UNIVERSITY OF NAPLES FEDERICO II

D.I.I. – DEPARTMENT OF INDUSTRIAL ENGINEERING

DOCTORAL PROGRAM IN INDUSTRIAL ENGINEERING
XXXI CYCLE

PH.D. DISSERTATION

EXPERIMENTAL AND NUMERICAL APPROACH TO INVESTIGATE TIRE AND ABS COMBINED INFLUENCE ON WET BRAKING PERFORMANCE OF PASSENGER CARS

COORDINATOR

CH.MO PROF. ING.
MICHELE GRASSI

SUPERVISORS

CH.MO PROF. ING.
RICCARDO RUSSO

CH.MO PROF. ING.
FRANCESCO TIMPONE

PH.D. CANDIDATE

SEBASTIAN ROSARIO PASTORE

“E il mio maestro mi insegnò come è difficile

trovare l’alba dentro l’imbrunire.”

Franco Battiato

Acknowledgements

I would like to thank my supervisors, Professors Riccardo Russo and Francesco Timpone, for the patient guidance and advice they have provided throughout my time as PhD student. My thanks also go to Professor Michele Russo, for the trust he has placed in me.

I would also like to thank the Reviewers of this thesis, Professors Wolfgang Fervers and Basilio Lenzo for their kind availability, patience and precise corrections.

I am also grateful to Andrea, Flavio, Sasha and all the Ph.D. and Master thesis students I met at the Department of Industrial Engineering, for the involving passion, technical suggestions and all the moments we spent together.

I would like to thank the Master thesis student Romualdo Pandolfi for his analytic contribution in the understanding of the ABS braking test and Bachelor thesis students Vincenzo Venanzio and Luca Prignano for their helpful support in the development of VELA.

I must express my gratitude to Michela and my family, for their continued support and encouragement. They were very understanding, especially in the hardest moments. They have been my strength.

These three years were very formative, I met many people who made me grow professionally and as a person. My sincere thanks go to whom supported me during my path, regardless the kind of way and contribution. With some of them, a true friendship was born that long distances have not ruined.

Abstract

This PhD activity is mainly focused on the study of the emergency braking test, where the tire behaviour can be influenced by the ABS system during such manoeuvre on wet roads. The main goal is to investigate and optimize the optimal shape of the longitudinal force characteristics of the tire in order to reduce the braking distance.

The only evaluation of the μ-peak could not be sufficient for reliable assessments but the whole shape of the longitudinal curve should be considered. Nowadays, the Wet Grip Index (WGI) is the parameter with which it is possible to classify the quality of a tire in wet conditions in the EU tire label and it is mainly based on maximum grip that a tire can perform interacting with the wet road. Understanding the optimal shape of the curve could also mean to understand if the WGI approach can give a complete evaluation of tire performance during the braking, or there could be something more to take into account.

A numerical approach was considered and a ABS logic has been modelled with the aim to replicate the fundamental strategies of a passenger car. A half vehicle model has been considered for this research work. A more physical approach on ABS modelling is proposed in this thesis, with the aim to estimate the optimal working range of the logic without any pre-set information.

Regarding the implemented tire model, the focuses were on trying to find a method to characterize the tire in wet conditions and understand how the longitudinal relaxation length can influence the ABS work in simulation environment. A method is proposed to get a possible estimation of the longitudinal relaxation length of the tire from vehicle measurements. Moreover, a study about the relaxation length evaluation with respect to the excitation frequency coming from the longitudinal slippage will be described in this thesis.

The emergency braking model was used to optimize the reference curve in order to reduce the braking distance. The analysis is focused on three parameters that can identify the longitudinal characteristics of the tire: the braking stiffness, μ-peak and drop down of the grip after the peak condition. The main outcome of the simulation results shows that the μ-peak could not be considered as the only critical parameter to evaluate the braking performance of the tire and that the drop-down of the grip seems to play a very important role to reduce braking distances.

Keywords: Vehicle dynamics, Vehicle control systems, Emergency braking, Forces and moments, Tire modelling, Relaxation length, Vehicle braking simulation, Tire characterisation, Viscoelastic characterisation, Vehicle testing.

Table of contents

Notation

a_x	Longitudinal vehicle acceleration	[m/s^2]
a_T	Shift factor (master curve)	
a_1	Distance from the centre of gravity to the front wheels	[m]
a_2	Distance from the centre of gravity to the rear wheels	[m]
c_{app}	Coefficient for the “Apply” phases in the brake pressure model	
c_{dump}	Coefficient for the “Dump” phases in the brake pressure model	
c_{hold}	Coefficient for the “Hold” phases in the brake pressure model	
d	Vehicle braking distance	[m]
d_{exp}	Experimental displacement by VELA	[m]
f	Frequency	[Hz]
f_c	Cut-off frequency	[Hz]
f_s	Sample rate	[Hz]
l	Wheelbase	[m]
m_{half}	Mass of the half vehicle model	[kg]
m_{veh}	Mass of the vehicle	[kg]
p_b	Brake pressure	[bar]
r	Rolling radius of the free-rolling tire	[m]
r_l	Loaded radius	[m]
r_0	Unloaded radius	[m]
t	Time	[s]
t_M	Monitoring time	[s]
u_x	Carcass longitudinal deformation	[m]

B_x	Stiffness factor – Pacejka tire model	
C_x	Shape factor – Pacejka's tire model	
D	Damping of rubber compound	[N·s/m]
D_x	Peak factor – Pacejka's tire model	
E	Module of elasticity in the spring-mass-damper model describing the rubber compound	[Pa]
E_x	Curvature factor – Pacejka's tire model	
F_{ad}	Force due to the adhesion contribution on the friction	[N]
F_{exp}	Experimental force by VELA	[N]
F_h	Force due to hydroplaning	[N]
F_{hys}	Force due to the hysteretic contribution on the friction	[N]
F_x	Longitudinal force of the tire	[N]
$F_{x,ss}$	Steady-state longitudinal force of the tire	[N]
$F_{x,1}$	Longitudinal force of the front tire	[N]
$F_{x,2}$	Longitudinal force of the rear tire	[N]
F_z	Vertical load	[N]
$F_{z,0}$	Nominal vertical load on the tire	[N]
$F_{z,1}$	Vertical force of the front tire	[N]
$F_{z,2}$	Vertical force of the rear tire	[N]
K	Stiffness of rubber compound	[N/m]
K_x	Longitudinal slip stiffness or Braking stiffness	[N/-]
$K_{x,s}$	Static longitudinal stiffness	[N/mm]
I_θ	Moment of inertia of the vehicle (y-direction)	[kg·m^2]
T	Temperature	[°C]
T_b	Wheel torque brake	[N·m]
T_g	Temperature of the Transition region	[°C]
T_p	Oscillation period for the sinusoidal input	[s]

V_r	Relative sliding speed	[m/s]
V_x	Longitudinal vehicle velocity	[m/s]
W_1	Static load on the front axle	[N]
W_2	Static load on the rear axle	[N]
α	Side slip angle	[°]
γ	Inclination angle	[°]
ε	Strain (deformation) of rubber compound	[-]
ε_{rp}	Pulsation of the harmonic force due to the roughness of the road profile	[1/s]
η	Viscous module in the spring-mass-damper model describing the rubber compound	
θ	Pitch angle	[rad]
κ	Longitudinal wheel slip	[-]
μ	Tire grip	[-]
μ_{brake}	Friction coefficient when the piston and the disc are in contact in the brake caliper	[-]
σ	Tension of rubber compound	[Pa]
σ_κ	Longitudinal relaxation length	[m]
σ_{κ,F_z}	Longitudinal relaxation length determined using the MF Tire model	[m]
$\sigma_{\kappa,slip}$	Longitudinal relaxation length determined using the MF Relax model	[m]
τ_f	Relaxation time	[s]
ϕ	Angular phase lag of the tire	[rad]
ω	Wheel angular velocity	[rad/s]
ω_{rp}	Spatial pulsation of the road profile	[1/m]
Γ	Relaxation module due to a step input deformation	[Pa]
Ω	Pulsation of the sinusoidal force applied to the rubber compound	[°]

ABS	Antilock Braking System
CAN	Controller Area Network
CoG	Centre of Gravity
DOF	Degree of Freedom
ECU	Electronic Control Unit
$EBCM$	Electronic Brake Control module
GPS	Global Positioning System
WGI	Wet Grip Index

List of Figures and Tables

1. Introduction

The main goal of this activity was to investigate the interaction between the tire and the ABS system during an emergency braking manoeuvre with the aim to optimize the shape of the longitudinal force characteristic of the tire, the so-called "μ-slip" curve, in order to reduce the braking distance. The main idea of the proposed model is to support tire manufactures to better understand how to handle tire characteristics during their development loops, with the focus on pure longitudinal braking test. The topic is related to one of the branches of research pursued by the Applied Mechanics Research Group of the Department of Industrial Engineering at the University of Naples Federico II, which already carried out similar studies in the past [1][2].

The Wet Grip Index (WGI) is the current parameter with which it is possible to classify the quality of a tire in wet conditions in the EU tire label and it is mainly based on maximum grip that a tire can perform interacting with the wet road. The understanding of the optimal shape of the curve implies to focus on the WGI approach for the complete evaluation of tire performance during the braking. The only evaluation of the μ-peak could not be sufficient to make a reliable assessment but the whole shape of the longitudinal curve should be taken into account to evaluate the behaviour of the tested tires [2][3]. In Figure 1-1, an overview of the ABS and tire "communication" is shown.

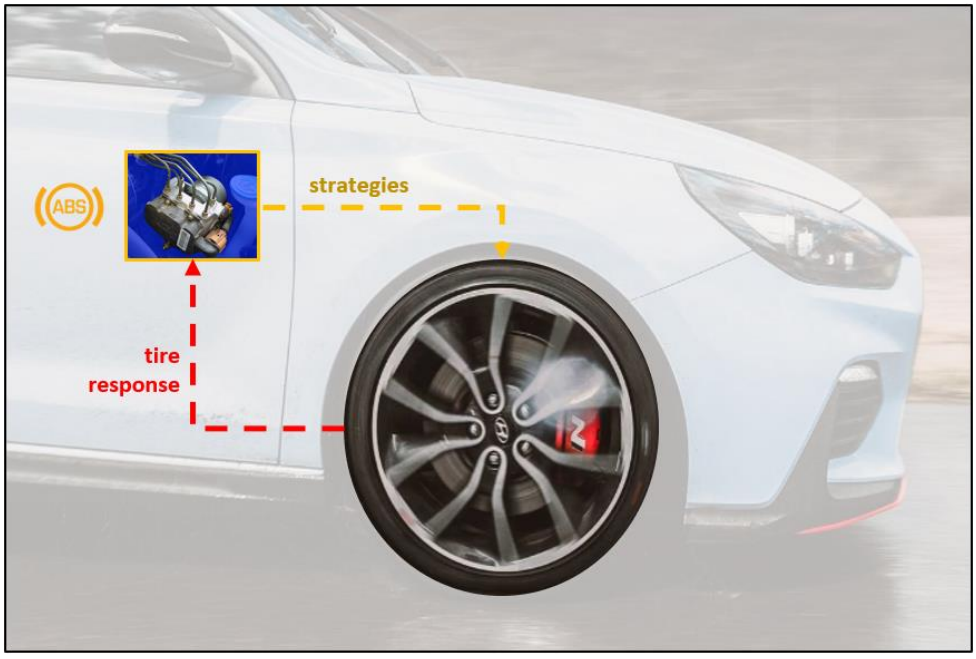

Figure 1-1 – Overview of the interaction between the ABS system and the tire during an emergency braking manoeuvre.

In Chapter 2 the background of the activity is described. A literature study about the WGI, ABS and tire modelling will be shown to better introduce the main reasons behind the development of this PhD work.

In Chapter 3 some details about the theory vehicle dynamics for the emergency braking will be shown by explained the global longitudinal equations that characterize the vehicle behaviour, focusing in particular on: the longitudinal load transfer, maximum deceleration, braking distribution, admissible braking domain variation and centre of gravity variations.

In Chapter 4 the pneumatic tire is described, in terms of construction features, viscoelastic characteristics of the rubber, mathematical models to describe the viscoelastic behaviour itself, forces and moments and tire modelling definitions in order to introduce what this analysis wants to focus on.

In Chapter 5, two experimental activities will be shown. The first one is related to outdoor test with a passenger car, with the aim to highlight the different behaviour that the same ABS logic can show with the two different tires that have been studied (Tire A and Tire B). Finally, vehicle and F&M results coming from trailer measurements are compared. The second experimental activity is related to the understanding of the longitudinal relaxation length parameter (with an indoor test with a test rig for tire forces and moments evaluations), that can be defined as the circumferential distance that a tire needs to generate the force, when the so-called “slip ratio” is applied as input. The relaxation length dependencies with the vertical load, slip ratio amplitudes and excitation frequencies have been investigated.

In Chapter 6, the numerical approach and the analysis of the simulation results are shown. The chapter can be divided in three steps. The first one was to study the strategies of the ABS logic: in this thesis, a case study will be proposed, where the strategies of a commercial logic coupled with two different tires have been investigated (Chapter 5). Therefore, the logic will try to replicate the strategies of the studied vehicle with a similar approach findable in the literature, with a great focus on the definition of the working range of the logic. In fact, a more physical approach on the estimation of the optimal working area is proposed, which can guarantee the stability and the maximum longitudinal performance of the tire.

The second step was to simulate the braking manoeuvre: once modelled and validated the state-flow ABS logic in Simulink environment, based on the behaviour of a real vehicle, the focus has been to characterize the tire model for wet conditions. Based on some recent research activities present in the literature, some formulas have been implemented in the semi-empirical model, in order to model the ABS simulation more reliable. The starting point has been to use the standard (Pacejka’s MF-Tire 5.2) model that has been adapted to the different longitudinal characteristics of the two studied tires that have been characterized with a trailer on wet surface at only one vertical load.

In fact, the third step is focused on the characterization of the investigated tires in wet conditions, it has been considered to measure forces and moments with a trailer on wet roads. The test has been done at a one load, that is around the maximum load that the test vehicle can generate during the emergency braking manoeuvre. Then, some a “starting” tire model has been adapted to the longitudinal measurements from tests with trailer. Considering the vertical load used for trailer measurements as reference, the corresponding curve has been considered as reference curve. Moreover, a method to characterize the relaxation length directly from vehicle measurements on wet surface has been considered, in order to characterize the MF-Relax model parameters and make the dependency of the longitudinal relaxation length on the longitudinal slippage of the tire during the braking.

Finally, the analysis of the simulation results is shown. The goal was to modify the reference curve and understand how to optimize the curve to reduce the braking distance: the study was mainly focused on the braking stiffness, μ-peak and drop down of the grip of the tire after the peak. To connect the simulation results with viscoelastic properties of the rubber, it has been developed an in-house made instrument called V-ELA, described in the Appendix of this essay.

In Chapter 7 the conclusions and future developments will be debated. As conclusions, the focus will be on ABS and tire modelling, the relaxation length dependency and the influence of the μ-slip curve on the vehicle performance because of the interaction with the tire. As future developments, the focus will be on the dependency of the friction on the longitudinal velocity and hydroplaning, a frequency analysis (in terms of ABS and tire response) and a proposal of a method to improve rubber characteristics starting from simulation outcomes.

In the Appendix, some alternative methods are proposed. A method to characterize the vertical load sensitivity of the tires is shown in the first subparagraph. In the second subparagraph, a mathematical relation has been found to fit the experimental relaxation length across the excitation frequencies that have been considered in the test procedure and that can be proposed to improve and increase the reliability of the response of the tire model for ABS braking simulations (as described in Chapter 5). Finally, a small and transportable instrument called V-ELA has the aim to estimate the stiffness and damping compliances of the rubber directly from the tire with a different approach with respect to the standard DMA test is shown. This instrument can be applied as shown in the future developments (Chapter 7), by applying a simplified Persson's theory-based approach. The V-ELA can play an important role to connect the results from braking simulation and compound characteristics.

The data used for the current analysis are made available for use by the Department of Industrial Engineering at University of Naples "Federico II", thanks to the collaborations the department had built up with several companies during the years. Because of non-disclosure agreements, there will not be any direct mention about original raw data, absolute values or results, instruments and tires used. All the data will be shown as normalized with respect to a specific constant value, but the trends and rankings will be kept allowing the reader to understand the described methods.

2. Background of the activity

Nowadays, tire manufacturers take care of the braking performance on wet surfaces, that is a critical safety feature and it is related on how quickly human drivers will be able to stop while they are driving a vehicle. The tire plays a crucial role in a vehicle's stopping distance and those ones with excellent grip have shorter braking distances on slippery roads, which is essential for keeping the driver safe when it rains. In the following paragraphs, the background of the activity is introduced, by focusing on the description of the Wet Grip Index, the reviews of the ABS for passenger cars and the tire models which can be considered for the kind of study proposed.

2.1 Wet Grip Index

Since the development of the first motor driven vehicle in 1769 and the occurrence of first driving accident in 1770, engineers were determined to reduce driving accidents and improve the safety of vehicles [5]. It is obvious that efficient design of braking systems is to reduce accidents. Vehicle experts have developed this field through the invention of the first mechanical Antilock-Braking System (ABS) which have been designed and produced in aerospace industry in 1930 [5].

There are different standards that can be followed, like the Danish Roads Standards and Guidelines conditions [6] or the Tire Labelling Regulation by ETRMA [7]. In Europe, EU Tire Labelling classifies tire wet braking performance with a parameter called Wet Grip Index (WGI) in different performance classes. In the current labelling regulation, three tire performance parameters are included: Fuel efficiency, Wet grip, and Rolling noise measured value (in dB). The three performance parameters are specified in the label, as shown in the following Figure 2-1.

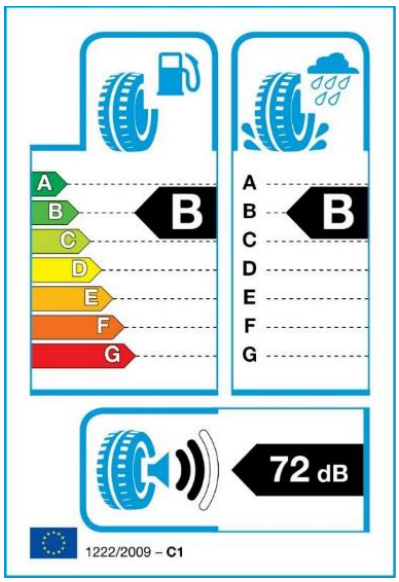

Figure 2-1 – An example of EU tire labelling [7].

The wet grip refers to the safe performance of tires, i.e. it reflects the capability of a tire to brake on a wet road. It is determined based on the Wet Grip Index according to the A-G ratings (from shortest to the longest braking distances). The effect is influenced by vehicles and driving conditions but in the case of full braking, the difference between the G and the A classes could be up to 30% shorter braking distance for a set of 4 identical tires [7].

The value of the wet grip index is calculated based on either the average deceleration when the test is carried out with a commercialized vehicle with ABS system equipped or the peak brake force coefficient when a F&M trailer is used, which is unit-less and compared to a Standard Reference Test Tire (SRTT) [4][8]. The wet grip index is shown on the label as a marked letter on the A-G scale. Normally, the measurements from the F&M trailer and the commercialized vehicle are considered as equivalent [8].

It is well known that wheels will slip and lockup during severe braking or when the braking manoeuvre is carried out on a slippery road surface (wet, icy, etc.) [5]. This usually causes a long stopping distance and sometimes the vehicle will lose steering stability [5]. The ABS is recognized as an important contribution to road safety as it is designed to keep a vehicle steerable and stable during heavy braking events by preventing wheel lock [9]: its target is to manipulate the wheel slip so that a maximum friction is obtained and the lateral stability is maintained, in order to reach the shortest distance while maintaining the directional control.

Nowadays, the link between emergency braking manoeuvre and ABS is one of the main topics for tire companies. In order to reduce investments in tire development and manufacturing for indoor and outdoor tests, simulated approaches are considered to predict the stopping distance [10][11][12].

Moreover, the behaviour of tires on wet surfaces is of considerable interest from the vehicle safety point of view, as many accidents occur on slippery roads. To achieve acceptable performance on wet surfaces, it is essential to maintain the effective contact between the tire rubber compound and the road, removing water from the contact area as much as possible. This means that the tire tread should have a suitable pattern to facilitate the flow of fluid from the contact area (hydroplaning phenomenon), and the surface of the pavement should have an appropriate texture to facilitate drainage as well. To provide good skid resistance, road surfaces must fulfil two requirements: an open macro-texture to facilitate gross draining, and micro-harshness to produce sharp points that can penetrate the remaining water film [13].

2.2 ABS – Antilock Braking System

According to the Society of Automotive Engineers (SAE), the goal of ABS is: “The application of ABS to a vehicle can provide improvements in the vehicle performance under braking compared to a conventional brake system. Improvement is typically sought in the areas of stability, steerability, and stopping distance. In addition to minimizing stopping distance, vehicle stability is another aspect to straight line braking that must be considered. For the case of straight-line braking with the steering held fixed in the straight-ahead position, the vehicle should brake in a straight line in the presence of external disturbances … Preservation of steering control and stability during braking are prime goals of the application of ABS to vehicles” [9].

The reason for the development of antilock brakes is very simple. Under braking, if one or more of a vehicle wheels lock (begins to skid) then this has several consequences:

- braking distance increases;
- steering control is lost;
- tire wear will be abnormal.

The obvious consequence is that an accident is far more likely to occur. The application of brakes generates a force that impedes a vehicles motion by applying a force in the opposite direction.

Antilock braking systems (ABS) were conceived originally for trains in the early 1900s [9]. These systems were first applied to passenger vehicles and light trucks by Bosch in 1936. The first commercial systems

entered production in the 1960s and Bosch began supplying a hydraulic ABS system to Mercedes-Benz in October 1978. Research on improving ABS systems continues today with the development of hybrid and full electric vehicles where regenerative braking may be used to recover some of the kinetic energy that would otherwise be lost to heat due to the application of friction brakes [14][15][16][17].

The Antilock Braking System (ABS) is an electro-hydraulic device which aim is to prevent tires from locking during braking. Specific road tests performed by manufacturers involved in ABS (i.e. car, tires, braking systems and control system producers) have shown that it assures vehicle stability, directional control and, especially on slippery surfaces, minimizes the stopping distances, even in panic braking [5][18], under several grip conditions. It is also used to get more realistic vehicle simulations results regarding braking manoeuvre for several assessments in the transportation field, since it is a mandatory car active safety system [19].

One of the most popular ABS is the system proposed by Bosch [18]. The algorithm considers wheel angular deceleration, measured with specific sensors, to recognize the incipient wheel locking of one or more wheels [18]. In Figure 2-2 below, it is possible to see an overview of the Bosch ABS logic, where the vehicle speed, wheel acceleration and brake pressure are shown during a common braking manoeuvre.

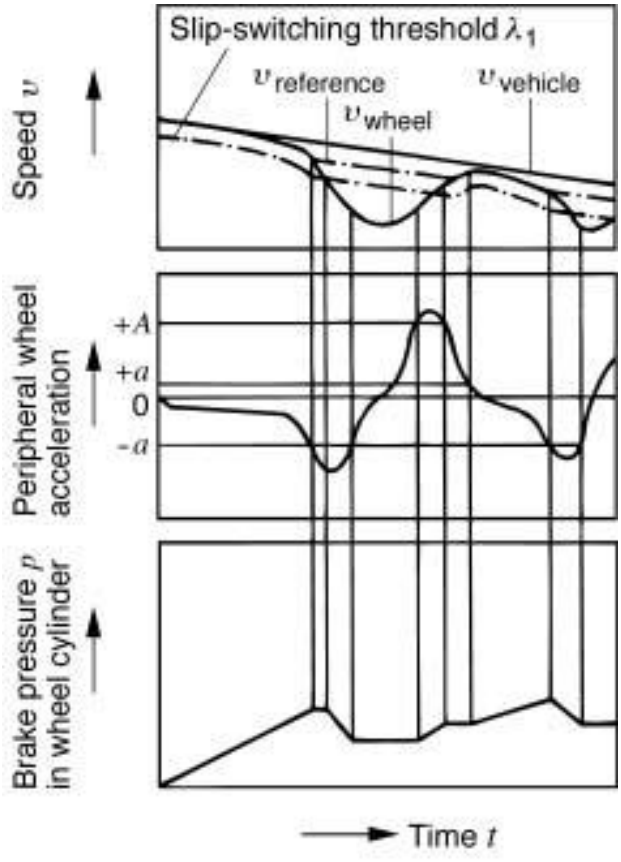

Figure 2-2 - Bosch ABS logic based on wheel acceleration/deceleration thresholds [18].

The ABS logic presented by Bosch, can manage the brake pressure in the calipers through some proper criteria and the monitoring of the wheel acceleration signal. These criteria are based on some pre-set wheel acceleration thresholds, as shown in the figure above.

A fundamental role is played by the estimation phase of the tire and road conditions. It is commonly recognized that it is not easy to estimate the tire and road friction forces and coefficient accurately because of the nonlinear system, parameters uncertainties, and signal noises. Therefore, the big effort of the researchers is to study different approaches for the determination of the possible thresholds of the

longitudinal slip. There are studies based on the observation of tire forces by the discrete Kalman filter, and the road friction coefficient estimated by a recursive least square method consequently [11][20]. Other approaches expect to pre-define look-up table for the low, med and high friction conditions to use when the road conditions are different [1].

Normally, the logic behind ABS strategy cannot be disclosed. Due to limited information from literature, particularly on the setup of longitudinal acceleration thresholds also due to industrial secret, it is not possible to understand how companies define their strategy to set these values, as also defined by Persson [21]. Sivaramakrishnan et al. describe that the ABS algorithms regulate the brake pressure following a set of rules that are based on wheel longitudinal slip and deceleration thresholds and that the most commercial ABS systems are designed to use wheel deceleration/acceleration thresholds to decide the brake pressure actuation [3]. These values could be defined based on different experimental activities, where it could be possible to set best values at the initial phase of the braking. It could be possible to switch from a dataset to another based on the best compromise for those conditions, consistent with company definitions [1].

Below, there are some other approaches to model the ABS logics proposed by the literature, as an overview of the current research work about modelling the ABS logics. The following points are partially extracted from the ALY, Ayman A., et al. technical review [5].

A *PID controller* can be used to improve the performance of the ABS. In this case, the slip-based logic sets two different thresholds with which it can manage the braking performance, by trying to follow a target that represent the max performance reachable. The PID controller is simple in design but there is a clear limitation of its performance. It does not possess enough robustness for practical implementation [5][22].

The *Optimal Control Methods based on Lyapunov approach* is a nonlinear output feedback control law for active braking control systems. The control law guarantees bounded control action and can cope also with input constraints. closed-loop system control algorithm that allows detecting without the need of a friction estimator, if the closed-loop system is operating in the unstable region of the friction curve, thereby allowing enhancing both braking performance and safety. Since the changes in the road conditions implies continuous adaptation in controller parameter, an adaptive control with Lyapunov approach is considered. Some nonlinear output feedback control law for active braking control systems are also proposed [5][23].

With the *Robust Control based on Sliding Mode Control method* is a systematic approach which is provided with the aim to solve the problem of maintaining stability and consistent performance in front of modelling imprecisions. The design of sliding-mode controllers under the assumption of knowing the optimal value of the target slip is introduced, where the main limitations are the optimal slip estimation and the tracking of the estimated optimal value [5][24][25][26][27][28].

The *Adaptive Control based on Gain Scheduling Control method* incorporates the wheel slip constraint as a priori into control design so that the skidding can be avoided. A control structure of wheel torque and wheel steering is proposed to transform the original problem to that of state regulation with input constraint [5][29].

The main advantage of the *Fuzzy Sliding Mode Control (FSMC)* design method is that it requires fewer fuzzy rules than Fuzzy Control does. The Fuzzy Control and FSMC are both effective methods, their major disadvantage is that the fuzzy rules should be previously tuned by time-consuming trial-and-error procedures [5][30][31]. To solve this problem, an *Adaptive Fuzzy Control (AFC)* based on the Lyapunov synthesis approach has been extensively studied [32][33]. A fuzzy controller is the main tracking controller, which is used to mimic an ideal controller, and a robust controller is derived to compensate the difference between the ideal controller and the fuzzy controller. The *Self-Learning Fuzzy Sliding Mode Control (SLFSMC)* has the advantages that it can automatically adjust the fuzzy rules, like the AFC, and can reduce the fuzzy rules, similar to the FSMC [5]. In order to obtain high performance even in the worse road conditions, the *Fuzzy Model Reference Learning Control (FMRLC)* has been proposed [34]. It uses a learning mechanism which observes the outputs and adjusts the rules in a direct fuzzy controller so that the overall system behaves like a “reference model” which is able to characterize the desired behaviour [5].

2.3 Tire models for ABS simulations

To understand a certain strategy of the ABS system, it is important to know tire characteristics in terms of forces generated between the tire and the road during the braking.

In the literature, several tire-road contact models can be found. The most popular one is the Pacejka MF-Tire model [35], that is based on a steady-state formulation and introduces the transient behaviour of the tire as a first-order differential equation (up to 8Hz) of relevant quantities such as the slip angle and the longitudinal slippage.

The transient behaviour can mainly define the relaxation length [36][37][38][39], which will be described in Chapter 4 and Chapter 5. In the case of low frequency manoeuvres and large wavelength road irregularity, steady-state or nearly steady-state tire models correctly predict the tire behaviour. However, if the frequency of the manoeuvre increases or the road wavelength decreases, more complex tire models are necessary in order to reproduce the fact that the tire , being a partially viscoelastic solid, changes its dynamic behaviour and thus the forces at the hub as a function of excitation frequency [40]. Pacejka also proposes the "Enhanced Nonlinear Transient tire model" that couples MF-Tire model with a single DOF model that reproduces the contact patch dynamics [36][40]. The Enhanced Nonlinear Transient tire model requires the integration of a second order differential equation (and of the first order differential equation of the slippage) whose coefficients are a function of the vertical load and of the slippage. To reduce the computational effort, a new dynamic tire-road contact model is proposed, based on a first order differential equation like the differential equation proposed by Pacejka. In their so-called "MF-Relax model", the relaxation length is a function not only of the vertical load but also of the slippage. They also found that the relaxation length also depends on the excitation frequency, but there was no clear relation between and the excitation frequency: for this reason, this dependency was not included in the MF-Relax model. The dependency of the control system strategies and the time delay for tire response it is also a topic on which researchers are focusing on. In fact, some studies show how the longitudinal relaxation time characterizes the time available for an agile wheel torque control and longitudinal tire slippage control to enhance vehicle mobility and energy efficiency [37].

Other models are able to better predict the tire dynamic behaviour even in cases of high slippages or combined slippages such as Pacejka's Enhanced Nonlinear Transient tire model (up to 30Hz) [36].

Moreover, some research activities highlight the Rigid Ring model (see Figure 2-3) could take tire eigenmodes into account (due to the ABS work and the short wavelength of road irregularities). It is an high frequency (up to 100Hz) extension of MF-Tire, that has been developed for ride comfort, road load and vibration assessments and that considers the belt and the rim as a rigid ring and disk respectively, with their masses and inertias linked through a system of springs and dampers in horizontal, vertical and torsional directions [3][41].

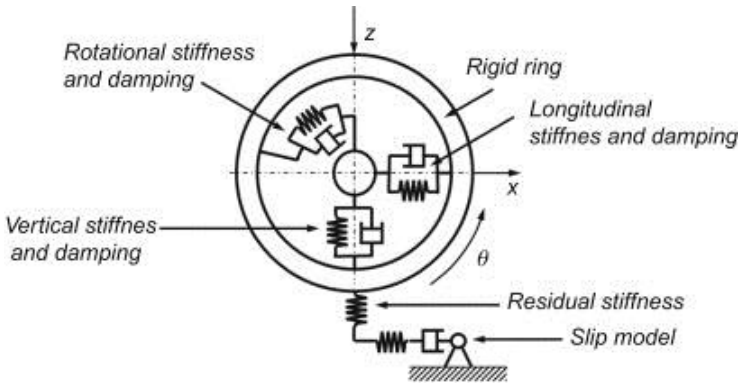

Figure 2-3 – Scheme of the Rigid Ring model [42].

This kind of a model can help in the prediction of the vehicle dynamics response in critical situations in which active control systems (such as ABS, ESP, etc.), having an abrupt response, intervene to avoid accidents [40]. In fact, during such manoeuvres, tires experience very fast transient behaviour: having a reliable tire model means being also able to simulate these situations, helping the vehicle designer and/or the control engineer to setup a safer vehicle in less time.

The choice of using more complex and accurate models often leads to very complex and hardly understandable results. It could be more difficult to characterize more parameters not easily measurable. The approach followed in this essay is focused on a simpler MF-Tire model, with some alternative evaluation regarding the transient behaviour modelling.

3. Theory of braking manoeuvres

Every day, people can recognize the importance of a vehicle to faithfully follow the desired path as well as the relevance of achieving such a condition without “extreme” driving skills needed. It is essential to formulate an adequate vehicle dynamics model for a reliable prediction and analysis of real vehicle behaviour and stability performances. Obtaining a complete and accurate prediction with a model that tends to be as complex as possible, often leads to very complex and hardly understandable results. Moreover, complex models often involve physical quantities and parameters difficult to be measured with satisfying accuracy. Therefore, in such cases, it is far better to start with the formulation of simpler models, which involve fewer parameters and Degrees of Freedom (DOFs), still proving to be accurate enough in order to describe the main characteristics of the motion.

In this chapter a complete vehicle dynamics model is shown, able to describe its behaviour during the braking. The main interest is to study the vehicle behaviour in all those situations where its stability is a crucial requirement.

3.1 Longitudinal dynamics

It is possible to study the braking and acceleration conditions just studying the longitudinal motion of the vehicle. The braking manoeuvre is usually more studied than the acceleration one because it is the opposite manoeuvre and the involved forces are much lower when the vehicle is accelerating (generally there are only two driven wheels). Moreover, studies about the braking manoeuvres are more related to safety reasons, important topic for passenger cars. The goal is to brake the car in the shortest possible distance. This theoretical approach also matches with the main purpose of the thesis.

Trying to only describe the basic features, we can indicate the following assumptions [43]:

- braking efforts are the same between right and left side because, otherwise, we would have yaw moment;
- the vehicle moves on flat road, as a geometrical plane;
- the vehicle is moving in a straight line and in absence of side force disturbance;
- side slip angles of the four wheels are equal to zero, all the tires are in pure braking condition.

Usually, during the braking we have pitch oscillations of the sprung mass (assumed rigid). In uniform braking conditions, (with constant braking forces), the pitch movement exists only at the starting instants, when forces are applied abruptly. During the rest of braking there is a constant pitch angle. Therefore, excluding the short initial transient, suspensions play a marginal role: we can represent the vehicle as a single rigid bodywork in translational direction.

The same axle’s wheels are located always in the same conditions (grip, vertical load and braking force) to allow the vehicle’s rotational balance around a vertical axis.

3.1.1 Vehicle model for braking manoeuvres

In this paragraph, a simple vehicle model during the braking: in the following Figure 3-1, the reference system and the forces to consider during the studied manoeuvre is shown.

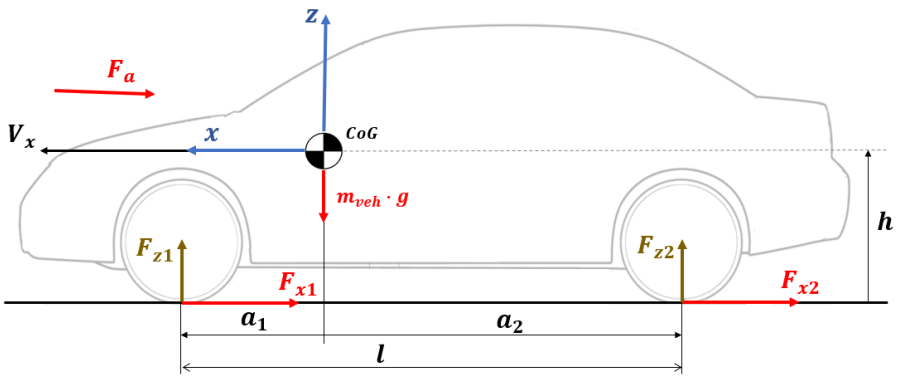

Figure 3-1 - Scheme of the vehicle in braking conditions.

Based on the scheme proposed in the Figure 3-1, the distance between the centre of gravity's position and the front axle will be referred to as a_1, while the distance occurring between the rear axle and the centre of gravity itself will be referred to as a_2. The total length existing between the axles, defined as l, is currently known as "vehicle's wheelbase":

$$l = a_1 + a_2 \tag{3.1}$$

with F_{z1} and F_{x1} we can indicate the vertical and longitudinal forces acting by the road on two front axle's wheels (the same for F_{z2} and F_{x2} forces on the rear axle). The longitudinal forces are assumed as positive in braking conditions.

There is also an aerodynamic force F_a(or drag force) that is not necessarily horizontal if there is lift or downforce. However, except in the case of racing cars equipped with flaps, aerodynamic effects are substantially negligible during emergency braking of passenger cars. It is also precautionary since it has a small contribution with respect to the braking forces that the tires can generate while they interact with the road [43].

Even rolling resistance is modest, around 1.5% of the total weight of the vehicle; only in the case of uphill driving we do not have negligible forces opposed to the motion, compared to any braking forces themselves.

A fixed reference system with the road has been considered to describe the vehicle's motion: the x_0 axis is parallel with the road and directed in the sense of motion and the z_0 vertical axis is directed upwards. The vehicle speed is indicated with u and its longitudinal acceleration (negative braking) with $\dot{u}$. The following equations (3.2):

$$\begin{aligned} m_{veh}\dot{V}_x &= -\left(F_{x,1} + F_{x,2}\right) \\ 0 &= F_{z,1} + F_{z,2} - m_{veh}g \\ 0 &= \left(F_{x,1} + F_{x,2}\right)h - F_{z,1}a_1 + F_{z,2}a_2 \end{aligned} \tag{3.2}$$

are describing the model depicted in Figure 3-1.

The inequalities (3.3) are expressing the limits of braking forces due to grip:

$$\left|F_{x,1}\right| \leq \mu F_{z,1}, \qquad \left|F_{x,2}\right| \leq \mu F_{z,2} \tag{3.3}$$

where μ is indicated as coefficient of friction, defined as the ratio between the longitudinal force and the corresponding vertical load.

The following inequalities:

$$F_{z,1} \geq 0 \text{ and } F_{z,2} \geq 0 \tag{3.4}$$

are expressing that the road is a unilateral bond. The equations (3.3) and (3.4) also regulate vehicle dynamics in acceleration conditions. The only difference is in the longitudinal forces' sign. Obviously, if the traction is only at one axle, a longitudinal force is zero (rolling resistance is not considered, as defined before).

3.1.2 Longitudinal load transfer

There is not a load transfer if the vehicle is in free rolling conditions ($\dot{V}_x = 0$), the so-called static loads W_1 and W_2 are exercised on the axles. as show in the equations (3.5):

$$W_1 = \frac{m_{veh} g a_2}{l}, W_2 = \frac{m_{veh} g a_1}{l} \tag{3.5}$$

it depends only on the position of the centre of gravity in the absence of aerodynamic actions. In braking condition there is an increase of the vertical load ΔF_z on the front axle and a corresponding decrease on the rear one (the opposite situation in case of acceleration). The load on the front axle in dynamic condition is obtained by:

$$\begin{aligned} 0 &= -mV_x h - F_{z,1} a_1 + mg a_2 - F_{z,1} a_2 \rightarrow \\ F_{z,1} &= \frac{mg a_2}{l} - \frac{mh}{l} V_x = W_1 - \frac{mhV_x}{l} \end{aligned} \tag{3.6}$$

starting from the equations (3.2). While, the following ones:

$$\begin{aligned} 0 &= -mV_x h + F_{z,2} a_2 - mg a_1 + F_{z,2} a_1 \rightarrow \\ F_{z,2} &= \frac{mg a_1}{l} + \frac{mh}{l} V_x = W_2 + \frac{mhV_x}{l} \end{aligned} \tag{3.7}$$

are describing the load on the rear axle. In the diagram, the intercepts represent static loads. As shown in Figure 3-2, the load transfer depends linearly on the longitudinal acceleration.

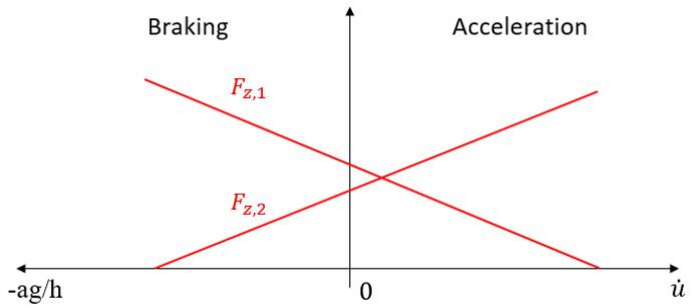

Figure 3-2 - Static loads at the axles as a function of the longitudinal acceleration [43].

In fact, the load transfer depends on the h/l ratio (relation between the height of the centre of gravity and the vehicle's wheelbase). The distribution of the braking forces between the front and rear axles ($F_{x,1}/F_{x,2}$) has no influence on ΔF_z.

The condition $F_{z,2} = 0$ (in ordinary motor vehicles) is obtained for $\dot{V}_x = -a_1 g/h$ corresponds to the detachment from the ground of the rear wheels and then the longitudinal rollover of the vehicle.

3.1.3 Maximum deceleration

The maximum deceleration is achieved when all wheels are on the grip limits:

$$F_{x,1} = \mu F_{z,1} \text{ and } F_{x,2} = \mu F_{z,2} \tag{3.8}$$

where the inequalities (3.3) are changed by the above shown equalities Under these extreme conditions, it is straightforward to obtain:

$$\left|\dot{V}_x\right|_{max} = \mu g \tag{3.9}$$

widely used in control systems. In fact, before locking, it must estimate the max deceleration of the vehicle in order to know the μ coefficient. In common passenger vehicles, considering that under high friction conditions are valid at $\mu < a_1/h$, the slippage of the tires always theoretically occurs before the rollover. Combining the above equations:

$$\begin{aligned} F_{x,1P} &= \mu F_{z,1P} = \mu \left(W_1 + \frac{mh}{l}\mu g\right) \\ F_{x,2P} &= \mu F_{z,2P} = \mu \left(W_2 - \frac{mh}{l}\mu g\right) \end{aligned} \tag{3.10}$$

the values of the two braking forces F_{X1}= F_{X1P} and F_{X2}= F_{X2P}, at the limit condition ($\dot{V}_x = -\mu g$). Therefore, the relation (3.11):

$$\frac{F_{x,1P}}{F_{x,2P}} = \frac{F_{z,1P}}{F_{z,2P}} = \frac{a_2 + \mu h}{a_1 - \mu h} \tag{3.11}$$

shows that the braking force distribution depends on variable forces magnitudes and this indicates that the same vehicle must reach the optimal conditions for a given μ coefficient.

3.1.4 Braking force distribution

This following essay wants to show what happens when the limit of grip the two axles is reached at the same time and when one of the two braking forces is fixed and the other one assumes the maximum value (equal to the limit of grip). Considering the above reported equations:

$$\begin{aligned} F_{x,1} = \mu F_{z,1} = \mu\left(W_1 - \frac{mh}{l}\dot{u}\right) = \\ = \mu\left[\frac{mga_2}{l} - \frac{h}{l}\left(-F_{x,1} - F_{x,2}\right)\right] = \mu\left[\frac{mga_2}{l} + \frac{hF_{x,1}}{l} + \frac{hF_{x,2}}{l}\right] \end{aligned} \tag{3.12}$$

which will be separated by vehicle axle.

In fact:

$$F_{X1}\left(1-\mu\frac{h}{l}\right)=\mu\left[\frac{mga_2}{l}+\frac{hF_{X2}}{l}\right]$$
$$F_{X2}\left(1+\mu\frac{h}{l}\right)=\mu\left[\frac{mga_1}{l}-\frac{hF_{X1}}{l}\right] \quad (3.13)$$

the equations (3.3) are related respectively to the front and rear axles. When the only front brake:

$$F_{x,1O}=\frac{\mu W_1}{\left(1-\mu\frac{h}{l}\right)} \quad (3.14)$$

with $F_{x,2}$ = 0. While, for the only rear brake:

$$F_{x,2O}=\frac{\mu W_2}{\left(1+\mu\frac{h}{l}\right)} \quad (3.15)$$

when $F_{x,1}$ = 0. The Figure 3-3 is showing the admissible are for the brake forces distributions that can be possible to find for different braking manoeuvres.

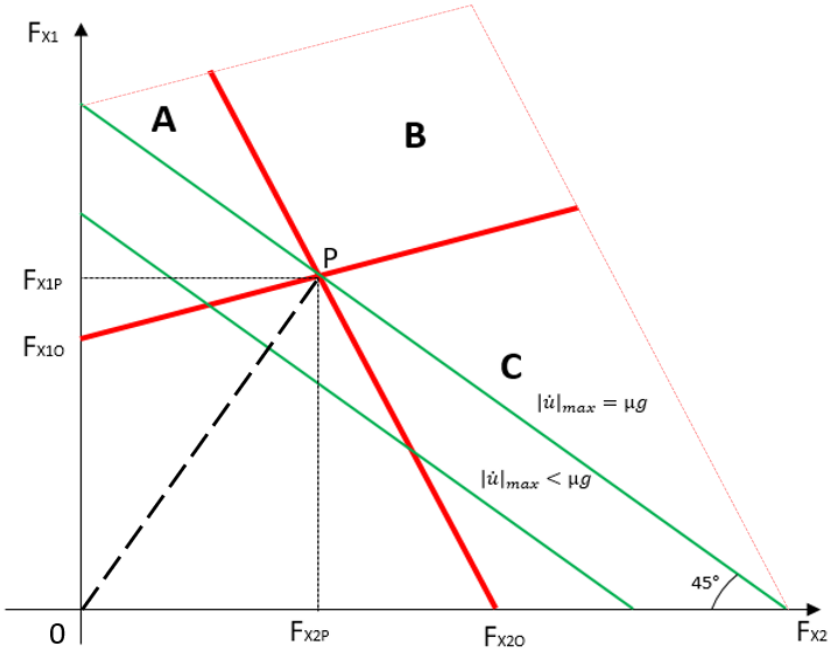

Figure 3-3 - Admissible area of possible brake forces distributions [43].

The equations (3.13) indicate two straight lines: their slopes depend on μ, h and l. The equation $-F_{x,1}-F_{x,2}$= m$\dot{V}_x$ indicates the so-called iso-deceleration line (with a 45° inclination). With the straight line $-F_{x,1}-F_{x,2}$= mg, that has to pass through the point P, it is possible to realize the maximum possible deceleration for each ($F_{x,1P}$, $F_{x,2P}$).The area under the quadrilateral is called "admissible braking domain": all the forces ($F_{x,1}$, $F_{x,2}$) in the domain do not cause the wheel lock. Therefore, the main goal of the ABS is to keep the working zone in this area, as close as possible to the point P.

The areas in the figure represent:

A. front wheels locking;

B. both rear and front wheels locking;

C. rear wheels locking.

For an iso-deceleration straight with ($\dot{u} < \mu g$), we are inside the area where there are a lot of pairs ($F_{x,1}$, $F_{x,2}$) of braking forces without locking. For $|\dot{V}_x|_{\max} = \mu g$ (point P) there is no choice for braking force distributions without wheel locking.

The deceleration is smaller with the $F_{x,1O}$ force: with a lower load transfer there will be less vertical load on the front axle and the limit braking force $F_{x,1O}$ (from ground to front) is smaller than $F_{x,1P}$. As it is possible to observe below:

$$F_{x,1O} > \mu W_1 \ , \qquad F_{x,2O} < \mu W_2 \tag{3.16}$$

Obviously, at rear we have the opposite case. The $\overline{OP}$ straight line (3.17) equation in Figure 3-3:

$$F_{x,1} = \frac{a_2 + \mu h}{a_1 - \mu h} F_{x,2} \tag{3.17}$$

is showing that the highest load transfer, from rear to front, is possible at the point P. There are the maximum load on front and the maximum braking limit force $F_{x,1P}$.

3.1.5 Admissible braking domain variation

It is possible to plot the admissible braking areas corresponding to varying grip levels. In general, μ_1 is entirely contained in μ_2 area when $\mu_1 < \mu_2$. It is not possible that a domain with a higher coefficient of adhesion can intersect with a domain with a lower coefficient of adhesion. The one with the lower coefficient of adhesion is contained always in that one with the highest coefficient of friction.

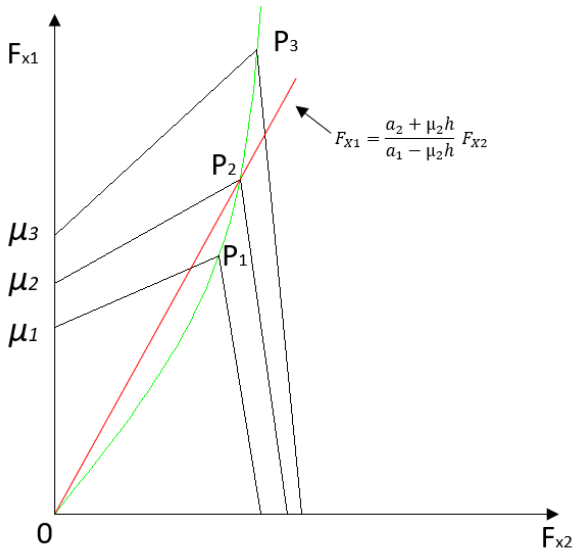

Figure 3-4 - Area of all admissible braking combinations for three different grip coefficients. The parabola represents the limit points of the braking areas [43].

In Figure 3-4 it is possible to see three regions obtained for increasing values of the coefficient of adhesion $\mu_1<\mu_2<\mu_3$ and suppose a braking system designed to have the optimum performance when $\mu = \mu_2$ that we can distribute the braking forces between front and rear axle according to the line through the origin and P_2:

$$F_{x,1} = \frac{a_2 + \mu_2 h}{a_1 - \mu_2 h} F_{x,2} \tag{3.18}$$

where, in this way, it is not possible to meet all the endless $F_{x,1}$, $F_{x,2}$ forces, but only those belonging to the straight line.

3.1.6 Vehicle's centre of Gravity variations

Normally, the centre of gravity can vary only vertically and longitudinally, considering a symmetrical vehicle to the XZ plane. It is observed that the maximum permissible deceleration is not a function of the position of CoG. In fact, μg is obtained in the following conditions:

$$\begin{aligned} F_{x,1} &= \mu F_{z,1} \\ F_{x,2} &= \mu F_{z,2} \end{aligned} \tag{3.19}$$

when $F_{x,1}$ and $F_{x,2}$ reach the limit of grip at the same time. Assuming that the CoG has an only longitudinal movement (and not in height), the vertexes of all the possible admissible domains must always be on the line of the maximum admissible deceleration.

In any case, for the proposed model in Paragraph 6.2, no longitudinal and vertical variations of the CoG will be taken into account (that means no effect of weight distribution due to CoG variations). Therefore, the only load transfer will be considered, generated by the effect of the longitudinal deceleration during the braking, as shown in the equations (3.6) and (3.7).

3.2 ABS description and overview of test procedures

3.2.1 Technical description

During severe braking scenarios, a point is obtained in which the tangential velocity of the tire surface and the velocity on road surface are not the same such that an optimal slip which corresponds to the maximum friction is obtained. During the braking, the longitudinal slip κ (that will be better explained in Paragraph 4.5.3) is defined as:

$$\kappa = \frac{V_x - \omega r}{V_x} \cdot 100 \tag{3.20}$$

where ω, r, and V_x represent the wheel angular velocity, the wheel rolling radius, and the vehicle forward velocity, respectively.

When the vehicle has a constant velocity, $V_x = \omega r$, therefore $\kappa = 0$. In severe braking, it is common to have ω = 0 while κ = 1, which is called wheel lockup. Wheel lockup is undesirable since it prolongs the stopping distance and causes the loss of direction control [16][17].

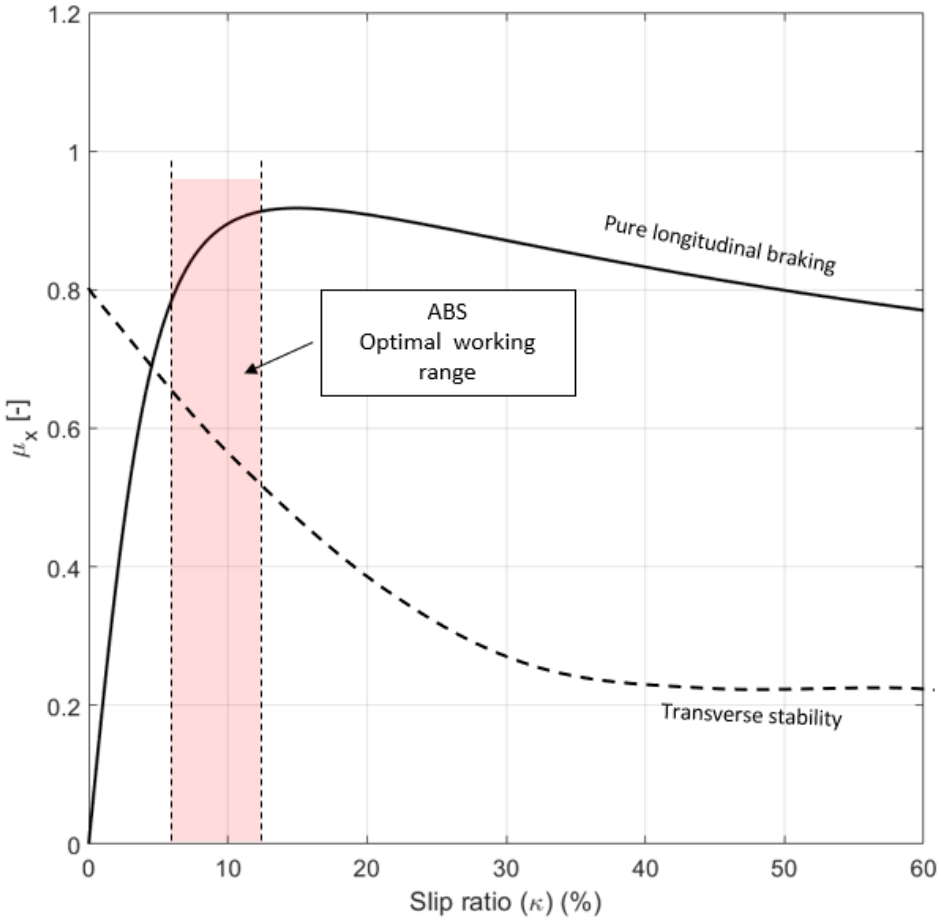

Figure 3-5 - Relationship between braking coefficient and wheel slip.

In Figure 3-5 it is shown that the slide values for stopping/traction force are proportionately higher than the slide values for cornering/steering force (dashed curve). A locked-up wheel provides low road handling force and minimal steering force.

The main benefit from ABS operation is to maintain directional control of the vehicle during heavy braking. In rare circumstances the stopping distance may be increased however, the directional control of the vehicle is higher than if the wheels are locked up.

As described in the ALY, Ayman A., et al. technical review [5], the main difficulty in the design of ABS control arises from the strong nonlinearity and uncertainty of the problem. ABS systems are designed around system hydraulics, sensors and control electronics.

The block diagram in Figure 3-6 shows the block representation of an antilock brake system. It shows the basic functionality of the various components in ABS systems and shows the data/information flow. The wheel sensor feeds the wheel spin velocity to the Electronic Control Unit (ECU), which is based on some underlying control approach would give an output signal to the brake actuator control unit. The control logic is based on the objective to keep the wheels from getting locked up and to maintain the traction between the tire and road surface at an optimal maximum. The task of keeping the wheels operating at maximum traction is complicated given that the friction-slip curve changes with vehicle, tire and road changes.

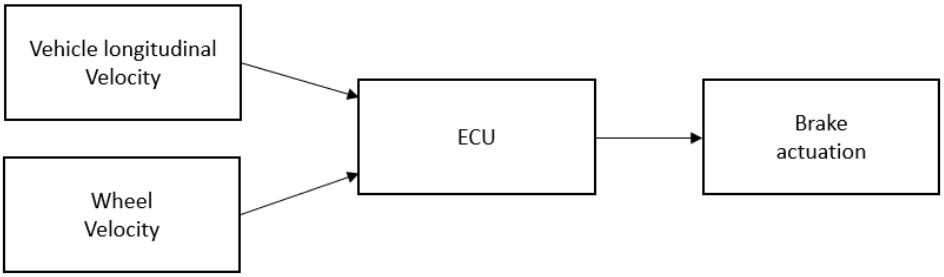

Figure 3-6 – Flow chart of a typical antilock braking system.

Typical ABS components include: vehicle's physical brakes, wheel speed sensors (up to 4), an electronic control unit (ECU), brake master cylinder, a hydraulic modulator unit with pump and valves. Some of the advanced ABS systems include accelerometers to determine the deceleration of the vehicle.

As shown in Figure 3-7, the ABS system consists of a conventional hydraulic brake system plus antilock component. It includes a vacuum booster, master cylinder, front disc brakes, rear drum brakes, interconnecting hydraulic brake pipes and hoses, brake fluid level sensor and the brake indicator. The ABS components include a hydraulic unit, an electronic brake control module (EBCM), two system fuses, four-wheel speed sensors (one at each wheel), interconnecting wiring, the ABS indicator, and the rear drum brake.

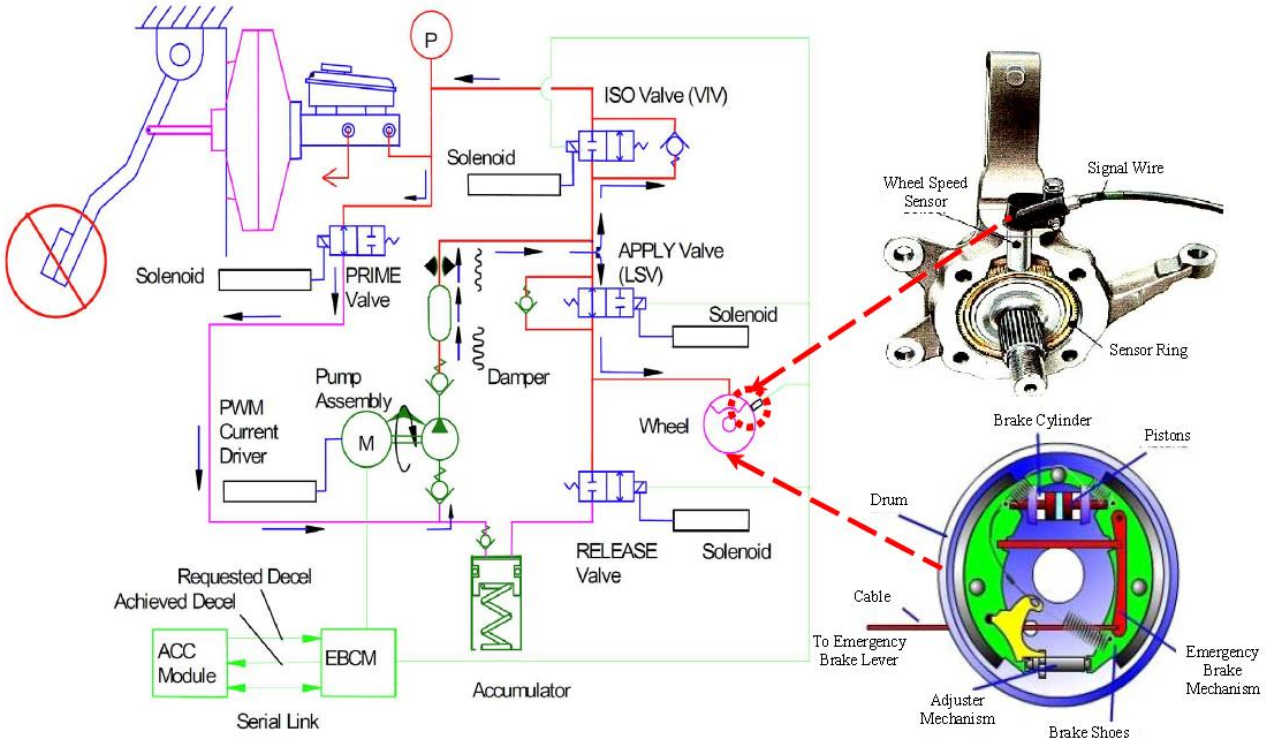

Figure 3-7 - Conventional scheme of the ABS components [5].

Most ABS systems employ hydraulic valve control to regulate the brake pressure during the anti-lock operation. Brake pressure is increased, decreased or held. The amount of time required to open, close or hold the hydraulic valve is the key point affecting the brake efficiency and steering controllability.

As also described by Sivaramakrushnan et al. [7], ABS algorithms regulate the brake pressure following a set of rules that are based on wheel slip and/or wheel deceleration thresholds. Most commercial ABS systems

are designed to use wheel deceleration/acceleration thresholds to decide the pressure state. The system used in their study is based on the Bosch HVE Version 1 ABS algorithm [19], which was comparable to a commercial ABS system. Sivaramakrushnan et al. also define that a future work will focus on exploring how to provide information to the ABS controller to adapt its thresholds and maximize the management of tire performance to reduce stopping distance.

3.2.2 Procedures for ABS braking assessment

There are several test procedures described by the Society of Automotive Engineers [9] to evaluate the performance of the ABS, namely:

- straight line braking on high and low friction surfaces;
- stability and controllability in response to steering inputs;
- braking in a turn;
- μ-split braking test.

The utilization of the available friction force is a fundamental aspect of any brake system design. The yaw velocity (or yaw rate) response to steering may be used as a measure of both stability and steerability.

For the case of braking in a turn, lateral load transfer occurs from the inside to the outside wheels. The ABS algorithm's control of the longitudinal slip on the inside and outside wheels at similar slip values usually results in a rigid body motion that increases the radius of the turn.

In the split friction test, the emergency stop manoeuvres will exceed the friction available on the low coefficient side, once again resulting in imbalanced longitudinal forces. The resulting rigid body moment will tend to steer the vehicle to the higher coefficient surface.

4. The pneumatic tire for passenger cars

The tire is the contact element of the vehicle with the road. It has the task of transferring to the vehicle forces deriving from its interaction with the ground and to absorb part of the road asperities. It is presented as an elastic toroidal open to the lower surface, mounted on a rigid axial symmetric element called rim, which constitutes its connection with the vehicle and with which it realizes the complex of the wheel (Figure 4-1).

Figure 4-1- Tire mounted on rim.

Once mounted on the rim, the tire is inflated with air at a certain pressure. The wheel is fixed to an element of the vehicle called the hub (also axial symmetrical), by means of a bolted joint. The wheel-hub set is therefore constrained to the rest of the vehicle by means of supports, generally roller bearings, which guarantee the free rotation around the axis of symmetry and allow the required exchange of forces.

The tire can absorb small obstacles and the irregularities of the road, in order to improve the comfort of the passengers, the integrity of the vehicle in time and the continuity of the contact to the ground. The deformability is also necessary to create a contact zone with the road of sufficiently high dimensions such as to generate the desired grip with the road. The outer surface of the tire in contact with the ground is called “tread”. The portion of the tread instantly in contact with the road is commonly referred to as “contact area” or “ground footprint”. Another feature that is required is the resistance necessary not only to sustain the mass of the vehicle, but also to withstand adequately the high forces of inertia that are generated on the vehicle during the motion. It must also be able to absorb the least amount of energy possible during its motion and therefore present the slightest resistance to rolling, in view of the maximum mechanical efficiency of the vehicle, in order to optimize the usage with the minimum environmental impact.

4.1 Tire characteristics

In this paragraph, a general overview of the tire is shown. The tire has a composite structure that consists of a carrier that is the carcass formed by flexible reinforcing fibres, that are extensionally resistant and

immersed in a deformable rubber matrix that is in contact with the ground (Figure 4-2). The carcass has the function of resisting the stresses caused by the inflation pressure, the applied load and the forces transmitted between the tire and the ground, whether vertical, lateral or longitudinal, contributing to the comfort and to the uniformity of rolling.

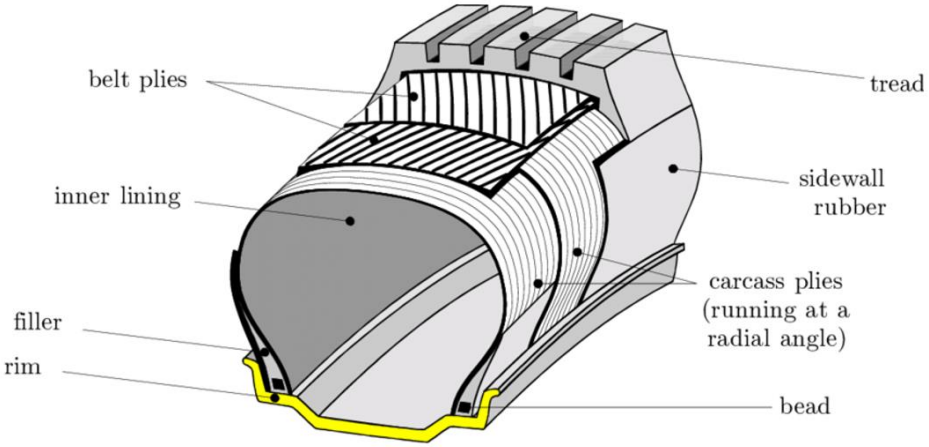

Figure 4-2 - Pneumatic tire structure.

The rubber forming the matrix is a mixture of synthetic rubbers of different quality and other components (additives), this mixture is called compound. It is made up of elastomers that combine with reinforcing additives and sulphur necessary for the vulcanization process. Elastomers are made up of long polymer chains that in a state of thermodynamic equilibrium are enveloping themselves like wool balls, tangled together. If a mechanical stress is applied, the molecules tend to unravel. When the stress is removed, the molecules will relax again in the braided state. While a normal solid state of equilibrium corresponds to the minimum potential energy, for elastomers the equilibrium is reached when the entropy reaches its maximum. Reinforcing additives help the tires to resist wear better and to make them more rigid, without them the tires could only cover a few hundred kilometres. The reinforcement filler generally used is carbon black or silica.

The sulphur used to carry out the vulcanization, by bridging between several chains, allows the polymerization of the polymer, allowing the formation of a chemically stable macromolecule, very resistant, endowed with great capacity of elastic deformation (no plasticity). The vulcanised rubber preserves the described properties even at high temperatures, whereas, instead, the unvulcanised natural rubber shows an increasingly higher plasticity. For this reason, the tires obtained by vulcanization are thermosetting. Obviously, the curing should not be pushed excessively, in order to avoid excessive rigidity of the final product.

The main components of the tires are described as follow:

- the tread, the portion in contact with the road; In the case of passenger vehicle tires, it is furrowed in various ways by circumferential and transverse grooves: these canals, deep several millimetres, provide for the drainage of the water which may be present on the road and they promote cooling by convection. In special cases, they can be made in order to promote the advancement on the snow, on the mud, the ground, the sand and incoherent grounds. The set of these channels constitutes the carving of the tread and splits the same into dowels.
- the shoulders, side border areas of the tread, which confer further resistance and rigidity towards cutting efforts;
- the beads, i.e. the two edges of the tire intended to lean on the rim, characterised by a support base and a point;

- the sidewall, lateral zone of the tire, bounded by the shoulder on the top and by the bead on the bottom, accompanied by the centring threads that identify the surface of the support on the balconies of the rim;
- the inner lining, that is a thin layer of special waterproof compound that covers the inner part of the tire.

Concerning the carcass, the reinforcement wires are arranged in several unidirectional groups with single-row development and are separated from the wires of the adjacent ones by thin layers of rubber to avoid mutual rubbing and premature wear. The materials which make up the tire must meet specific requirements. In passenger tires, the reinforcement is made up of steel wires and fibres of rayon and nylon. The reinforcement structure, thus constituted, is completed by two steel rope rings each drowned in one of the two beads. The circling rings are two additional reinforcement elements, the canvases surround each other, transmitting to these the important tensile forces from which they are stressed during the use.

4.2 Viscoelastic behaviour of the rubber

Like almost all polymer matrix composites, the constituent compound of the tires shows a viscoelastic behaviour. In addition to elasticity, it is characterised by an intrinsic viscosity which is highly dependent on temperature. These materials deviate to some extent from Hooke's law and exhibit behaviour that has elastic and, at the same time, viscous characteristics, presenting a relationship between efforts and time-dependent deformation. Creep and relaxation are among the phenomena that highlight the viscoelastic behaviour of materials.

Creep consists of the gradual increase of deformation under the action of a constant applied load. If we suppose to apply the load history using a step function ($H\ (t)$), the deformation will undergo a seemingly instantaneous increase and grow with time (Figure 4-3, a case), up to t_1.

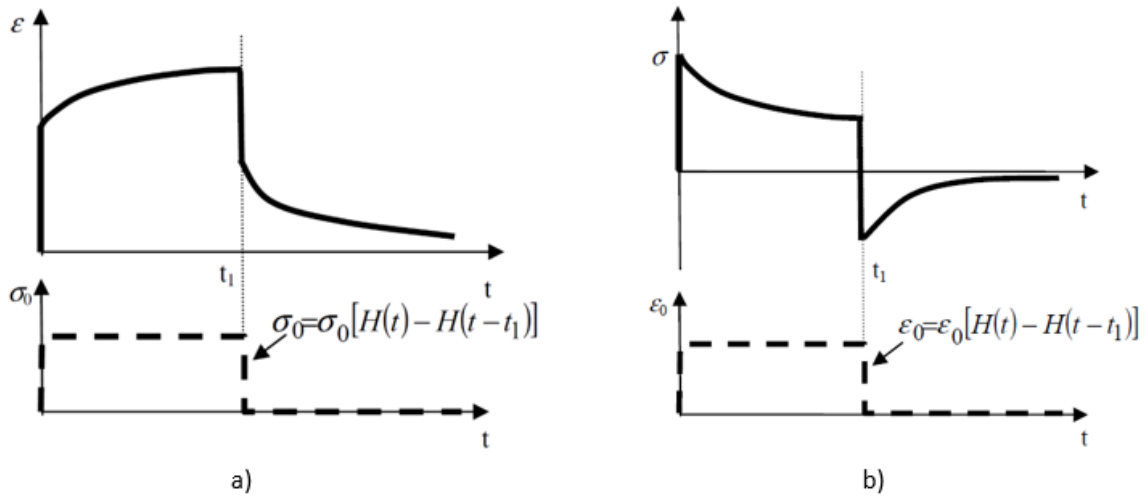

Figure 4-3 – Creep (a) and relaxation (b) phenomena [44].

It is possible to define a displacement modulus at creep J, variable over time:

$$J(t) = \frac{\varepsilon(t)}{\sigma_0} \tag{4.1}$$

from the ratio between the deformation obtained and the applied load level. The relaxation is the dual phenomenon of creep and consists in the gradual decrease of the load when a constant deformation is applied to the material. The stress pattern in the material to the instantaneous application of the deformation entails a seemingly instantaneous response, followed by a progressive reduction of the load. This trend is represented in the first part of the graphs in Figure 4-3, case "b".

The relaxation module is defined based on the response to a step deformation:

$$\Gamma(t) = \frac{\sigma(t)}{\varepsilon_0} \tag{4.2}$$

where the ε_0 is the deformation as step input. Another class of phenomena characterizing the viscoelastic behaviour is the response to the application of a deformation (or load) with cyclical pattern, as represented in the equation (4.3):

$$\varepsilon(t) = \varepsilon_0 \, sin(2\pi f t) = \varepsilon_0 sin(2\pi \frac{t}{T_p}) \tag{4.3}$$

where f is the frequency and T_p the oscillation period. As shown in Figure 4-4, in an elastic material the deformation-induced load is in-phase with the applied sinusoidal deformation.

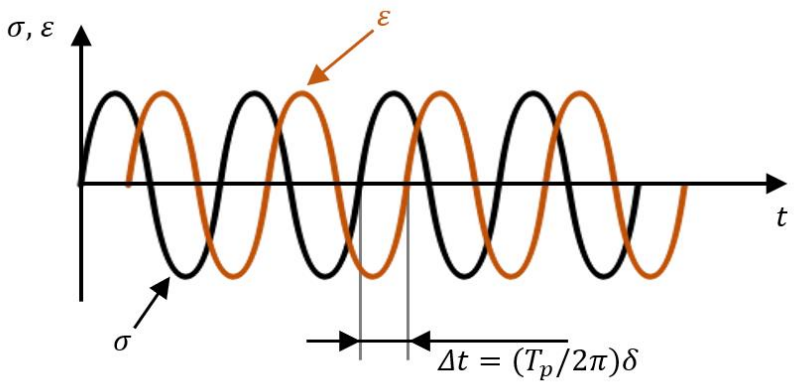

Figure 4-4 - Phase due to a sinusoidal load.

The response in deformation is then expressed as:

$$\sigma(t) = \sigma_0 \, sin(2\pi f t + \delta) \tag{4.4}$$

where δ is the phase angle representing the lag between the deformation as input and the load response. Depending on how the material responds to the stress, different values of the phase shift angle can be generated (Figure 4-5): when the material is a viscoelastic system as is generally with polymers δ is variable between 0° and 90°.

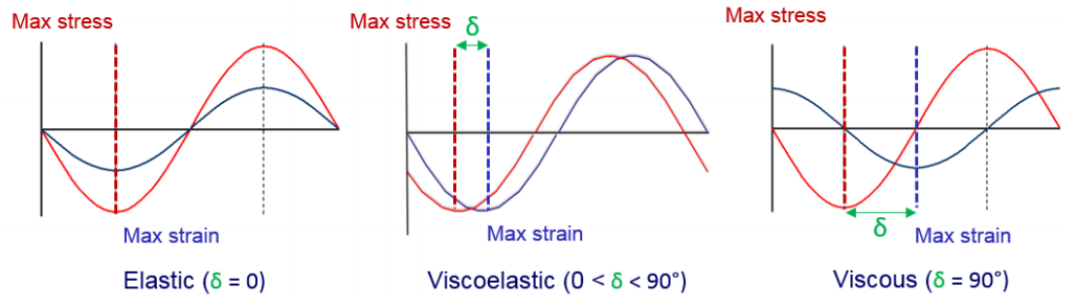

Figure 4-5 - Stress and strain cyclical deformations: elastic, viscous and viscoelastic materials [45].

Developing the equation (4.4) with the usual trigonometric relationships, it is possible to get the following relation:

$$\sigma(t) = \sigma_0 \, sin(2\pi f t)\cos(\delta) + \sigma_0 \, cos(2\pi f t)\sin(\delta) \tag{4.5}$$

which shows that the agent stress is the sum of two contributions, the first is in phase with the deformation and the second in quadrature. The two types of response of the viscoelastic material, the one typical of the elastic solid and the one of the viscous fluids. It is possible to write the equation (4.5) as follow:

$$\sigma(t) = \varepsilon_0 E' \, sin(2\pi f t) + \varepsilon_0 E'' cos(2\pi f t) \tag{4.6}$$

where, the E' describes the ability of the rubber to reversibly store elastic energy and is named "Storage modulus" or conservative module, while the E'' describes, instead, the ability of the sample to dissipate energy in the form of heat through viscous creep. Since this energy is not recoverable, it takes the name of "Loss modulus" or dissipative module. Both the two modules are defined by:

$$E' = \frac{\sigma_0}{\varepsilon_0}\cos(\delta) \quad E'' = \frac{\sigma_0}{\varepsilon_0}\sin(\delta) \tag{4.7}$$

as function of the phase angle. Finally, it is possible to define a further important parameter, the so-called “Loss tangent”, equal to the ratio between the "Loss modulus" and the "Storage modulus":

$$\tan(\delta) = \frac{E''}{E'} \tag{4.8}$$

and its value is a measure of the relationship between energy dissipated in the form of heat and the potential energy stored during a complete stress cycle. For this reason, it is known as a dissipation factor. Representing in complex notation the deformation and the effort with the expressions:

$$\begin{aligned} \varepsilon(t) &= Im(\varepsilon_0 e^{i\Omega t}) \\ \sigma(t) &= Im(\sigma_0 e^{i(\Omega t+\delta)}) \end{aligned} \tag{4.9}$$

with which the complex module E^*. It can commonly be defined as:

$$E^* = \frac{\sigma}{\varepsilon} = \frac{\sigma_0}{\varepsilon_0} e^{i\delta} = \frac{\sigma_0}{\varepsilon_0}[\cos(\delta) + isin(\delta)] = E' + iE'' \tag{4.10}$$

and its representation is given as an example in Figure 4-6.

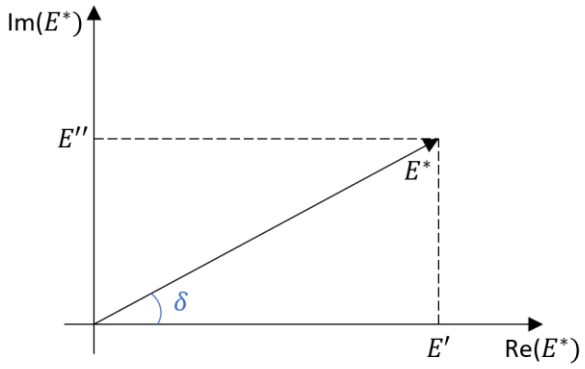

Figure 4-6 - Complex modulus representation.

4.2.1 Hysteresis

The introduction of the complex module, which has been shown to be intrinsically linked to the phenomena of the relaxation and creep, allows to identify the form of the response to a generic sinusoidal force application. In fact, it can be assumed the following relation:

$$\varepsilon = \varepsilon_{max}\sin(\Omega t) \tag{4.11}$$

as time-history for deformation. While, the result in terms of effort is shown by:

$$\sigma = Dsin(\Omega t + \delta) = |E^*|\sin(\Omega t + \delta) \tag{4.12}$$

due to the sinusoidal deformation as input. The equations (4.11) and (4.12) can be interpreted as parameter equations and an ellipse as shown in Figure 4-7.

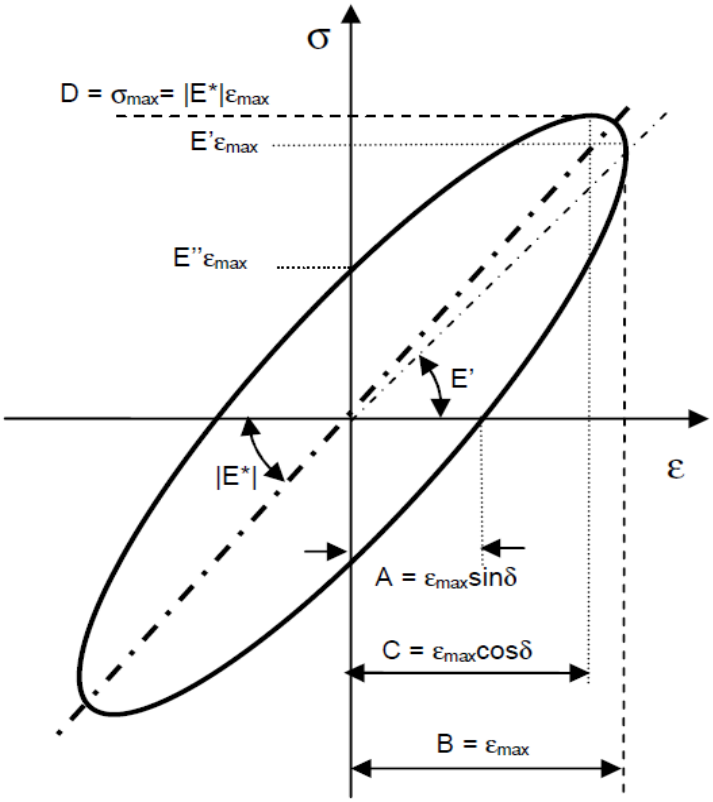

Figure 4-7 - Stress-deformation relationship [44].

The ellipse defines a loop that is called hysteresis cycle. The cycle has an elliptical shape for linear viscoelastic materials, but it appears in some cases sharper and this aspect is a clear sign of nonlinear viscoelastic behaviour. The area enclosed by the hysteresis cycle represents the work dissipated during a cycle. The ellipse intercepts with axes identify important properties of the viscoelastic material. In particular it is possible to demonstrate that the intercept with the deformation axis is obtained for the value $A = \varepsilon_{max} sin(\delta)$ that the abscissa corresponding to the point of maximum effort is equal to:

$$C = \varepsilon_{max} \cos(\delta)$$
$$\tan(\delta) = A/C \tag{4.13}$$

where, for geometric reasons, the larger the A/C ratio the wider the area enclosed by the elliptical figure, which in turn represents the dissipated energy during a cycle. Therefore, the δ value is directly related to the dissipative effects. It is possible to observe how the slope of the line drawn from the origin to the point of the cycle corresponding to the attainment of the maximum deformation provides immediately the module in phase.

4.2.2 Temperature-frequency effects on complex modulus

Factors that greatly influence the values of the complex module and (as a result) the $tan(\delta)$, are the temperature and frequency of application of the load. As far as temperature is concerned it is possible to identify three zones which correspond to three different behaviours of the material (Figure 4-8, a).

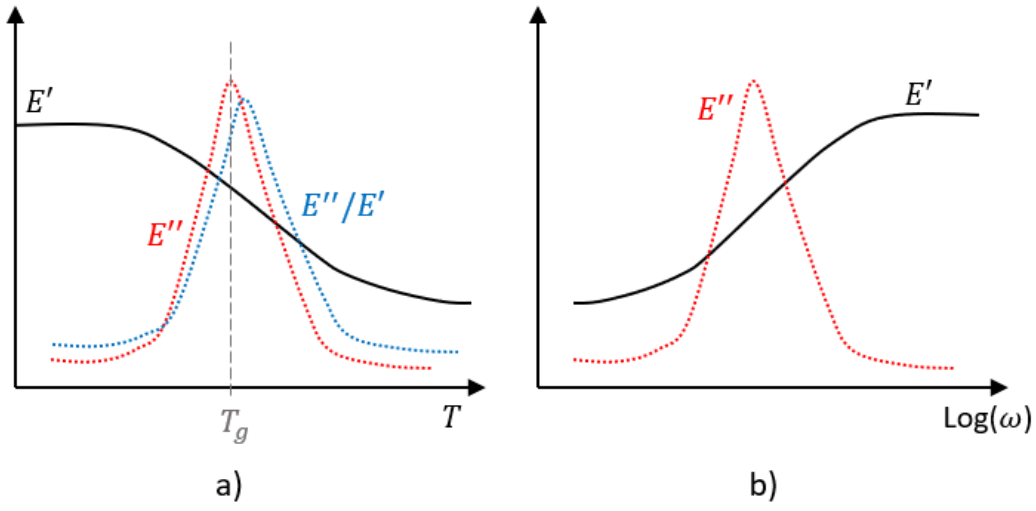

Figure 4-8 - E', E'' and tan(δ) across the temperature (a) and the excitation frequency (b).

In the first zone, for temperatures below the glass transition temperature T_g, the module is independent on temperature and the material is vitreous and elastic: in fact, it is evident that the "Storage modulus" assumes very high values while the "Loss modulus "relatively low values, therefore the area is not very dissipative.

There are maximum values of the "loss modulus" and $tan(\delta)$ at the glass transition temperature, while the "storage modulus" tends to decrease. This region, therefore, is extremely dissipative by presenting the maximum hysteretic grip (see Paragraph 4.4).

In the last zone, the material shows a decreasing of the modules, with the reaching of the minimum values of the three different parameters: this gives a little dissipative rubbery behaviour to the material. Even when the temperature is constant, the complex module varies when the frequency is changes (see Figure 4-8, b).

At very low frequency excitations the polymeric chains tend to align themselves, the process takes place in a quasi-static way because they have all the time to vary their disposition, dissipating little energy. At very high frequency, the chains between two successive states of equilibrium do not have time to lengthen and the excitation shifts from the chains to the intermolecular links, which are much more rigid and less dissipative, so E' reaches very high values while E'' tends to zero.

By exciting, instead, the material with pulsations close to those ones close to the "relaxation time", τ_f., i.e. the average time that a polymer chain takes to disturb an existing equilibrium and watch it decay back to equilibrium. In this case, the loss modulus E'' reaches its maximum values making the material extremely dissipative: in general, the peak in the loss modulus is a direct consequence of the structural relaxation process and its dependence on strain rate. As the temperature increases, τ_f decreases: this means that the pulsation for which E'' reaches its maximum (maximum dissipation zone and maximum grip), is higher. When the temperature decreases, $\tau_f$increases and the maximum grip area moves towards lower pulsations. The behaviour in the three zones can be summarised as follows:

- "Rubber region": a rubbery and little dissipative area (high temperatures or low frequencies)
- "Glass region": hard and not very dissipative zone (low temperatures or high frequencies);
- "Transition Region": intermediate zone where the maximum dissipation (temperature next to T_g, frequency of at τ_f) is maximal.

If we try to consider tires that have the region of maximum dissipation at a temperature T_2 (summer), around Ω_0, by mounting them during the winter when the temperature T_1 is lower than T_2, it will work at the pulsation Ω_0 (linked to the speed of slipping and the road) and the rubber will be located in the glassy area with a lower dissipation (low grip). The complex module is a function of Ω and the absolute temperature T. When the frequency and temperature vary, with an appropriate shift operation it is possible to combine the effect of frequency and temperature in a single variable called “reduced frequency”.

The rubber friction is dominated by the viscoelastic properties of the rubber. Williams, Landel and Ferry demonstrated the correlation between the effects of temperature and speed. equivalence for viscoelastic properties could be described by the universal function “WLF transformation equation” [46].

Generally, the transformation is carried out by measuring the friction coefficient over a logarithmic speed range, with the highest speed low enough to make the temperature increases in the contact zone negligible. The experiments are then repeated for a range of temperatures. If the data are plotted as function of log speed the curves for different temperatures are seen to be segments of a single, so called “master curve”. This curve is obtained by horizontal displacements (shift factors) to the curve for a convenient reference temperature: stable friction values are obtained if the slope of the curve of friction coefficient vs. $log\ a_T v$ (where $log\ a_T$ is the shift factor) is positive. Once it turns negative, stick-slip sets in.

4.3 Mathematical models to describe the viscoelastic behaviour

To represent the behaviour of a viscoelastic material it is necessary to use models that consist of combinations of springs and dampers.

4.3.1 Kelvin-Voigt model

This model represents the behaviour of a viscoelastic material, such that its elastic response to an applied stress is totally recoverable, but delayed: the deformation is not produced instantaneously, but progressively over time. The elastic response of the material manifests itself with a delay due to the viscous friction present inside the material itself. The model consists (Figure 4-9) of a spring and a damper connected in parallel: under the application of a load the elastic spring response is delayed by the dissipative element. If the stress is removed after a certain time, the deformation reached at that time is totally recoverable, but in an infinite time.

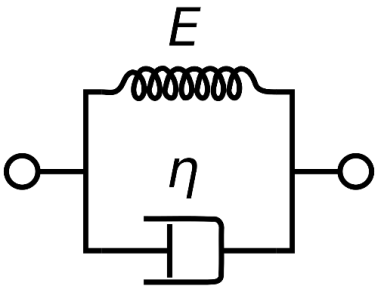

Figure 4-9 - Kelvin-Voigt model.

In order to find the stress-strain relation, we observe that the same deformation affects both the spring and the damper while the stress is the sum of:

$$\sigma = \sigma_E + \sigma_\eta \tag{4.14}$$

where that due to the spring, σ_E and the one due to the damper σ_η. Starting from the equation (4.14):

$$\sigma = E \cdot \varepsilon + \mu \frac{d\varepsilon}{dt} \tag{4.15}$$

which represents the constitutive equation of the Kelvin-Voigt model. This model works properly at low frequencies, where only the spring intervenes and has little influence on the damper. Conversely, at high frequencies, the damper becomes very rigid, completely dissipating the energy supplied from the outside.

4.3.2 Maxwell model

The Maxwell model involves the use of a series-connected spring and damper (Figure 4-10). By applying a constant force, this determines an effort to which both elastic and viscous elements are subjected. The total deformation is instead given by the sum of the elastic deformation and the viscous deformation.

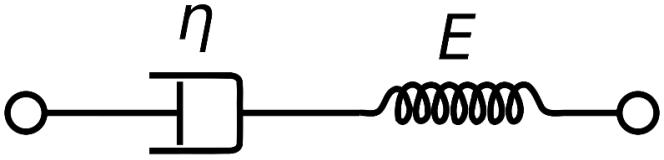

Figure 4-10 - Maxwell model.

With a constant effort applied one has an instantaneous elastic deformation, followed by an increasing deformation linearly in time; By removing the load at a certain moment, it recovers instantaneously and

integrally only the elastic deformation, while the viscose one is not recoverable (Figure 4-13). The following equation (4.16):

$$\varepsilon = \varepsilon_E + \varepsilon_\eta \tag{4.16}$$

to find the binding strains-deformation it is observed, while the deformation is the sum of ε_E and ε_η due to respectively the stiffness and the damping effects.

4.4 Tire road interaction and rubber friction: Adhesive, Hysteretic and Abrasive components

Tire traction describes the force transmitted between tire and road under several circumstances. It is a prerequisite for controlled steering, acceleration and braking of self-propelled vehicles. Normally, the frictional force changes at the different sliding conditions (from the free rolling to the full sliding) [13]. Therefore, two aspects must be considered:

- The mechanics of force transmission of elastic wheels under limited slip;
- Rubber friction.

Rubber friction differs from friction between hard solids because the first one depends on the load and strongly on speed and temperature, while in hard solids it is virtually independent of these parameters. Although the effect of load is more important for soft rubbers on smooth surfaces, while it is not so important for tire compounds on roads which are always sufficiently rough and the effect of the load dependence is smaller [47]. The experiments conducted by Coulomb referred to only metallic surfaces. Later, Bowden and Tabor [48] conducted numerous researches on the subject, directing their attention to the behaviour of the tires, for which the laws formulated by Coulomb were not valid. The phenomena related to grip for polymeric materials differ in fact from those mentioned for metals, mainly because of the strong dependence on load, temperature and relative speed.

An effective generalized friction model was formulated by Kummer (Figure 4-11) as part of an analysis and test program on the interaction between tires and road. This model took into account, for the first time, resistant forces generated by three components: adhesion, deformative hysteresis and wear.

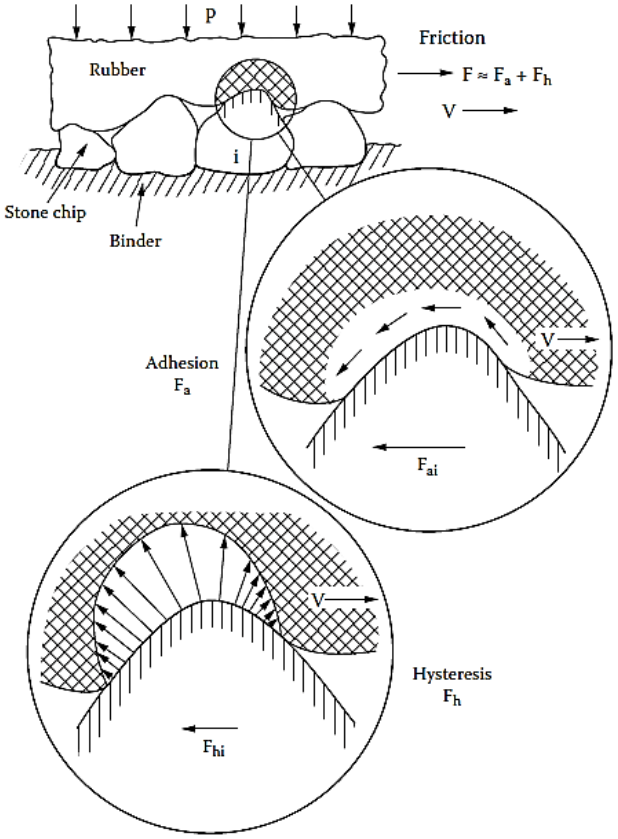

Figure 4-11 - Phenomenon of rubber friction on the asphalt [49].

Kummer [50] considered the forces that are generated between a single road element and a tire. The grip with the road asperity is responsible for the actual surface of contact and the total force is sum of the three contributions:

$$F_{tot} = F_{ad} + F_{hys} + F_w \tag{4.17}$$

where F_{tot} is the total friction resistance generated between a tire in contact with a dry road surface. It is the sum of different contributions:

- F_{ad} is the contribution of the adhesion force;
- F_{hys} is the contribution attributed to the loss of energy by deformation due to the hysteresis of the rubber;
- F_w is the loss of cohesion due to wear and tear.

Kummer posited that F_{ad} and F_{hys} are not independent because the adhesion is able to increase the extent of the contact area and hence the area in which hysteretic deformations occur. Each of these forces varies depending on the type of materials (polymers and additives of the tires, materials constituting the road surface), the conformation of the surfaces in contact (surface state of the tire, roughness of the Road), of the local micro-slip speeds, temperature and normal load.

There are basically two mechanisms related to molecular adhesion, which can generate friction forces between rubber and rigid rough surfaces. As first effect, the value of the current contact area can be considered: rubber generally has a rather low modulus of elasticity, so the forces of adhesion can deform the material and force it to follow the profile of the surface on which it is supported. An influence on the value of the contact area can also influence the value of the friction coefficient. In the case of friction between tire and road paving can be considered an irrelevant phenomenon, with good approximation. This

is mainly due to the fact that the materials commonly used for the realization of the tread have an elastic modulus of about 10-15 MPa, a fairly high value in the field of elastomers.

The second effect considers an area in which the rubber and the surface are in contact. Between the molecules of the two bodies some interactions are made; typically, the Van der Waals forces are established, namely adhesion at the molecular level.

The adhesive friction is generated by the formation of molecular bonds (due to the lower hardness of the tread compared to road paving) between the two surfaces (the polymer chains on the tread surface are approaching the micro-roughness of the asphalt) that, during the interaction, lengthen up to a distance much higher than the one considered for the asperities generating the friction force for adhesion. When the internal tension of the bonds exceeds the maximum value tolerable by the same one, there is the rupture: the molecular chain will undergo a dissipative process of the accumulated energy (that can be assumed equal to the one in case of a loaded spring to which the load is suddenly removed) and then reattach itself again to the substrate. The process is called "Stick & Slip" and it is often referred to as one of the major makers of the noise that is generated when the tires are rolling on the road. It is possible to schematize the molecular chain of the rubber as a sort of spring and its elongation involves an elastic force that opposes the motion (see Figure 4-12).

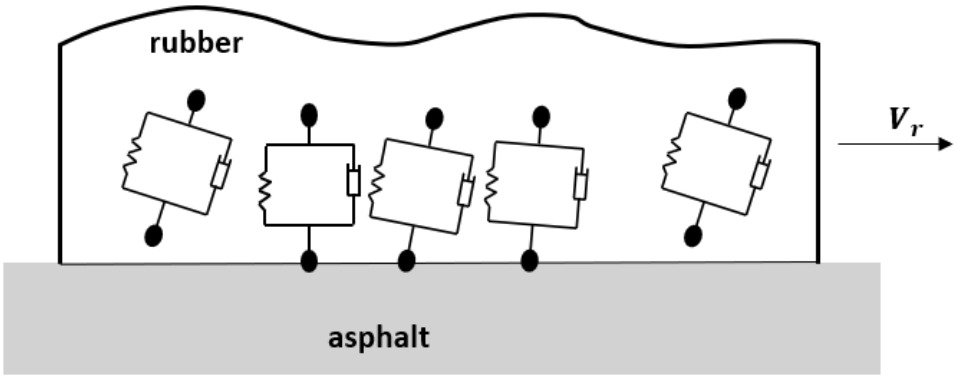

Figure 4-12 - "Stick & slip" mechanism for the adhesive friction generation.

The force given by the single bond is very weak, however the resultant of the set of these actions is not negligible and may represent even more than the 50% of the total friction force.

It defines the friction coefficient for adhesion, the relationship between the adhesion force (F_{ad}) and the normal load acting on the sample. It is experienced that it varies with the sliding speed and temperature.

The essential condition for the development of molecular adhesion is that the rubber is in direct contact with the road surface. In this case, the adhesion mechanism can be optimal and the two surfaces must be free of contaminants at the contact points (in particular, it is thought that the limit distance is of the order of μm), otherwise van der Waals bonds cannot be formed (for example, in case of wet or dirty surface) and molecular adhesion is not able to give any contribution. The value of the friction force generated by this process is the function of the actual contact area, which, is dependent on the elastic properties of the material, the normal force and the surface roughness. In fact, the contact area can be considered independent of the sliding speed and the same can be confirmed for F_{ad}.

The contribution of the adhesion is more important for flooring that can be defined as “smooth”, with a bigger contact area than the one it is possible to obtain on a road paving with high roughness. Therefore, since the Van der Waals interactions are strongly dependent on the actual contact area, in the case of smooth surfaces their contribution will be very relevant. The opposite can be said for the contribution of the hysteresis; In the ideal boundary situation of perfectly smooth surface, it would be in fact null.

Assuming that the road profile is described by an harmonics shape having wavelength λ and amplitude h (and that it is the same for all planes parallel to that) and resting on a road surface a rubber block with a perfectly smooth surface and the vertical force acting on that element. It is also assumed for the moment that the rubber can perfectly follow the profile. When the rubber block slides on the surface, due to the roughness of the latter, it is subjected to harmonic forces having a pulsation equal to:

$$\varepsilon_{rp} = V_r \omega_{rp} \tag{4.18}$$

where V_r is the relative sliding speed while ω_{rp} represents the spatial pulsation of the road profile. The following equation:

$$\omega_{rp} = 2\pi/\lambda \tag{4.19}$$

is giving the latter parameter. Therefore, the rubber is subject to cyclic deformations with also dissipation of energy, due to the internal friction. It is possible to analyse what happens when the rubber crawls on the single roughness: using the simple model of spring and damper in parallel to represent its point in contact with the surface, it is that this undergoes a compression-release cycle. Due to the presence of the damper, this entails a loss of energy. Furthermore, the deformation of the rubber on the roughness is asymmetric (Figure 4-13). This asymmetry generates a force field having a non-zero result according to the direction parallel to the motion, which generates the frictional force [51][52][53].

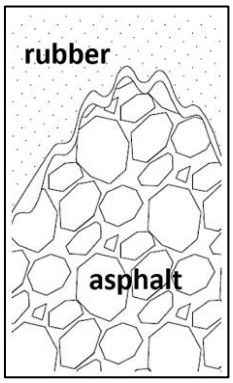

Figure 4-13 - Surface as sum of 2 sinusoidal lines, the rubber cannot fill all the cavities.

However, for convenience it can be considered a surface as the sum of two sinusoids of different wavelength and for which the ratio between the amplitude and the wavelength is the same (Figure 4-13).

When the rubber is pressed against the surface with enough pressure to follow the largest asperities, the interface pressure at the bottom of a valley is much lower than at the top of a peak. Therefore, thanks to the high local pressure the rubber can fill the small roughness that occurs in the high parts of the large roughness. However, downstream the pressure may not be enough to force the material into contact with the valleys of the smallest bumps. This means that the harmonics with a small wavelength can only partially contribute to the oscillating deformation of the rubber. The fundamental problem is to be able to evaluate the effective contact area; it is clear, in fact, that where a direct contact is not taking place, asperities cannot impose any displacement and therefore cannot cause any loss of energy.

The hysteretic component can be described by saying that when the rubber crawls on a rough surface it undergoes an oscillating stress and not all the deformation energy accumulated in the loading phase is returned in the unloading phase. Part of this energy is dissipated as heat due to the internal damping of the material, and therefore this phenomenon, as well as the complex module E^*, will depend on the temperature and the stress frequency, as already explained in the Paragraph 4.2.2.

The abrasion forces are instead detectable by observing that some solid surfaces can remove particles of material from the rubber during the motion. Generally, these particles do not remain attached to the moving surface and this phenomenon can intervene on contaminated surfaces for which the coefficient of friction from adhesion is very low. Therefore, the resistance to motion is due only to the break due to mechanical cutting action due to the roughness. The ratio between the abrasion force and the normal load is defined as coefficient of friction due to abrasion.

When the value of the friction coefficient from adhesion is high, the removal of material derives from the high strain tensions during the sliding, with consequent fracture of the material. In this case, it must be considered that there is also an adhesive component in the force that contrasts the motion. The same mechanism of abrasion wear is associated with this kind of friction.

Since the three described friction mechanisms always intervene simultaneously, it was considered necessary to introduce a new classification of tire wear, adopting the definitions of:

- cohesive wear, determined by the energy required for breaking the material (alternatively defined toughness),
- interface wear defined for high levels of energy dissipated by friction in very thin layers of material and characterized by high temperature increases.

Based on these new definitions, abrasive and fatigue wear must be considered cohesive wear phenomena, while adhesive wear (due to cyclic regeneration of the intermolecular bonds) must be considered a phenomenon of interface wear.

4.5 Introduction to Forces and Moments of the tire

Tire forces and moments are complex nonlinear functions of the tire usage variables that are established by driver inputs and vehicle responses. On a laboratory test machine or an over-the-road testing device, the test conditions are established by the need to explore the expected range of usage. To allow communication, modelling, and use of the resultant data, a formal language has been developed for describing inputs to the tire and the force and moment responses developed by the tire [13].

Both the SAE tire Axis System and the ISO Wheel Axis System have their origins at the road since the source of tire forces and moments is at the road surface. In the following, the first mention of a term defined within a terminology document is capitalized to identify the fact that it is a universally defined term.

4.5.1 The SAE and ISO tire axis systems

The SAE and ISO tire axis systems (Figure 4-14) are right-handed, three-axis, orthogonal, cartesian coordinate system with the origin at the contact centre in the road plane. The road plane is the plane tangent to the road surface at the contact centre. The contact centre is the point in the road plane where the line defined by the intersection of the Wheel Plane (the plane halfway between the rim flanges) to road plane is cut by the projection of the Spin Axis onto the road plane.

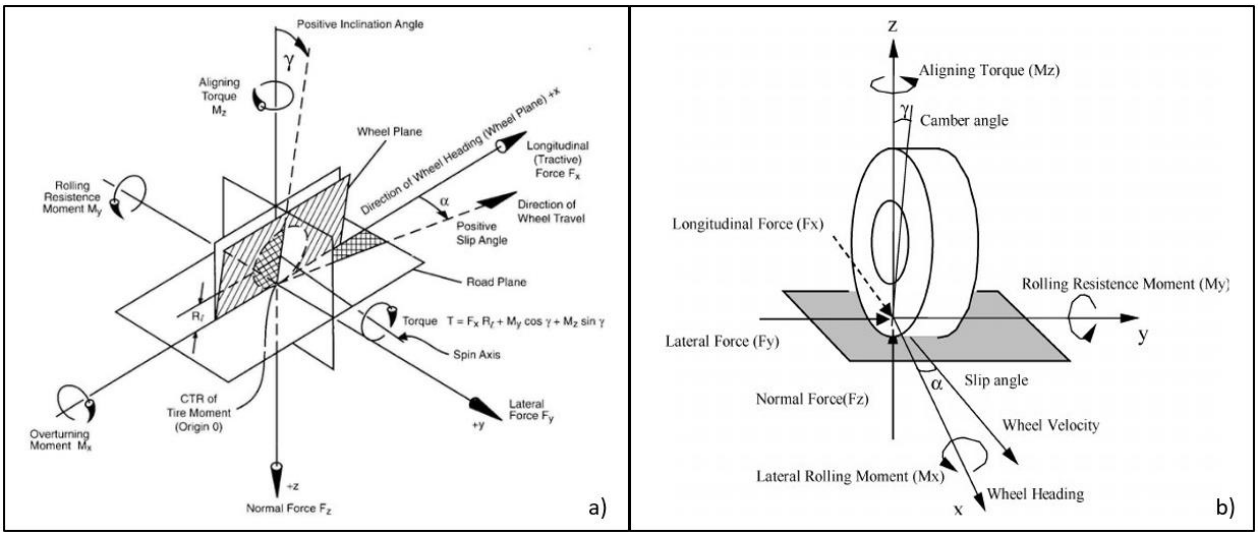

Figure 4-14 – The SAE (a) and ISO (b) reference systems [13].

Therefore, the contact centre is defined by the wheel, not the tire. It is defined in terms of the wheel because the tire is flexible and the exact location of its centre of contact at any given moment is not determinable

The SAE X-axis is along the line defined by intersection of the wheel plane with the road plane, the contact line. Positive X is in the intended rolling direction for the tire. The SAE Y-axis is along the projection of the spin axis onto the road plane. Positive Y is to the right when the system is viewed from the rear looking in the positive X-direction. The SAE Z-axis is defined by the cross product of +X into +Y. It is perpendicular to the road plane with its positive sense into the road plane [54].

The ISO Wheel Axis System is defined in ISO 8855 [54]. Some of the elements forming the wheel axis system have slightly different names and symbols than they have in the vehicle axis system. In a practical sense, the wheel axis system represents a 180° rotation of the tire axis system about the X-axis (or X-axis in ISO terms) resulting in positive Z being upward and positive Y being to the left. In the wheel axis system, a positive slip angle is associated with a right turn. Again, a positive inclination angle moves the top of the tire to the right with respect to the contact centre when viewing the tire from behind looking in the positive X direction.

4.5.2 General definitions of the tire forces and moments

Since the precise effective location at which the road applies forces to the tire is unknown, the origin of the tire axis system is arbitrarily defined by the wheel and road geometry. Three forces and three moments are normally required to define how the road interacts with the tire. Each of the three forces acts along its associated axis in the tire coordinate system. For example, F_x acts along X-axis. The positive direction for each force is the same as the positive direction for its associated axis. The three forces are defined as follows:

- Longitudinal force F_x, is the force of the road on the tire along the X-axis. It accelerates or decelerates the vehicle dependent on whether the tire is driven or braked. If F_x is positive, the tire is driven, and it is called driving force. If F_x is negative, the tire is braked and it is called braking force.
- Lateral force F_y, is the force of the road on the tire along the Y-axis. It forces the vehicle to move to the left or right when a certain slip angle or inclination angle is applied (or both at the same time).

- Normal force F_z, is the force of the road on the tire along the Z-axis. It is the contact force between the road and tire. It is negative in case of SAE sign convention.

Each of the three moments acts about its associated axis in the tire axis system. For example, M_x acts about X'. The right-hand rule is applied. The positive sense for each moment is clockwise about the positive branch of its associated axis when looking away from the tire axis system origin along the positive branch of the axis. The three moments are defined as follows:

- the Overturning moment (M_x) is the moment about the X-axis. It accounts for the effect of left-to-right displacement of the point of action of the normal force with respect to the contact centre. M_x influences camber behaviour.
- the Rolling resistance moment (M_y) is the moment about the Y-axis. It accounts for the fore-aft displacement of the point of action of normal force with respect to the contact centre.
- the Aligning moment (M_z), is the moment about the Z-axis. It accounts for the point of action of the shear forces, F_x and F_y, within the road plane.

Tire force generation depends on several variables, and inputs such as inflation pressure and driving speed. The used variables are defined in this paragraph. Tire load, which is characterized in terms of Normal Force (F_z), is the most important tire usage variable: it largely determines the tire structural deformations. The normal force is a crucial player in the generation of frictional forces and, hence, in this whole discussion.

The Loaded Radius (r_l) is the distance from the spin axis to the contact centre in the wheel plane. This is an important geometric variable in tire force and moment studies. It is dependent on normal force, inflation pressure and the tire 's structure.

Besides the already described slip ratio (κ) that is important for the longitudinal dynamics of the tire, there is also the Slip angle (α) to evaluate the lateral behaviour that is measured from the X'-axis to the direction of wheel travel, trajectory velocity, V_x, the velocity of the contact centre across the road, lies in the road plane. The slip angle α is positive clockwise around the positive branch of the Z'-axis. A positive slip angle is associated with a left turn.

The Inclination angle (γ) measures the tilt or camber of the wheel plane with respect to the Z'-axis. Inclination angle is measured from the Z'-axis to the wheel plane within the Y'Z' plane. It is positive clockwise around the positive branch of the X'-axis. The top of a tire showing a positive inclination angle is moved to the right with respect to its contact centre, as seen from the rear. The Inclination angle is positive when the top of a tire leans to the right. The Camber angle is defined as positive, if the tire is leaning outward on a vehicle. Thus, on the right side of a vehicle camber angle is equal to inclination angle, but on the left side of a vehicle camber angle is the negative of inclination angle [13].

Longitudinal force generation depends on angular velocity about the spin axis and on the relationship of the instantaneous angular velocity to the angular velocity existing when the tire is in free rolling conditions in a straight line. The moment or torque that is applied from the axle to the tire is what determines the tire angular velocity. Thus, the torque applied about the spin axis is also important in the generation of longitudinal force. Spin angular velocity, ω, is the angular velocity of the tire about the spin axis.

The Wheel Torque is the external moment applied to the tire about the spin axis. The torque causes the tire to operate in either a driven or braked state. When the wheel torque is higher than zero, it is called Driving Torque, while when it is lower than zero, it is called braking torque (T_b).

4.5.3 Braking effort and longitudinal slip

When a driving torque is applied to a pneumatic tire, a tractive force is developed at the tire – ground contact patch [13]. At the same time, the tire tread in front of and within the contact patch is subjected to compression. A corresponding shear deformation of the sidewall of the tire is also developed.

Shear deformations at the tread elements happen when they are entering the contact region, the distance (per rotation) that the tire travels when subject to a driving torque will be less than the one in free rolling conditions. This phenomenon is usually defined as longitudinal slip. When a driving torque is applied, the longitudinal slip is usually defined by:

$$\kappa_{tr} = \left(1 - \frac{V_x}{r\omega}\right) \cdot 100\% \tag{4.20}$$

where V_x is the linear speed of the tire centre, ω is the angular speed of the tire, r is the rolling radius of the free-rolling tire.

As the tractive force developed by a tire is proportional to the applied wheel torque under steady-state conditions, slip is a function of tractive effort. At first, the wheel torque and tractive force increase linearly with slip because, initially, slip is mainly due to elastic deformation of the tire tread. This corresponds to section $O - A$ of the curve shown in Figure 4-15. A further increasing of wheel torque and tractive force results in part of the tire tread sliding on the ground. Under these circumstances, the relationship between the tractive force and the slip is nonlinear. This corresponds to section $A - P$ of the curve. The maximum tractive force of a pneumatic tire on hard surfaces is usually reached somewhere between 15 and 20% of longitudinal slip.

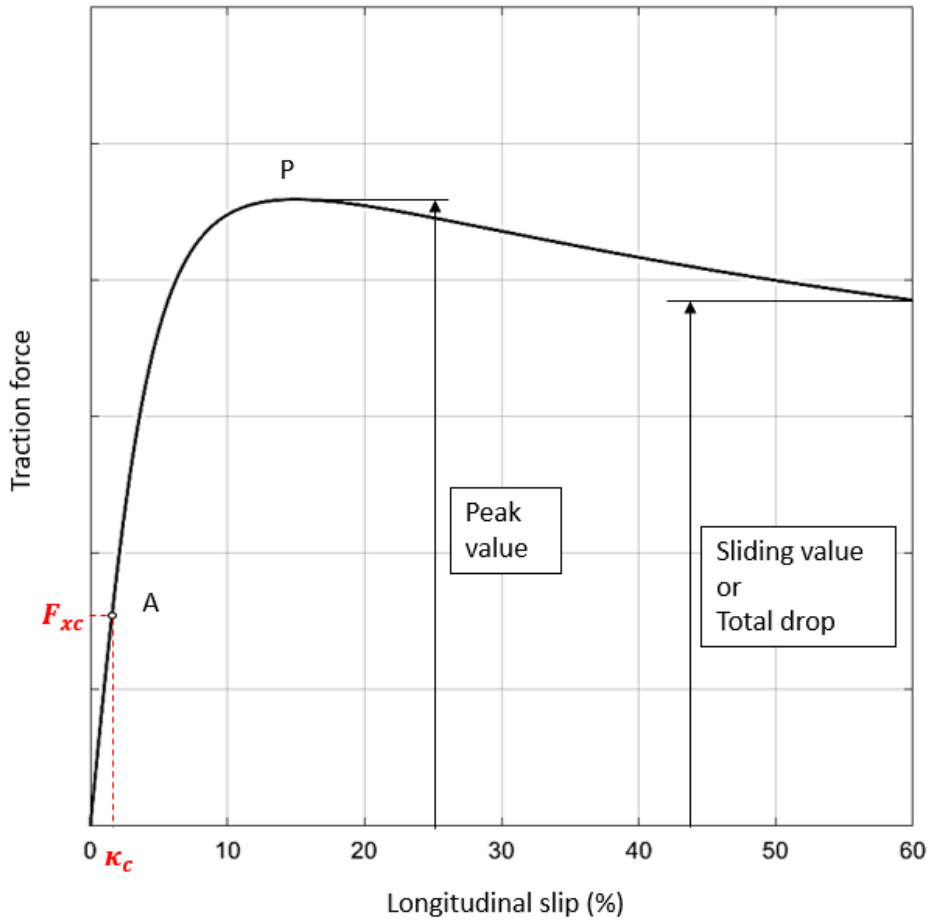

Figure 4-15 - Longitudinal characteristic of the tire.

Any further increase of slip beyond that results in an unstable condition, with the tractive effort falling rapidly from the peak value $\mu_p F_z$ to the pure sliding value $\mu_s F_z$, as shown in Figure 4-15, where F_z is the normal load on the tire and μ_p and μ_s are the peak and sliding values of the coefficient of road grip,

respectively. The unstable zone is commonly recognized as the one the ABS tries to avoid in order to guarantee the steerability of the vehicle.

In case a braking torque is applied to the tire, a stretching of the tread elements occurs when they are entering the contact area, in contrast with the compression effect for a driven tire. Therefore, the distance that the tire travels when a braking torque is applied will be higher than the one in free rolling conditions. The severity of braking is often measured by the skid of the tire, which is defined as:

$$\kappa_{br} = \left(1 - \frac{r\omega}{V_x}\right) \cdot 100\% \tag{4.21}$$

where for a locked wheel, the angular speed ω of the tire is zero, whereas the linear speed of the tire centre is not zero. Under this condition, the skid is denoted as 100%.

A simplified theory for the relationship between the braking effort and the skid can also be developed. It should be mentioned that according to the definitions of slip κ_{tr} and skid κ_{br} given by the equation (4.22), the following equation:

$$|\kappa_{tr}| = \left|\frac{\kappa_{br}}{(1 - \kappa_{br})}\right| \tag{4.22}$$

is giving the parameters for slip κ_{tr} and skid κ_{br}, respectively [13]. If no sliding takes place on the contact patch, the relationship between the braking effort and the skid can be established by replacing $K_{x,tr}$and κ_{tr} in $F_x = K_{x,tr}\kappa_{tr}$ with $K_{x,br}$ and $\kappa_{br}/(1 - \kappa_{br})$, respectively

$$F_x = K_{x,br} \left|\frac{\kappa_{br}}{(1 - \kappa_{br})}\right| \tag{4.23}$$

where F_x is the braking effort acting in the opposite direction of motion of the tire centre, and K_{br} is the slope of the braking effort – skid curve at the origin

$$K_{x,br} = \frac{\partial F_x}{\partial \kappa_{br}} \tag{4.24}$$

with $\kappa_{br} = 0$.

Using the definition of skid given by the equation (4.22), it is interesting to note from equation (4.23) the nonlinear relationship between braking effort and skid, even at low slip, where no sliding takes place between the tread and the ground.

The critical value of skid $\kappa_{br,c}$, at which sliding between the tread and the ground begins, can be established by replacing the tire longitudinal stiffness K_{tr} and the longitudinal slip κ_{tr} in the equation that defines the trailing part of the contact patch:

$$\kappa_c = \frac{\mu_p F_z}{k_t {l_t}^2} = \frac{\mu_p F_z}{2K_{x,tr}} \tag{4.25}$$

where the k_t is the tangential stiffness of the tread block and l_t is the contact length of the tire.

Assuming the longitudinal strain is a measure of the longitudinal slip κ_{tr} of the tire, it is concluded that if the whole contact patch is in adhesion region, the relationship between the tractive force F_x and the slip κ_{tr} is linear. This corresponds to the region between points O and A as shown in Figure 4-15. Therefore, coming the following equation:

$$\frac{\partial F_x}{\partial x} = k_t x\, \kappa_{tr} \rightarrow F_x = \int_0^{l_t} k_t x\, \kappa_{tr}\, dx = \left(\frac{k_t {l_t}^2}{2}\right)\kappa_{tr} = K_{x,tr}\, \kappa_{tr} \tag{4.26}$$

where x is the distance between the tractive force per unit contact length in the adhesion region and the front contact point. The term $\left(\frac{k_t {l_t}^2}{2}\right)$ may be taken as the slope K_{tr} of the braking force – slip curve at the origin, that is:

$$\frac{\partial F_x}{\partial \kappa_{br}} = k_t l_t \kappa = \frac{\mu_p F_z}{l_t} \tag{4.27}$$

The equation (4.28) allows to calculate the critical value of skid $\kappa_{br,c}$:

$$\kappa_{br,c} = \frac{\mu_p F_z}{2K_{br} + \mu_p F_z} \tag{4.28}$$

at which sliding between the tread and the ground begins, can be established by replacing K_{tr} and κ_{tr} in the equation (4.26) with K_{br} and $\kappa_{br}/(1 - \kappa_{br})$, respectively. The corresponding critical value of braking effort $F_{x,c}$ is given by:

$$F_{x,c} = \frac{K_{br}\, \kappa_{br}}{1 - \kappa_{br,c}} = \frac{\mu_p F_z}{2} \tag{4.29}$$

beyond which sliding between the tread and the ground begins. When sliding takes place in part of the contact patch (i.e., $\kappa_{br} > \kappa_{br,c}$), the relationship between the braking effort and the skid:

$$F_x = F_{x,s} + F_{x,c} = \mu_p F_z \left(1 - \frac{\mu_p F_z}{4K_{tr}\, \kappa_{tr}}\right) \tag{4.30}$$

can be established by replacing K_{tr} and κ_{tr} in the relationship between the total force and the slip when part of the tread is sliding on the ground. It is shown in the following equation:

$$F_x = \mu_p F_z \left[1 - \frac{\mu_p F_z (1 - \kappa_{br})}{4\, K_{br}\, \kappa_{br}}\right] \tag{4.31}$$

where K_{tr} and κ_{tr} are replaced with K_{br} and $\kappa_{br}/(1 - \kappa_{br})$, respectively. While the theory described above represents a simplified model for the highly complex phenomenon of tire – ground interaction, it has been proven to be useful in representing tire behaviour in the simulations of the dynamics of passenger cars. The significant difference between the peak values μ_p and the sliding value μ_s of the friction coefficient indicates the importance of avoiding wheel lock-up during braking (κ_{br} = 100%) or wheel spinning during acceleration (κ_{tr} = 100%). This is one of the impetuses to the development of antilock brake systems and traction control systems for road vehicles.

4.5.4 Performance of tires in wet conditions

Some investigations on the influence of tread pattern and speed on braking performance in wet conditions, show that there is a marked difference in the coefficient of road grip between patterned tires, including the ribbed and siped tires, and smooth tires on wet asphalt and concrete surfaces. The tread pattern increases the value of the coefficient of road grip and reduces its speed dependency. In contrast, there is little pattern effect on wet quartzite surfaces, and a high level of road adhesion is maintained over the entire

speed range. Thus, it can be concluded that the advantages of a patterned tire over a smooth tire are prominent mainly on wet surfaces [13].

Tread pattern can function satisfactorily on a wet road only when the grooves and sipes constitute a reservoir of enough capacity and its effectiveness decreases with the wear of the tread. The decline in value of the coefficient of road grip with the decrease of tread depth is more pronounced on smooth than on rough roads, as rough roads can provide better drainage.

When a pneumatic tire is braked on a wet surface, the motion of the tire creates hydrodynamic pressure in the fluid. The hydrodynamic pressure acting on the tire builds up as the square of speed of the tire and tends to separate the tire from the ground. At low speeds, the front part of the tire rides on a wedge or a film of fluid. This fluid film extends backward into the contact area as the speed of the tire increases. At certain a speed, the hydrodynamic lift developed under the tire equals the vertical load, the tire rides completely on the fluid, and all contact with the ground is lost. This phenomenon is usually referred to as hydroplaning [55]. For smooth or close-patterned tires that do not provide escape paths for water and for patterned tires on flooded surfaces with a fluid depth exceeding the groove depth in the tread, the speed at which hydroplaning occurs may be determined based on the theory of hydrodynamics. Based on the following equation:

$$F_h \propto \rho_h A {V_x}^2 \tag{4.32}$$

it can be assumed that the lift component of the hydrodynamic force F_h is proportional to the tire –ground contact area A, fluid density ρ_f, and the square of the vehicle speed V_x. Moreover, the level of energy loss from viscoelastic rubber compounds used in the tread under dynamic deformation depends not only on the viscoelastic properties of the tread compounds, but also on the mode of deformation.

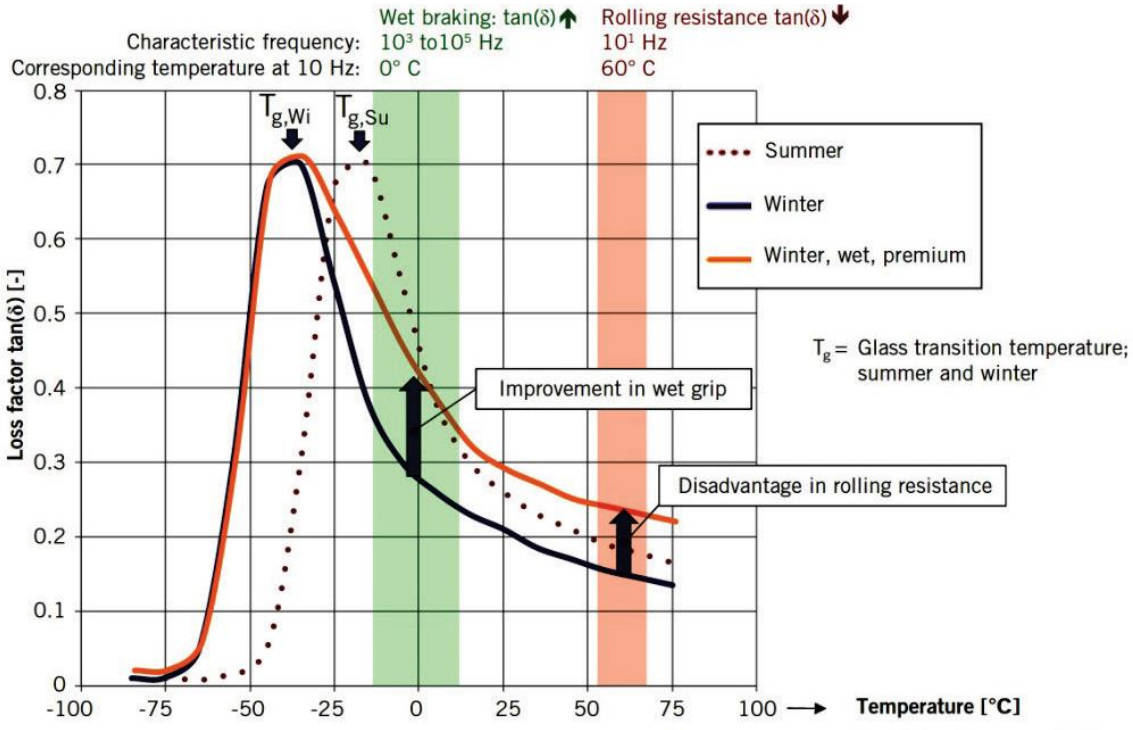

Figure 4-16 – Loss factor curves across the temperature: trade-off between wet grip and rolling resistance [56].

The course of changes in the value of the loss factor depending on the temperature of the rubber (Figure 4-16) allows to determine the qualitative effect of the rubber mixture on the tire performance characteristics,

namely the wet grip and the rolling resistance of the tire (hysteresis loss). In this figure, the marked area (including the direction of change) in which the value of the tan(δ) determines the mentioned properties of tires: normally, improving the wet grip implies the worsening of the rolling resistance [56].

4.6 Tire modelling

Normally, semi-empirical tire models require tire measurements for parameterization. These models are typically used for vehicle dynamic simulations. Two well-known semi-empirical tire models are the Magic Formula and the SWIFT model. The Magic Formula is a tire handling model that can deal with slip, camber and transient responses up to about 8 Hz. The SWIFT model is a dynamic model to describe tire behaviour for in-plane (longitudinal and vertical) and out-of-plane (lateral and steering) motions up to about 60-100 Hz and it can deal with arbitrary road unevenness.

4.6.1 Pacejka's Magic Formula

Over the years, many different mathematical functions have been used to approximate the tire 's behaviour in the most possible precise way, generally with poor results. One of the most reliable and wide-spread non-linear models able to simulate and to represent the tire as a vehicle component in a vehicle simulation environment is the so-called Magic Formula (as shown in Figure 4-17), developed by the Dutch Professor Hans Pacejka [7].

His approach consists in improving the purely mathematical models by introducing some experimental raw data, so that a higher accuracy is achieved. This approach is defined "semi-empirical" because the model is based on measured data but may contain structures that find their origin in physical models.

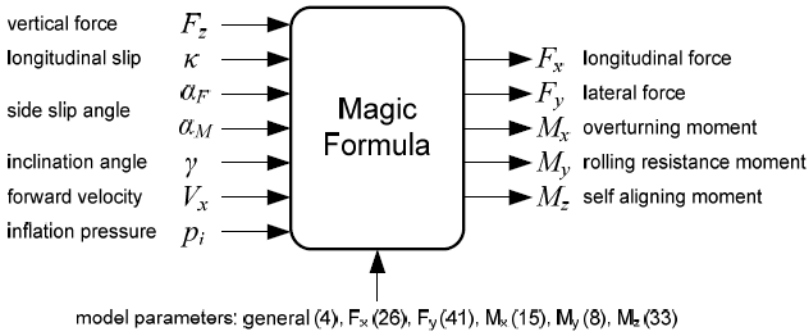

Figure 4-17 - Inputs and outputs for the Pacejka's Magic Formula tire model [36].

The Pacejka's tire model could greatly help in the prediction of the vehicle's dynamic response in critical situations in which active control systems (such as ABS), having an abrupt response, intervene to avoid accidents [40] (see Chapter 2). In fact, during such manoeuvres, tires experience very fast transients: having a reliable tire model means being able also to simulate these situations thus helping the vehicle designer and/or the control engineer to setup a safer vehicle in less time.

It is an empirical tire model used to estimate the steady-state tire forces and moment characteristics. It was devised in 1985 by TU-Delft and Volvo, but the model was not formulated from a physical point of view and the results were not accurate. In 1993 Michelin developed a purely empirical model using Magic Formula to describe the longitudinal force generation at combined slip [7].

The input variables are very important, and it is essential to understand the meaning of both. The longitudinal wheel slip κ is defined in equation (4.33):

$$\kappa = -V_x - r\omega V_x \tag{4.33}$$

such that for a positive longitudinal force F_x (braking force), the sign of κ is negative. Thanks to these implementations, and to very accurate studies on the analytical models, Hans Pacejka developed a semi-empirical tire model able to calculate the steady-state forces and moments exerted by the tire s during their normal working conditions.

Regarding the tire 's behaviour, the main physical quantities we are interested in the friction forces F_x and F_y (longitudinal and lateral forces exerted between tire and road surface) and the M_z moment (self-aligning torque).

The "slip parameter" is the input variable to determine the above-mentioned quantities. The slip is able to characterize the tire's working conditions of the specific performed manoeuvre: in case of longitudinal dynamics the slip ratio (indicated with the "k" symbol) will be used, in case of lateral dynamics the slip angle, or its tangent function (indicated with $\tan\alpha$) will be used.

The Pacejka's formulation has the following structure:

$$Y = Y(X) \tag{4.34}$$

the output variables F_x, F_y and M_z are indicated with the "Y" symbol, while the input parameters slip ratio κ and α with the "X" symbol. Then, the "Magic Formula", which allows to determine the desired physical quantities starting from the above-mentioned input parameters.

The slip ratio (κ) is determined thanks to the resolution of the wheel's dynamics. The exact Pacejka's 'Magic Formula' expression is reported below:

$$\begin{aligned} Y(X) = D\sin\{C\tan^{-1}[B(X+S_H) \\ - E(B(X+S_H) - \tan^{-1}(B(X+S_H)))]\} + S_V \end{aligned} \tag{4.35}$$

B, C, D, E, S_H and S_V are experimental coefficients depending on the analysed tire. The following list shows the description of the mentioned parameters:

- Stiffness Factor B;
- Shape factor C;
- Peak value D;
- Curvature factor E;
- Horizontal shift S_H:;
- Vertical shift S_V.

For given values of the coefficients B, C, D and E the curve passes through the origin and shows an anti-symmetric shape with respect to the origin itself. Despite this, the experimental curves often do not pass through the Origin: introducing the so-called "shift coefficients" in two directions (S_H and S_V), the analytical results can fit the experimental data as precisely as possible (Figure 4-18).

Consequently, the curve plotted in the (X, Y) reference system does not pass through the Origin, while in an adequate (x, y) reference system the curve does pass through its origin. Obviously, the two different reference systems can be obtained one from the other by means of simple rigid translations, being:

$$\begin{cases} Y(X) = y(x) + S_V \\ x = X + S_H \end{cases} \tag{4.36}$$

where the shift coefficients at the origin in the experimental curves are mainly due to the ply-steer (lateral force generated by the tire because of asymmetries in its carcass in the plies' distribution and tread pattern) and to the tire's conicity.

The above reported formulation is able to produce a characteristic curve which closely matches measured curves of lateral and longitudinal friction forces, as well as the curve describing the trend of the self-aligning torque, also taking into account the vertical load acting on the considered wheel and its camber angle, which are already included in the reported parameters: as a matter of fact, all the various factors are functions of normal load and wheel camber angle.

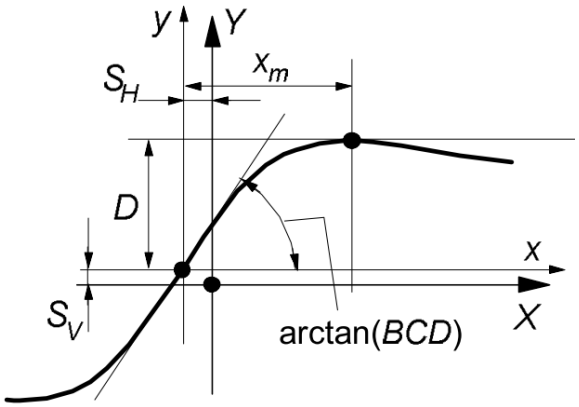

Figure 4-18 - Plot of Pacejka's Magic formula [36].

The D parameter represents the curve's peak value, while the product BCD represents the curve slope at the origin $x = y = 0$. As the shape factor C is used to control the limits of the range of the sine function, determining the final shape of the curve, and D affects the function's maximum, the slope at the origin can be modified by means of interventions on B.

Finally, the E factor is used to modify the function's curvature around its peak, as well as the peak's horizontal position.

In the Figure 4-19, the effect of the various parameters is shown for a reference tire, in order to make their roles clearer.

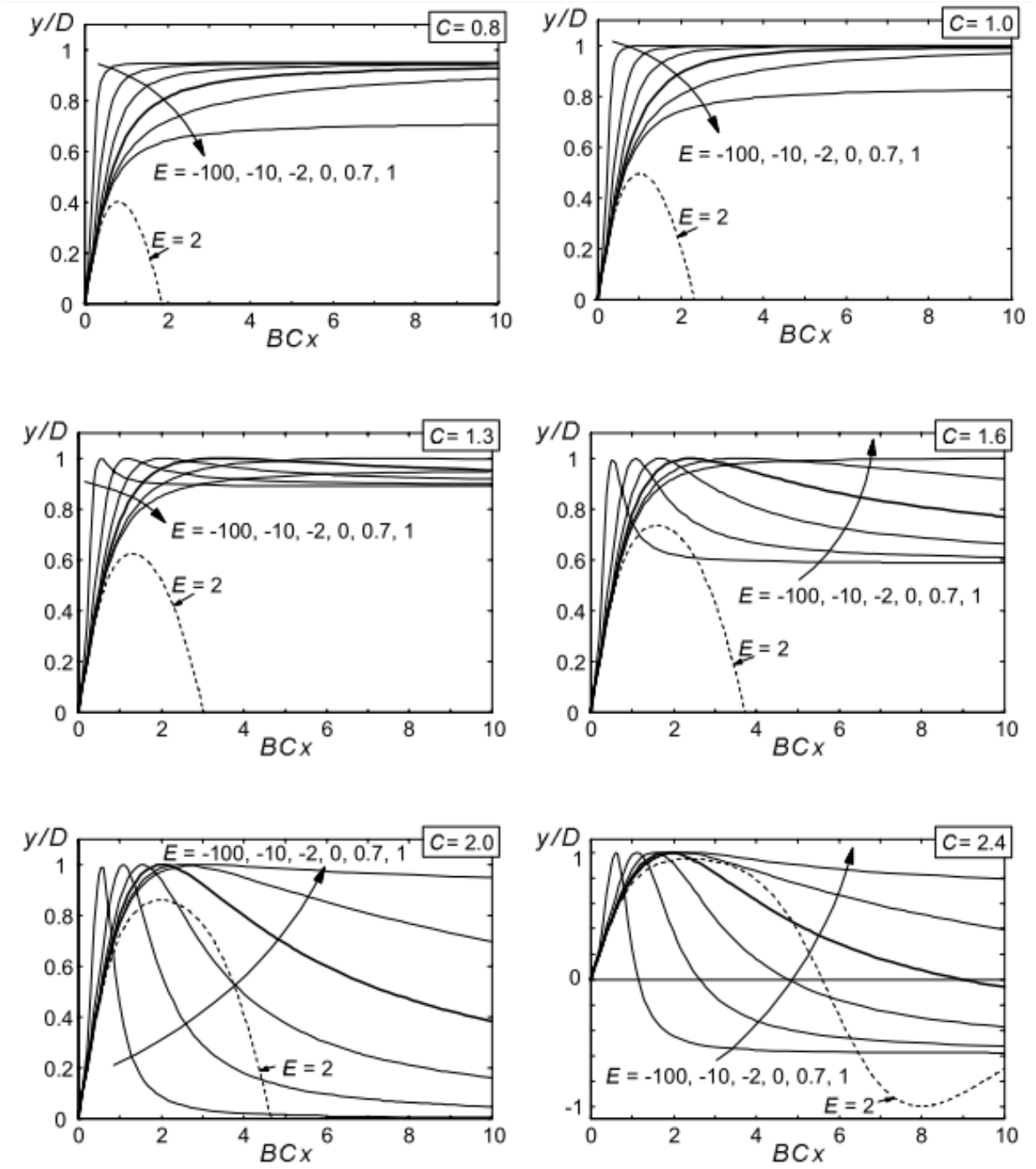

Figure 4-19 - Different Plots of Pacejka's 'Magic Formula', for the same tire and for different values of the experimental coefficient C [36].

It is fundamental to underline that the above reported expression for the "Magic Formula", as well as the following curves, are only valid in case of pure interaction conditions.

Regarding the tires' behaviour, this essay is referring to the "pure longitudinal interaction" in case of a vehicle driving in straight direction, while changing its longitudinal speed (acceleration or brake).

4.6.2 Transient Behaviour and relaxation length

In the literature, several different dynamic tire-road contact models can be found. The most popular one is Pacejka's MF-Tire model that is based on a steady-state formulation and introduces the transient behaviour of the tire as a first-order differential equation of relevant quantities such as the slip angle and the longitudinal slip. However, it has been shown that this model does not correctly predict the tire behaviour in case of high slippages such as those encountered during ABS braking.

The previous Magic Formula equation is valid for the steady-state tire behaviour. When driving, however, the tire requires some response time on changes of the inputs. In tire modelling terminology, the low frequency behaviour (up to 15 Hz) is called transient behaviour. It provides two methods to model transient tire behaviour:

- Stretched String;
- Contact Mass.

The stretched string tire model can be used for accurate transient tire behaviour. The tire belt is modelled as stretched string, which is supported to the rim with lateral (and longitudinal) springs. Stretched String Model for Transient tire behaviour shows a top view of the string model. When the tire is rolling, the first point having contact with the road adheres to the road (no sliding assumed). Therefore, a lateral deflection of the string arises that depends on the slip angle size and the history of the lateral deflection of previous points having contact with the road. Instead, the contact mass model is based on the separation of the contact patch slip properties and the tire carcass compliance. Instead of using relaxation lengths to describe compliance effects, the carcass springs are explicitly incorporated in the model. The contact patch is given some inertia to ensure computational causality. This modelling approach automatically accounts for the lagged response to slip and load changes that diminish at higher levels of slip. The contact patch can deflect in longitudinal, lateral, and yaw directions with respect to the lower part of the wheel rim and the contact patch itself uses relaxation lengths to handle simulations at low speed [57].

In this essay, the stretched string model will be considered as shown in the following Figure 4-20 and equations.

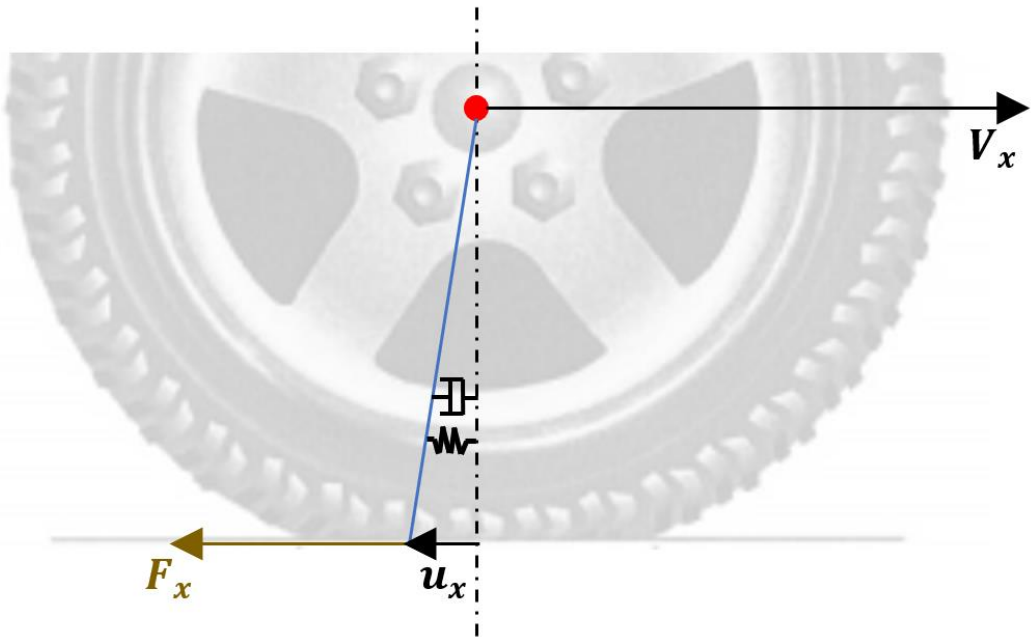

Figure 4-20 – Longitudinal tire deflection during braking.

In order to calculate the longitudinal deflection u_x of the string in the first point of contact with the road, the following differential equation is valid:

$$\tau \dot{F}_x + F_x = F_{x,ss} \tag{4.37}$$

where τ is the time constant that depends on the ratio between the longitudinal relaxation length and the longitudinal velocity of the wheel centre. The $F_{x,lag}$ can be expressed as function of the longitudinal displacement at the contact point between the tire and the road, the equation (4.41) can be sown as below:

$$\frac{\sigma_\kappa}{V_x} K_{x,s} \frac{du_x}{dt} + K_{x,s} u_x = K_x \kappa \tag{4.38}$$

with $\frac{\sigma_\kappa}{V_x} K_{x,s}$ the damping coefficient and $K_{x,s}$ the stiffness coefficient (as shown in Figure 4-20). Since $K_x = \sigma_\kappa K_{x,s}$, the equation (4.38) becomes:

$$\sigma_\kappa \frac{du_x}{dt} + |V_x| u_x = \sigma_\kappa V_{sx} \tag{4.39}$$

with $V_{sx} = V_x \kappa$.

In the following chapter, some experimental tests were carried out to determine how the relaxation length parameter, that appears in the first order differential equation of the slippage varies as a function of the working conditions i.e., of the normal load and the amplitude and the excitation frequency of the longitudinal slippage.

5. Experimental approach

The tires used for the test are typical commercial tires that can be used for different climatic conditions. One of them can be identified with a clear peaky shape of the longitudinal curve (described in Paragraph 4.5.3), while the second one with a smoother shape. As introduced in Chapter 2 and contrarily to what is expected by considering the grip of the peaky and smooth curves, this following Paragraph 5.1 will show that the smoother tire has a better behaviour than the peaky one in wet conditions and the WGI can reward the peaky tire. In order to highlight it, an experimental activity has been carried out. The paragraph 5.2 is focused on the experimental relaxation length characterisation. From the simulation results in Chapter 6, it seems to be clear that the relaxation length can affect the ABS strategies. The experimental activity tries to highlight the dependencies of the longitudinal relaxation length on some parameters like vertical load, excitation frequency and longitudinal velocity.

5.1 Outdoor wet braking test description and results

The goal was to test and evaluate the two tire specifications (shown in Figure 5-1) with the same passenger car, by investigating the braking distances and getting some vehicle measurements in order to analyse vehicle behaviour. The tested tires will be called “Tire A” and “Tire B” and they will refer to the peaky and the smooth µ-slip curves, respectively. The data are made available for use by the Department of Industrial Engineering at University of Naples “Federico II”.

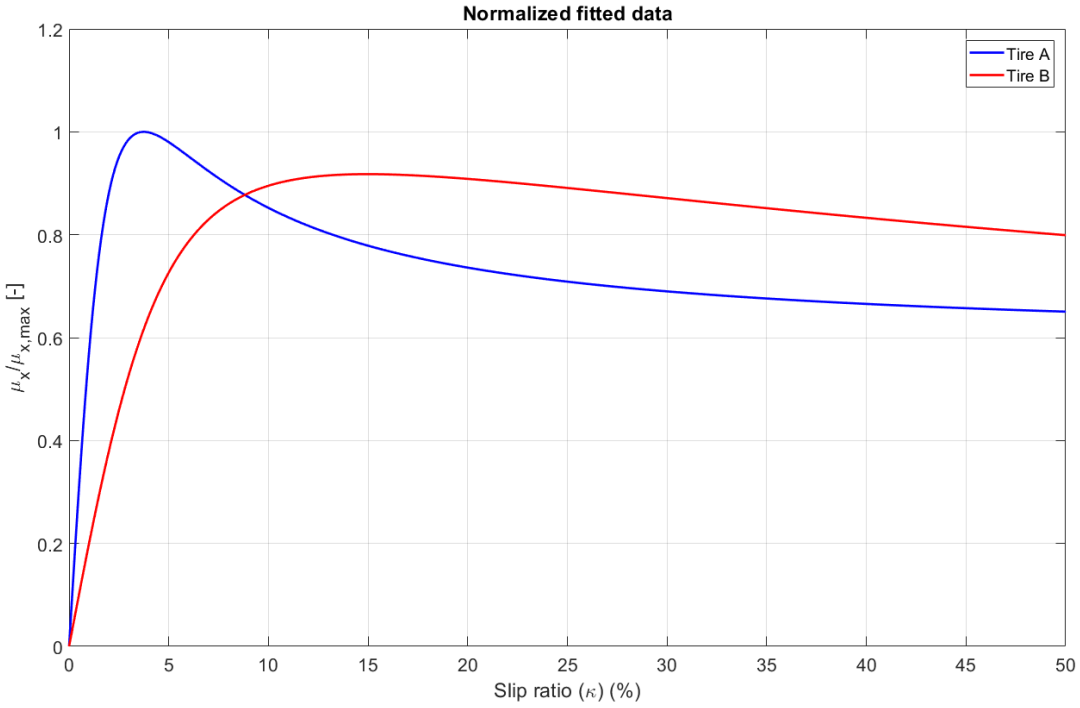

Figure 5-1 – Comparison of the curve’s shapes between Tire A and Tire B. Normalized data.

Initially, some longitudinal braking test have been executed with the F&M trailer in order to get the curves of the studied tires. Based on the peak level that can be seen in Figure 5-1, It can be assumed that the WGI will give a higher rating to Tire A with respect to Tire B. The test has been carried out around the maximum vertical load of the vehicle that can be reached when the full load transfer is completed.

The second step was to do objective measurements of the vehicle behaviour during the emergency braking manoeuvre. The vehicle technical specifications of interest are listed in the Table 5-1 below.

Table 5-1 - Test vehicle specification.

Technical specification	
Front/Rear [%/%]	60/40
Mass [kg]	1400
Length[mm]	4255
Width [mm]	1799
Wheelbase [mm]	2637
Wheel mass [kg]	28
Height of CoG [m]	0.54

The data listed in the table above have been useful to characterize vehicle model parameters, which is described in Chapter 6, Paragraph 6.1.

Outdoor tests have been carried out on a straight line, by using a common test procedure, as inspired by the standard tests for wet braking [8]. In general, the vehicle braking is a complex process predetermined by many factors that may be casual ones, such as the parameters of the structure of the vehicle and the ones of the road coating as well as mental and physiological peculiarities of the driver, so the maximum possible number of them should be assessed in order to describe braking in detail [58]. The braking distance is mostly impacted by:

- the initial velocity;
- the time of response of the driver;
- the time for the increase of deceleration;
- the time of variation of the settled deceleration;
- the time of moving with released brakes;
- and the settled deceleration.

There are several standards that consider more than one initial velocity to evaluate the braking performance [6][58], that is not a goal of this research activity. In fact, in this essay the speed range for braking distance measurements is set as suggested by Wet Grip Index method [8]:

- V_i = 80 kph (initial velocity);
- V_f = 20 kph (final velocity).

The Wet Grip Index method does not consider V_x = 0 kph but 20 kph as final velocity. It can be considered mainly due to the quite fist changes of the slip signal and the study of the ABS strategies at very low velocities is not the goal of this analysis. In fact, as also explained in Chapter 1, the main goal is more related to tire behaviour under the same vehicle. In Figure 5-2 is shown a passenger car during an emergency braking test on wet surface.

Figure 5-2 –A passenger car during a wet emergency braking test.

As already described, this is a pure longitudinal manoeuvre: only the ABS control on the front right tire has been studied, by admitting that it can be considered the same also for the left wheel, because of the symmetry of the vehicle and the manoeuvre.

Tire A and Tire B have been tested on the proving ground designed for a continuous irrigation of test tracks. In addition to braking distances measured on the same surface, some measurements have been carried out during the objective tests. A list of the considered channels from vehicle measurements is shown in the Table 5-2, with the description of the channels acquired and corresponding units.

Table 5-2 - Outdoor test measurements for emergency braking test.

Instrument	**Channel**	**Units**
Inertial Platform	a_x	m/s^2
	V_x	m/s
	d	m
	θ	rad
	Brake switch	[on, off]
Encoder	ω	rad/s
Pressure sensor	p_b	bar

In order to characterize the vehicle during the braking, the following instruments have been used:

- Inertial Platform with GPS sensor and integration of vehicle sensors via CAN bus;
- Encoder on Front-right wheel;

- Pressure sensor mounted on brake calipers of front axle wheels.

In the following Figure 5-3 the main signals acquired during the test are shown. The following data have been normalized with respect to the maximum value among the 2 compared signals (Tire A and Tire B) shown per each plot, in order to keep any difference between the compared signals.

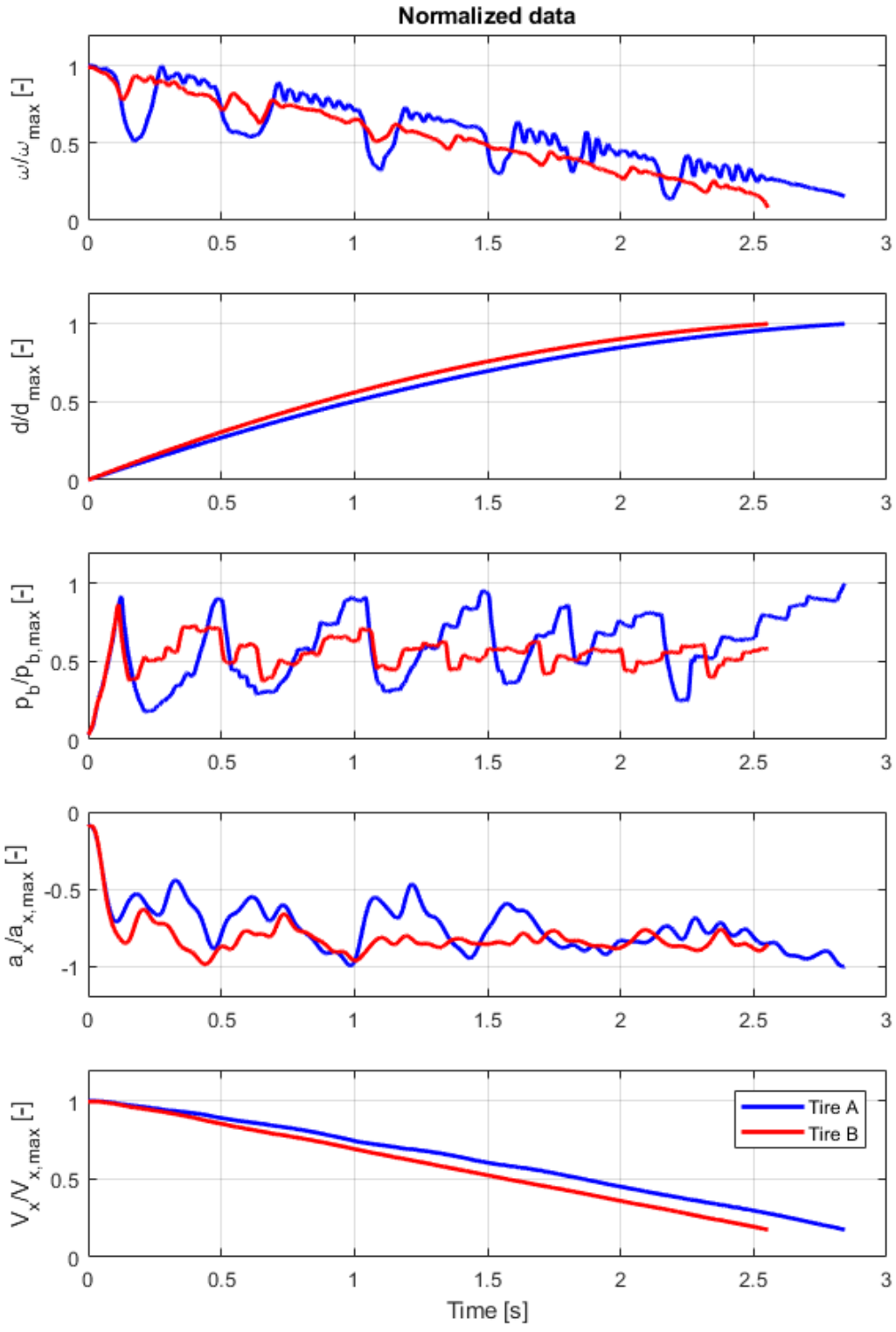

Figure 5-3 - Normalized data of the acquired signals.

The figure clearly shows how the same control logic on the same surface can differently manage 2 different tires. The sample rate considered for vehicle data acquisition is f_s = 500 Hz. The binary Brake Switch signal has been useful to cut the full acquisition by every run.

In order to measure different useful signals and verify the repeatability of the results, 5 runs have been considered for both studied tires at the same conditions. Below, the Table 5-3 with the average distances and longitudinal decelerations for both peaky and smooth curve. Tire A has been chosen as reference because it is the one that should perform better than Tire B based on WGI approach and the results will be shown:

$$ratio\ \% = \frac{variable_{Tire\ B}}{variable_{Tire\ A}} \cdot 100 \tag{5.1}$$

as ratio between the parameter under evaluation for Tire B and the reference Tire A.

Table 5-3 - Comparison of the averaged braking distances between Tire A and Tire B; the results are expressed as percentage with respect to the reference tire (Tire A).

Average of the 5 runs	**Tire A (%)**	**Tire B (%)**
Brake distance	100	89
Longitudinal deceleration	100	114

According with what explained at the beginning of the current chapter, the results highlighted the Tire B with better performance than Tire A. The same can be seen if the average longitudinal decelerations are analysed in the following Figure 5-4, that is one of the 2 methods used for WGI.

As explained in Chapter 1 and 2, the ABS tries to reach and keep the maximum performance of the tire, while the WGI refers to the assessment of the peak value of the tire. This experimental activity shows that Tire B has a better performance with respect to Tire A in wet conditions: with the same vehicle and the same ABS, there is a reduction of the stopping distance d by 12.3%, despite the shape of the curves in Figure 5-1 and the WGI would not suggest this outcome. In fact, as already described in Chapter 1, the 2 methods are considered as equivalent.

An initial analysis can define that in wet conditions more difficulties could be present to keep the μ-peak, in particular in case of a peaky shape, as for the Tire A. It will be better investigated in the next Chapter 6.

In Figure 5-4 it is possible to observe a different behaviour for the same ABS logic: the smooth tire is showing a more concentrated working area, with lower peaks and higher minimum values with respect to the peaky tire (Tire A). Evidently, the smooth spec allows a finer control, with lower increases and decreases of the pressure in the brake calipers.

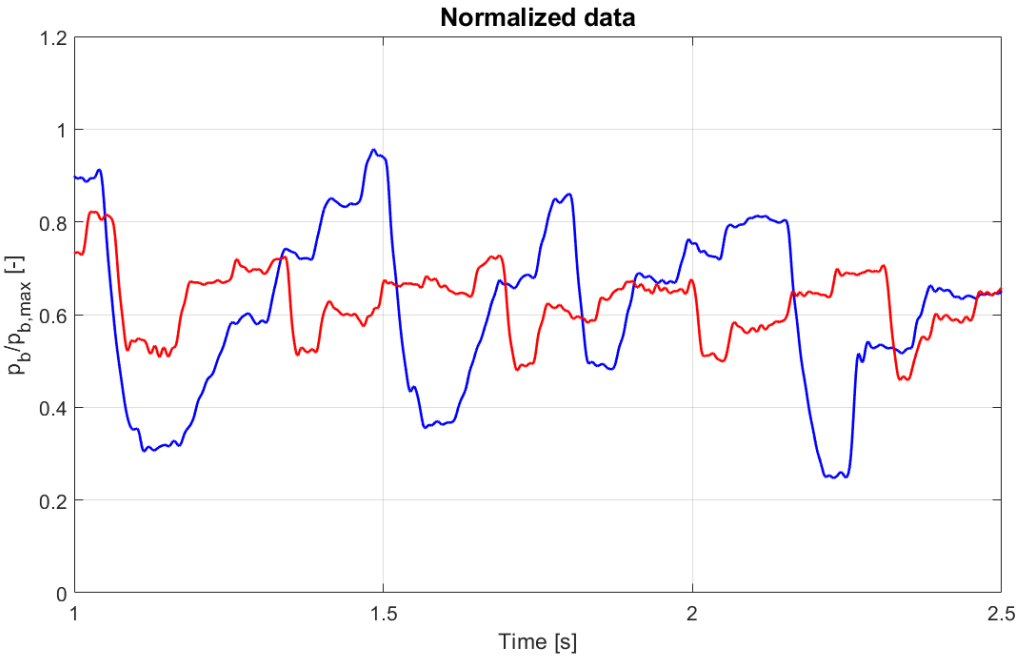

Figure 5-4 - Comparison between normalized brake pressure between Tire A (blue) and B (red) for the same vehicle for a certain run.

A further analysis that can be done is related to the assessment of the brake pressure signal. As it is possible to see from Figure 5-5, the studied ABS can have different approaches with 2 different tires. It can be assumed that it is able to calibrate itself to different tires with different characteristics and performance. In order to better highlight it, the following two points have been considered to evaluate:

- the root mean square (RMS) value of the brake pressure signal, in order to understand which kind of average brake torque the vehicle is applying to the tire;
- the standard deviation (STD) of the brake pressure signal, in order to understand how spread out the brake pressure values are.

In the following graphs (Figure 5-5 and 5-6), the above-mentioned values are shown as percentage values, in order to compare Tire A (as reference tire) and Tire B.

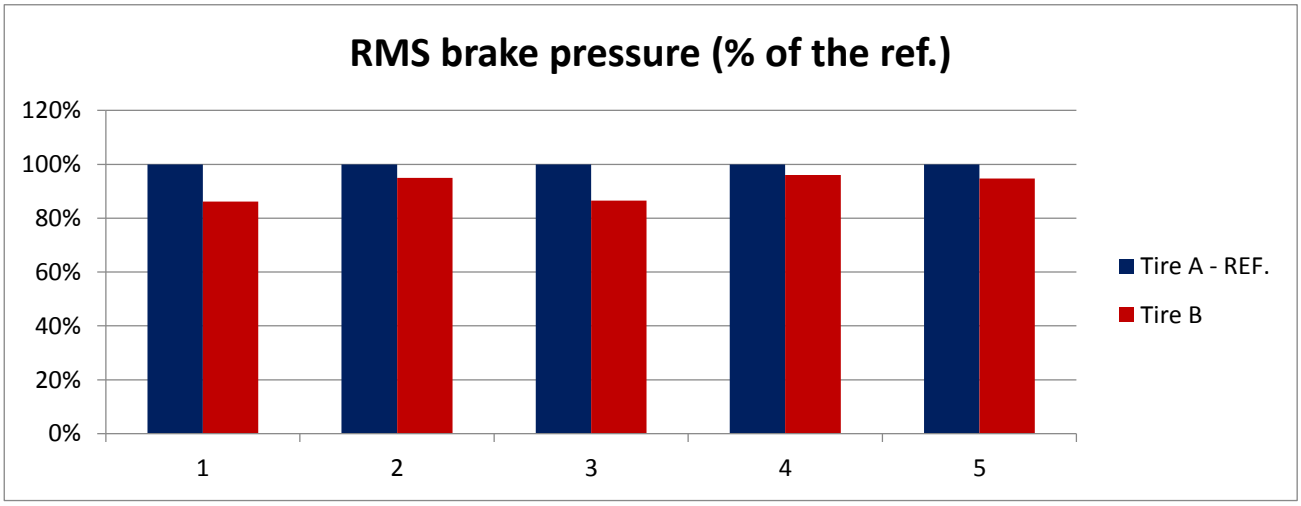

Figure 5-5 – Comparisons between RMS values of the brake pressure signals for Tire A and B.

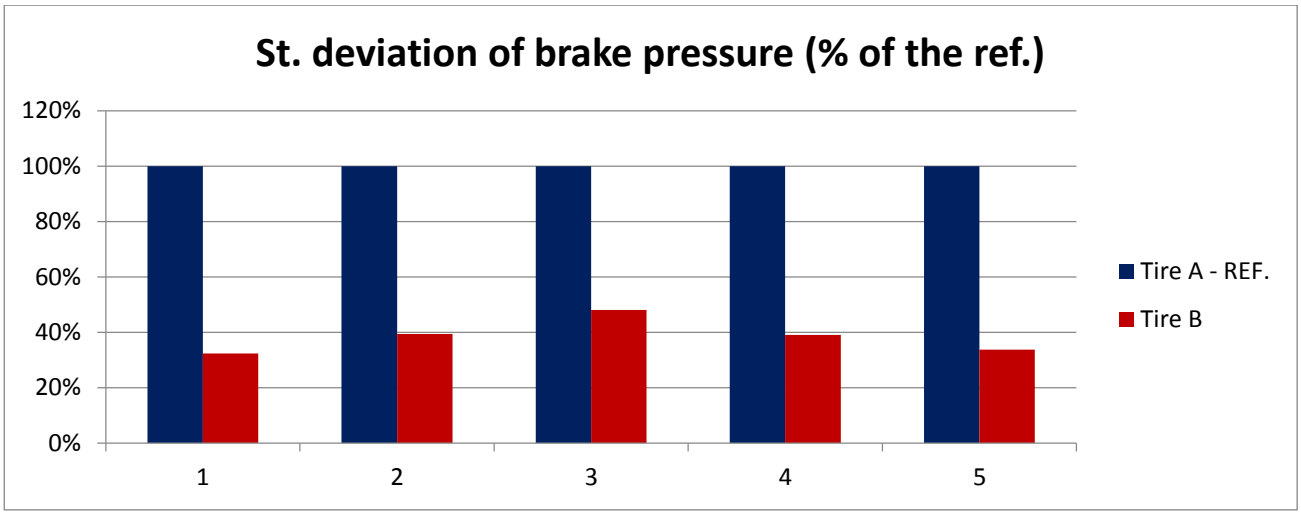

Figure 5-6 – Comparisons between STD values of the brake pressure signals for Tire A and B.

Since the ABS strategies influence the final braking distance, this last one seems to be dependent on the 2 above-described parameters. Practically, since the brake torque is connected to the longitudinal force that the tires, with the RMS value it is possible to know how much force the vehicle can generate. As consequence of the WGI definition, the higher the RMS the higher the force and the lower the braking distance should be if a linear dependency between longitudinal force and brake torque is considered. Therefore, Tire A should always perform better than Tire B.

In the following Figure 5-7, the best braking distance cases have been compared. Even in this case and despite quite close RMS values between the two tires, it is clear that they have a very different standard deviation.

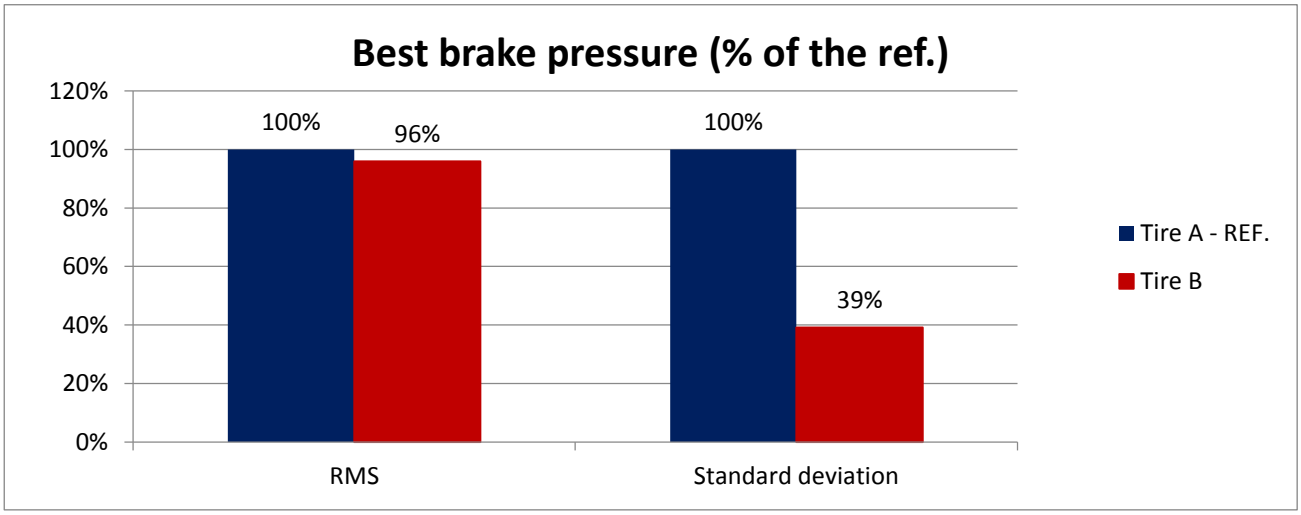

Figure 5-7 - Comparisons between RMS and STD of the brake pressure signals for Tire A and B: best braking distances cases among the 5 runs analysed.

As shown in Table 5-3, Tire B can stop the vehicle in a lower braking distance (around 12.3%). This means the RMS is not the only parameter to be considered shorter, but another good parameter can be found in the STD, where the dispersion of the signal is highlighted.

5.2 Longitudinal relaxation length characterization

An experimental test was carried out to determine how the relaxation length parameter that appears in the first order differential equation of the slippage (4.43) varies as a function of the working conditions i.e., of the normal load, of the excitation frequency, and of the slippage. These tests allowed to verify the limits of Pacejka's MF-Tire model when trying to reproduce the tire transient behaviour. In this paragraph, the main goal is to analyse different tire models for the calculation of the relaxation length [40]:

- MF-Tire 5.2 transient model;
- MF-Relax model.

In Braghin et al. research work [40], they made a comparison among the MF-Tire 5.2, Enhanced nonlinear transient tire model and the MF Relax model proposed by them. In the following paragraph a test procedure for longitudinal relaxation length calculation will be described, with an assessment of the MF-Relax model that will be adopted for the model described in Chapter 6. The size of the tested tire is different from the ones used for the outdoor tests but it can be acceptable since the analysis wants to investigate the relaxation length dependencies on the above-mentioned parameters instead of evaluating absolute values.

5.2.1 Test setup description

Tests are performed with a test bench that allows to measure tire force and moments while it is interacting with the surface. Normally, this test rig for forces and moments measurements does not allow to test tires on the asphalt and in wet condition. In fact, a dedicated sandpaper wraps the rolling metal belt at the desired velocity, in order to replicate the asphalt grip (Figure 5-8).

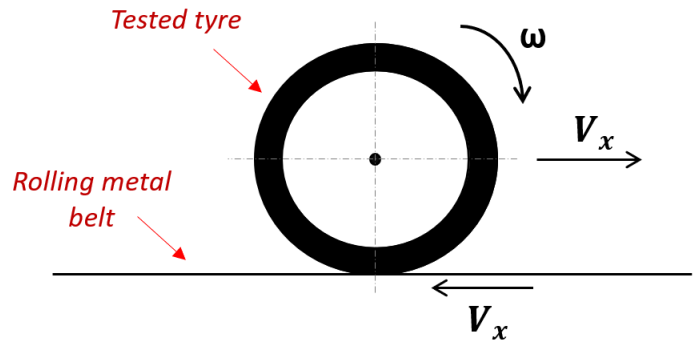

Figure 5-8 - Scheme of the test bench used for forces and moments measurements.

Moreover, the mentioned test bench allows to apply several longitudinal and lateral slippages, inclination angle and vertical loads, according to the ISO reference system described in the Paragraph 4.5.1. The data have been filtered by using a low-pass filter as shown in the Table 5-4 below.

Table 5-4 - Filtering details.

Filter	**Order**	**Cut-off frequency**
Butterworth, low pass	6	based on the frequencies of the slip ratio sine signals + 3 Hz

The main conditions are described in Table 5-5.

Table 5-5 - Overview of the test conditions considered for the relaxation length procedure.

Channel	Units	Type of signal	Magnitude	Frequency [Hz]
κ	%	Sinusoidal	0.5, 1, 2	0.1, 0.5, 2, 4, 6, 8
F_z	% of the nominal load	Constant	60, 100, 120	-
γ	°	Constant	0	-
V_x	kph	Constant	V_1, V_2, V_3 (with $V_1 > V_2 > V_3$)	-

The choice to consider the slip ratio range between 0.5 and 2 % depends essentially on the purpose to keep the linear range of the longitudinal curve of the tire for the evaluation of the relaxation length dependencies. and verify how the MF Relax model can fit the experimental data. An example of the filtered measured signals is shown in the following Figure 5-9, where the green and yellow points identify the peaks in the force and slip ratio signals, respectively.

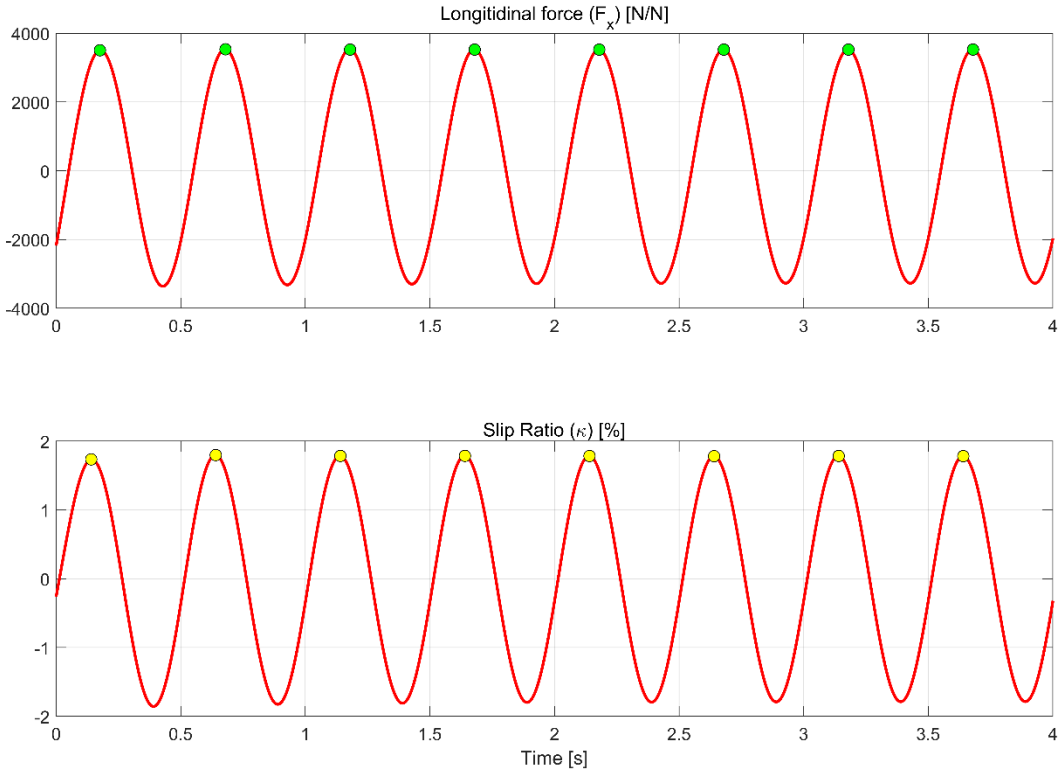

Figure 5-9 – Filtered input (longitudinal slip) and output (longitudinal force) of the test procedure.

The calculation of the relaxation time and length will be described in the next paragraph.

5.2.2 The influence of Slip ratio on longitudinal relaxation length

The relaxation length of the tire can be defined as the circumferential length that tires must cover in order to generate a force, if a certain slip is applied. In the following picture, the measured transient tire behaviour is shown for different frequencies. The following first order transfer function is related to the linear transient tire [39] and based on the low-pass filter Laplace notation:

$$\frac{F_x}{\kappa} = K_x \left(\frac{1}{\frac{\sigma_\kappa}{V_x} s + 1} \right) \tag{5.2}$$

where the K_x is the steady-state longitudinal slip stiffness, while in the brackets the transient behaviour is represented [40][39]. In the following Figure 5-10, it is represented the Bode diagram of the transient response of the tire for the 3 analysed longitudinal velocities, at the nominal load and 1% of the longitudinal slip.

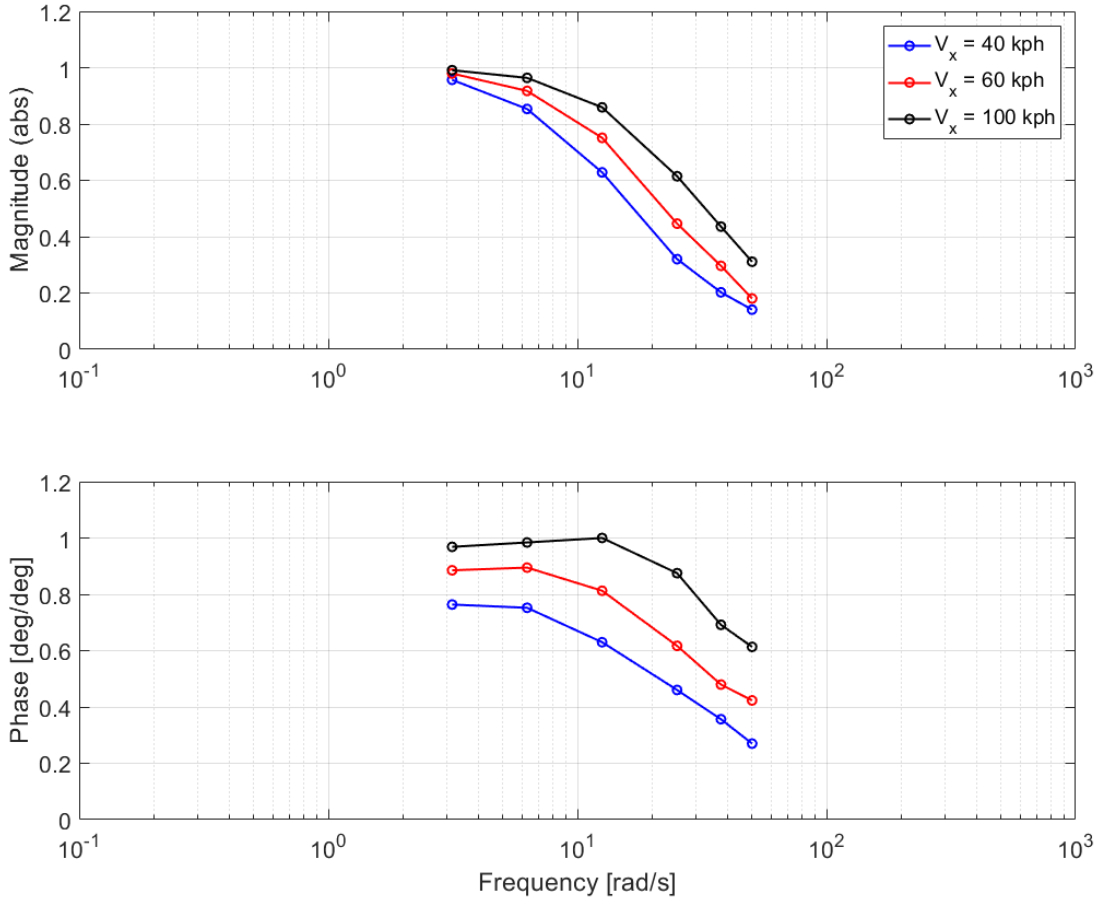

Figure 5-10 – Measured transient response of the tire represented in the bode diagram for the 3 analysed longitudinal velocities (F_z = 100%, κ = 1%). Normalized Phase values.

The steady-state longitudinal slip stiffness K_x is calculated using the linear equation:

$$K_x = \frac{F_x}{\kappa} \tag{5.3}$$

where the transient relation can be neglected. In fact, the linear relation between F_x and κ allows to determine the longitudinal slip stiffness K_x. The low frequency behaviour can be considered for this calculation, where the tire shows the steady-state behaviour.

In this paragraph, the method for the relaxation length calculation is based on the evaluation of the time delay between the correlated peaks of the sinusoidal input between the Longitudinal slip (input) and the Longitudinal force (output). In the Figure 5-11 the scheme of the angular distance that the tire needs to build-up the longitudinal force is shown.

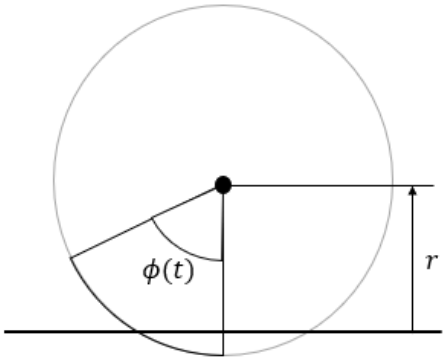

Figure 5-11 - Scheme of the angular distance that the tire needs to generate force.

The approach that has been used consists to calculate the relaxation length:

$$\sigma_\kappa(t) = r \cdot \phi(t) \tag{5.4}$$

where, r is the rolling radius of the free-rolling tire (calculated as the ratio between longitudinal velocity V_x and wheel rotational speed ω in free rolling conditions) and $\phi(t)$ can be calculated from the wheel speed $\omega(t)$, that is a measurement available from the test results. It can be defined as shown below:

$$\phi(t) = \int_{peak\ of\ \kappa}^{peak\ of\ F_x} \omega(t)\, dt \tag{5.5}$$

The rolling radius r for the tested tire is approximately 0,31 m. In this paragraph, the dependency between the relaxation length with vertical load, slip ratio and excitation frequency (that has been set as frequency of the slip ratio sine signal) will be investigated. The $\phi(t)$ represents the *phase lag* of the tire, between the Longitudinal slip as input (κ) and the Longitudinal force as output (F_x). A similar approach has been explained in Wei et al. study, with a focus on lateral relaxation length [59].

In the Figure 5-12, 5-13 and 5-14, it is possible to observe that the relaxation length shows a decreasing trend when the excitation frequency is increasing. The results are shown at the same velocity and slip ratio amplitude. The figures also highlight that a higher vertical load tends to increase the relaxation length values per each excitation frequency. Therefore, it is possible to summarise that the higher the vertical load the higher the relaxation length is.

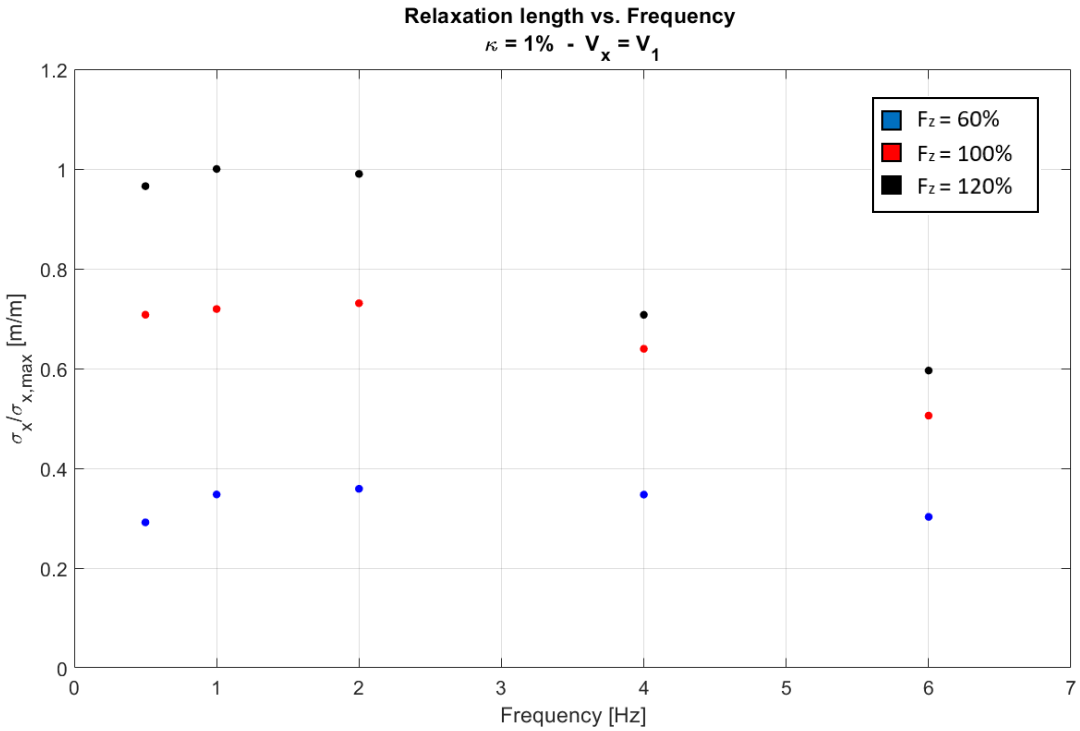

Figure 5-12 – Influence of the vertical load on the relaxation length across the excitation frequencies, calculated by "peak to peak" method, at the velocity V_1. Normalized data.

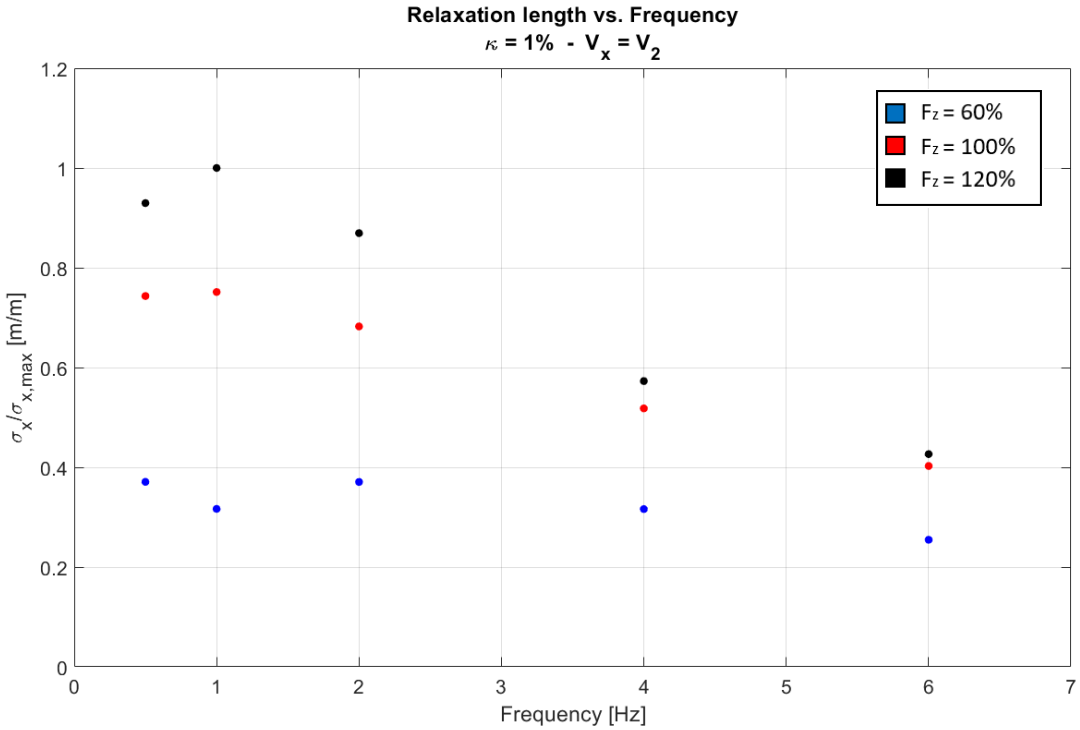

Figure 5-13 – Influence of the vertical load on the relaxation length across the excitation frequencies, calculated by "peak to peak" method, at the velocity V_2. Normalized data.

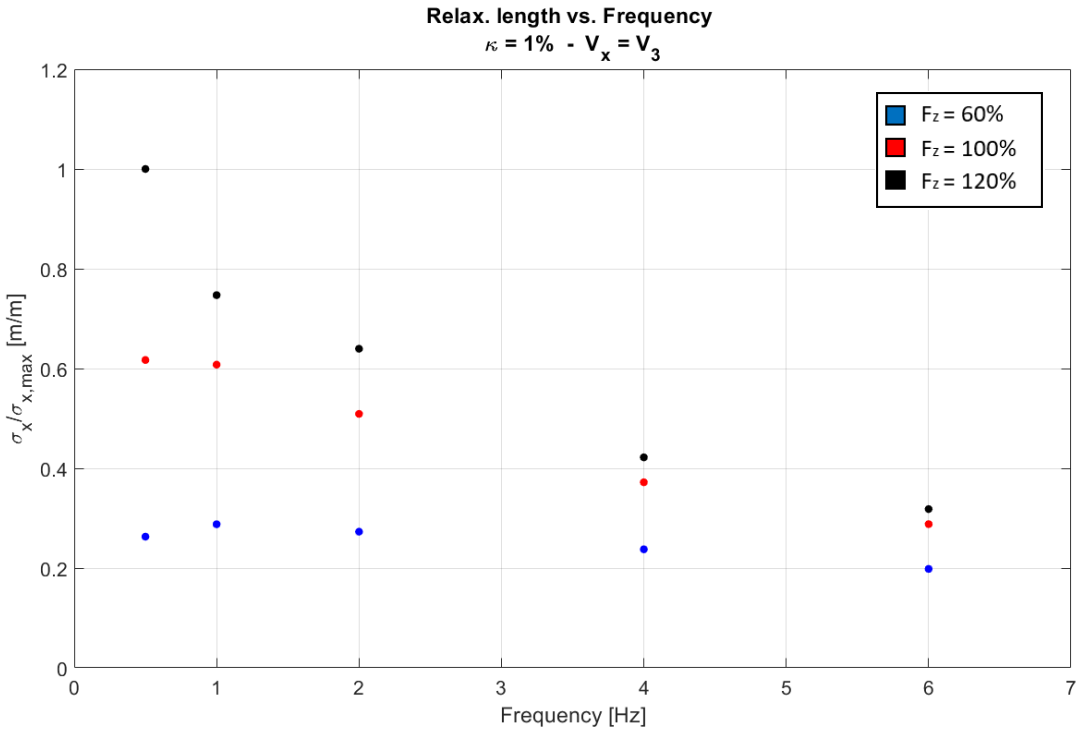

Figure 5-14 – Influence of the vertical load on the relaxation length across the excitation frequencies, calculated by "peak to peak" method, at the velocity V_3 and $\kappa = 1\%$. Normalized data.

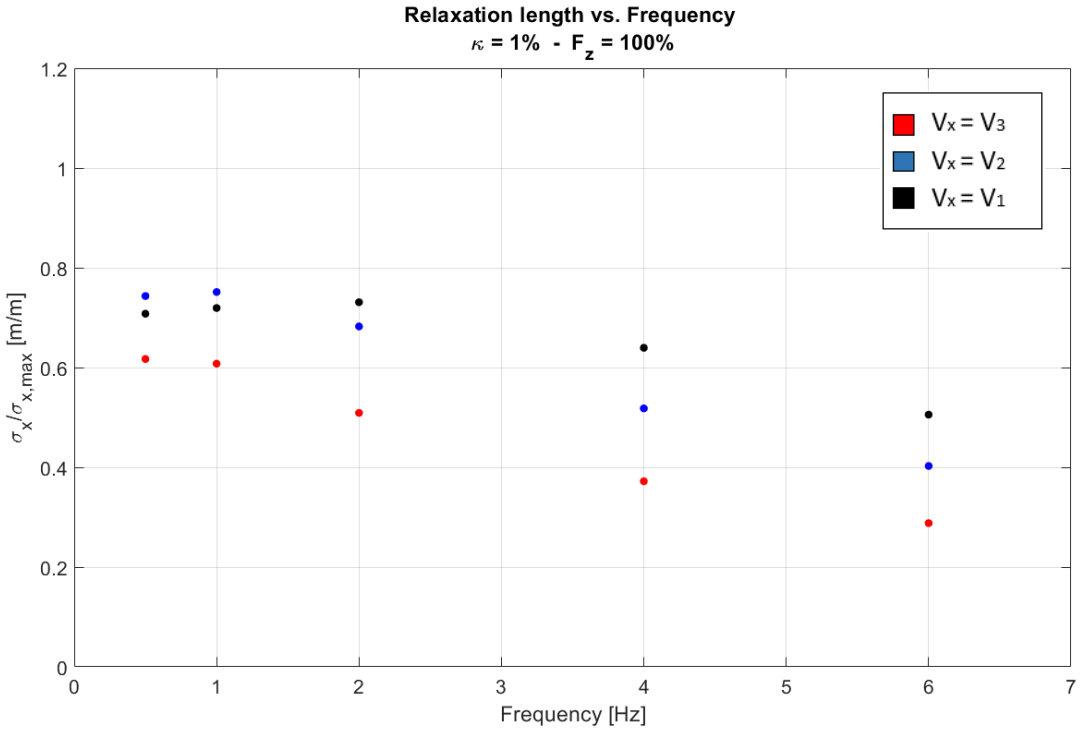

Figure 5-15 – Influence of the longitudinal velocity on the relaxation length (normalized) across the excitation frequencies, calculated by "peak to peak" method, at the nominal load $F_z = 100\%$ and $\kappa = 1\%$.

Experimentally, it has been observed that the relaxation length is also dependent on the longitudinal velocity across the excitation frequencies. In the Figure 5-15, three longitudinal velocities have been compared at the same slip ratio amplitude and vertical load (the nominal one). In this case, it is possible to summarise that the gap between low and high velocity (40 and 100 kph) increases when the frequency is increasing.

In the next figures Figure 5-16, 5-17 and 5-18 the relaxation length dependency on the longitudinal slip amplitude is investigated, with the aim to understand which frequency range is where the amplitude shows a higher influence.

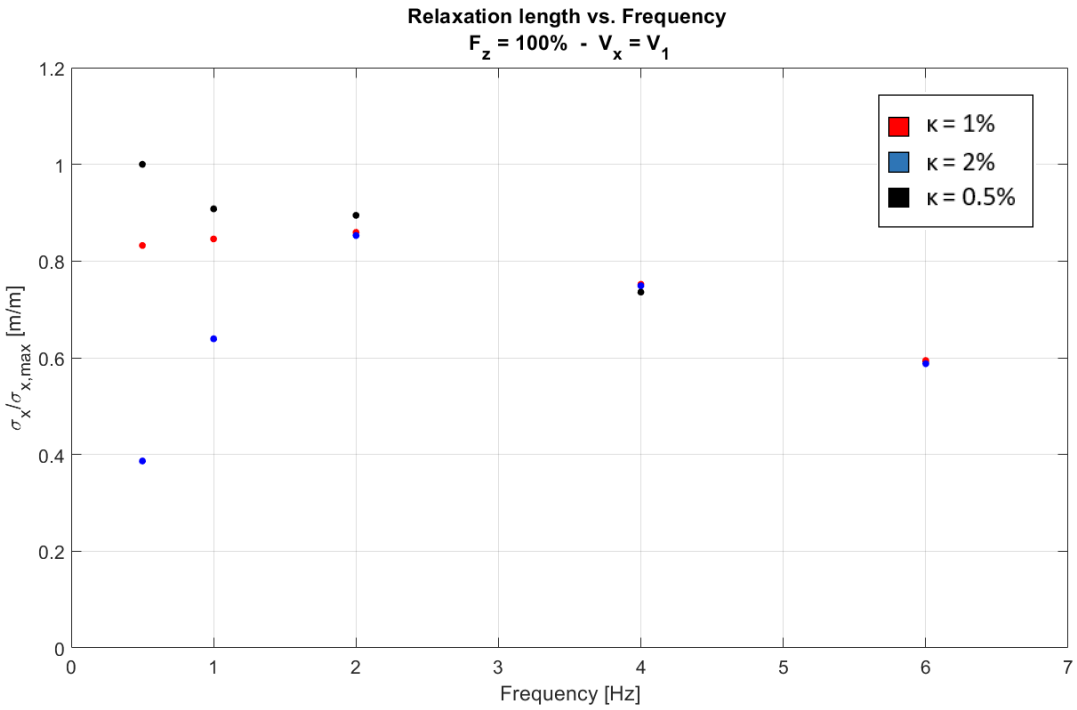

Figure 5-16 – Influence of the Slip Ratio amplitude on the relaxation length (normalized) across the excitation frequencies, calculated by "peak to peak" method, at the nominal load $F_z = 100\%$ and velocity V_1. Normalized data.

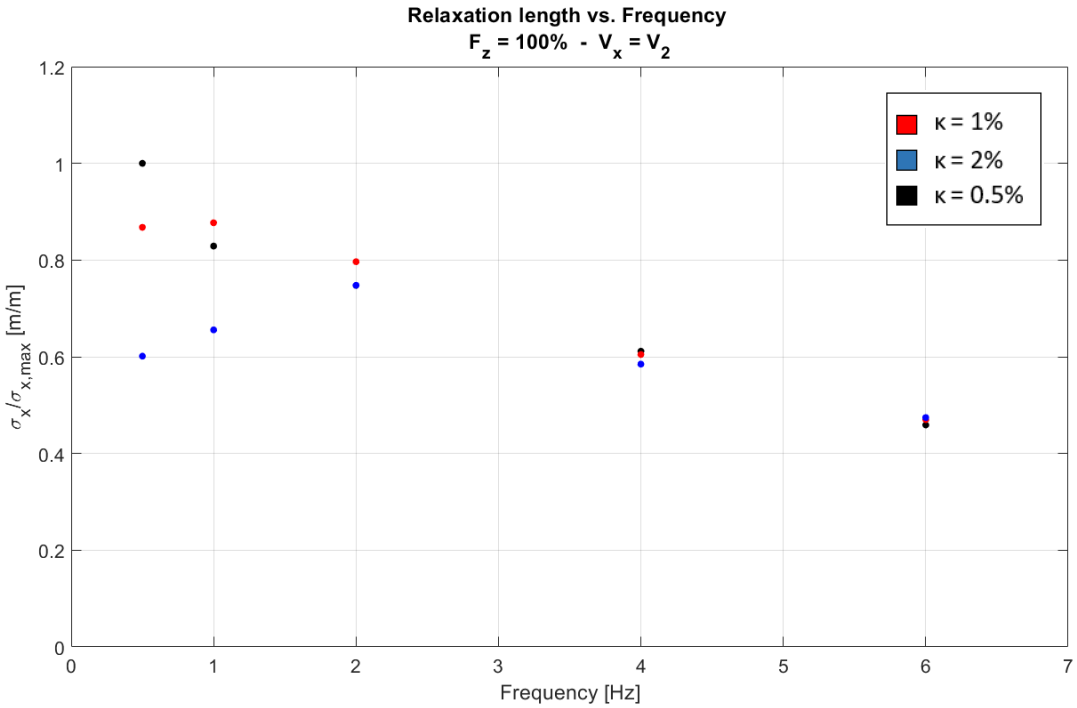

Figure 5-17 – Influence of the Slip Ratio amplitude on the relaxation length (normalized) across the excitation frequencies, calculated by "peak to peak" method, at the nominal load $F_z = 100\%$ and velocity V_2. Normalized data.

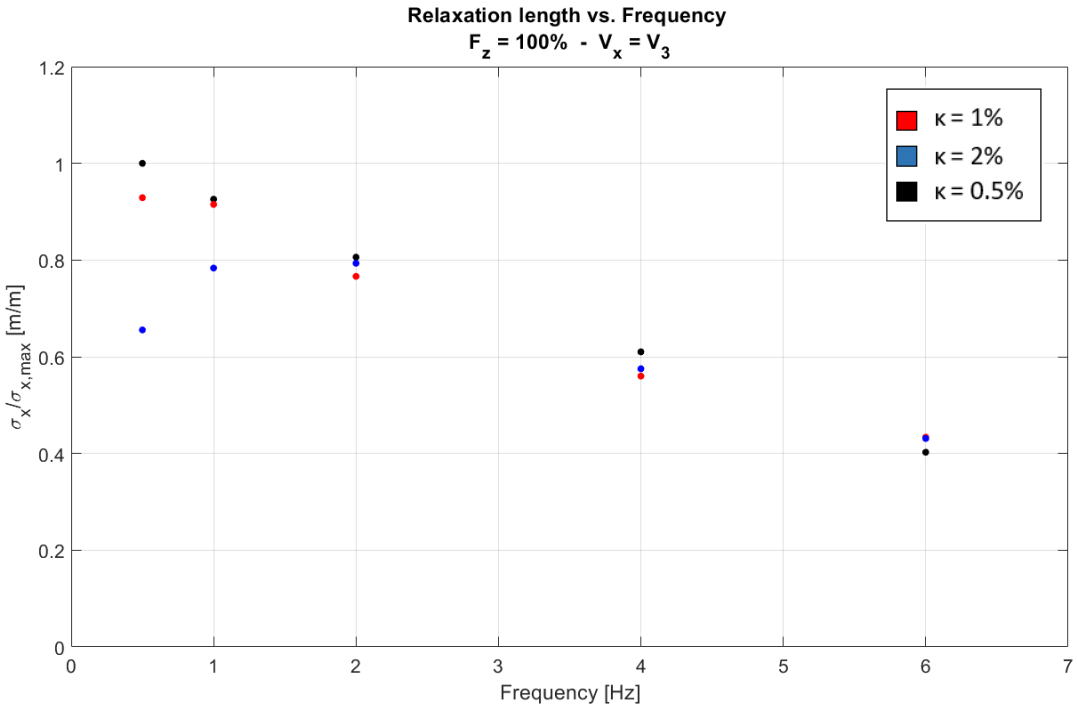

Figure 5-18 – Influence of the Slip Ratio amplitude on the relaxation length (normalized) across the excitation frequencies, calculated by "peak to peak" method, at the nominal load $F_z = 100\%$ and velocity V_3. Normalized data.

At low frequencies, a high variation of the relaxation length is visible at different amplitudes of the longitudinal slip: the relaxation length is higher at 0.5% than the ones at 1% and 2% in the frequency range

[0, 2 Hz]. In this range, the higher the amplitude, the lower the relaxation length. This can be explained with the analysis of the braking stiffness K_x with respect to the velocity, as shown in the Figure 5-19 below.

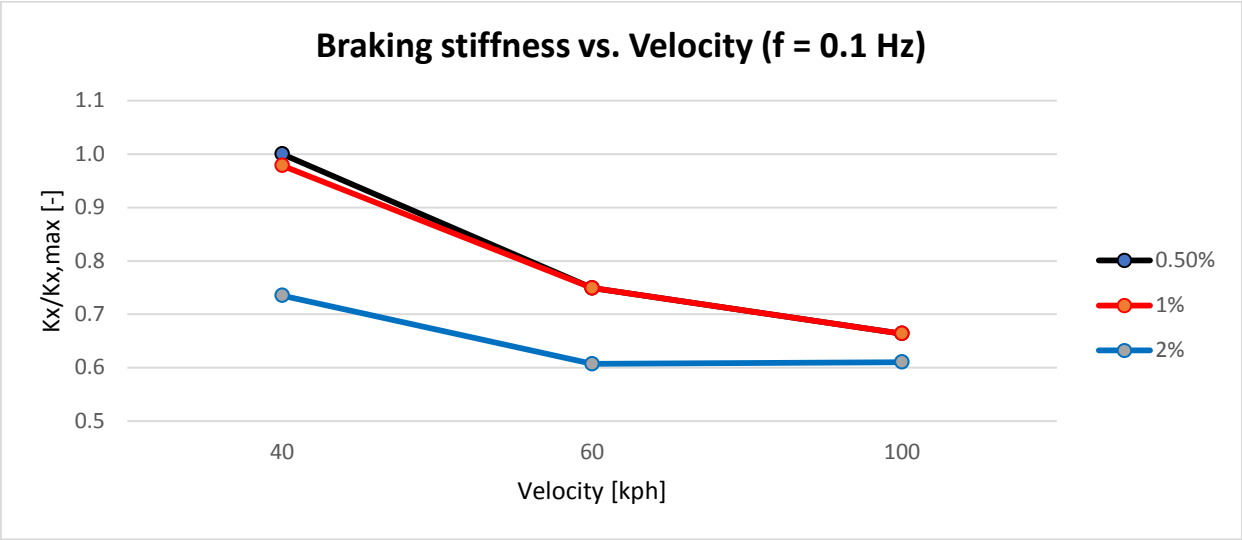

Figure 5-19 – Braking stiffness variation across the longitudinal velocity, at $F_z = 100\%$ and $f = 0.1\%$ Normalized data.

The K_x is similar at 0.5% and 1% across the longitudinal velocities, while the 2% shows lower values of the braking stiffness. It could happen that there are nonlinearities of the force generated by the tested tire at the 2% of slip ratio. This can explain the differences at low frequencies, since the relaxation length can be considered as ratio between the braking stiffness and the static longitudinal stiffness [36][60].

This is also in accordance with what explained in Braghin et al. study, where they define that the MF Relax model can better fit experimental data at lower frequencies with respect to the MF Tire and the Enhanced Nonlinear Tire models [40]. After that, the relaxation length is similar per each amplitude and tends to decrease when the excitation frequency is increasing, as also shown above. this variation becomes always lower when the excitation frequency increase (from 0.5 to 6 Hz).

5.2.3 MF-Tire & MF-Relax model assessment

The first step towards the determination of the longitudinal contact force in transient manoeuvres is the calculation of the relaxation length σ_κ as shown in the following equation:

$$\sigma_\kappa = F_z(PTX1 + PTX2 \cdot df_z)e^{-PTX3 \cdot df_z}\left(\frac{r_0}{F_{z0}}\right) \tag{5.6}$$

that is a function of just the applied normal load F_z. The variables shown in the equation (5.8) are:

- $PTX1$, $PTX2$, and $PTX3$ are three parameters that must be determined experimentally;
- F_{z0} is the reference normal load (i.e., the reference load used during the identification of MF Tire model's coefficients);
- df_z is the relative variation in the normal load with respect to the reference normal load ($df_z = (F_z - F_{z0})/F_{z0}$);
- r_0 is the unloaded radius of the tire.

Based on what was shown in the previous Paragraph 5.2.2, the MF-Relax model has been used for the braking simulations that will be better explained in the next Chapter 6. This model is based on MF-Tire model, the only difference is that the relaxation length does not only depend on the normal load but also on the slippage magnitude:

$$\sigma_{\kappa,slip} = \left(\sigma_{\kappa,Fz} - OTX1\right)e^{-OTX2\cdot\kappa} + OTX1 + OTX3 \cdot \kappa \tag{5.7}$$

being $\sigma_{\chi,Fz}$ the relaxation length determined using the MF-Tire model, $OTX1$, $OTX2$ and $OTX3$ the three coefficients that must be experimentally determined and κ the measured slippage.

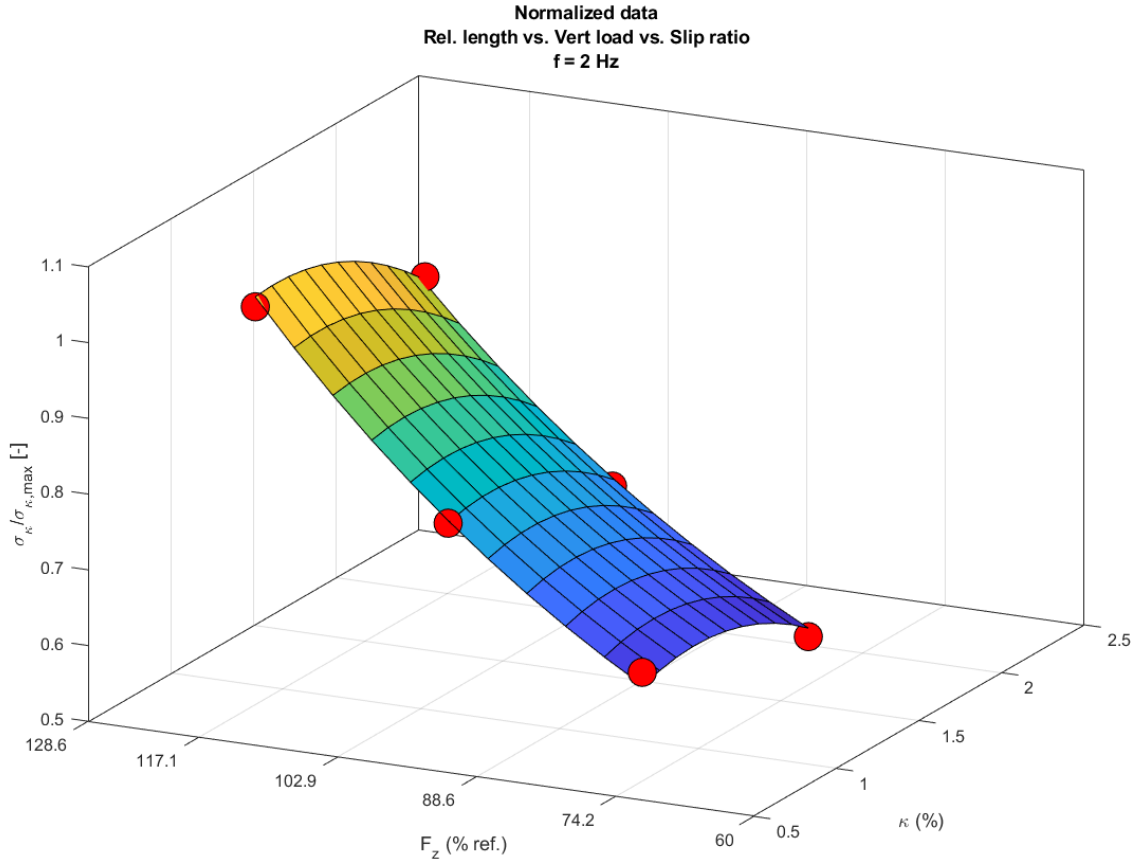

Figure 5-20 - Relaxation length as function of Vertical load and Slip ratio: example of the MF-Relax based interpolation surface, with the red points representing the σ_κ calculated from the filtered data.

The above-shown Figure 5-20 represents the interpolation of the relaxation length with respect to the vertical load and slip ratio, thanks to the MF-Relax model. This approach has been considered for the simulation model that will be described in Chapter 6, where a method for longitudinal relaxation length characterisation from vehicle measurements will be introduced. Moreover, the proposal of a model to fit the dependency between the relaxation length and the excitation frequencies will be shown in the Appendix, Paragraph A.2.

6. Numerical approach and simulation results

The topic of the ABS braking is one of the most studied in the field of the vehicle dynamics. A common approach for the braking manoeuvre study is to model and simulate the main characters influencing the vehicle behaviour: the vehicle, ABS model and tire (Figure 5-1). As part of this study, a Half Vehicle model, a reverse-engineered ABS model and a specific tire model are described in the following paragraphs.

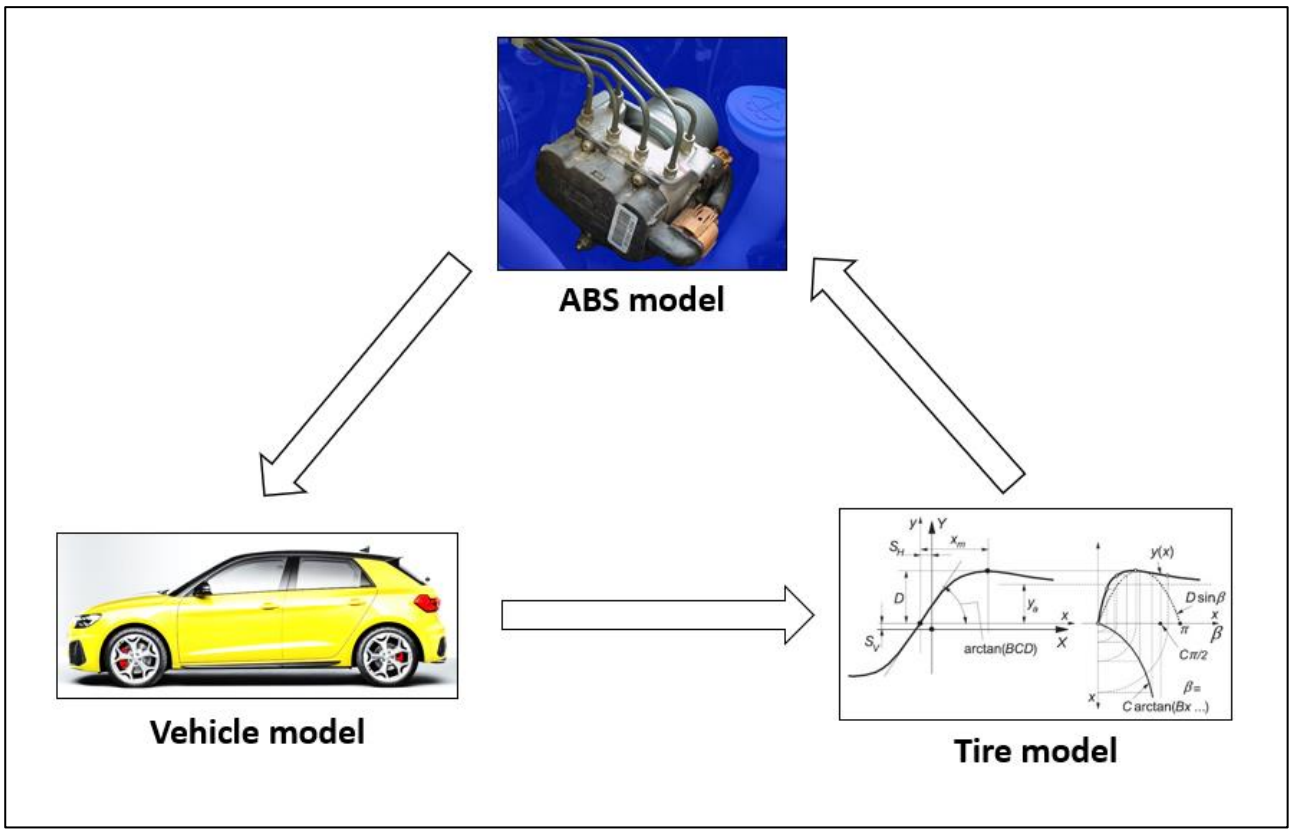

Figure 6-1 – Scheme of the full braking model.

Theoretically, for a complete description of the physical phenomena it would be necessary to consider a large number of variables and parameters. Practically, a series of simplifying hypotheses and approximations are formulated to take into account only the elements that are crucial for the description of the studied phenomena. The model maker must distinguish negligible phenomena occurring in the investigated manoeuvre. The logical steps that allow to solve the problem that we have posed are:

- identification of the real system and the kind of phenomenon;
- identification of necessary and sufficient independent variables to describe the model (Lagrangian coordinates);
- formulation of the physical model to reproduce the phenomenon of the real system that is studied;

- the building up of a mathematical model through the writing of equations (also by means of graphical interface).

Through a series of simplifying hypotheses, we reach the construction of physical and-mathematical models characterized by parameters, such as:

- size and dimensions of the car to be reproduced (see Table 5-1, Paragraph 5.1);
- suspended and unsprung masses of the vehicle, stiffness and damping of the suspension system, etc. (physical).

In order to make the model by considering the basic simplifying assumptions, the first approach could initially be to think about how to realize a very accurate model. However, this choice has some disadvantages, as shown below:

- the mathematical formulations can be extremely complex;
- the number of parameters necessary for the description of the model increases considerably, limiting its flexibility;
- measurements could be difficult for some parameters;
- it is particularly difficult to highlight the causal relationships that link the modelling of the phenomena to the results obtained.

The equations of motion of these physical-mathematical models are then written once the initial conditions are assigned, the equations can be implemented by providing, finally, the laws of motion. Appropriate numerical calculation codes can simulate different kind of test manoeuvres: in fact, it is possible to reproduce "assisted braking" by implementing a control algorithm that performs the functionalities of an anti-lock system.

All the data used for the validation of the model and the analysis which will be shown are made available for use by the Department of Industrial Engineering at University of Naples “Federico II”.

6.1 Half-vehicle model

The vehicle model shown in Figure 6-2 considers the pitching and the additional loading of the front axle during braking [61]. It is mainly based on the assumptions assumed for the vehicle model described in Paragraph 3.1, including suspension compliances. Conversely the rear axle-load is reduced during braking. In the horizontal direction front and rear tire models provide the brake force in response to the wheel slip. The weight of the unsprung masses is neglected; the vertical tire-load variation will contain low frequencies due to the absence of the wheel-hop mode in the model. Furthermore, the road is assumed to be flat. The front and rear axle properties and the front and rear tire parameters have been considered identical on both axles.

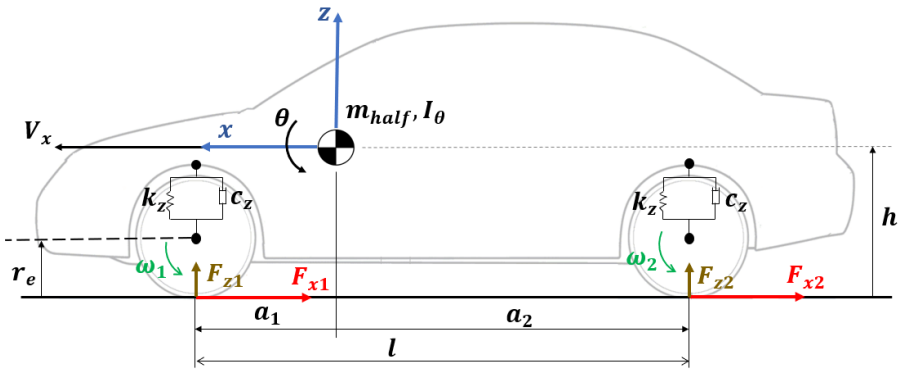

Figure 6-2 - Scheme of the Half vehicle model for the ABS simulations.

The horizontal dynamic:

$$m_{half} \cdot a_x = F_{x,1} + F_{x,2} \tag{6.1}$$

The vertical and pitch dynamics:

$$\begin{aligned} m_{half}\ddot{z} &= m_{half}g - 2c_z\dot{z} - 2k_z z - c_z(a_1 - a_2)\dot{\theta} - k_z(a_1 - a_2)\theta \\ I_\theta\ddot{\theta} &= -(h - z)\left(F_{x,1} + F_{x,2}\right) - c_z(a_1 - a_2)\dot{z} - k_z(a_1 - a_2)z \\ &\quad - c_z({a_1}^2 + {a_2}^2)\dot{\theta} - k_z({a_1}^2 + {a_2}^2)\theta \\ F_{z,1} &= c_z\left(\dot{z} - a_1\dot{\theta}\right) + k_z(z - a_1\theta) \\ F_{z,2} &= c_z\left(\dot{z} + a_2\dot{\theta}\right) + k_z(z + a_2\theta) \end{aligned} \tag{6.2}$$

where z denotes the vertical degree of freedom of the centre of gravity, x denotes the horizontal direction and V_x is the vehicle speed, taken positive in driving direction. Below, the used Simulink half-vehicle model is shown. As it can be seen in the above equations (6.2), for the proposed vehicle model, one of the simplifications that has been considered is that the vertical load is dependent on the elongation of the suspension. The wheel dynamic is shown in Paragraph 6.3.2, equation (6.15). In the following Figure 6-3, an overview of the model as Simulink block is shown.

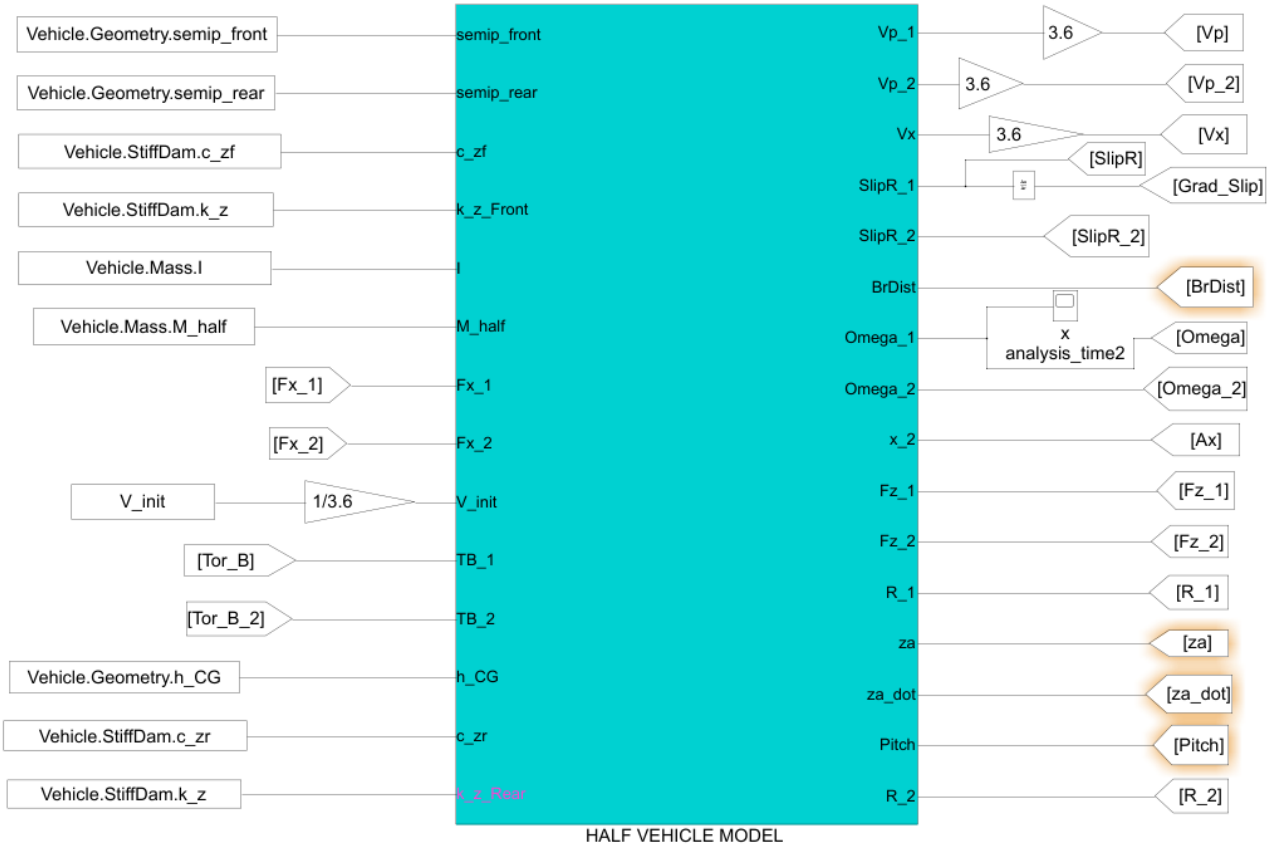

Figure 6-3 - The vehicle model in Simulink environment.

The pitch degree of freedom is denoted with θ. The suspension stiffness is denoted k_z and the damping c_z. The front and rear axles are located at a_1 and a_2 with respect to the centre of gravity. F_z denotes the

normal load and F_x is the longitudinal force taken positive in driving direction in Figure 6-1. Braking typically results in a negative F_x, but in the following paragraphs the $F_x$signal will be considered as positive during braking manoeuvre, for convenience. An additional suffix i is introduced showing "1" for the front axle and a "2" for the rear axle. The moment arm (h-z) of the brake forces will be approximated with h, so by neglecting products of variations, nonlinearity in the pitch model has been avoided.

6.1.1 Validation of Vehicle model

The braking tests considered for the validation have been carried out by starting from an initial speed of 140 kph up to stop the vehicle, with a very low deceleration value in order to avoid ABS activation. A scheme of the used approach for vehicle model validation is shown in Figure 6-4.

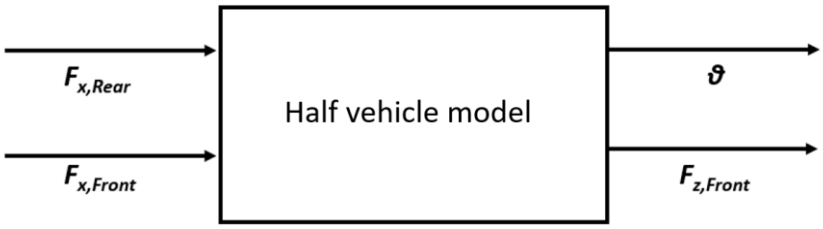

Figure 6-4 - Validation process for the vehicle model.

For a correct validation, it has been useful to give as input the longitudinal force F_x, acquired by a wheel force transducer (Figure 6-5) that has been mounted on the front-right wheel.

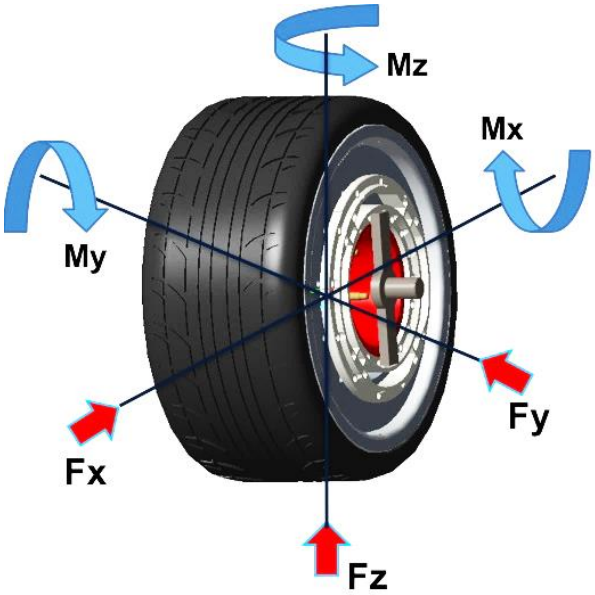

Figure 6-5 – Wheel force transducer measurements.

For the rear longitudinal force a proportional coefficient has been obtained by knowing half vehicle mass, longitudinal force $F_{x,1}$ and longitudinal acceleration a_x. Therefore, by using longitudinal second order differential equation as shown below:

$$m_{half} \cdot a_x = F_{x,1} + F_{x,2} \quad \Rightarrow \quad F_{x,2} = F_{x,1} - m_{half} \cdot a_x \tag{6.3}$$

the tire longitudinal force at the rear axle $F_{x,2}$ has been calculated. In Figure 6-6 the two longitudinal forces at the front (measured) and rear (calculated) axels are shown from the free rolling condition (until around 2 seconds) to the normal braking manoeuvre (from 2 to around 9 seconds). In Figure 6-7 the measured longitudinal acceleration at the CoG of the vehicle model is shown for the not emergency braking manoeuvre. This parameter has been considered as input of the Half vehicle model for the validation.

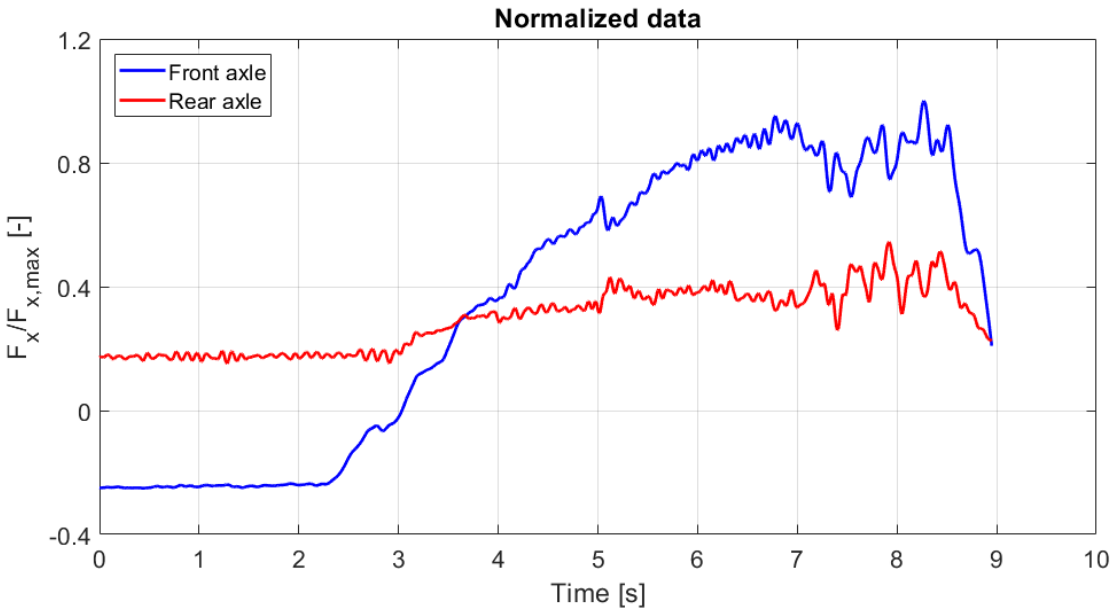

Figure 6-6 - Longitudinal force variation for a normal braking between the front and rear axle (vehicle measurements).

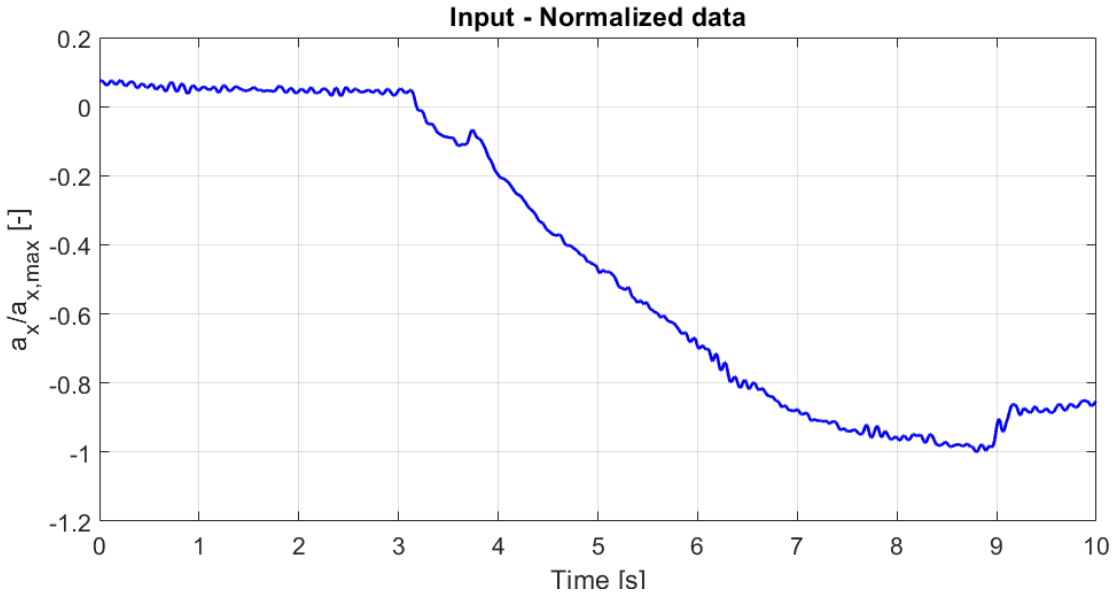

Figure 6-7 – Longitudinal acceleration measured as input of the vehicle model for the validation.

After, the simulated pitch angle θ and vertical load F_z (of the front right wheel) have been considered as the output of the system and compared with the measured ones (Figure 6-8). They are also useful to verify

the entity of longitudinal load transfer, which plays a fundamental role for ABS model work, which will be described in the next paragraphs.

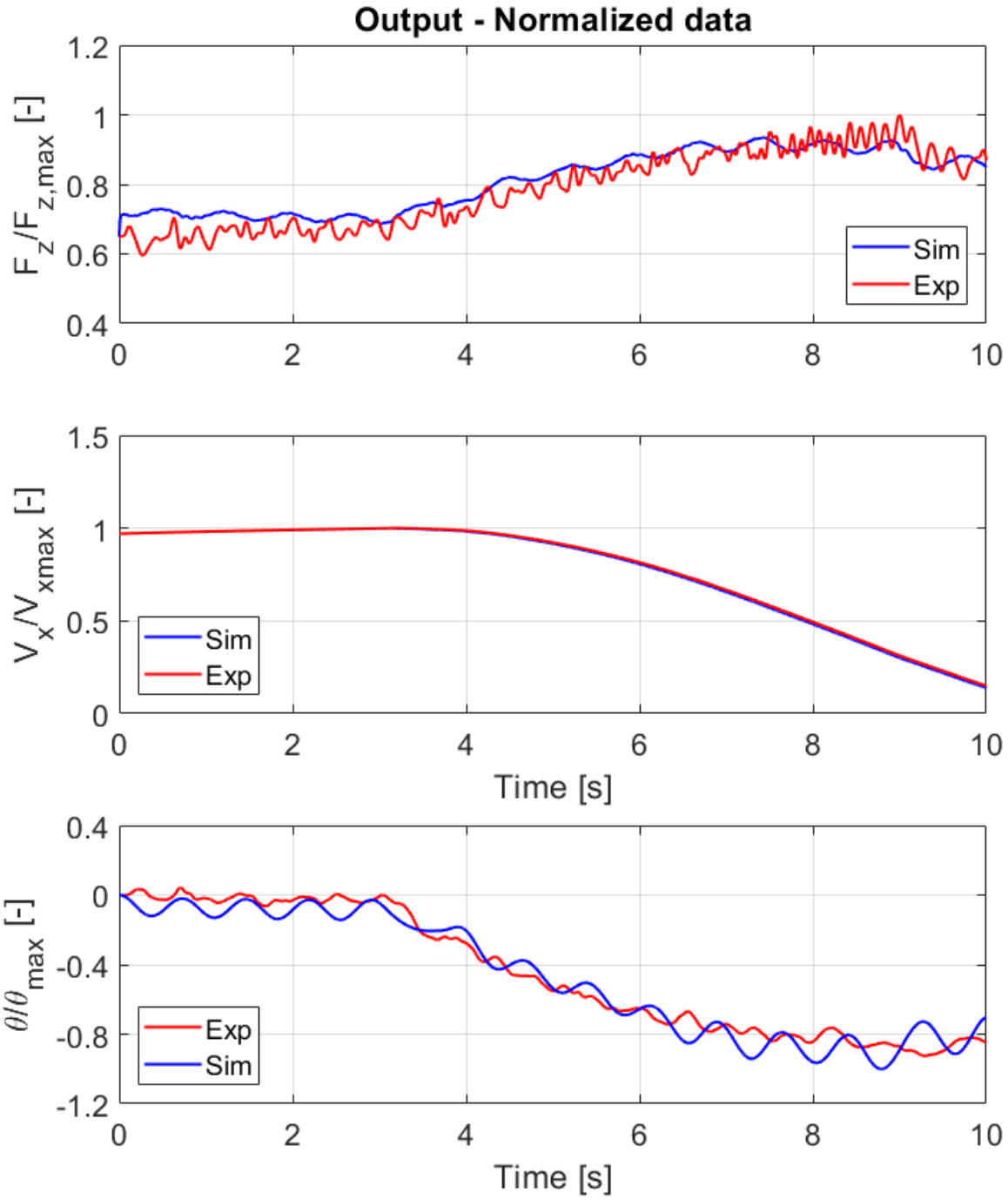

Figure 6-8 - Validation of the vehicle model by focusing on the simulated pitch angle θ and vertical load F_z (of the front right wheel).

6.2 Reverse engineering of a slip-based ABS control logic model

As already mentioned in Chapter 1, normally the ABS logics are based on wheel deceleration and wheel slip. Considering that there are still road surfaces and situations for which ABS could be improved, researchers have been trying to find a more mathematical approach to realize the algorithm. It is supposed

that the ABS could be more stable and robust on more slippery road surfaces. This mainly concerns wet, snowy, and icy roads. As described before, usually it is not possible to clearly know ABS algorithms that are used on current passenger cars. Therefore, a slip-based ABS model will be described in this sub-paragraph, with the aim to allow a good replication of the behaviour of the commercial passenger car's ABS during the emergency braking manoeuvre.

The longitudinal velocity from GPS has been used for the calculation of the of the slip ratio parameter during the braking. There are different ways with which an ABS system can estimate it [1], but a complete ABS logic understanding is not the main goal of this current essay. The assumption that has been made is to consider the V_x coming from the GPS quite similar to the one estimated by the logic itself. Therefore, the simulated longitudinal velocity that has been taken into account is obtained by integrating the longitudinal acceleration at the centre of gravity of the vehicle model.

The proposed logic is based on a PID approach (see Chapter 1) that does not need to be preliminarily tuned in order to set some fundamental slip thresholds that will be predefined per each surface condition. It will be based on a target slip following (see Paragraph 2.2 and Paragraph 3.2) and it will try to reduce the error between the target slip to reach and a specific slip value that can occur during the braking.

The hydraulic circuit of a braking system is an extremely complex system (see Paragraph 3.2). Several assumptions were made with the aim to simplify the modelling approach and remove factors that had low influence on ABS performance:

- the ABS logic is assumed to estimate vehicle speed and monitor wheel slip ratio;
- pressure in the master cylinder is assumed to be a constant value;
- braking torque at the axle is linearly proportional to the pressure in the brake line;
- mechanical delay in converting the pressure in the brake line to torque is taken to be a constant value in time;
- the rate of increase and decrease of pressure during different brake states remain constant and cannot be changed during the simulation;
- a minimum speed is required for the operation of the ABS system below which the braking module switches to manual braking.

An initial identification phase of slip ratio's thresholds is expected for the modelled logic. Some experimental observations showed that this fundamental phases can be found at the beginning of the braking manoeuvre (t_{lag} = 0 ÷ 0.15 s): in fact, the initial shape of brake pressure is the same for all the runs and both specs Tire A and Tire B, where the ABS is still not working. This phase is needed to give the system the possibility to optimize itself: a passenger car can break at several conditions and with different tires. In this sense, it is important to optimize its strategies based on the current tire-road interaction conditions.

In the Figure 6-7, the variability of the brake pressure signals is shown and where it is possible to observe how the same ABS logic can show a different kind of control based on the tire it has to control. In this case, Tire B is allowing a finer control than Tire A.

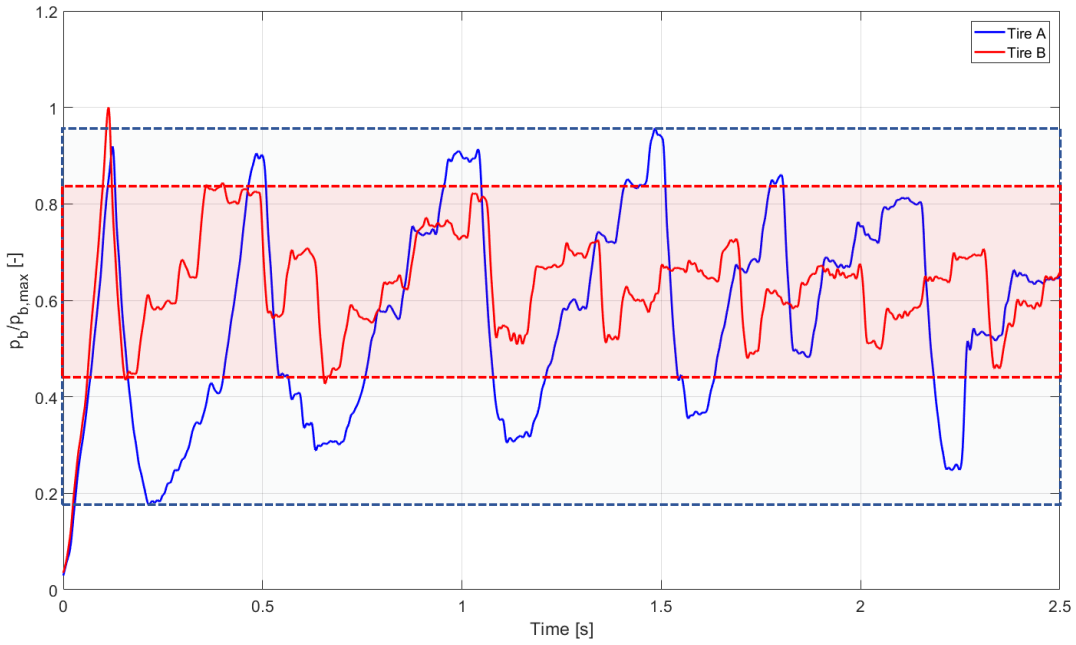

Figure 6-9 - Difference between the 2 studied tires with the same vehicle: the variability of the brake pressure is lower for the Tire B, where the ABS show a finer control. The red line refers to Tire B, the blue one to Tire A. Normalized data.

In the following Figure 6-10, the ABS State-flow model is shown.

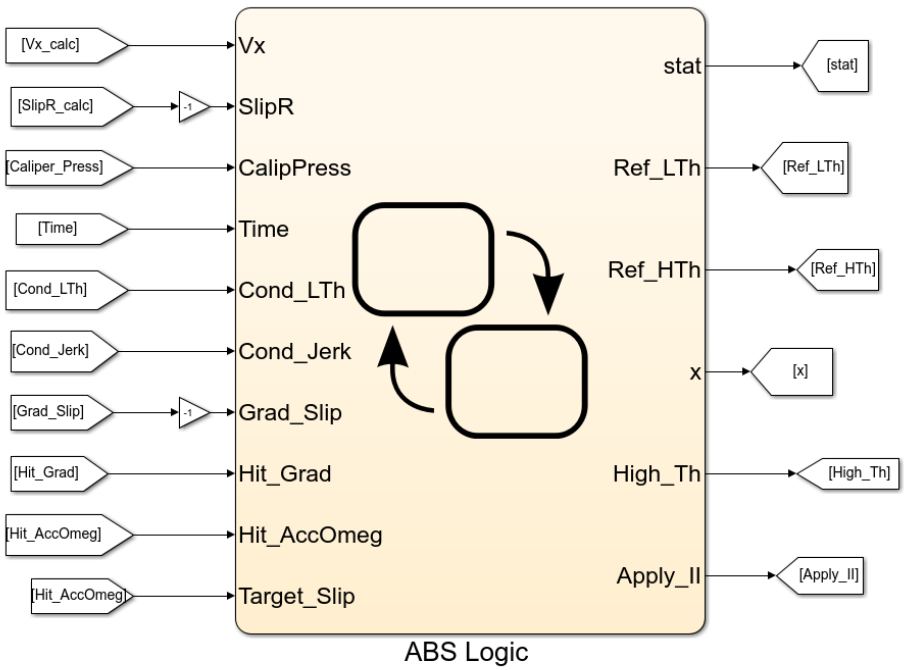

Figure 6-10 - State-flow ABS logic in Simulink environment with inputs and outputs.

There are examples in the literature (Paragraph 2.2) describing how to estimate grip conditions where, in particular, they are based on reference slip ratio values or pre-set look-up tables and pre-fixed thresholds

values that require many tests for their identification [1]. Therefore, the main goal has been to realize a logic in Simulink environment that could reliably represent the ABS operations that have been observed experimentally.

In order to obtain with described above, a reverse engineering of the logic has been made with 2 main purposes. The first one was to try to get more information on the management of the μ-slip curve from braking simulation. Knowing the strategies of the ABS, it can be possible to have a clearer idea on how to handle tire characteristics. The second purpose was to propose a PID slip-based ABS logic which can adapt itself to the tire road interaction characteristics during the check phase which is expected during the initial part of the emergency braking. This model does not need to be preliminarily tuned in order to set particular thresholds because of its physical approach and the use of some conditions on some signals of interest that can help to predict the incoming instability (peak condition).

6.2.1 Inputs and outputs

Target of the proposed logic is to predict tire behaviour without any pre-set value, based on a more physical approach (that means based on the physics of the tire during the wet test) by monitoring signals as the longitudinal slip ratio, velocity and acceleration. Since the ABS unit is responsible for braking control, the proposed model has a limited set of inputs and outputs:

- longitudinal slip and the wheel acceleration, as inputs;
- strategies to control the brake pressure, defined with a mathematical model, as outputs.

In the following figure, the scheme of the required inputs and outputs of the proposed model is shown.

Figure 6-11 – Scheme of the required inputs and outputs of the proposed ABS model.

Therefore, it is possible to divide the ABS work in 2 main sequential actions:

1. “Slip ratio’s thresholds estimation phase” of the current tire-road interaction;
2. Control cycle phase.

The above-mentioned phases will be shown in the following paragraphs. In the following, the “Slip ratio’s threshold estimation phase” is described. The μ-slip curve of tire is estimated in this phase. This estimation indirectly considers different conditions in terms of weather (dry or wet), temperature, tire characteristics (summer, winter or all-season). In this way it is possible to maximize the performance and the braking distance as consequence.

6.2.2 Slip ratio’s thresholds estimation phase

In the Slip ratio’s thresholds estimation phase, the control logic can estimate the tire longitudinal behaviour: the brake pressure linearly increases and the ABS is not working. By monitoring the slip ratio signal and its rate, it is possible to estimate some slip thresholds that represent how the μ-slip curve can manage the slip of that tire in the studied conditions. Differently from the approaches showed in Paragraph 2.2, for the proposed algorithm it is not needed to estimate forces and friction or to pre-set look-up tables:

the longitudinal forces can indirectly be recognized by monitoring slip ratio signal, its rate and wheel acceleration. This is a quite transient phase, where different parameters are changing very quickly. The goal is to set 2 thresholds:

- the *Upper bound*, to identify μ-peak (the transition point between the stable and instable zones);
- the *Lower bound*, to identify the transition zone between the linear and non-linear sections of the curve.

In this way, an Optimal Slip Ratio range is defined (as shown in Figure 3-6), and it represents the target interval where slip ratio signal must be to maximize the performance. The Upper bound definition considers the jerk signal, that is the variation in time of the wheel angular acceleration, as shown in the Figure 6-12, below.

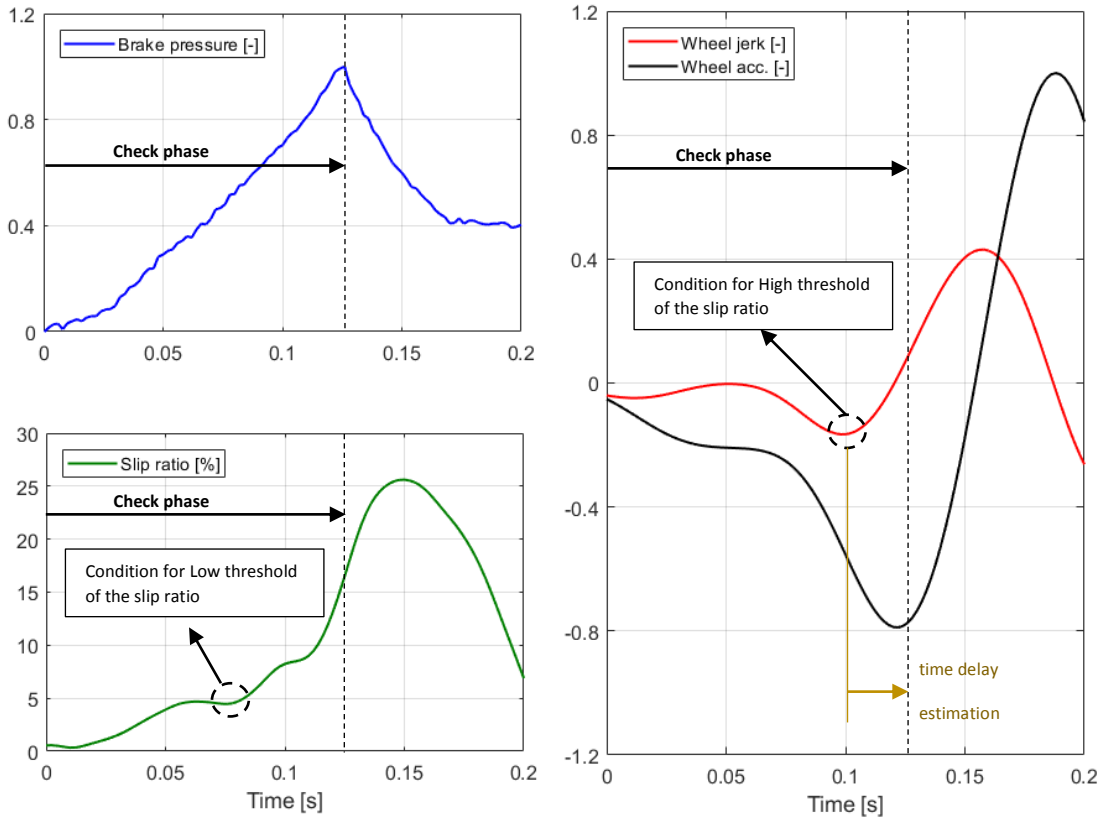

Figure 6-12 - Evaluation of the slip thresholds through the analysis of the wheel acceleration and jerk (normalized data).

Some precursors of instability have been identified by observing the signals and some criteria have been implemented to detect the mentioned precursors. This is a common approach that can be found in the literature to evaluate the instability conditions of a system [62][63]. A criterion to detect the precursor on the wheel jerk has been defined for μ-peak identification: it has been observed that the slip ratio value at the local minimum of the wheel jerk signal corresponds to one at the μ-peak (as shown in Figure 6-12). In order to manage the quite noisy jerk signal, it has been necessary to filter wheel acceleration with a very low cut-off frequency (10 Hz): despite this, a good correlation with the investigated system behaviour can be found, for this specific checking phase. Furthermore, wheel jerk has been also multiplied by a scaling value because of its high values.

In the bottom left picture in the Figure 6-12, it is possible to identify κ values at μ-peak condition through the condition on the wheel jerk signal and, after a constant time lag (experimentally observed), we can observe the brake pressure decreasing.

In order to trigger the Lower bound threshold, it seems to be very important to focus on the inflection points of the slip ratio, as can be observed in Figure 6-12. From the simulation, it has been seen that it can be directly influenced by the relaxation length of the tire (see Paragraph 6.4.1). The scheme in Figure 6-13 tries to explain why the inflection point of the slip ratio signal (measured at the rim) should represent the effect of the relaxation length on the braking.

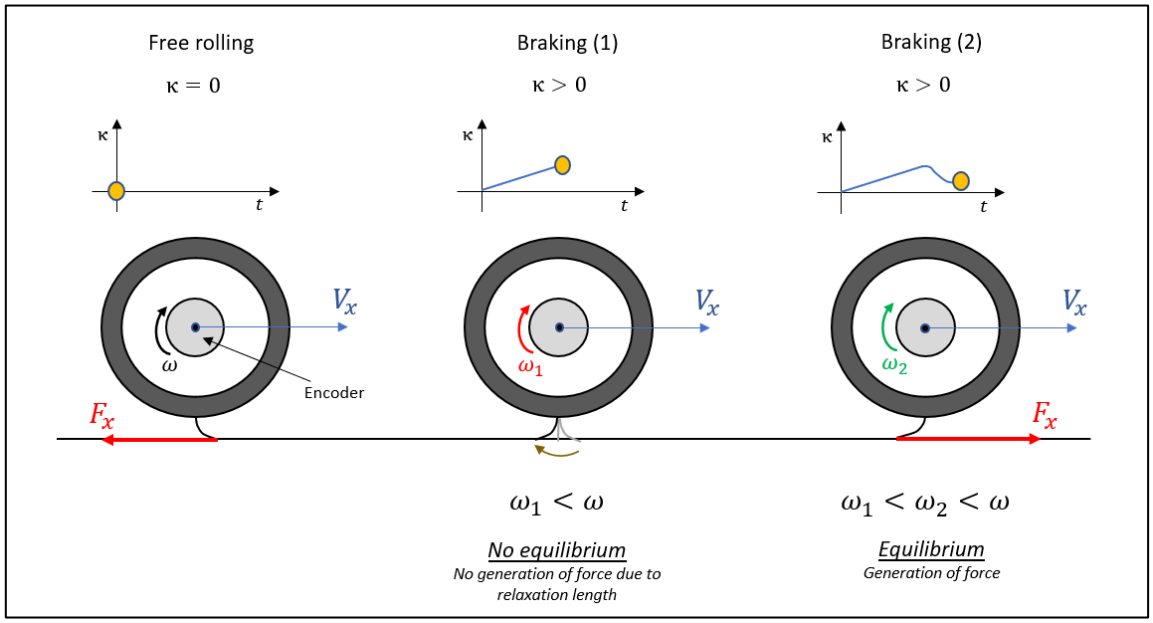

Figure 6-13 – Scheme of the tire behaviour in the initial phase of the braking. Effect of the relaxation length on the estimation of the low slip threshold. The signs are referred to the adapted sign convention used for the braking simulations.

When the emergency braking starts, the slip ratio signal is showing a quite linear increase while the tire is still not generating braking force due to the relaxation length. The sudden generation of the force in Braking (2) is essential for the wheel equilibrium and it leads to a slight wheel acceleration which is represented by the local minimum point in the slip ratio signal.

For this analysis, it has been preferred to filter up to 100 Hz to prevent loss of important information from the acquired signals.

In the following Figure 6-14 and Figure 6-15, the reference thresholds during the slip ratio's thresholds estimation phase are shown: the identified criteria allow identifying for all the 5 runs and both low and upper bounds the analysed specs, with a good approximation.

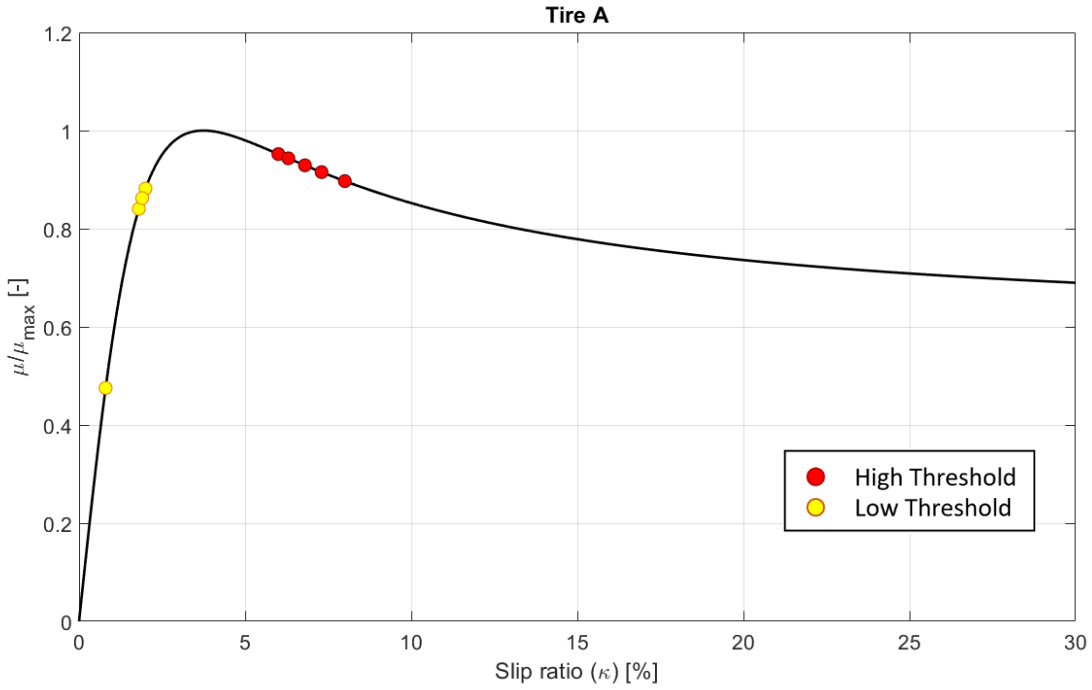

Figure 6-14 - Estimation of the ABS range in the slip ratio's thresholds estimation phase per each run for Tire A. The red points identify the high thresholds, while the low ones are identified by yellow points. Normalized data.

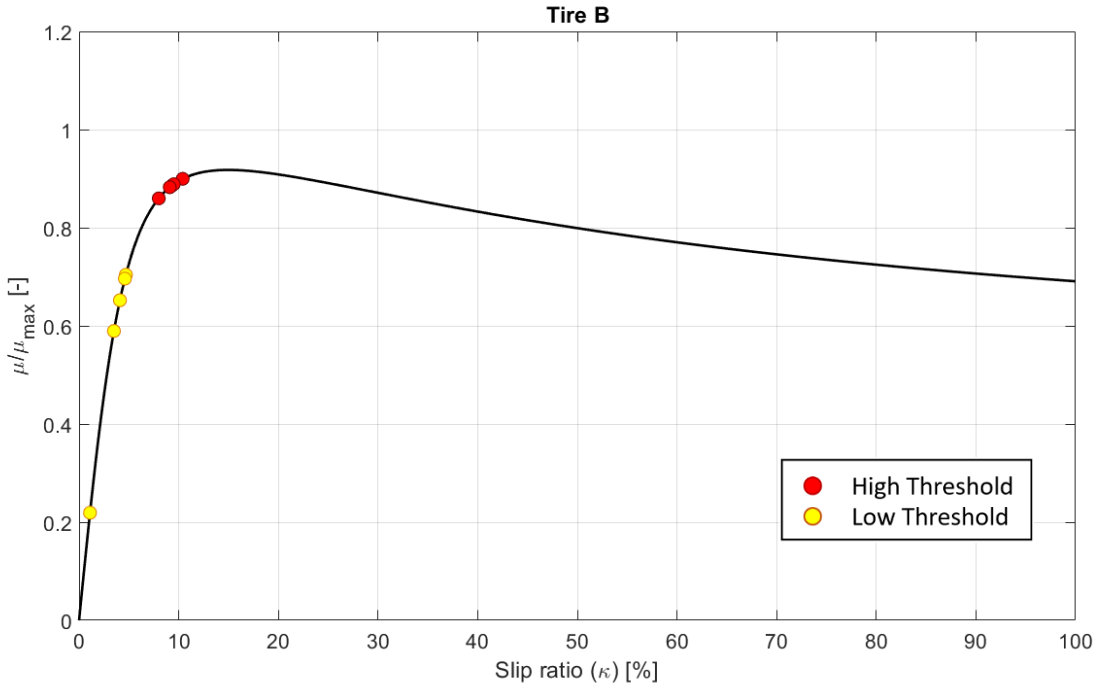

Figure 6-15 - Estimation of the ABS range in the slip ratio's thresholds estimation phase per each run for Tire B. The red points identify the high thresholds, while the yellow ones the low thresholds. Normalized data.

Regarding the peak condition, it is possible to observe the system effort to keep the high threshold very close to the maximum value because of its evident target to obtain, in order of priority, steerability and braking distance reduction.

As shown in Figure 6-12, a time lag t_{lag}can be identified as the delay between ECU computation and effective braking actuations, with which it is possible to find a good correlation with experimental results. After the estimated time lag, the Slip ratio's thresholds estimation phase ends and the 2 thresholds have been set. In the following Figure 6-16 and Figure 6-17, the occurrences of the slip ratio during an experimental braking test have been shown for both the tested tires in order to compare the working area due to the ABS influence and the optimal working range estimated during the Slip ratio's thresholds estimation phase of the ABS model.

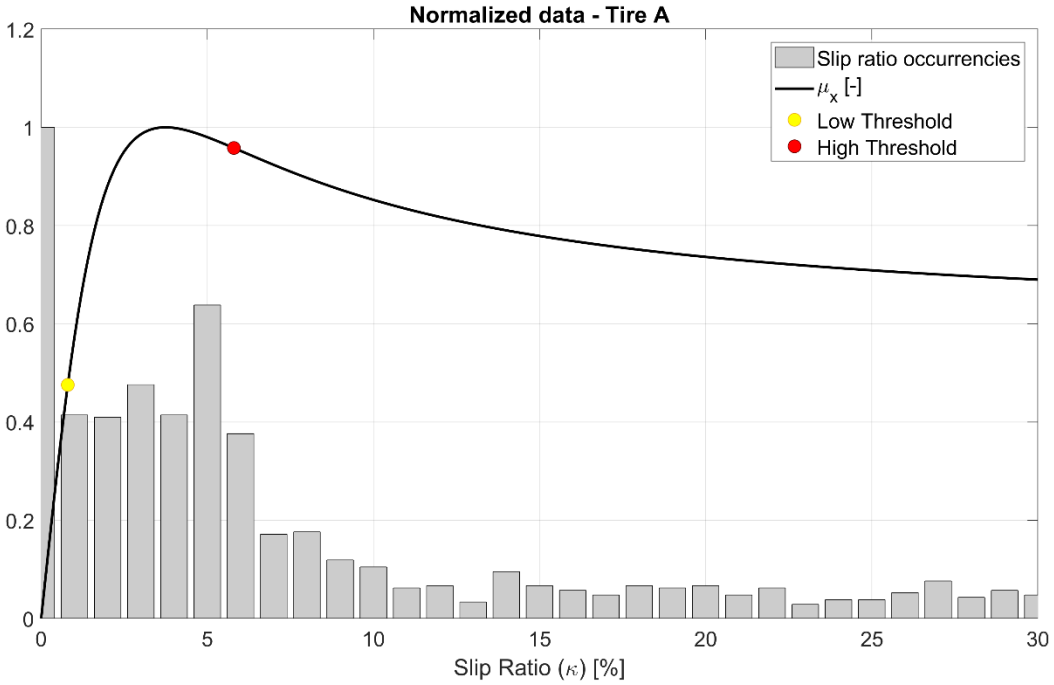

Figure 6-16 - Occurrences of the slip ratio signal during a braking test for Tire A. The red and yellow points identify the working range.

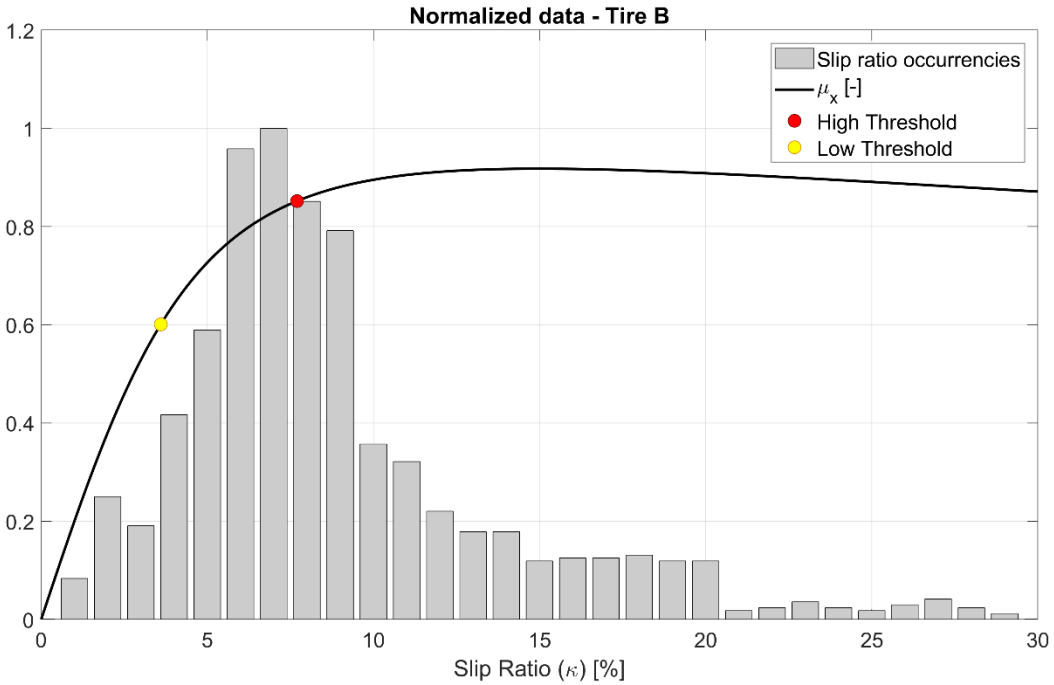

Figure 6-17 - Occurrences of the slip ratio signal during a braking test for Tire B. The red and yellow points identify the working range.

It is significant to consider the slip ratio occurrences are in a certain area where a possible working range is identified. The occurrences allow to know in which area the slip ratio is more present, that is a clear indication of the ABS work. Evidently, there are 2 different areas for the peaky and smooth tires because of the different slip ratio ranges where they reach the maximum grip values. Despite some thresholds updating criteria that can occur, it should demonstrate its capability to keep as fine as possible the optimal κ range during the manoeuvre.

For the reverse-engineered logic, an updating criterion for the reference low threshold is not expected, a clear criterion it has not been identified. Once the above-described thresholds have been set, a new control cycle starts and the control logic tries to keep the longitudinal slip of the tire within the optimal working range. Evidently, the experimental observations have allowed to conclude that the control logic restarts from the reference low threshold set in the slip ratio's thresholds estimation phase at the beginning of a new control cycle, every time.

6.2.3 Control Cycle and updating criteria

The μ-slip curve has been estimated and the optimal working range has been identified in the estimation phase. As consequence, the logic has been able to estimate the reference curve for that braking manoeuvre, where it takes directly into account tire characteristics, weather conditions and temperature by monitoring slip ratio.

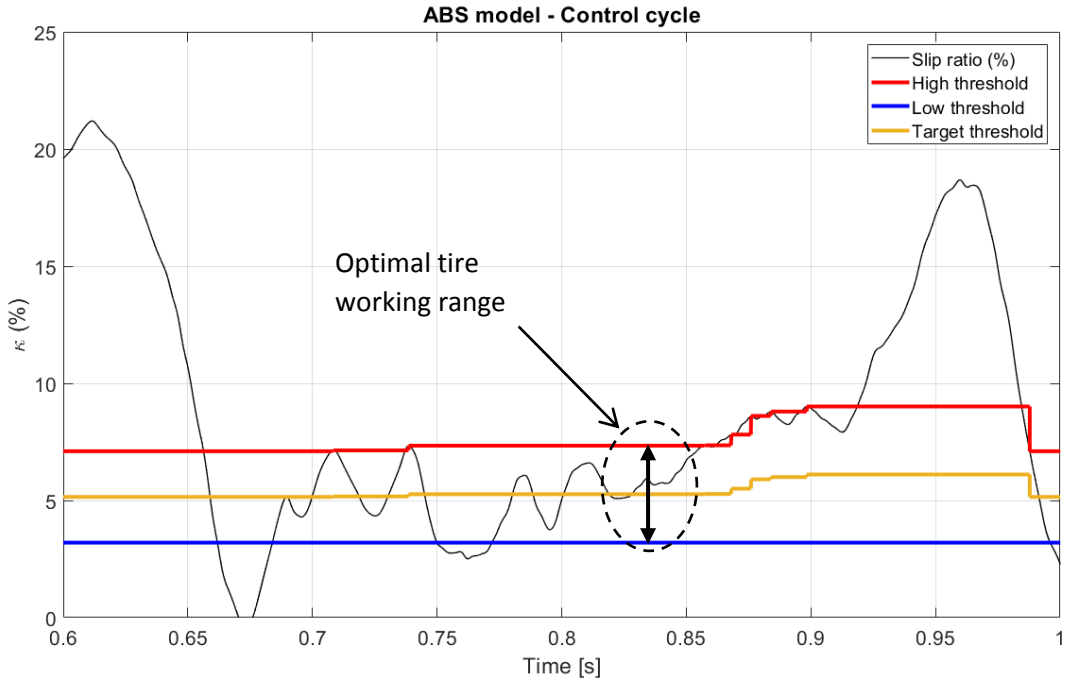

Figure 6-18 – Updating and the High and Target thresholds during a control cycle. The low threshold is kept as constant. The area in between the Low and High thresholds defines the estimated optimal working area of the tire.

As show above in Figure 6-18, after the Slip ratio's thresholds estimation phase some different control cycles are expected to maximize the performance. Initially, they start based on reference slip thresholds but, as the manoeuvre advances, the system can expect thresholds variations, for the upper one. The reverse-engineered criteria for the updating of the upper threshold must respect the following conditions.

If the slip ratio signal is within the range defined by the 2 thresholds set during the estimation phase, no actions are expected from the logic. If slip ratio signal is higher than reference upper threshold, the system will monitor the slip ratio signal variations for a certain time has been defined as "Monitoring Time" t_M, identified around 0.01s.

The criteria consider the following points:

1. If $t < t_M$ and the slip ratio shows a peak and it is showing a decreasing phase after an increasing one, there will be an updating of High Threshold that will be set with the highest reached κ value;
2. If $t > t_M$ and the slip ratio does not show a peak showing only an increasing phase, there will not be an updating of High Threshold that will be kept the same.

The condition 1 expects that control cycle can continue because of the absence of instability issues; the condition 2 expects the reaching of the μ-peak and, after that, the damping phase the ABS can restart with a new control cycle by stating for reference thresholds identified during slip ratio's thresholds estimation phase.

The reverse-engineered model considers the updating of the only upper threshold. This means that it considers μ-slip curve variations which are not always the same because of different causes (such as longitudinal velocity or hydroplaning) and, therefore, it expects μ-peak variations during the braking (see Paragraph 7.2.1).

6.2.4 Brake pressure mathematical model

Another aspect, that cannot be underestimated, is a good brake pressure modelling. It is clear that a reliable response of brake pressure into the brake chambers is needed, because of different torques with which brakes will stress the tire structure. Therefore, it is important to have the correct response, in order to expect the ABS behaviour as close as possible to real working. In an ABS system, the brake pressure is regulated by means of electromagnetic valves that are installed in the Hydraulic Control Unit (HCU) [10]. The pressure can be regulated through three states:

- Apply, where the pressure is increased;
- Hold, where the pressure is kept as constant;
- Dump, where the pressure is released.

As already specified at the beginning of this paragraph, the braking torque at the axle is linearly proportional to the pressure in the brake line, by following the equation below:

$$T_b = Gain \cdot p_b \tag{6.4}$$

with

$$Gain = 2 \cdot A_p \cdot \mu_{brake} \cdot R_p \tag{6.5}$$

where the $2 \cdot A_p$is the area of the pistons on the brake disk, $\mu_{brake}$is the friction coefficient when the piston and the disc are in contact and the radius R_p is the between the centre of the piston and the centre of the disc.

In the literature it is possible to find similar approaches [10]. In this essay, the hydraulic brake has been modelled with a mathematical approach as shown below:

$$\begin{aligned} p_{APP}(t) &= p(t_{i-1}) + c_{app,1} t_i; \\ p_{DUMP,1}(t) &= p(t_{i-1}) + c_{dump,1} t_i + c_{dump,2} {t_i}^2, \\ p_{DUMP,2}(t) &= p(t_{i-1}) + c_{dump,3} t_i; \\ p_{HOLD}(t) &= p(t_{i-1}) + c_{hold,1} t_i + 2{t_i}^2. \end{aligned} \tag{6.6}$$

It has been observed that a specific set of coefficients cannot be considered for all the tires characteristics and surface conditions. In fact, based on the external conditions, some different brake strategies and different sets of parameters must be considered for the above-mentioned mathematical relationships, in order to validate the reverse-engineered model. It will be discussed in the next paragraph.

6.2.5 Validation of the reverse engineered ABS logic

For the validation of the control logic, it has been necessary to consider that for the correct work of the brake model has to be tuned. A set of 10 parameters (2 of them for the “Slip ratio’s thresholds estimation phase”, while the other 8 ones related to the “Applying”, “Holding” and “Damping” phases) of the brake model will be taken into account for the tuning. These parameters have been optimized based on the outdoor test results: as for a common ABS logic, the slip ratio will be considered as input signal, while the brake pressure as the output of the model to validate. The validation will be handled by comparing the simulated and experimental brake pressure signals, by setting specific thresholds for the correlation coefficients between the simulated and experimental signals [64].

In the following Figure 6-19, the setup of the complete model for validation is shown. For the validation phase of the logic, the vehicle model is not required: the goal is to feed the model with the experimental slip ratio signal that is the results of the combination of the vehicle and tire work.

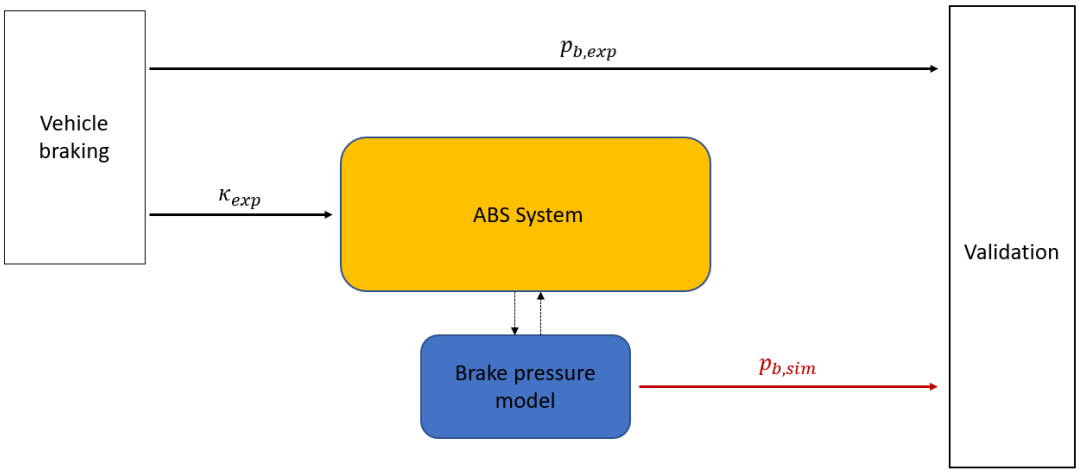

Figure 6-19 - Setup of the full emergency braking model used for the validation.

The optimization has been conducted by considering the Matlab function "lsqnonlin" [65], that solves nonlinear least-squares (nonlinear data-fitting) problems.

$$x = lsqnonlin(fun, x_0) \tag{6.7}$$

As shown in the equation above, it starts at the point x_0 and finds a minimum to the sum of squares of the functions described in function *fun*.

Moreover, it is possible to set or change the values of these parameters using the setup of the optimization, with the Matlab function "optimset".

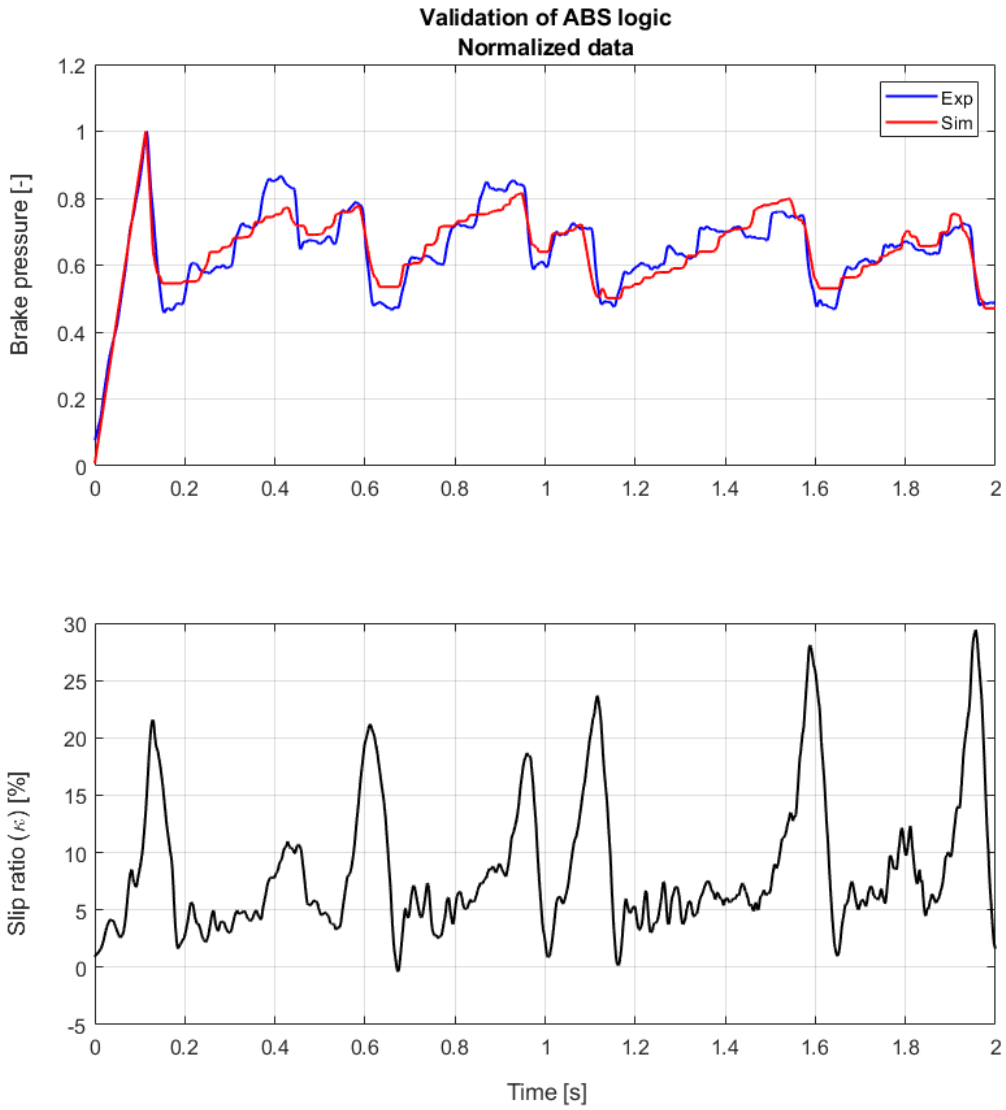

Figure 6-20 – Example of validation of the state-flow ABS logic in the case of Tire B, with the identification of the parameters related to the brake pressure.

Looking at the simulated and experimental signals in Figure 6-20, it can be observed that the reverse-engineered model can show a good replication of the investigated braking system. This result is quite important for two main reasons: the first one is that it shows that despite the alternative estimation approach, the model can allow to get results close to the real system, while the second reason is that the described ABS model can help in the understanding of the interaction between system and the tire.

6.3 Tire modelling for braking simulation

Regarding the emergency braking manoeuvre, the pure longitudinal slip equations can reliably replicate tire behaviour. In fact, in an emergency braking test, the effect of lateral force and self-aligning moment can be neglected.

The following equations:

$$\begin{gathered}\kappa_x = \kappa + S_{Hx} \\ C_x = PCX1\ \lambda_{Cx} \\ D_x = \mu_x\ F_z \\ \mu_x = (PDX1 + PDX2 \cdot dF_z)(1 - PDX3 \cdot \gamma^3)(1 + PPX3 \cdot dp_i + PPX4 \cdot {dp_i}^2) \\ E_x = (PEX1 + PEX2 \cdot dF_z + PEX3 \cdot {d_{fz}}^2)(1 - PEX3 \cdot sgn(\kappa_x))\ \lambda_{Ex} \\ K_{x\kappa} = (PKX1 + \mathrm{PKX2} \cdot dF_z) exp(PDX3 \cdot dF_z)(1 + PPX1 \cdot dp_i + PPX2 \cdot {dp_i}^2) F_z \lambda_{Kx\kappa} \\ B_x = \frac{K_{x\kappa}}{C_x D_x}\end{gathered} \tag{6.8}$$

are referring to the longitudinal equations describing the steady-state conditions of the tire. Moreover, the shift factors are shown in the equations (6.10):

$$\begin{gathered}S_{Hx} = (PHX1 + PHX2 \cdot dF_z)\ \lambda_{Hx} \\ S_{Vx} = (PVX1 + PVX2 \cdot dF_z) F_z\ \lambda_{Vx} \lambda_{\mu x}\end{gathered} \tag{6.9}$$

which are considered as zero in this essay. When the inputs are far outside the measurement range (e.g. extremely high vertical loads or very large inclination angles) the extrapolation capabilities of the model can possibly fail. Therefore, as shown below:

$$\begin{gathered}\kappa_{min} < \kappa < \kappa_{max} \\ \gamma_{min} < \gamma < \gamma_{max} \\ p_{i,min} < p_i < p_{i,max}\end{gathered} \tag{6.10}$$

the slip rato, camber angle and inflation pressure must be kept within the mentioned range for reliable results. In the following work, it has been considered two different approaches: the classical calculation of the relaxation length as the only function of the vertical load and the alternative "MF-Relax model" proposed by Braghin et al. [40], where the relaxation length is a function not only of the vertical load but also of the slippage (see Chapter 5, Paragraph 5.2.3).

The first step towards the determination of the longitudinal contact force in transient manoeuvres is the calculation of the relaxation lengthσ_κ that is a function of just the applied normal load F_z,

$$\sigma_{\kappa,slip} = \left(\sigma_{\kappa,Fz} - OTX1\right) e^{-OTX2 \cdot \kappa} + OTX1 + OTX3 \cdot \kappa \tag{6.11}$$

where $OTX1$, $OTX2$, and $OTX3$ are three parameters that have to be determined experimentally from vehicle data (Paragraph 6.3.3), $\sigma_{\kappa,Fz}$ is the relaxation length from the MF-Tire model and κ is the longitudinal slip of the tire. The scaling factor related to this equation that takes into account the influence of the road conditions and of the vehicle is neglected in this work. Once the relaxation length is known, the following first order differential equation in the longitudinal deformation of the tire carcass u is solved:

$$\sigma_\kappa \frac{du_x}{dt} + |V_x| u_x = -\sigma_\kappa \kappa \, V_x \tag{6.12}$$

with V_x being the longitudinal speed component of the hub and κ: being the slippage. From the longitudinal deformation of the tire carcass u_x, the equation (6.14):

$$\kappa' = \frac{du_x}{dt} sgn(V_x) \tag{6.13}$$

allows to determine an equivalent slippage κ'. Finally, it is possible to calculate the longitudinal tire -road contact force:

$$F_x = F_x(\kappa', \gamma, F_z) \tag{6.14}$$

through the well-known steady-state MF-Tire model equations. Below, an overview of the Simulink tire model is shown in the Figure 6-21 below.

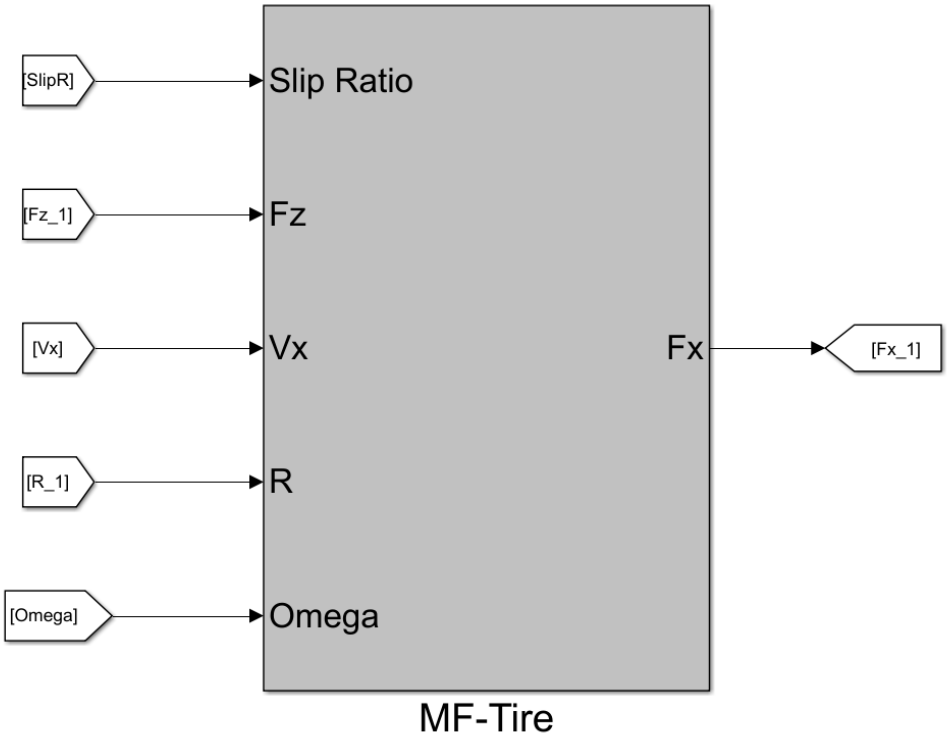

Figure 6-21 - Tire model including the MF-Relax for transient behaviour, implemented in Simulink environment.

6.3.1 Tire characterization approaches on wet surfaces from vehicle data

It is expected that tire performance can change between dry and wet surfaces under the same conditions. During this research work, it has not been possible to characterize tire longitudinal behaviour on the indoor test rig in wet conditions for both the studied tires Tire A and Tire B, while it has been possible to measure the longitudinal force of the same tire with a trailer on the proving ground, in wet conditions, at an only vertical load. Moreover, some alternative procedures have been considered to characterize the transient

and steady-state behaviours from vehicle and trailer measurements (that will be shown in the Appendix of this Thesis).

Therefore, the methods to characterize the tire models are listed below:

1. adapting the reference Pacejka's coefficients [57] to the longitudinal force curves got from tests with trailer in wet conditions at the testing normal load;
2. the longitudinal relaxation length of the tested tires estimated from vehicle data (transient behaviour).

Below, a description of the step 1, that has been adopted to characterize the tire models used for braking simulations is depicted (Figure 6-22).

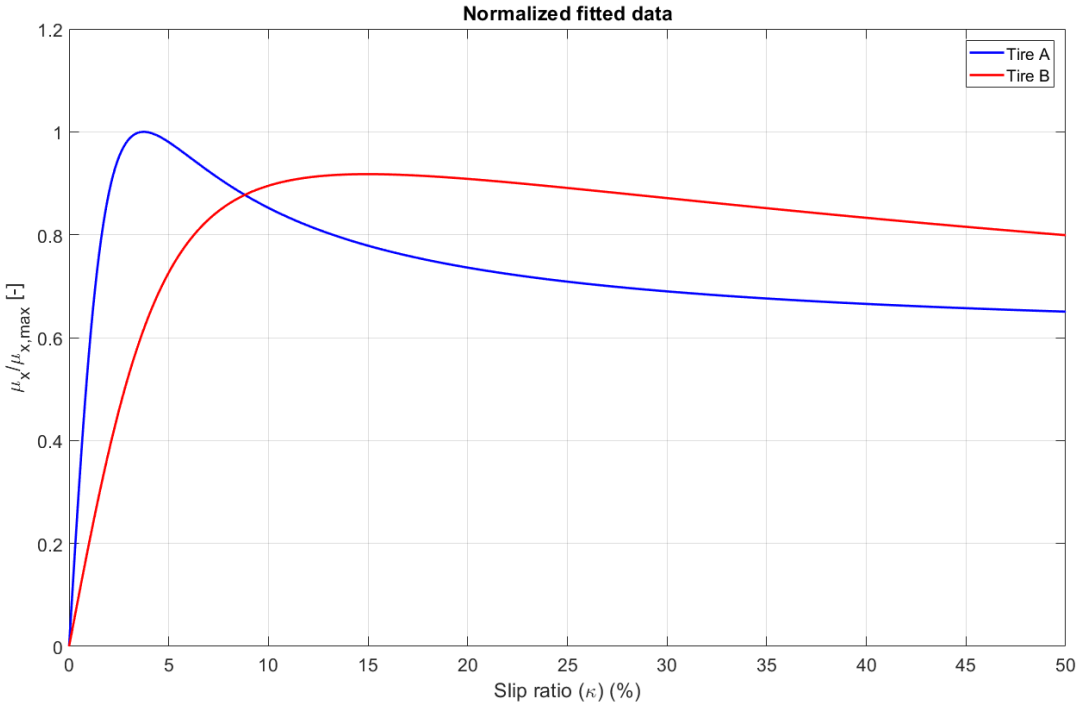

Figure 6-22 - Normalized curves of the studied tires in wet conditions.

In the Figure 6-20, it is possible to observe how the tires behave at the maximum reachable vertical load. Some specific microparameters from Pacejka's MF-Tire model have been modified in order to replicate the same shape that is possible to see from outdoor tire characterisation with trailer. In particular, the coefficients $PCX1$, $PEX1$, $PEX2$, $PEX3$ and $PEX4$ have been optimized to reach the proposed aim; they represent, respectively:

- Shape factor for longitudinal force ($PCX1$);
- Longitudinal curvature at nominal vertical load ($PEX1$);
- Variation of curvature with vertical load squared ($PEX2$);
- Factor in curvature while driving ($PEX4$).

Once reached the desired shape, the tire model remains constrained to the same load sensitivity of the reference model. In order to characterise the load sensitivity of the tire, an alternative method will be proposed in the Appendix (Paragraph A.1), where the load sensitivity of the tested tires is estimated from the vehicle data (at the steady-state behaviour).

6.3.2 Calculation of longitudinal force, vertical force and slip ratio

The longitudinal force F_x, it can be usually measured thanks to a wheel force transducer that can replace the rim, but its use was not considered during ABS braking tests because of its big mass and moment of inertia could affect the ABS work, not allowing to obtain realistic results. The method proposed in this research work allows to estimate the longitudinal and vertical forces from vehicle measurements.

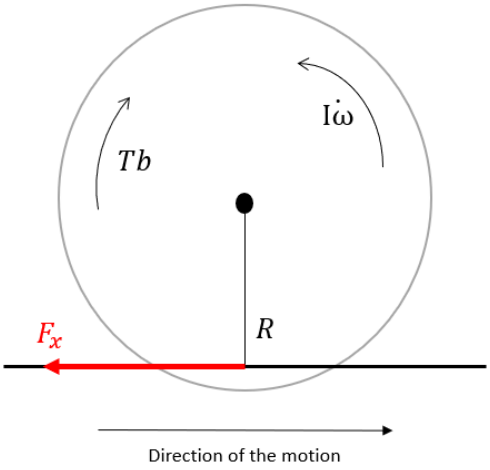

Figure 6-23 - Wheel equilibrium.

Therefore, it has been preferred to carry out with common rims, in order to avoid any influences on ABS work (see Paragraph 6.2). For the proposed calculations (6.14) and (6.15), the wheel equilibrium:

$$F_x = \frac{T_b + I \cdot \dot{\omega}}{r} \tag{6.15}$$

has been isolated, as shown Figure 6-23. The same has been repeated for the vertical load F_z. A calculation of this force is proposed [43]:

$$F_z = a_x \cdot m_{half} \cdot \frac{h}{l} + F_{z,0} \tag{6.16}$$

by focusing on the vertical load variation of the front axle. With the mass m_{half}, the analysis is directly related to one tire of the front axle, since vehicle is considered symmetric as one of the initial hypotheses. In the Figure 6-23, the longitudinal slip and the calculated longitudinal force and vertical load are shown.

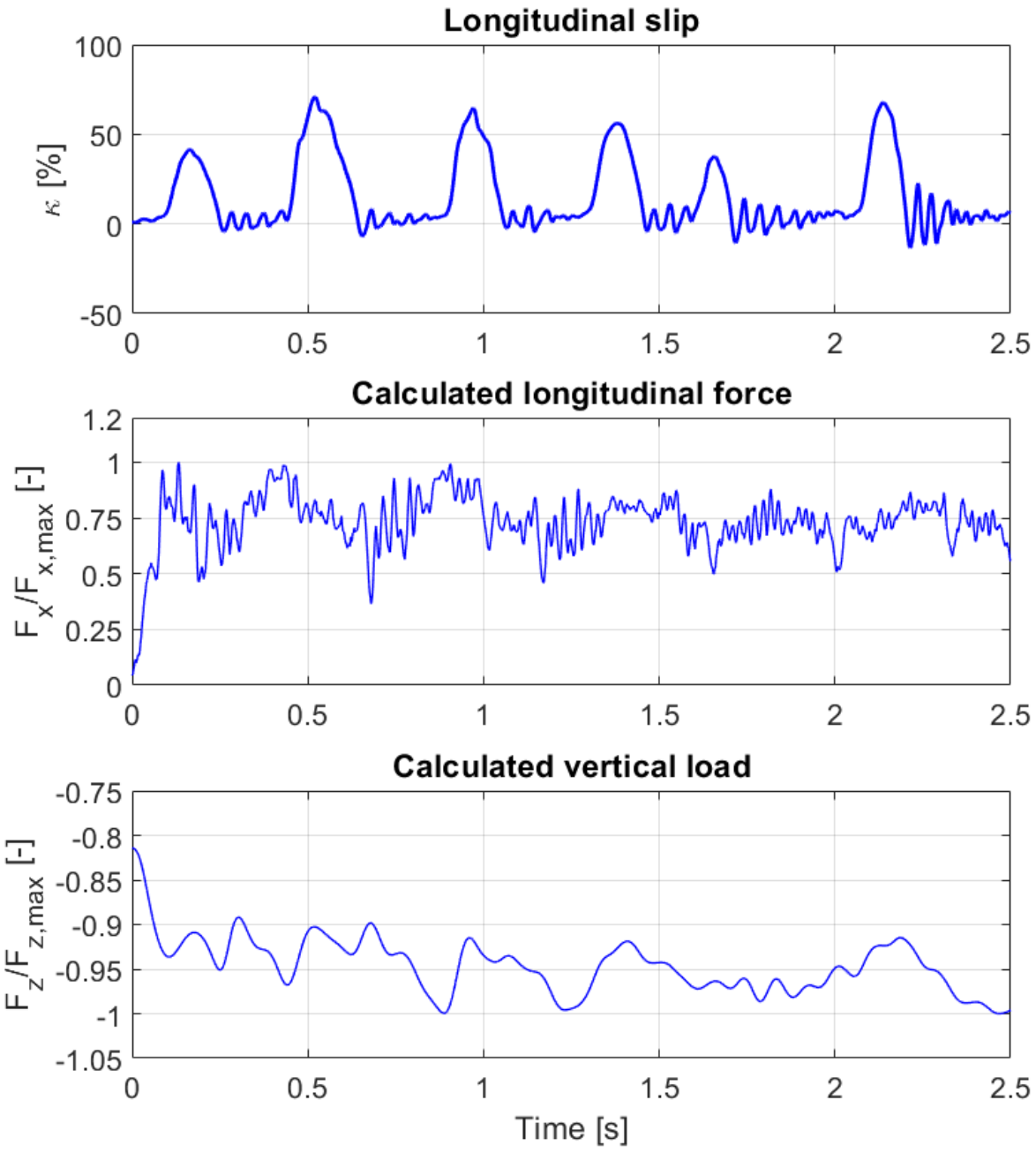

Figure 6-24 - Calculated F_x and F_z from vehicle data.

For convenience, a positive F_x (differently from what has been defined in Paragraph 4.5.1 and already shown in Figure 6-24) and a negative F_z will be considered. The vertical load that has been used corresponds to the maximum one reachable from the test vehicle, after the effect of the longitudinal load transfer that occurs during an emergency braking manoeuvre.

6.3.3 Estimation of the longitudinal relaxation length from vehicle measurements

Normally, a good correlation between both indoor and outdoor results is important for the validation of the procedures that have been made and the use of more reliable results and simulations [66][67]. In the current paragraph, a method for tire relaxation length calculation is proposed from vehicle measurements during the emergency braking test. It is important to mention that it has been necessary to calculate some quantities for this purpose (that were not possible to be measured), as shown in the last paragraph. This can also be considered as an approach to allow the relaxation length characterisation in wet conditions (that is not possible to do with indoor test benches).

The test can be considered at the steady-state conditions with regards to the vertical load and the camber angle. In fact, the estimated vertical load at which the data have been obtained it is always the same, around F_z = 4700N, while the camber angle can be considered as constant. A different assumption must be done for the longitudinal velocity, which is decreasing during the braking. Therefore, the results will be affected from the influence of the longitudinal velocity, as also shown in Paragraph 0 (the lower the longitudinal velocity, the lower the relaxation length). Looking at the equations related to the MF-Tire model (5.8) and related to the MF-Relax model (5.9), it can be assumed that there is not a direct dependency on the longitudinal dependency on the longitudinal velocity from the investigated models (even in the case of the MF-Relax model, where the dependency on the longitudinal slip can be seen as the a combined effect of the longitudinal velocity and peripherical velocity of the wheel). In fact, the longitudinal velocity is introduced in the first order differential equation (4.43).

For the calculation of the relaxation length, it has been calculated the delay between the peaks of slip ratio and F_x sinusoidal signals, similar to the approach described in the above-mentioned paragraph. In order to characterize the longitudinal relaxation length from vehicle measurements, the linear area of the longitudinal curve has been taken into account (Figure 6-25).

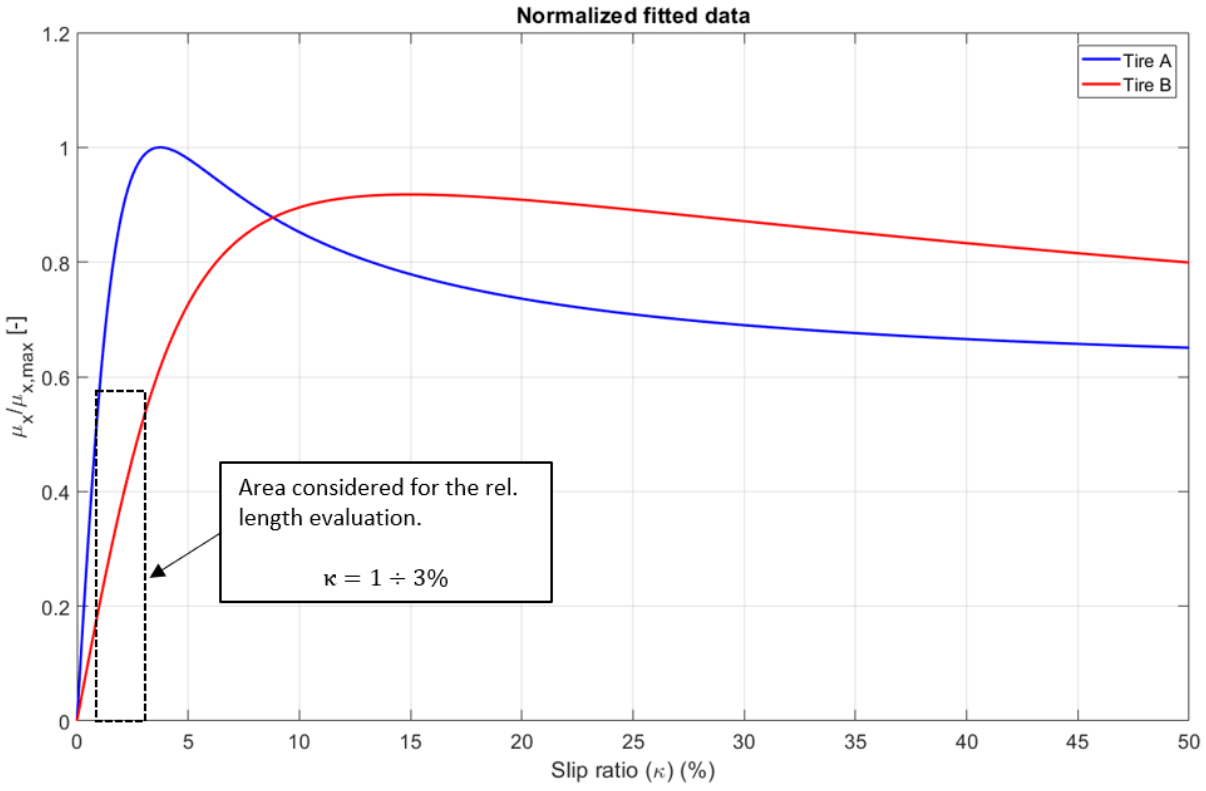

Figure 6-25 - Slip ratio range considered for relaxation length evaluations.

The first step of the procedure has been to consider the Fast Fourier Transform, since the Fourier analysis converts a signal from its original domain to a representation in the frequency domain and vice versa. In this way it is possible to get the amplitudes of the periodic signal of interest and at which frequency they are associated, as shown in Figure 6-26.

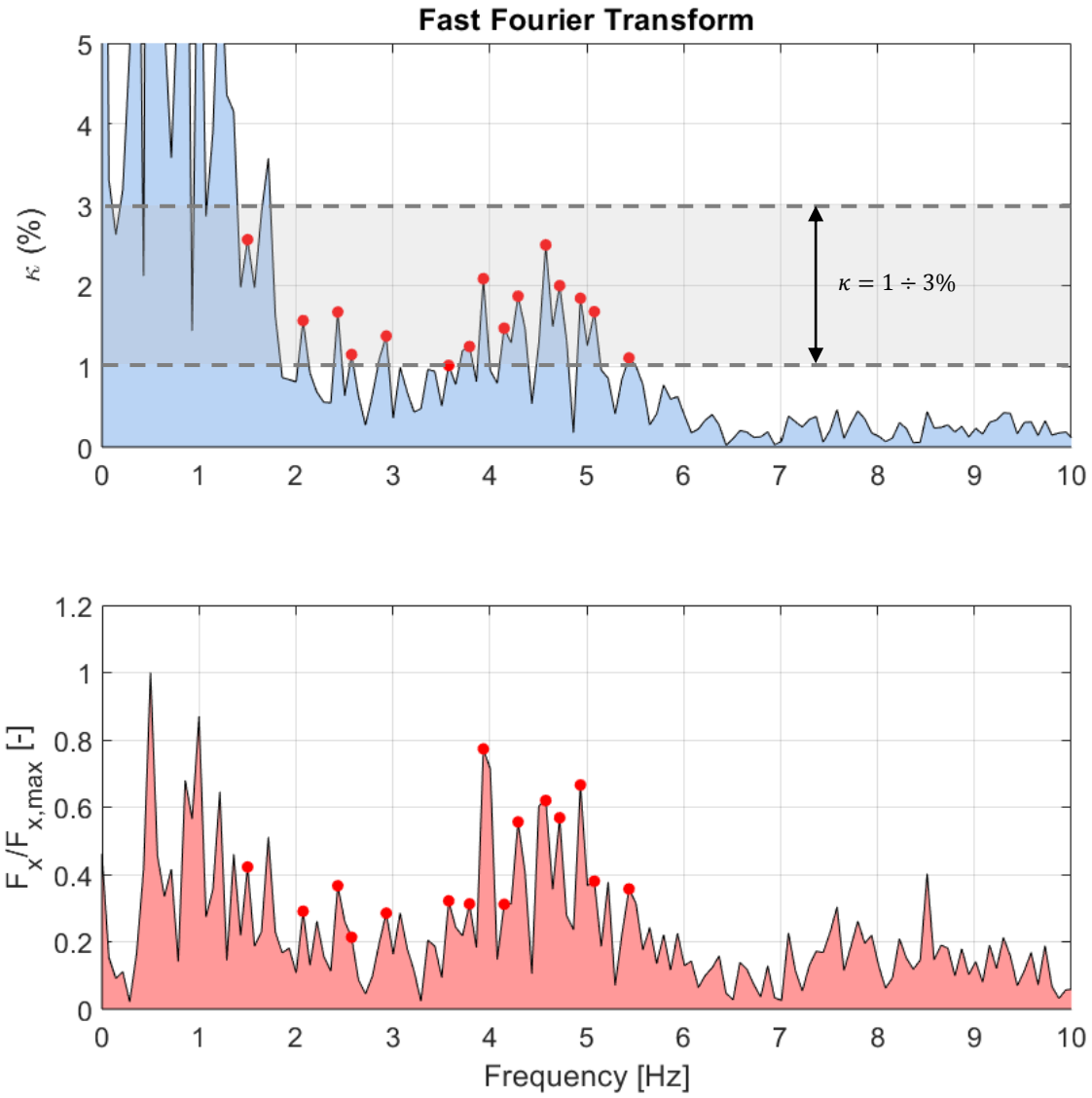

Figure 6-26 - Frequency analysis of the Slip ratio and Longitudinal force for Tire A and B during a whole braking run.

It is assumed that the range of slip is usually considered around 1-3 %, in order to try to keep a common slip range that can be found during the control cycle of the logic, before leaving the stable zone of the longitudinal curve (peak condition), as shown in Figure 6-23. In Paragraph 5.2 it is shown that at 2% of longitudinal slip, the tyre can already show a nonlinear dependency between the longitudinal force and the longitudinal slip itself (at least at low frequencies). However, it is also dependent on the tire characteristics and a not direct correlation of the results can be carried out between Paragraph 5.2 and the current one, since the tires are different. In any case, the MF Relax model may be able to catch relaxation length at different slip ratio (even in the nonlinear response of the tire) and then fit the different relaxation length values at different amplitudes of the slip.

Therefore, above shown amplitudes of the slip ratio signal have been selected, in the range 1-3%. The same peaks have been also useful to select the ones related to the longitudinal force. In this way, it can be possible to generate sinusoidal signals at different amplitudes and frequencies.

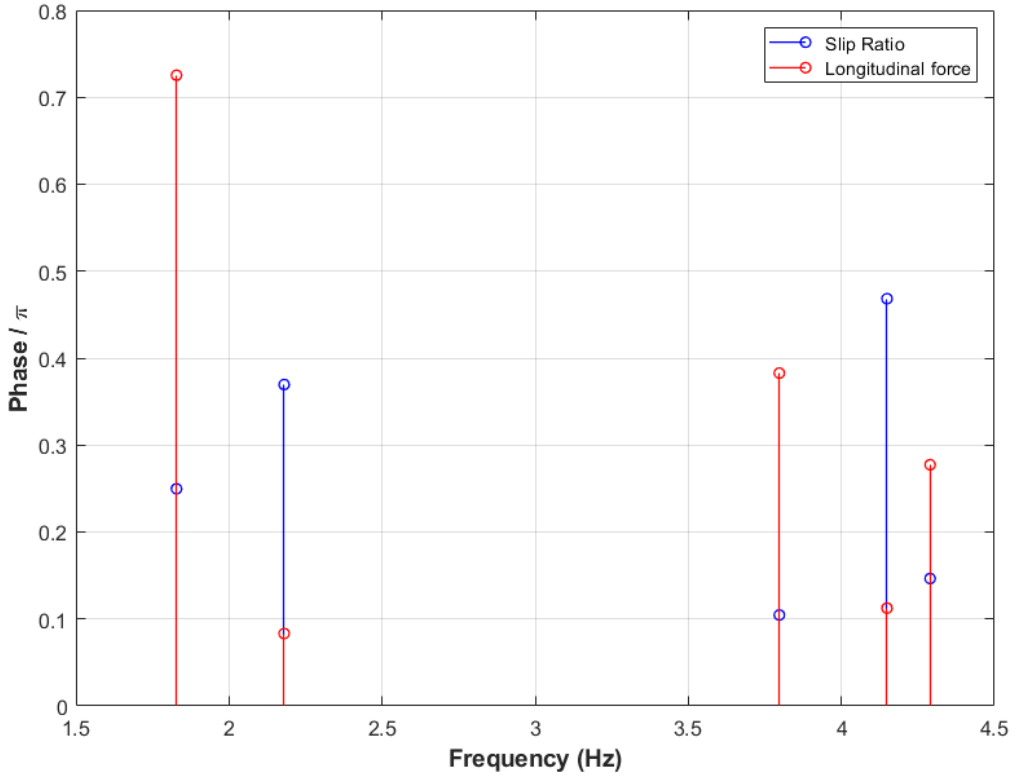

Figure 6-27- Phase delay between Slip Ratio and Longitudinal Force.

Moreover, the phase between the two signals is calculated, as shown in Figure 6-27. With this approach, it is possible to create the conditions to calculate the relaxation length, at different slip ratio amplitudes and frequencies. It is possible to see a trend of the relaxation length with respect to the slip ratio, even if the spread looks like quite wide (Figure 6-28 and Figure 6-29). This can be evaluated as a similar trend to the ones shown and analysed in the Paragraph 5.2

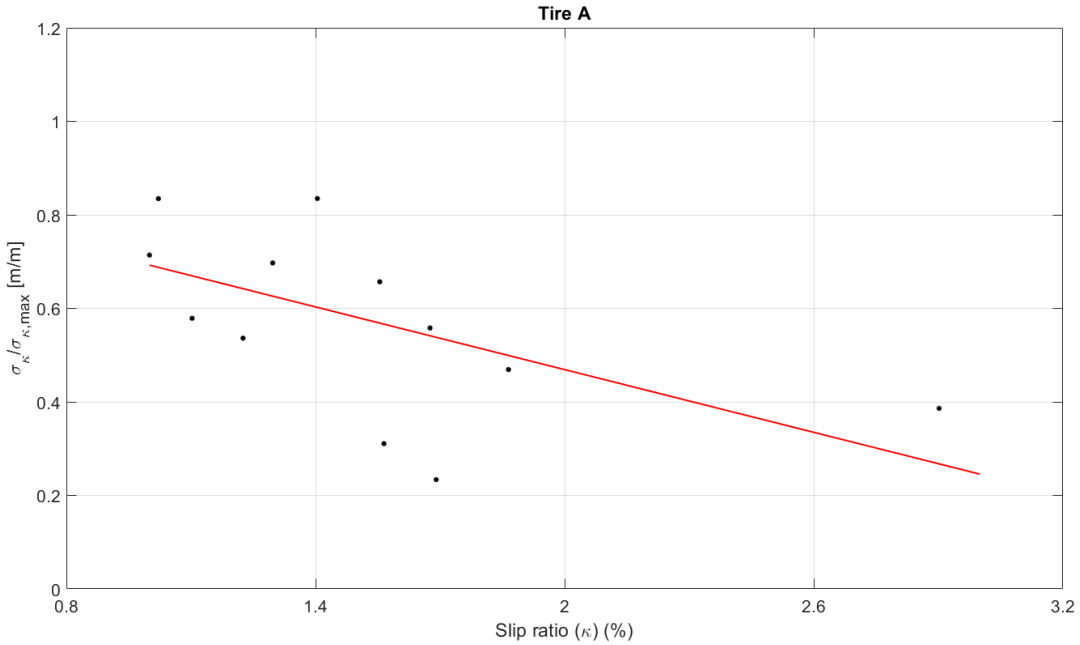

Figure 6-28 - Estimated relaxation length across the slip ratio from vehicle measurements for Tire A. Normalized data.

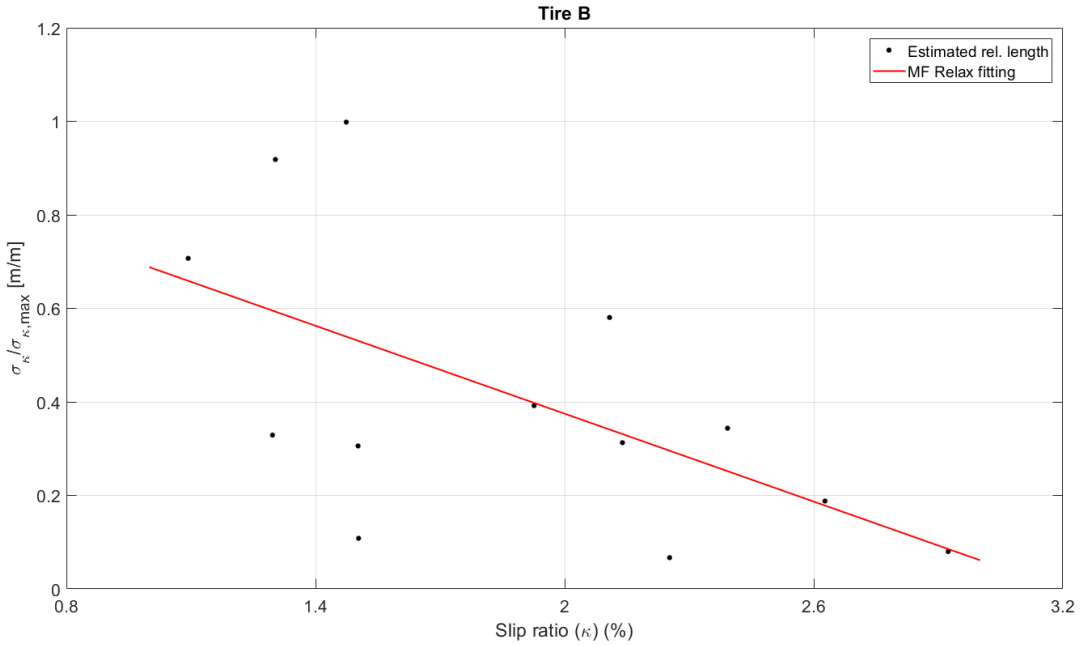

Figure 6-29 – Estimated relaxation length across the slip ratio from vehicle measurements for Tire B. Normalized data.

The described method allows to get a good trend of the relaxation length with respect to the slip ratio, as shown in Figure 6-28 and 6-29, where the fitted curve is obtained with the MF Relax model proposed by Braghin et al. in their study, as also explained in Paragraph 5.2.3. Trends and values of the longitudinal relaxation length that have been calculated can be defined as reliable, in agreement with the usual values that can be found in the literature [28][36][54].

6.4 Analysis of the simulation results

In the following paragraph 6.4.1 a general analysis of the braking simulation results with a particular focus on the relaxation length influence on the slip thresholds estimation and the braking distances. In the paragraph 6.4.2, the main target of the PhD activity is investigated by understanding which longitudinal curve parameter (the peak, the braking distance or the drop down of the grip after the peak) shows the biggest effect on the final braking distance

6.4.1 Emergency braking simulations

In this paragraph, the results from the complete braking model are shown. In Figure 6-30 and 6-31, an overview of the vehicle manoeuvre is shown of both Tire A and Tire B, with the main focus on: slip ratio signal (as input for the modelled logic), slip ratio thresholds and brake pressure signal (that is a direct consequence of the ABS model strategy).

As already mentioned, both the steady-state and the transient of the tire affect the ABS estimations and decisions.

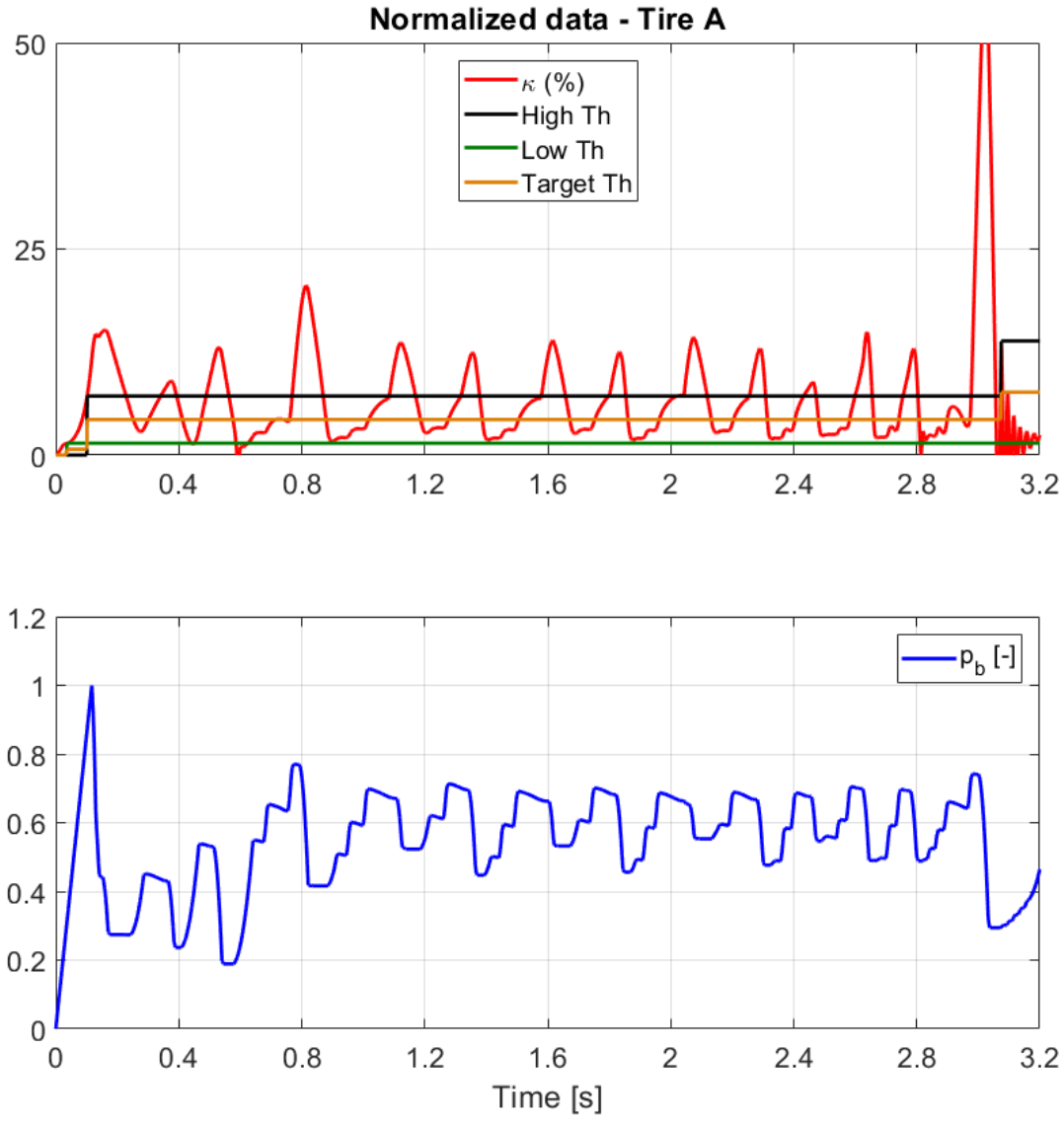

Figure 6-30 –ABS braking simulations for the Tire A model.

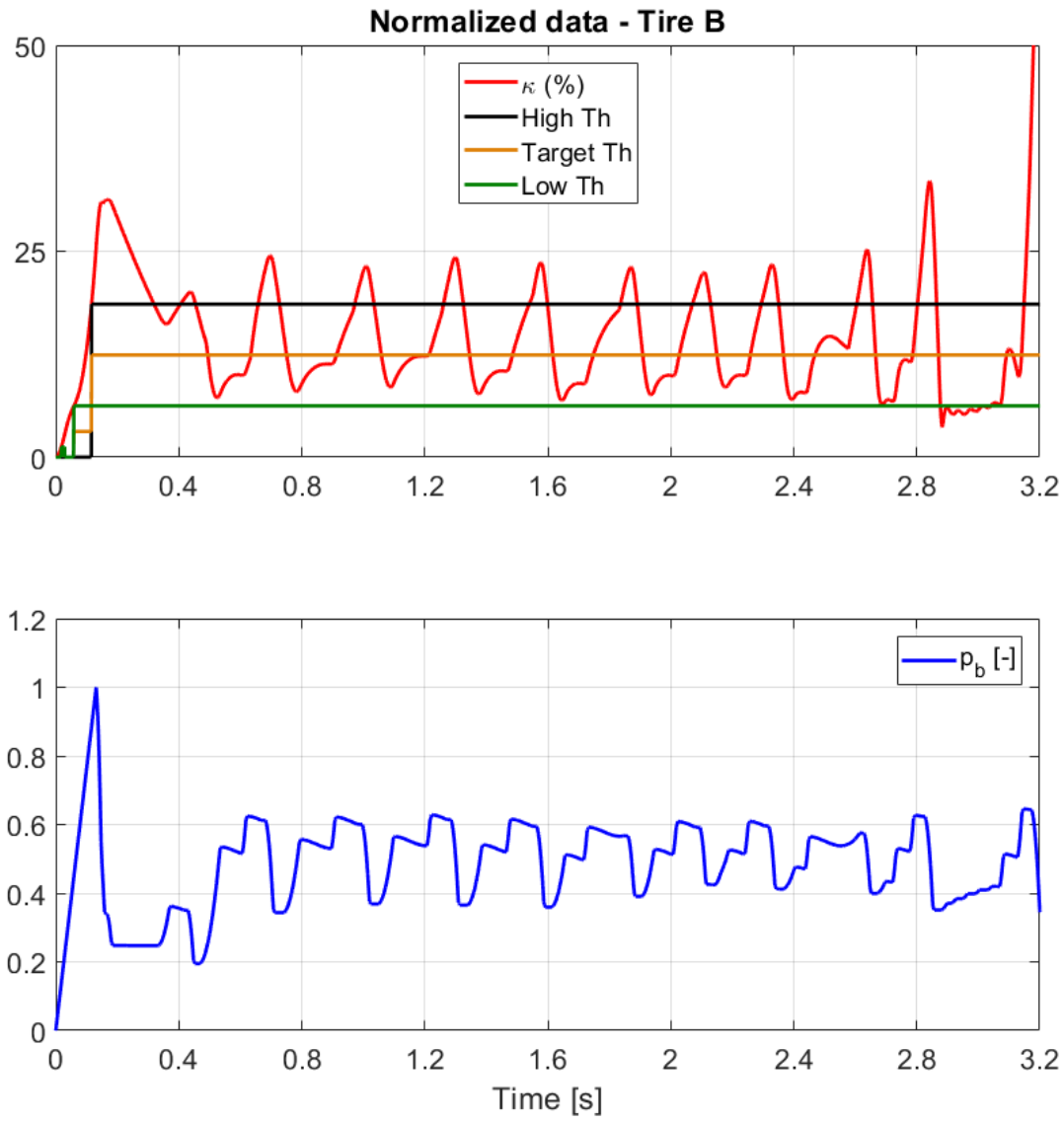

Figure 6-31 –ABS braking simulations for the Tire B model.

It has been observed that the relaxation length influences the setup of the slip thresholds during the estimation phase (explained in Paragraph 6.2.2), at the beginning of the emergency braking manoeuvre. The results of the simulation show a more realistic behaviour when the MF-Relax model for the relaxation length calculation (introduced in Paragraph 5.2.3) is implemented.

In fact, the MF-Relax model (characterized through vehicle measurements data on during braking test on wet surface) allows the ABS to set the low threshold; it is now possible to see a clearer inflection point in the slip ratio signal, similar to the one observed from the experimental data (Figure 6-32).

Apparently, the relaxation length generated by the MF-Tire model cannot be considered as fully realistic for the studied manoeuvre, since it is just considering the dependency on the vertical load. Therefore, the main focus was to verify the shape that the signal can have in order to allow the modelled ABS logic to work and estimates both the lower and upper bounds, as observed analysing the experiments.

The ranking or trends between the two considered specs is the main target of this analysis, instead of their effective braking distance. It is important to evaluate Tire A and B performances between experimental and

numerical results. This new approach allows to obtain a new and more realistic κ shape, as shown in the Figure 6-32 below.

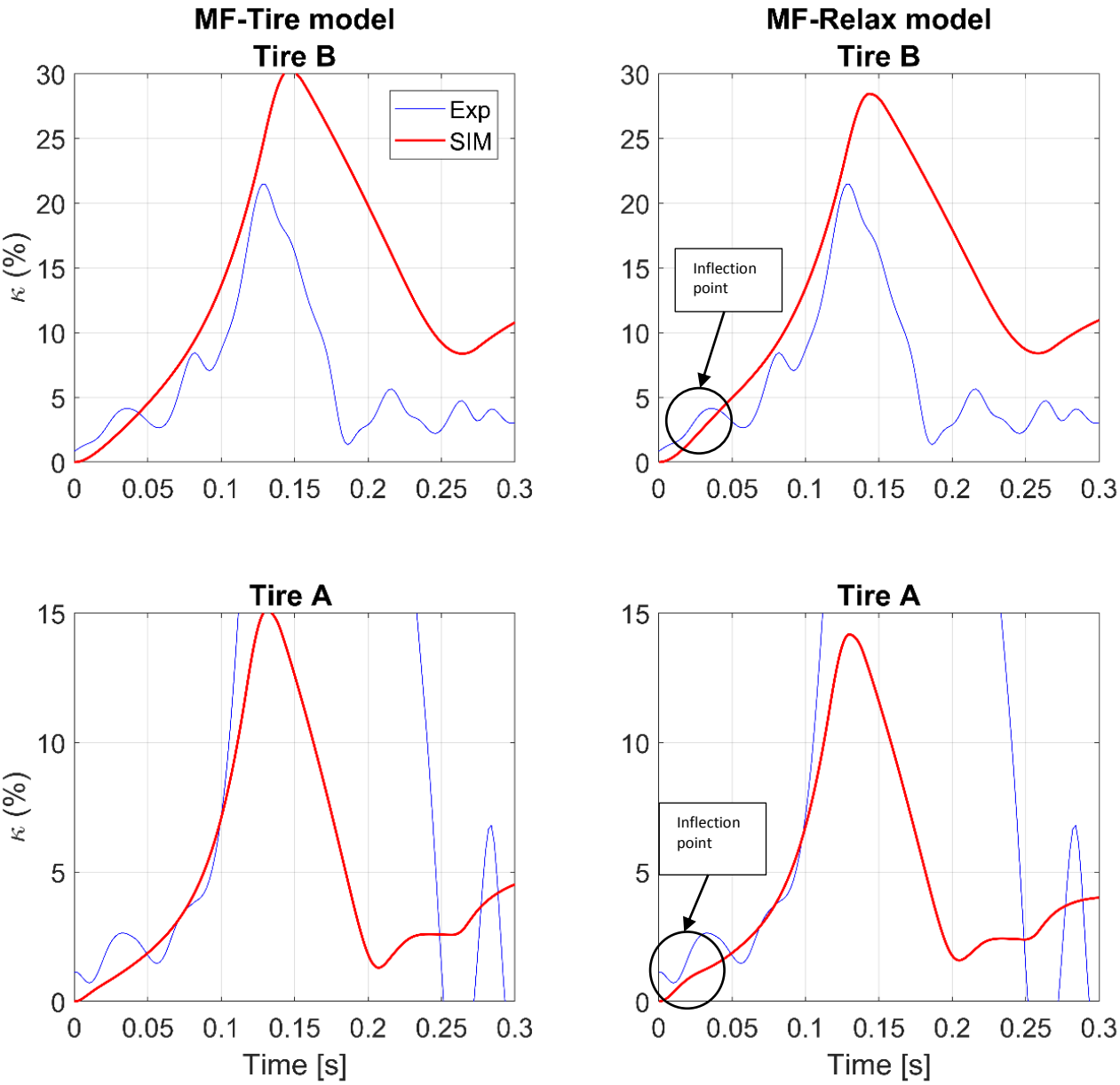

Figure 6-32 - Deflection points due to the relaxation length influence in the tire model.

A more realistic behaviour is visible in the κ signal and the reverse-engineered ABS can act and set reference thresholds. In the Figure 6-33, it is possible to identify the effective range used by the control system: the picture is showing the longitudinal forces coming from the simulation for the two tire models and the correlated low and high thresholds estimated by the ABS model.

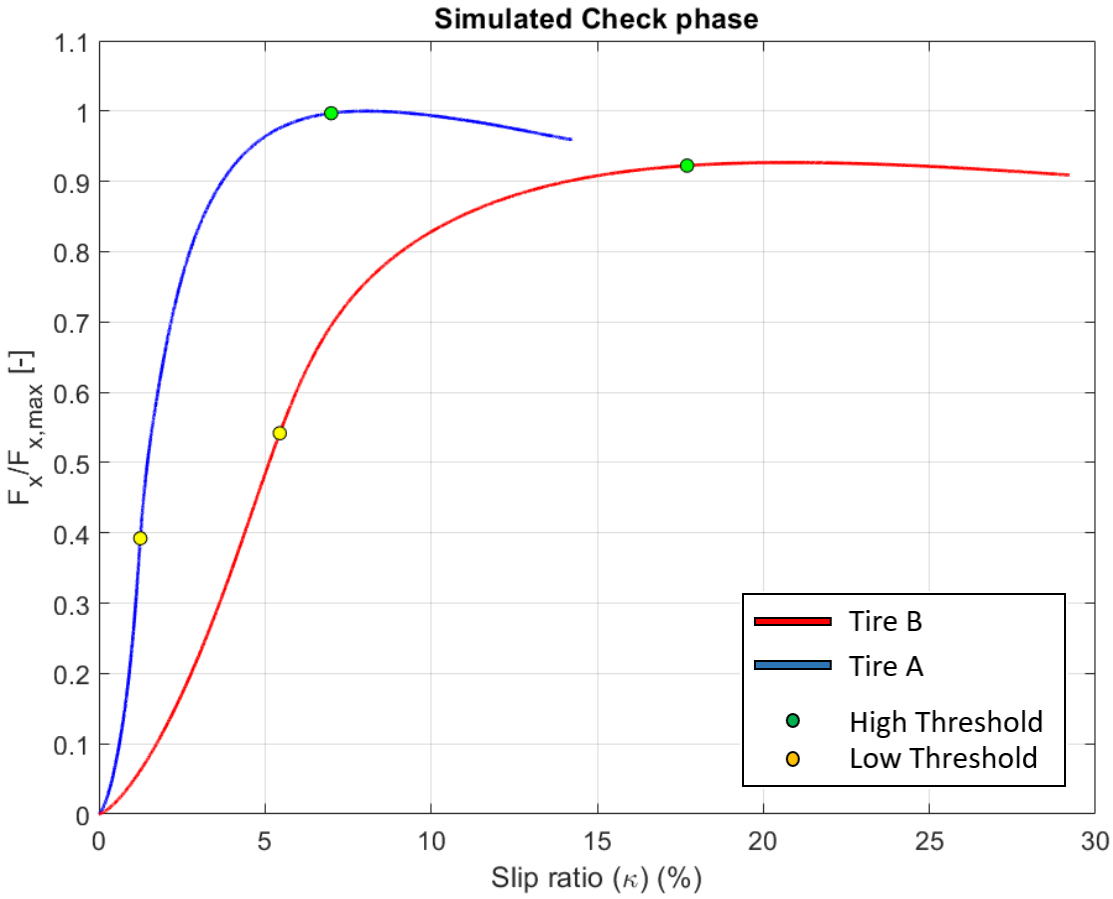

Figure 6-33 - Determination of the working range for 2 different tires with the implemented slip ratio's thresholds estimation phase in the ABS model.

The above figure shows the capability of the control system model to identify the desired range. In the Figure 6-34 and Figure 6-35, experimental and simulation results respect the same ranking, with smooth tire's thresholds higher than the peaky one, but with different percentage values.

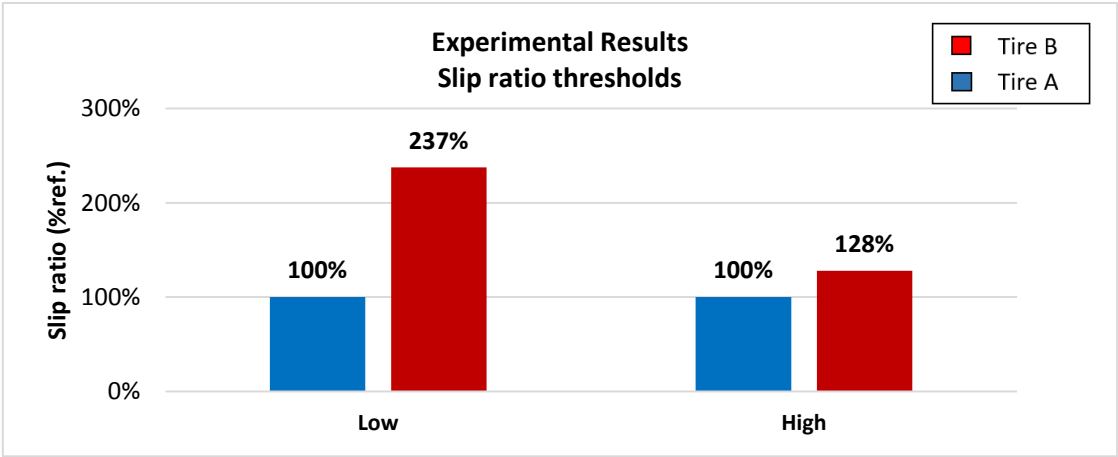

Figure 6-34 - Comparison between Low and High thresholds from experimental data.

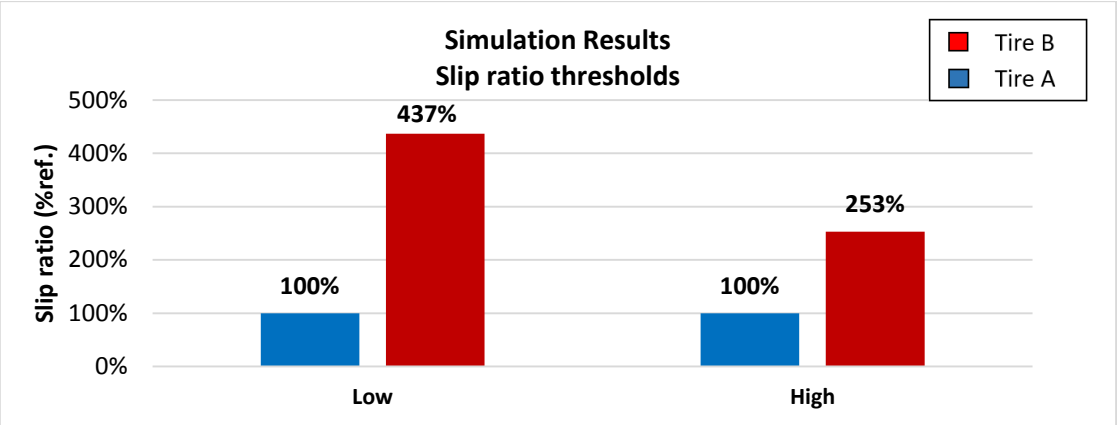

Figure 6-35 - Comparison between Low and High thresholds for simulated results.

The percentages from the experimental results has been calculated through the average values for both Low and High Thresholds on all the runs carried out.

In the following Figure 6-36, it is shown that in simulation it is not possible to see the same trend that has been seen during the experiments, despite the methods that has been used to improve the wet characterisation of the studied tires.

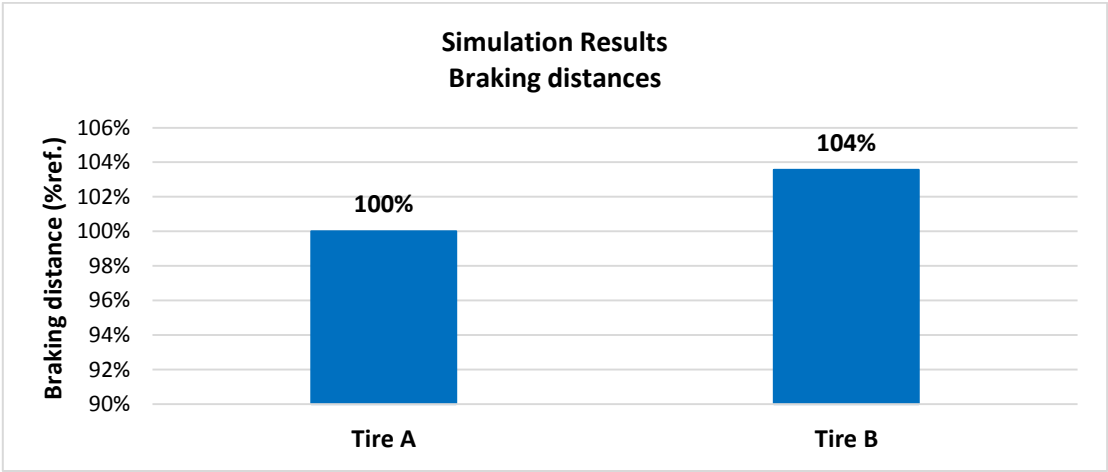

Figure 6-36 – Comparison of the simulated braking distances between Tire A and Tire B.

However, it cannot affect the analysis that will be described in the next paragraph, where a starting reference tire model will be modified with the aim to understand how the shape of the μ-slip curve can affect ABS behaviour and then the final test result.

6.4.2 Effect of the curve shape on braking performance

The previously described methods to characterize the tire have been proposed to allow to get the tire model to response as close as possible to the reality, in wet conditions. Moreover, it is important to specify that the MF-Tire model is not a physical model: therefore, it is not possible to evaluate and change tire characteristics through the implemented model [36]. However, since the improvements of the tire characteristics is one of the aims of more interest of tire companies, the main outcomes that this thesis wants to get are more related to the analysis of the longitudinal characteristics of the tire and the understanding of the optimal shape it must have in order to improve the braking.

In fact, inspired by the experimental investigations with the 2 studied tires Tire A and Tire B, in this paragraph the focus is on a reference tire model on which some change on the μ-slip curve have been done to understand how its shape can manage the performance. Connecting shape variations and tire features is not a straightforward work and it is not the direct goal of this thesis. In any case, as future development of the activity (Paragraph 7.2.3) a method for viscoelastic properties of the tire to improve tire behaviour during the braking will be proposed, thanks also to the development of the V-ELA, described in the Appendix (Paragraph A.3).

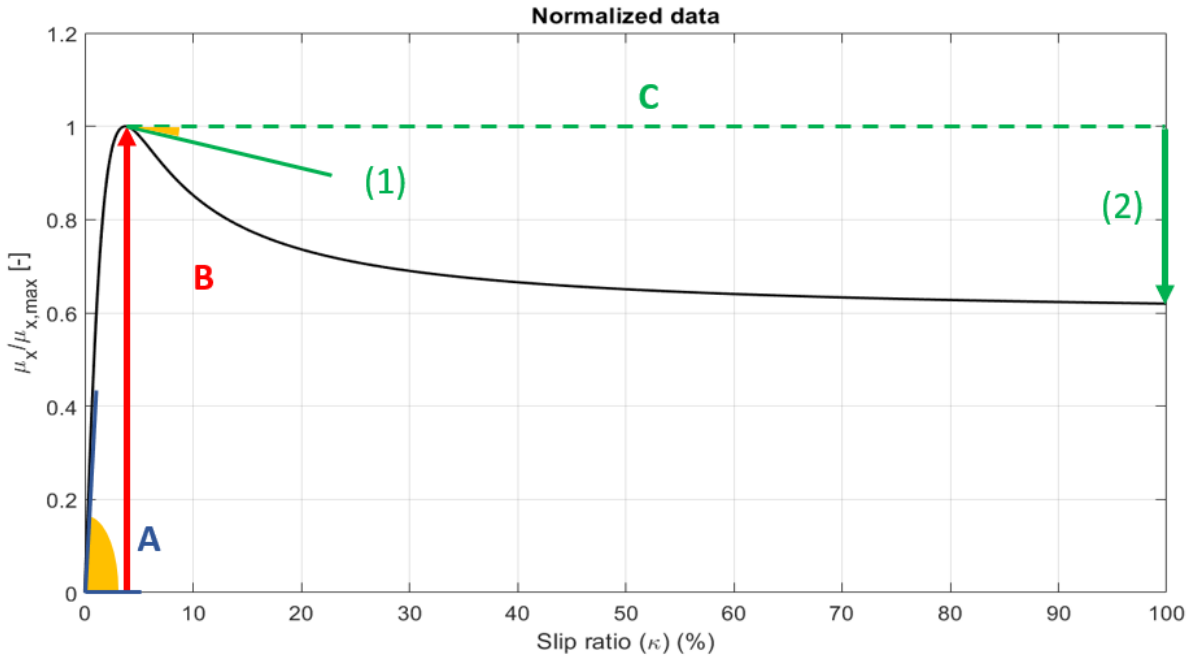

Figure 6-37 – Parameters that have been considered for the analysis of the μ-slip curve shape.

In this paragraph, some tire models were created by modifying F&M characteristics, to be evaluated during the braking simulations. It has been considered to focus on the shape of the longitudinal characteristic, as shown above in Figure 6-37:

A. The peak of longitudinal force μ_{max};
B. The braking stiffness K_x;
C. The drop down of the longitudinal force;
    1. Gradient of the drop $d\mu_{drop}$;

2. Total drop down.

As already explained in Paragraph 35, the peak is considered as the maximum value of longitudinal force (case B), while the "Braking stiffness" can be considered as the first derivative of the longitudinal force with respect the longitudinal slip around κ = 0% (Case A). The following equation:

$$K_x = \left.\frac{\partial F_x}{\partial \kappa}\right|_{\kappa=0} \tag{6.17}$$

will be considered for this analysis. The drop down of the longitudinal grip has been represented through 2 parameters: the "Total Drop" and the "Gradient of the Drop after the peak grip".

The "Total Drop" indicates the grip variation at the full sliding conditions of the longitudinal slip (κ = 100%), with respect to the reference curve.

The equation (6.9) is showing the "Gradient of the drop down after peak grip":

$$d\mu_{drop} = \left.\frac{\partial F_x}{\partial \kappa}\right|_{\kappa=\kappa_{\mu_{max}}}^{\kappa=\kappa_{\mu_{max}}+1\%} \tag{6.18}$$

which is defined as the decreasing zone of the interaction curve after the peak. It can also be defined as the first derivative of grip in the area of the peak. The considered range is between the slip ratio at μ-peak and the slip value as sum of the one at peak and 1%.Finally, all the parameters are expressed with an error factor with respect to the relative value of the reference curve:

$$e\% = \frac{x_{mod} - x_{ref}}{x_{ref}} \cdot 100\% \tag{6.19}$$

that will be proposed to evaluate the changes of the shape of the longitudinal curve.

Throughout this approach, several braking simulations have been run with the aim to observe if the peak has effectively the crucial role as defined in the WGI for European tire label (as already explained in Chapter 1).

In the following subparagraphs, some analysis will be shown with different shapes of the curves: the dotted curve is the reference one while the other curves will be the results of a "forced" modification of the reference curve, in order to isolate the investigated features and see how they can affect the simulated performance. It has been obtained by changing the related micro-coefficients of the MF-Tire model to match the critical parameters that have been identified in the list above.

Peak of the longitudinal force

It is the starting point of the assessment analysis. The approach was to maximize the peak, by keeping the braking stiffness and the drop as the same. The constant drop has been defined as the constant grip value at 100% of the slip ratio. The following analysis will refer to the μ_x-κ curve and the slip ratio range is 0-100%.

In order to keep the curves with a realistic shape, the peak variations have been handled as show below:

- around $\pm$10% of the peak value of reference curve;
- around $\pm$30% of the peak value of reference curve.

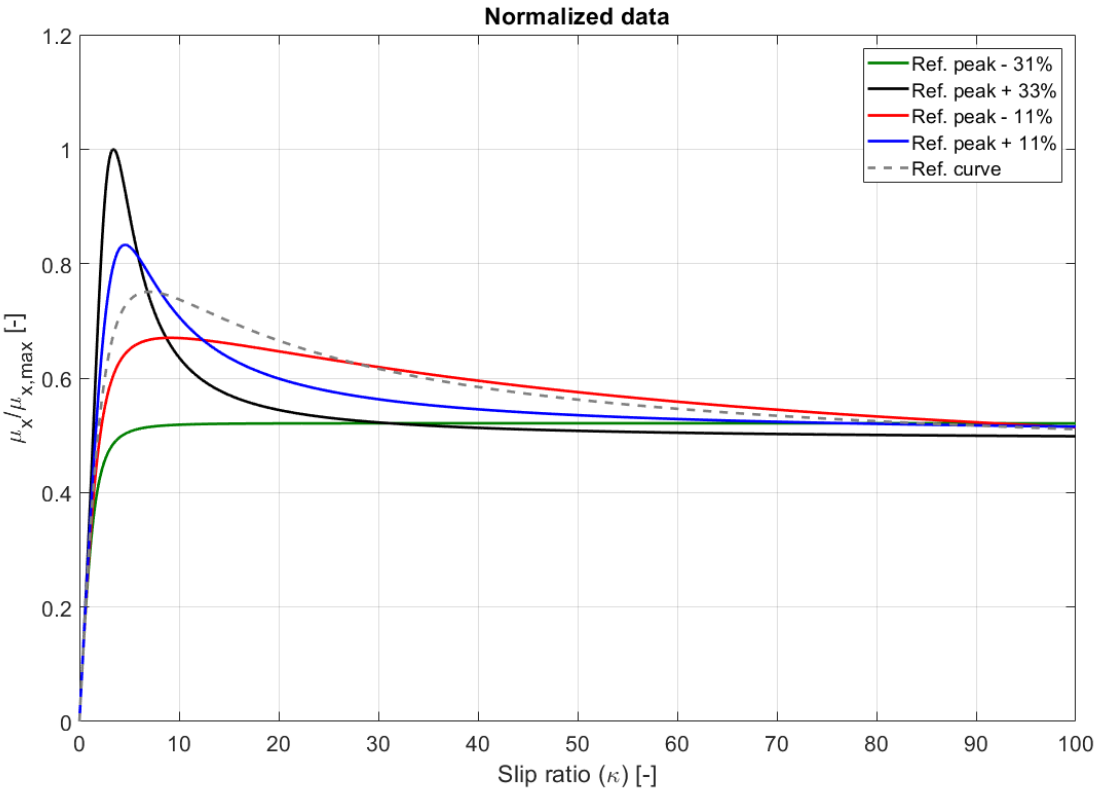

Figure 6-38 - Peak variations effect on the braking distance.

These 5 virtual tires have been introduced in the model to verify braking distance variations as results of the simulated braking manoeuvre, by using the modelled ABS state-flow logic. In Figure 6-39, the braking distance variations with respect to the reference model are shown per each μ-peak variation (as shown in Figure 6-38).

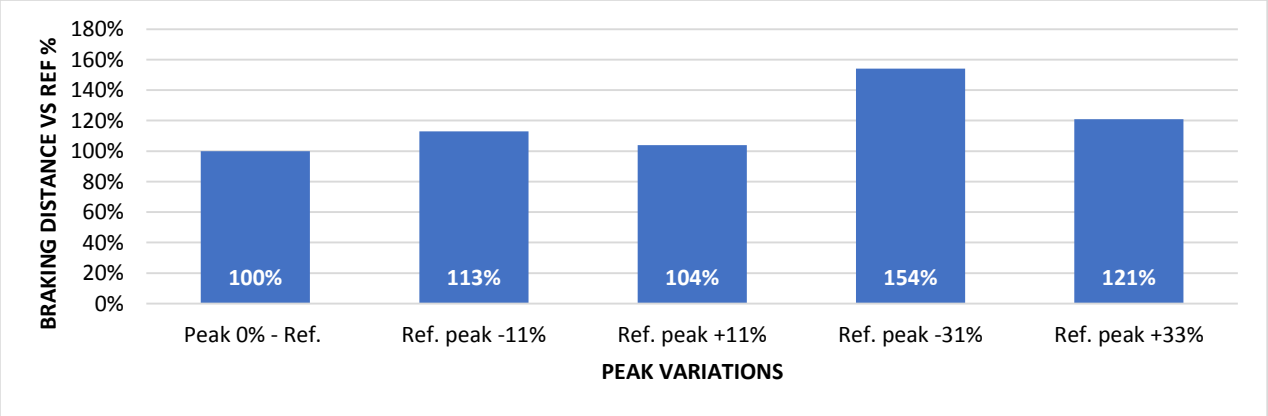

Figure 6-39 - Distance variations for the 5 virtual tires introduced: the 0% peak is the reference tire.

The braking distance with Peak 0% is set as reference. It is observed that the other tire characteristics show higher percentage values, where higher the percentage, higher the braking distance. This analysis is not showing a strict correlation between peak of the longitudinal grip and the braking distance, as also observable in Table 6-2.

Despite the ABS tries to keep the maximum grip zone, it seems to be clear that it is not the most important parameter to be optimized. In any case study the simulation showed a worsening of the performance.

Braking stiffness

A similar approach was also used for the braking stiffness evaluations. The braking stiffness of the reference model is modified in order to investigate the influence of this parameters on the braking distance. For the following analysis, μ-peak will be kept as constant and 2 cases will be shown:

1. Braking stiffness variations, with consequent drop variations;
2. Braking stiffness decreasing only, without any change for the other parameters.

The DOE that has been followed in this case:

Table 6-1 - DOE for braking stiffness evaluations.

	Braking stiffness variations				
Case 1 & 2	-80	-70	-60	-50	-40

This analysis shows the effect of the braking stiffness variations. The slip ratio range is 0-100%. Both case 1 and case 2 propose a braking stiffness increasing and decreasing:

- in case 1, the braking stiffness reduction is followed from an increased grip values over the μ-peak ("Drop decreasing" in Figure 6-40);
- in case 2, the drop @ κ=100% has been forced to reach the same values.

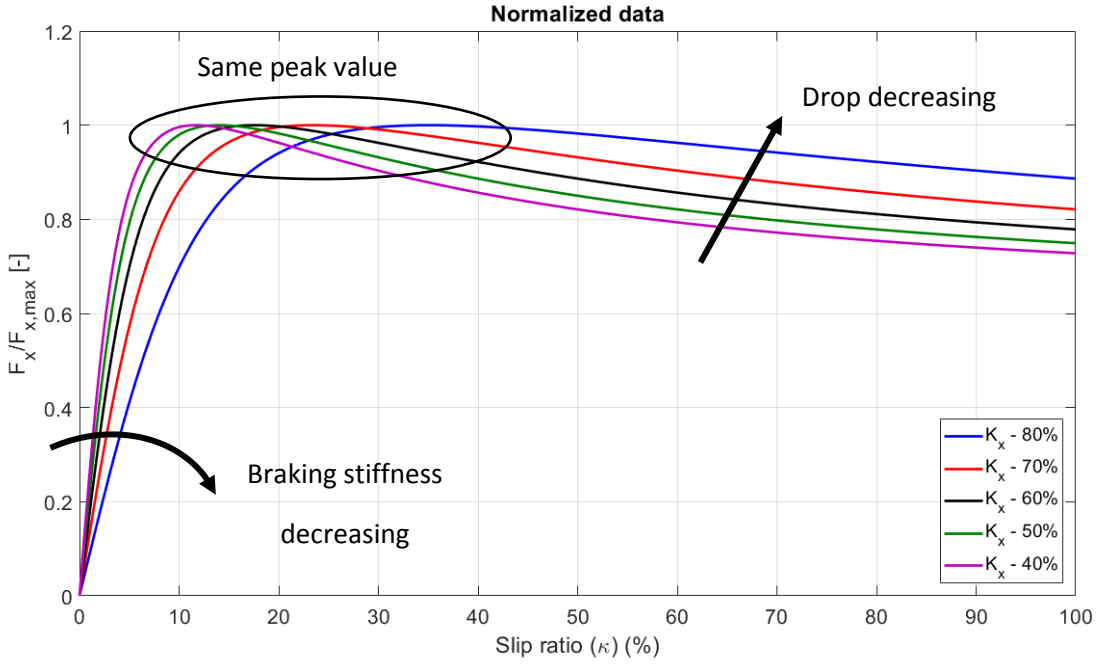

Figure 6-40 – Case 1: Braking stiffness variation with consequent variations of the total drop of the grip and its gradient at the peak.

In Case 1 it is possible to see that even keeping the peak as constant, the drop is changing with the braking stiffness. This is the result of the numerical behaviour of the MF-Tire model, that is based on the fitting of the forces and moments generated by the tire. It can be reasonable to consider the braking stiffness decreasing to increase the longitudinal grip level after the peak.

As shown in the Figure 6-40, the lower the braking stiffness, the lower the drop (the higher the grip level). A further and more fundamental analysis has been done to understand if the braking stiffness itself can improve the braking, by avoiding any kind of changes for the other studied parameters. It is shown in the following Figure 6-41.

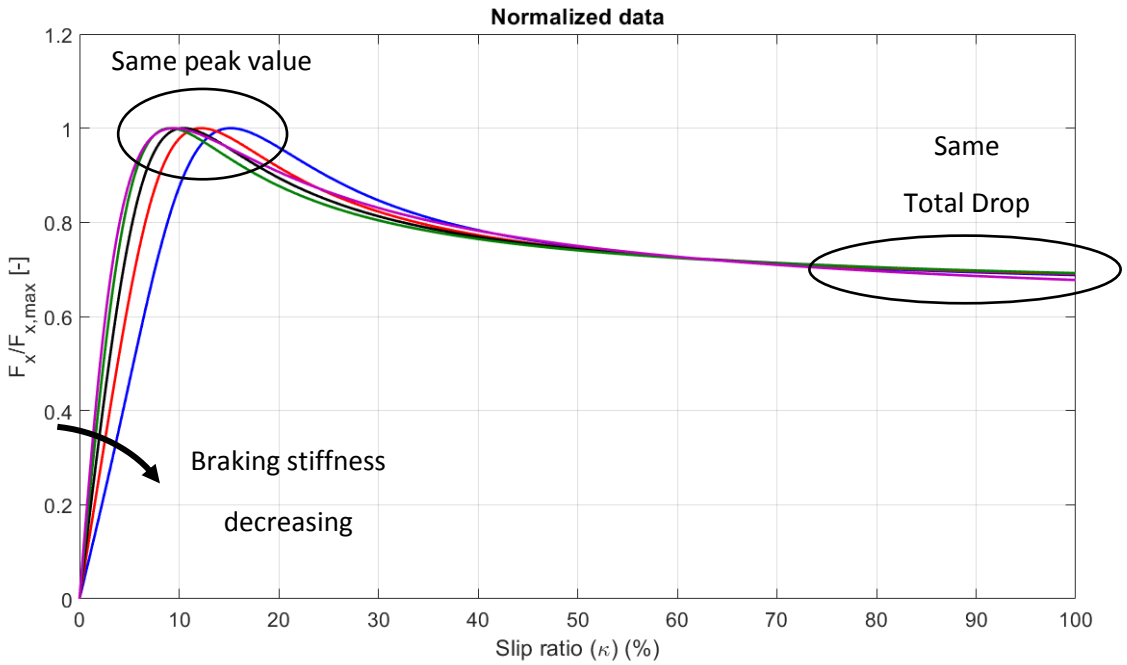

Figure 6-41 – Case 2: Braking stiffness variation by keeping the total drop of the grip and its gradient at the peak as constants.

In Figure 6-42, the braking distance percentages (as ratio between the braking stiffness coming from the modified curves and the reference curve) across the braking stiffness variations is shown. For the positive values of the braking stiffness variations there are not visible improvements: Case 2 stays around the 100%, showing the same results of the reference curve at different percentages, while the Case 1 slowly increases the braking distances when the breaking stiffness is higher.

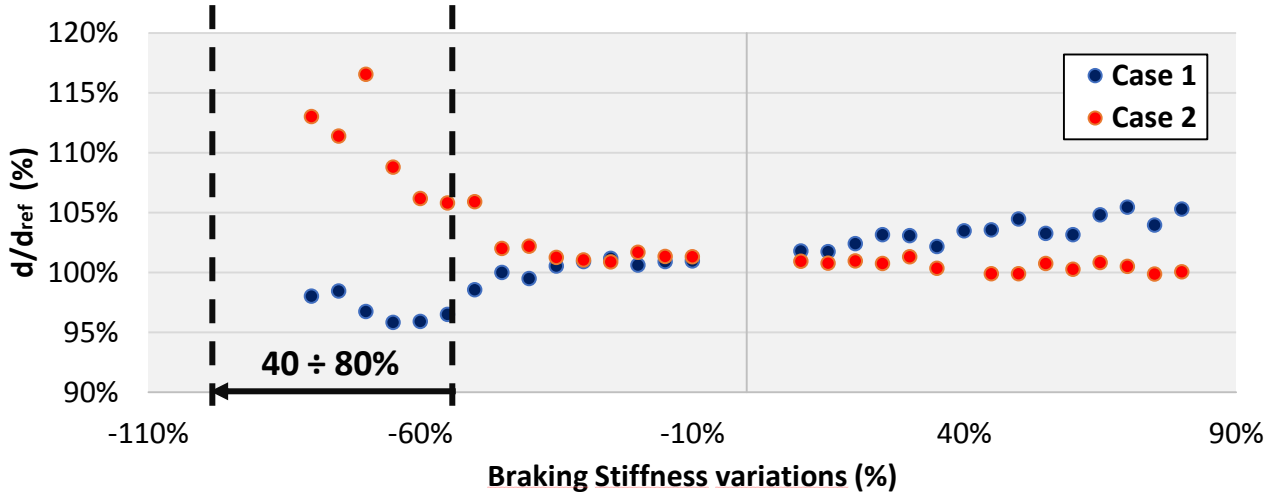

Figure 6-42 - Braking distance (d) percentages with respect to the reference braking distance for the 2 proposed cases. The lower is the percentage, the better is the result.

In case of negative percentage values of the braking stiffness variation (decreasing), Case 2 shows worst results, while Case 1 can reach the range 95%÷100% of the braking distance related to the reference curve, the "Braking stiffness variations" range between -90 and -50%. It is possible to see some improvements are visible in the braking stiffness range 35 ÷ 80%. The current analysis on the braking stiffness suggests that the improvements linked to the Case 1 should not directly depend on the braking stiffness itself but on the increasing of the grip over the peak value. In fact, forcing the drop to keep the initial shape (or the trend of the reference curve) does not allow to see any gain (120% of reference braking distance is reached for values lower than -60% of braking stiffness decreasing).

Drop of the longitudinal force

This analysis has been carried out by keeping the braking stiffness and the peak grip as constants. In Table 6-2, the Design of Experiment for the drop assessment is shown.

Table 6-2 - Design of Experiment for the drop assessment on μ-slip curve.

	Total drop of the grip (κ = 100%)		
	-10	**+10**	**+30**
Gradient at peak	-75	-82	-64
	-52	-34	-58
	+2	-2	-16
	+53	+75	+26
	-	-	+194

These variations have been carried out by changing the parameters of the MF-Tire model. The goal was to make 3 different examples, where the drop at the κ = 100% and the its gradient immediately after the peak can have different behaviours, with respect to the reference tire, as shown in Figure 6-43 and Figure 6-44.

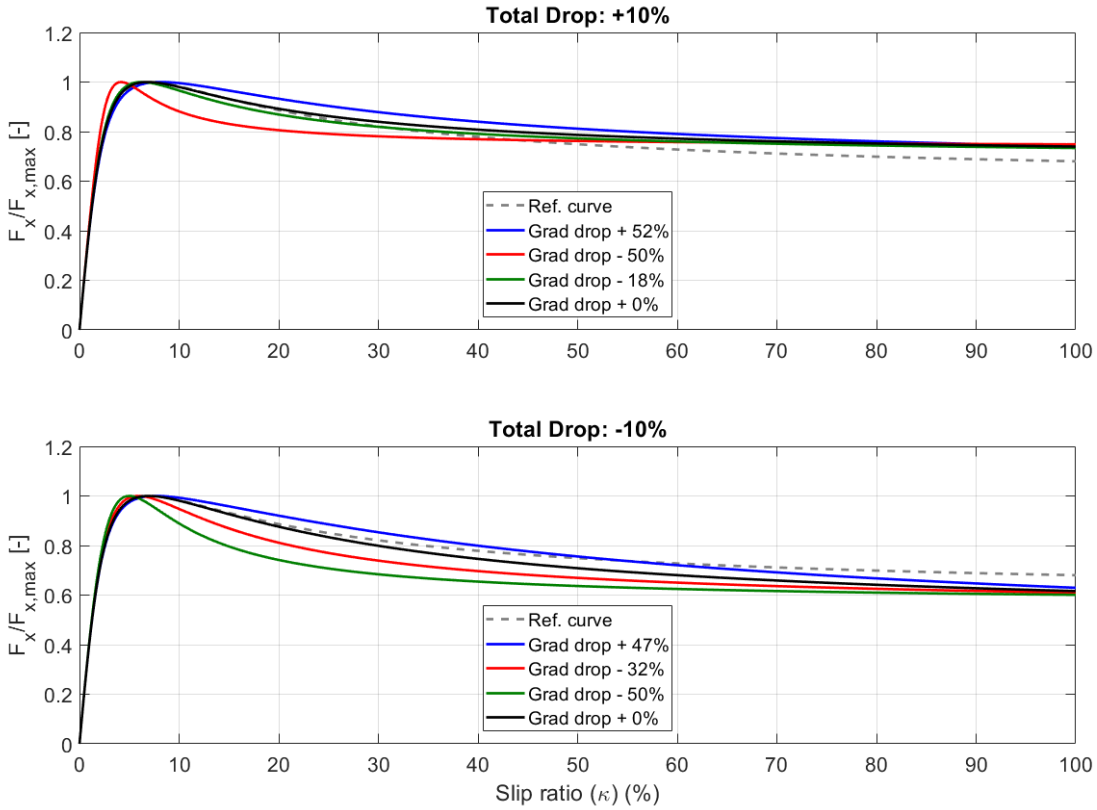

Figure 6-43 - Variation of the grip drop at the 100% of the slip ratio and its gradient at the peak of the curve.

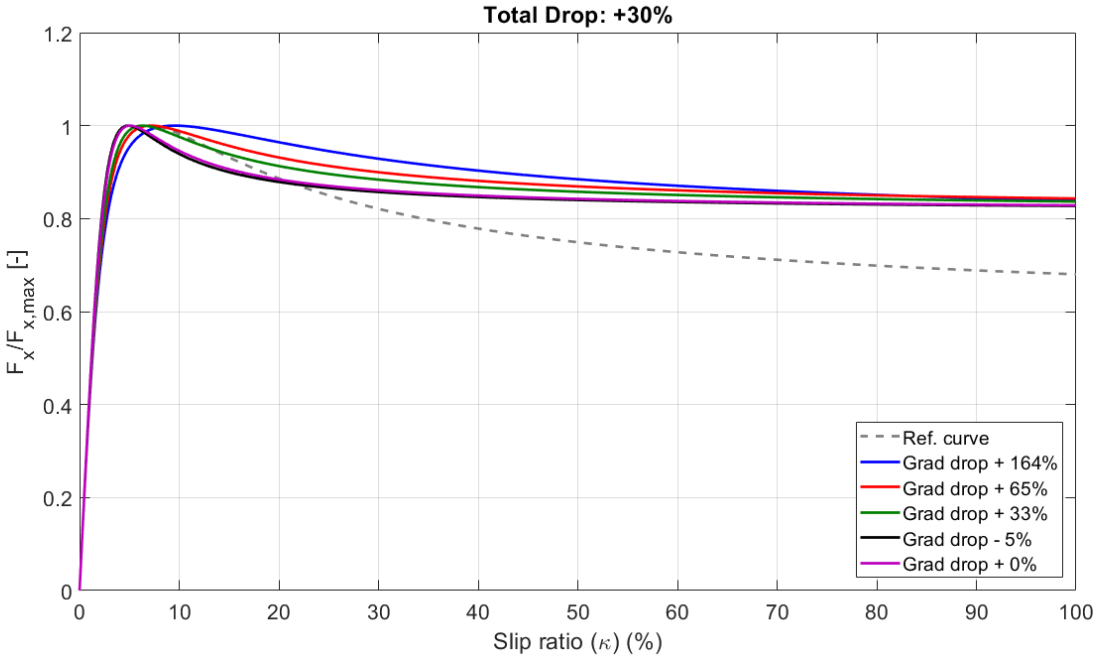

Figure 6-44 - Variation of the gradient of the drop down, with a total drop of +30% with respect to the reference curve at the κ=100%.

By handling the gradient of the drop of the grip at the peak, significant reductions of the braking distance can be seen, as shown in Figure 6-45.

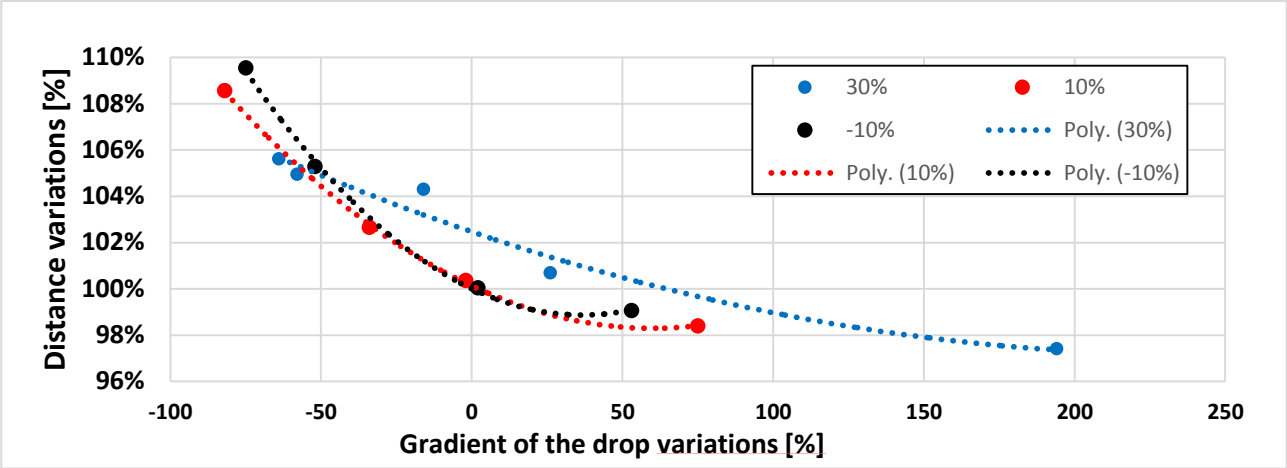

Figure 6-45 - Variations of the braking distance by managing the drop gradient tire grip after the peak condition.

The case where the virtual tires improve the performance are:

- Total drop = -10%, Drop gradient = +53%;
- Total drop = +10%, Drop gradient = +75%;
- Total drop = +30%, Drop gradient = +194%.

The gradient of the drop seems to have a great impact on the performance. Shape factor is a parameter that indicates the drop-in grip that occurs after crossing the optimal slip ratio. Steeper drop in grip leads to a smaller shape factor. Despite the different total drops (different colours in the above-shown Figure 6-45), the highest braking distance variations are visible for different gradients of the drop after the peak. Therefore, the sharper the drop after the peak, the worse the braking distance. This evaluation can also be correlated with Case 1 for braking stiffness variation, where a similar outcome that will be seen in the case of Drop of the force immediately after the peak.

Impact of each parameter on the braking distance from simulation

It is possible to summarize the analysis as shown in Table 6-3 below. With the R^2, the coefficient of determination, that is the proportion of the variance in the dependent variable that is predictable from the independent variables. It comes from the linear regression between the analysed parameters and the simulated braking distances. When the R^2 values are close to 1, it indicates there is a good correlation between the modified F&M parameters and the braking performance, while when they are closer to 0, it indicates there is a little correlation (or no correlation) with the braking distances.

Table 6-3 – Outcomes from the reference tire model changes, to understand the impact of each parameter on the simulated braking distance.

Parameters		R^2	+/- vs. 100%
Braking stiffness	no drop	0.0952	-
	drop variation	0.9316	+
Peak	-	0.2944	+
Drop gradient	Tot drop -10%	0.8563	-
	Tot drop +10%	0.8871	-
	Tot drop +30%	0.9286	-

The coefficient of determination is not the only parameter that has been considered. It has been necessary to define when the braking performance are improving. As already explained, in this study the lower the percentage related to the braking distances the better the performance. According to this, the percentages lower than the 100% for the reference, denote improvements. In Table 6-3, the "+/- vs. 100%" shows where improvements can be seen, with the positive sign indicating the cases where the simulated braking distances are not becoming lower than the 100%, while the negative sign indicating the cases with lower values.

Finally, as main outcome of the analysis, the cases of "Drop gradient – Tot. drop +30%", "Drop gradient – Tot. drop +10%" and "Drop gradient – Tot. drop -10%" show the best improvement due to the closest R^2 to 1 and the positive sign for the "+/- vs. 100%" parameter.

7. Conclusions and future developments

7.1 Outcomes of the research activity and future developments

The investigation of the emergency braking manoeuvre in wet conditions has been carried out through a numerical approach. Some analyses have been done to understand if the WGI approach ca be consider as fully exhaustive for this kind of assessment, as already introduced in Chapter 1 and Chapter 2. In the following subparagraphs the conclusions for this activity will be outlined.

7.1.1 ABS modelling

In order to understand how to improve the vehicle behaviour during a wet braking test, it had been necessary to understand how the ABS can interact with the tire during this manoeuvre. Based on the literature and the analysis of the proposed case study, the followed approach was to observe how a commercial ABS can work and try to make a model of it in Simulink environment. This model can:

- define similar strategies to the studied one;
- allow to study the tire behaviour under the influence of its strategies.

The modelled ABS is a slip-based logic, with a physical approach in the definition of the slip thresholds: during this slip ratio's thresholds estimation phase, some physical conditions have been defined to set the optimal working range for the logic.

It has been seen that the definition of the optimal working range is a direct consequence of the tire-road conditions: the ABS can monitor some fundamental vehicle signals with which it can estimate the already mentioned conditions (as the wheel acceleration).

For the definition of the high threshold (related to the identification of the peak of the curve), it has been necessary to treat the wheel jerk, appropriately filtered. The definition of the low threshold considers an inflection point of the slip ratio signal. It has been kept constant during the entire manoeuvre. Through the simulated approach, it has been seen that the low threshold can be influenced by the relaxation length of the tire. In order to get reliable simulations, it was important to use a tire model that could better replicate the longitudinal relaxation length.

7.1.2 Tire characterization

Another important point is to focus on the tire characterisation: this research work wanted to highlight the wet performance of the passenger cars and both the steady-state and the transient behaviour of the tire seem to play a very important role.

A method for the relaxation length identification from vehicle measurements has been proposed. This approach has been considered with the aim to estimate these physical quantities in wet conditions and directly from vehicle measurements.

Starting from a reference tire model (i.e. a Pacejka's tire model), it has been necessary to modify it through:

- Tire A and Tire B characterizations with a trailer on wet surface at 1 vertical load;

- extracting the load sensitivity, with which the peak values can be modified;
- estimating the relaxation length with a frequency analysis of the slip ratio and calculated longitudinal force signals.

It is necessary to specify that the points 2 and 3 have not been used in the simulations: these methodologies will be evaluated for future works on this topic.

Regarding the relaxation length, it has been proposed a method that tries to replicate the procedure used for the indoor test showed in Paragraph 5.2. The relaxation length has been estimated at a specific vertical load, close to the one the vehicle can reach after the complete longitudinal load transfer, during the control cycles.

7.1.3 Relaxation length dependency on the vertical load and the slip ratio amplitudes and excitation frequencies

In Paragraph 5.2 the longitudinal relaxation length has been calculated and analysed. The dependency on the vertical load, slip ratio amplitudes and excitation frequencies has been investigated. Moreover, the MF-Relax model has been validated by comparing the fitting with the experimental data, in order to include the dependency of the relaxation length on the slip ratio amplitudes in the implemented tire model. Its effect has been analysed during the ABS braking simulation.

Some more investigations are needed to understand if the $OTX1$, $OTX2$ and $OTX3$ parameters proposed by Braghin et al. needs to change with the vertical load. In this essay, they have been kept as constants.

In Chapter 6, a method for the relaxation length estimation from vehicle measurements and for fitting with the MF-Relax model has been shown.

Moreover, the variation of the relaxation length with respect to the excitation frequency (in terms of slip input), and an exponential dependency has been observed. Taking the cue from Braghin et al. study, a new model has been proposed (in the Appendix, Paragraph A.2) with which it could be possible to fit the relaxation length dependency on the excitation frequency during an ABS braking manoeuvre.

7.1.4 Influence of the shape of the μ-slip curve on the performance

The influence of the μ-slip shape on the braking performance has been investigated trough the numerical approach. The main outcome of the described activity is that (by using the same symbols used in Figure 6-35):

A. the braking stiffness K_x variations showed the better results when for lower value with respect to the reference curve;
B. μ-peak μ_{max} variations do not allow to improve ABS braking for the studied cases;
C. the gradient of the drop $d\mu_{drop}$ at μ-peak has a great impact on the braking distance.

Therefore, starting from a peaky curve (Tire A), some improvements have been obtained by making it more similar to Tire B curve shape. It has been seen that the bigger improvement was correlated with the $d\mu_{drop}$ parameter, by means the gradient of the drop down of tire grip after the peak. Obviously, the improvements can be a combination of the three different parameters. In this assessment, changing the parameters one by one had the main goal to show which one could have the most important influence on the final braking distance, starting from a specific curve.

As the WGI expects, the peak is an important parameter to evaluate because it gives an idea of the maximum performance that a specific tire can reach. This study wanted to show that probably it is not the only parameter to be evaluated for the proposed case study, the gradient of the drop can play an important

role due to the ABS influence and maybe it could be interesting to evaluate a combination of both parameters for the representative final index.

The numerical feedback of the model must be verified with the real tires to understand if it is possible to manage the same features from the simulation to the real tire. Future developments will expect to automatize the longitudinal curve shape variation, trying to reach the minimum distance from the starting tire.

7.2 Future developments

In this paragraph the future developments of the activity will be introduced and described. The focus will be on the dependency of the longitudinal velocity and hydroplaning phenomena, a frequency analysis of the ABS actuations and tire response during the manoeuvre and a proposal of a method to estimate rubber compound characteristics changes for the optimized curves coming from the simulation results.

7.2.1 Dependence on vehicle longitudinal velocity and hydroplaning phenomena

In the literature, it is possible to find many experimental studies that show a variation of the μ-peak in terms of both maximum grip value and slip ratio value at the peak of the curve [13][68][69]. Focusing on the last one, it is possible to observe the μ-peak moves towards higher grip and the rightmost slip ratio's values [13]. Based on the Stribeck curve theory [70], a possible friction model that could be implemented in the current tire model is [69]:

$$\mu = \mu_0 \cdot e^{\left[-\left(\frac{V_{rubber}}{V_{Stribeck}}\right)^a\right]} + b \cdot V_{rubber} \tag{7.1}$$

where μ_0 is the friction at theoretical "zero" speed, V_{rubber} is the longitudinal velocity of the rubber block, $V_{Stribeck}$ is the "Stribeck" speed, while a and b are the "shape" and "viscous" parameters respectively.

These phenomena can become annoying because of the so high difference of the curve's shapes for the same tire and they can mislead the logic on the real potentiality that can be used during the braking. It can be one of the reasons of the high threshold changes during the control cycles. The used tire model is not including the μ-peak variation across the slip ratio. Moreover, the hydroplaning can also affect the tire behaviour, as also shown in the equation in Chapter 4, Paragraph 4.5.4.

For future developments, it would be desirable to investigate the occurring phenomena during an emergency braking test that can affect the optimal performance form the starting point to the ending one of the manoeuvres and how to improve tire performance at the initial phase of the manoeuvre to allow a correct ABS working range estimation.

7.2.2 Frequency analysis

ABS actuation frequency

The ABS can show some actuations in high frequency that can stimulate some tire eigenmodes; in particular, it could be very useful to understand if low brake pressure magnitude can excite some tire eigenmodes during an emergency braking test. The modern ABS are not based only on the classical main 3 functions (Apply, Hold and Dump) but the Inlet and Outlet valves can act with high frequency brake pressure variations [71][72][73][74].

Based on these considerations, it could be interesting to investigate which the causes and the effects could be. In terms of causes, it would be interesting to understand the frequencies that the PWM control (Figure 3-7) can generate [1][75] for the ABS actuation frequencies. In terms of effects, the tire frequency response can significantly impact on the ABS control and then on the whole braking performance

Frequency response of the tire

The F_x signal shows different contributions at different frequencies that is not possible to generate with the used tire model. In Figure 7-1, the longitudinal force signal has not been obtained directly from Wheel

Force transducer during the emergency braking test because of some issues that can occur during the test. Therefore, the F_x has been calculated as described in the Paragraph 6.3.2.

In Figure 7-1, a comparison between experimental and simulated longitudinal forces in the frequency domain is shown. In particular, Tire A is showing that there are some force resonances in the range [20,30] and [40,50] that the tire model cannot fit.

The most important evidence in F_x frequency response is the particular behaviour between 20-30 Hz and 40-50 Hz for both Tire A and Tire B: from experiments, some resonance peaks are visible, due probably to some particular tire eigenmodes that can generate sensible tangential force variations at the different longitudinal velocities [71].

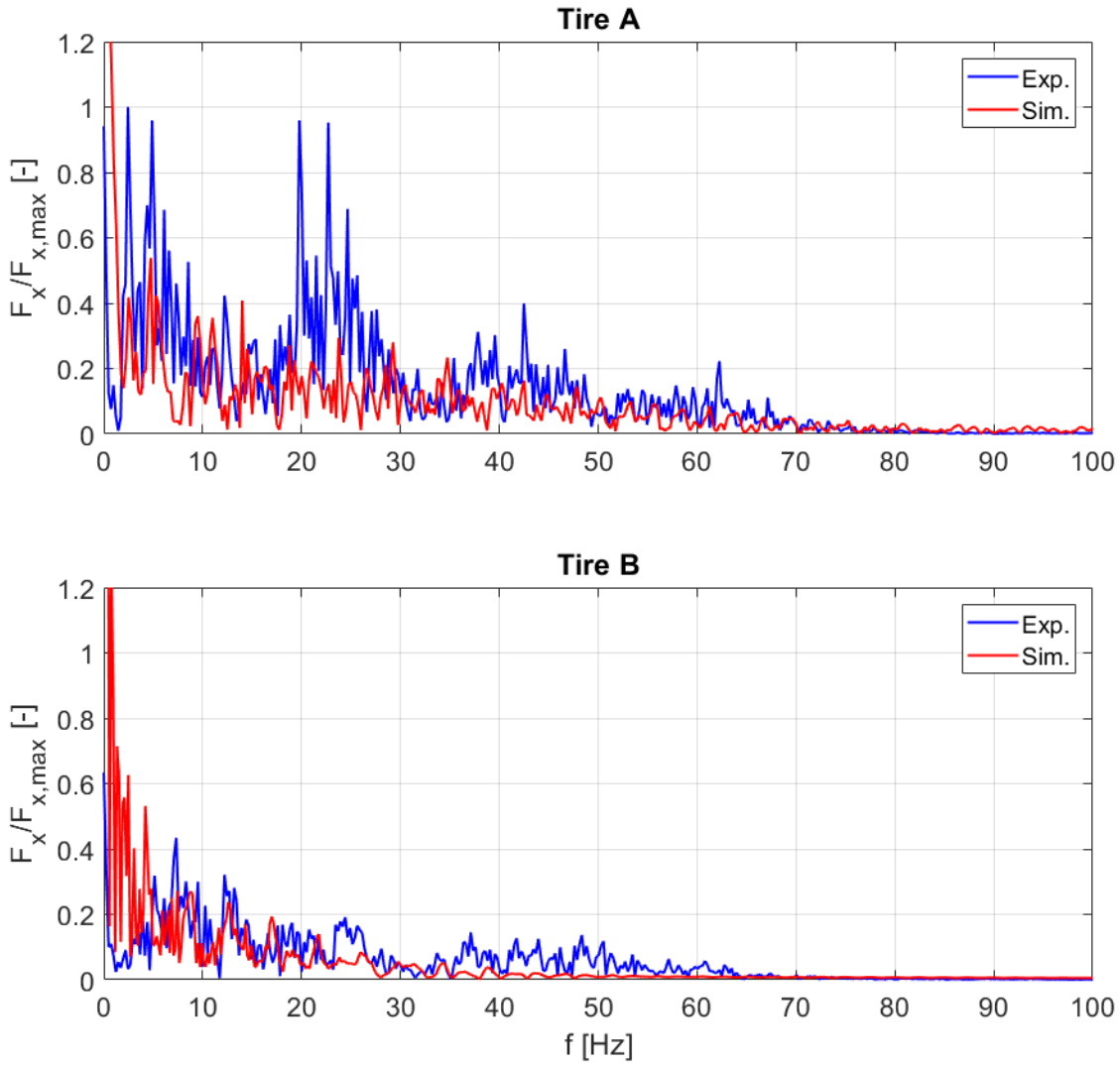

Figure 7-1 - Frequency analysis of the calculated longitudinal force for both the studied tires. Normalized data.

As expected, this condition can have an impact on braking performance and in order to manage this problem it is necessary to investigate the effective phenomena that occur.

The analysis of the calculated longitudinal force during the braking manoeuvre shoes that it is possible to instantaneously see where the highest frequencies occur. It is taken an example with Tire A in Figure 7-2,

where the calculated F_x is shown with respect to the time while the spectrogram of the same force signal is shown in Figure 7-3.

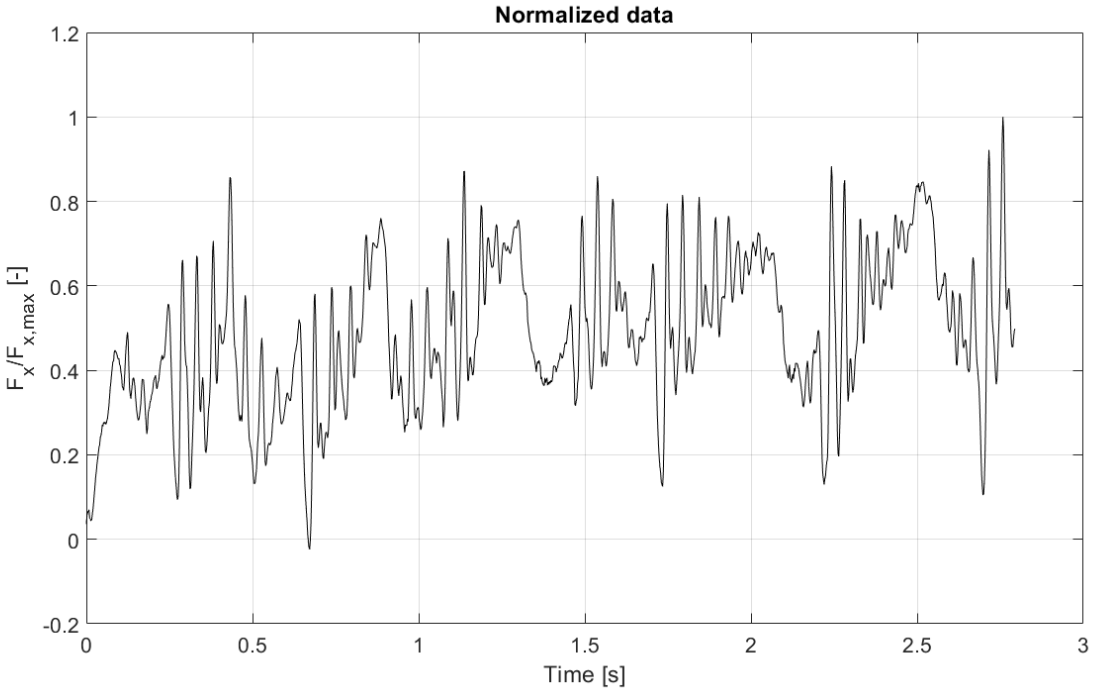

Figure 7-2 – Calculated longitudinal force from vehicle measurements.

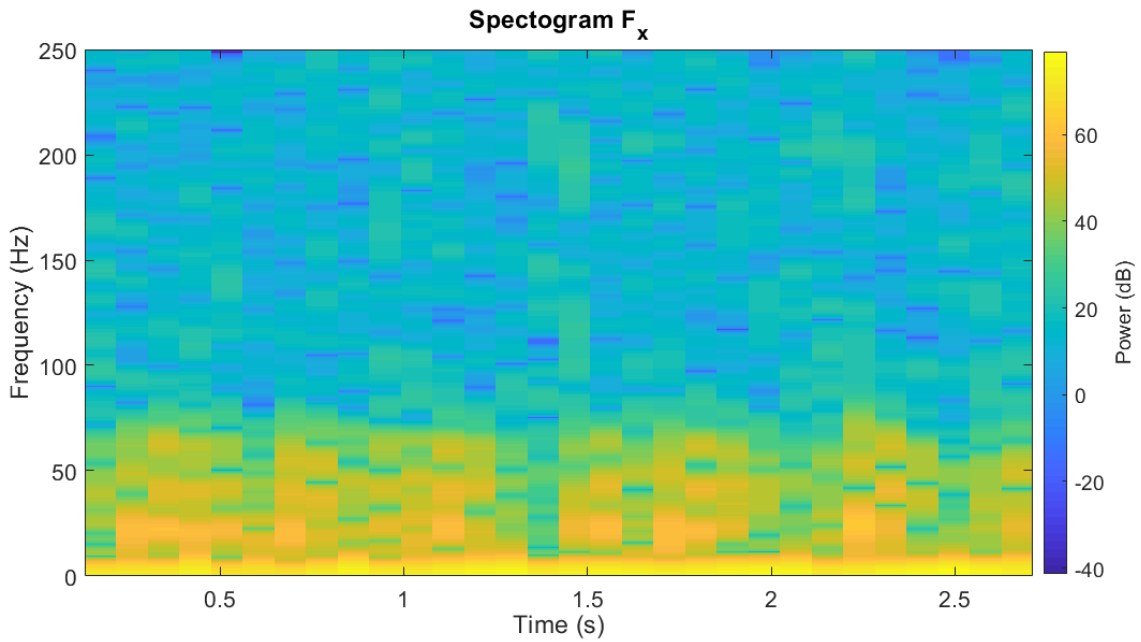

Figure 7-3 – Spectrogram of the longitudinal force calculated from vehicle measurements.

In these two figures, it is possible to observe that the higher frequency oscillations can be seen in the time signal just before the force drop-offs, which are caused by dropping the brake pressure. It is possible to find

similar outcomes in Tuononen et al. study [71][72], where the natural frequencies of the tire and their interaction with the ABS are analysed.

Some investigations with a Rigid Ring model will be considered as future development of this activity, in order to understand how the ABS frequencies can stimulate the eigenvalues of the tire and vice versa [12][76].

Rolling conditions

In Figure 7-4, a frequency analysis of a tire response is shown, where some resonance peaks are visible when the vehicle is travelling at a constant velocity (free rolling, κ around 0%). The data have been acquired with a Wheel Force transducer.

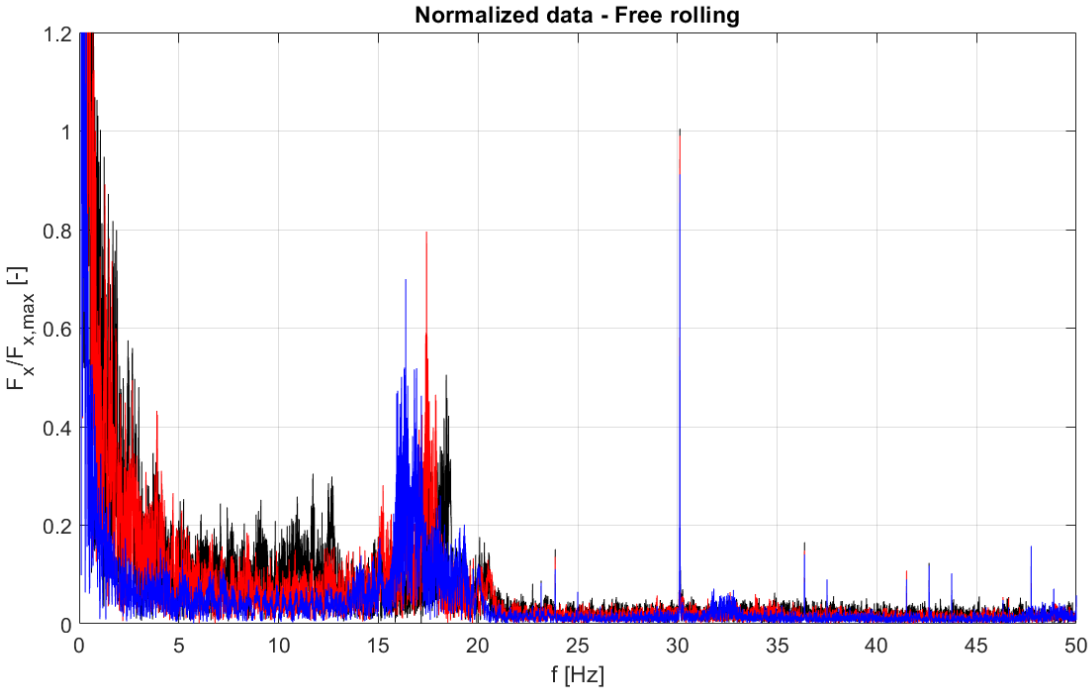

Figure 7-4 – Example of a frequency analysis of the F_x in free rolling conditions for the same tire on the same surface.

In free rolling conditions, there are some deformations of the tread blocks at the contact patch that produce some longitudinal force within a complete turn of the wheel. This F_x variations that can also be dependent on the rolling resistance [47], are also dependent on the wheel rotational velocity [77].

Therefore, tires can show a peak resonance also during free rolling conditions. It could be interesting to also investigate how the brake torque at that specific frequency of the peak resonance in free rolling condition tends to influence the magnitude of the resonance, how it is affecting the ABS work and how to model it for numerical evaluations. In fact, as already shown in Figure 7-1, some resonances due to the rotation are visible, which can increase the magnitude during a non-emergency braking manoeuvre for the generation of longitudinal forces. The braking torque M_y can produce a longitudinal force increment and, in the figure above, it is observable an increasing of the magnitude at ~20 Hz instead of that one at ~30 Hz because of some excited torsional eigenmodes: this could depend on the reachable M_y frequencies that can grow up the amplitude of the F_x values at the rim.

7.2.3 Proposal of viscoelastic moduli estimation from μ-slip curve

As future goal of the current research work, it will be considered to translate μ-slip variations in rubber properties. The next steps will investigate how to get reliable viscoelastic properties from the simulated manoeuvre. It is important to remind that during a wet manoeuvre there are additional phenomena such as the dynamic hydroplaning that can make tire design role more crucial than in dry conditions. In that case, the contact patch can be different because of tire construction. It has also to be considered that the current simulation does not consider the effect of both viscous and dynamic hydroplaning, which are related to low and high velocities, respectively.

A simple approach can be considered to estimate viscoelastic moduli from simulation results: it could help in case of low velocities, where the viscous hydroplaning should not play a crucial role on the performance. In this phase, rubber compound should have a significant impact [4].

In order to do that, it has been considered to use Persson's approach and link the E', E'' and $tan(\delta)$ to the grip [78]. The following equation is a proposal of a very simple approximation of Persson's theory [79]:

$$\mu \cong h'_{rms} \frac{Im\, E(\omega_0)}{|E(\omega_0)|} \tag{7.2}$$

where $E(\omega_0)$ is the complex viscoelastic modulus of the rubber and the h'_{rms} is a constant value that is assumed as h'_{rms} = 1.3, based on the latest development of Persson's theories (where the friction is due to viscoelastic losses and other mechanisms) which suggests the truncation of the spectrum of the surface should be such that the rms slope is fixed to the above mentioned value [79].

In Figure 7-5, the workflow for the estimation of viscoelastic properties is shown. The V-ELA (which will be described in the Appendix) is also included.

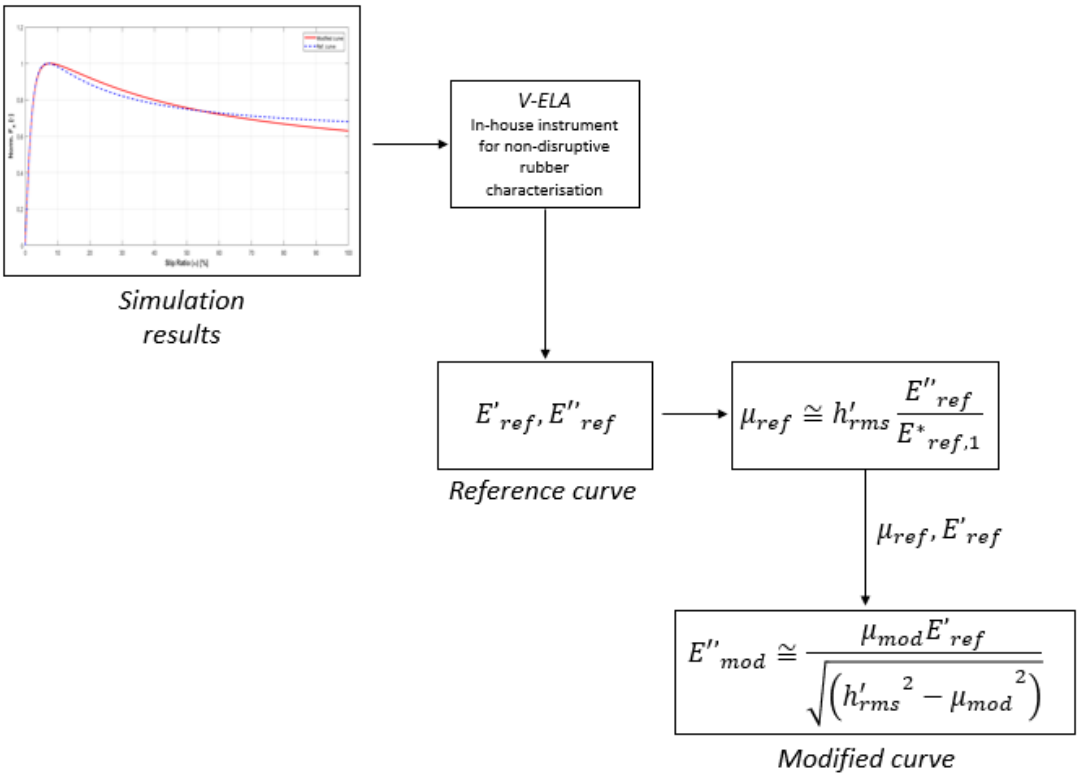

Figure 7-5- Scheme of the possible procedure to use for viscoelastic characterization and where the VELA can be involved.

The following Figure 7-6 is showing 2 curves: the reference curve and the modified one in the drop section.

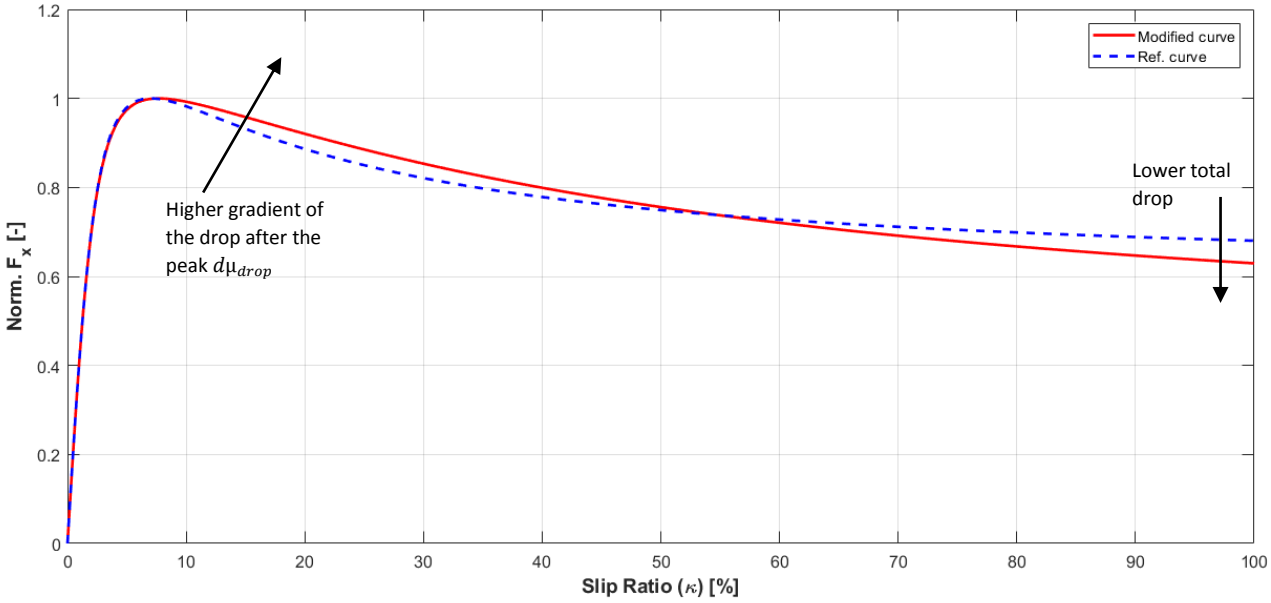

Figure 7-6 - Example of the results from simulation.

For the above showed normalized curves, the braking distances are shown in the table below.

Table 7-1 - Simulated braking distances.

Simulated braking distance [m]	
Ref. curve	**Modified curve**
30.49	30.25

The reduction is by 0.78%. It has been preferred to consider these 2 curves because they are just an example of improvement for tire performance related to the gradient of the drop of the grip. Especially in this case, the total drop is lower than the one showed by the reference curve, but the performance can improve because of the higher gradient of the drop after the peak condition of the curve ($d\mu_{drop}$).

Thanks to the using of the in-house developed V-ELA, it is possible to characterize the rubber with an indentation approach and obtain E', E'' and $tan(\delta)$, as described in the Appendix, Paragraph A.3.

The evaluation of the frequency at which the tire is touching the road is considered in the range of 7.3% (μ-peak) and 15% of the slip ratio. As described above, the considered reference range of the braking manoeuvre for this assessment is that one at low velocities, where we can expect the compound has a higher influence on the performance.

As example, it can be considered a reference velocity of 30 kph, as average of the longitudinal speed range 40÷20 kph during the considered braking manoeuvre test. For the mentioned velocity and the slip range 7.3÷15%, there is a frequency range of 3.6÷4Hz.

Thanks to the proposed equation (7.2), it would be possible to calculate the new E' and E'' from the modified curve, starting from the initial estimation carried out by the V-ELA.

The procedure proposes to:

1. Use a reference tire;
2. Estimate the E' and E'' moduli at different frequencies and temperatures;
3. Create the Pacejka's tire model;
4. Simulate the braking test;
5. Improve the performance, focusing on what we have seen in the Paragraph 6.3.2;
6. Use the grip values at different frequencies (according to the slip ratio range and longitudinal velocity to consider).

Once obtained grip values, it can be possible to use the equation (7.3), to calculate the E'':

$$Im\, E(\omega_0) \cong |E(\omega_0)| \frac{\mu}{h'_{rms}} \tag{7.3}$$

by keeping the $\mathrm{Re}(E^*)$ constant. Therefore, starting from a known storage modulus, a new E'' will be calculated that should increase the rubber grip for the identified frequencies [77].

The described simple model can be compared with the GrETA [80], a grip model that has been developed from Vehicle Dynamics research group at the University of Naples "Federico II", with the aim to analyse and understand the complex phenomena concerning with local contact between viscoelastic materials and rough surfaces.

References

[1] F. Timpone, “OPTIMIZATION OF THE BRAKING SYSTEM AND BRAKING CONTROL STRATEGIES OF THE VEHICLE BY SOFTWARE IN THE LOOP SIMULATION,” University of Naples “Federico II,” 2004.

[2] R. Russo, M. Terzo, and F. Timpone, “Software-in-the-loop development and validation of a Cornering Brake Control logic,” *Veh. Syst. Dyn.*, vol. 45, no. 2, pp. 149–163, Feb. 2007.

[3] S. Sivaramakrishnan, K. B. Singh, and P. Lee, “Influence of Tire Operating Conditions on ABS Performance,” *Tire Sci. Technol. TSTCA*, vol. 43, no. 3, pp. 216–241, 2015.

[4] S. Sivaramakrishnan, K. B. Singh, and P. Lee, “Experimental Investigation of the Influence of Tire Design Parameters on Anti-lock Braking System (ABS) Performance,” *SAE Int. J. Passeng. Cars - Mech. Syst.*, vol. 8, no. 2, pp. 2015-01–1511, Apr. 2015.

[5] A. A. Aly, E.-S. Zeidan, A. Hamed, and F. Salem, “An Antilock-Braking Systems (ABS) Control: A Technical Review,” *Intell. Control Autom.*, vol. 02, no. 03, pp. 186–195, 2011.

[6] P. Greibe, “Braking distance, friction and behaviour Findings, analyses and recommendations based on braking trials,” 2007.

[7] ETRMA, “EU Tyre Labelling Regulation 1222/2009 Industry Guideline on tyre labelling to promote the use of fuel-efficient and safe tyres with low noise levels,” no. July, 2011.

[8] T. Industry, “WET GRIP TEST METHOD IMPROVEMENT for Passenger Car Tyres (C1) Overview of Tyre Industry / ISO activities GRBP 68 th session,” vol. 15, no. September, pp. 12–14, 2018.

[9] “J2246A: Antilock Brake System Review - SAE International.”

[10] S. V. Sivaramakrishnan, “Discrete Tire Modeling for Anti-lock Braking System Simulations,” 2013.

[11] B. Hazen, “Masters Thesis: Design of an anti-lock brake algorithm based on wheel load measurements.”

[12] S. T. H. Jansen, P. W. A. Zegelaar, and H. B. Pacejka, “The Influence of In-Plane Tyre Dynamics on ABS Braking of a Quarter Vehicle Model,” *Veh. Syst. Dyn.*, vol. 32, no. 2–3, pp. 249–261, Aug. 1999.

[13] S. D. Gehman *et al.*, “Mechanics of pneumatic tires,” 1971.

[14] L. Valette, “2016 road safety statistics: What is behind the figures?,” *Eur. Comm.*, no. March, pp. 1–4, 2016.

[15] V. Ivanov, D. Savitski, K. Augsburg, and P. Barber, “Electric vehicles with individually controlled on-board motors: Revisiting the ABS design,” *Proc. - 2015 IEEE Int. Conf. Mechatronics, ICM 2015*, no. June, pp. 323–328, 2015.

[16] D. Savitski *et al.*, “The new paradigm of an anti-lock braking system for a full electric vehicle: experimental investigation and benchmarking,” *Proc. Inst. Mech. Eng. Part D J. Automob. Eng.*, vol. 230, no. 10, pp. 1364–1377, Sep. 2016.

[17] D. Savitski, V. Ivanov, B. Shyrokau, T. Pütz, J. De Smet, and J. Theunissen, “Experimental investigations on continuous regenerative anti-lock braking system of full electric vehicle,” *Int. J. Automot. Technol.*, vol. 17, no. 2, pp. 327–338, Apr. 2016.

[18] R. Bosch, *Bosch Automotive Handbook*, vol. Postfach, no. Plochngen. 2007.

[19] L. Pariota, S. R. Pastore, and F. Timpone, “Modelling components for the fuel consumption investigation in Model In the Loop environment: Parameter tuning for an ecological fully-adaptive cruise control system,” in *2016 IEEE 16th International Conference on Environment and Electrical Engineering (EEEIC)*, 2016, pp. 1–6.

[20] J. Zhao, J. Zhang, and B. Zhu, “Development and Verification of the Tire/Road Friction Estimation Algorithm for Antilock Braking System,” *Math. Probl. Eng.*, vol. 2014, pp. 1–15, Sep. 2014.

[21] B. N. J. Persson, “Rubber friction and tire dynamics,” *J. Phys. Condens. Matter*, vol. 23, pp. 15003–15017, 2011.

[22] Chih-Min Lin and Chun-Fei Hsu, “Self-learning fuzzy sliding-mode control for antilock braking systems,” *IEEE Trans. Control Syst. Technol.*, vol. 11, no. 2, pp. 273–278, Mar. 2003.

[23] M. Tanelli, A. Astolfi, and S. M. Savaresi, “Robust nonlinear output feedback control for brake by wire control systems,” *Automatica*, vol. 44, no. 4, pp. 1078–1087, Apr. 2008.

[24] H.-S. Tan and M. Tomizuka, “An Adaptive Sliding Mode Vehicle Traction Controller Design,” in *1990 American Control Conference*, 1990, pp. 1856–1862.

[25] Y.-K. Chin, W. C. Lin, D. M. Sidlosky, D. S. Rule, and M. S. Sparschu, “Sliding-Mode ABS Wheel-Slip Control,” in *1992 American Control Conference*, 1992, pp. 1–8.

[26] J. C. Gerdes and J. K. Hedrick, “Brake System Modeling for Simulation and Control,” vol. 121, no. September 1999, 2013.

[27] D. Cho and J. K. Hedrick, “Automotive Powertrain Modeling for Control,” *J. Dyn. Syst. Meas. Control*, vol. 111, no. 4, p. 568, Dec. 1989.

[28] E. Kayacan, Y. Oniz, and O. Kaynak, “A grey system modeling approach for sliding-mode control of antilock braking system,” *IEEE Trans. Ind. Electron.*, vol. 56, no. 8, pp. 3244–3252, Aug. 2009.

[29] Institute of Electrical and Electronics Engineers., *2004 5th Asian Control Conference : Melbourne, Australia, 20-23 July, 2004*. IEEE, 2004.

[30] C. Unsal and P. Kachroo, “Sliding mode measurement feedback control for antilock braking systems,” *IEEE Trans. Control Syst. Technol.*, vol. 7, no. 2, pp. 271–281, Mar. 1999.

[31] W. K. Lennon and K. M. Passino, “Intelligent control for brake systems,” *IEEE Trans. Control Syst. Technol.*, vol. 7, no. 2, pp. 188–202, Mar. 1999.

[32] C. C. Lee, “Fuzzy logic in control systems: fuzzy logic controller. I,” *IEEE Trans. Syst. Man. Cybern.*, vol. 20, no. 2, pp. 404–418, 1990.

[33] S.-W. Kim and J.-J. Lee, “Design of a fuzzy controller with fuzzy sliding surface,” *Fuzzy Sets Syst.*, vol. 71, no. 3, pp. 359–367, May 1995.

[34] R. E. Precup, S. Preitl, M. Balas, and V. Balas, “Fuzzy controllers for tire slip control in anti-lock braking systems,” in *2004 IEEE International Conference on Fuzzy Systems (IEEE Cat. No.04CH37542)*, vol. 3, pp. 1317–1322.

[35] H. B. Pacejka and E. Bakker, “The magic formula tire model,” *Veh. Syst. Dyn.*, vol. 21, no. 1, pp. 1–18, Jan. 1992.

[36] H. B. Pacejka, *Tire and Vehicle Dynamics*. Butterworth-Heinemann, 2006.

[37] V. V. Vantsevich and J. P. Gray, “Relaxation Length Review and Time Constant Analysis for Agile Tire Dynamics Control,” in *Volume 3: 17th International Conference on Advanced Vehicle Technologies; 12th International Conference on Design Education; 8th Frontiers in Biomedical Devices*, 2015, p. V003T01A038.

[38] C. L. CLOVER and J. E. BERNARD, “Longitudinal Tire Dynamics,” *Veh. Syst. Dyn.*, vol. 29, no. 4, pp. 231–260, Apr. 1998.

[39] G. Rill, “First Order Tire Dynamics,” in *III European Conference on Computational Mechanics*, Dordrecht: Springer Netherlands, 2008, pp. 776–776.

[40] F. Braghin and E. Sabbioni, “A Dynamic Tire Model for ABS Maneuver Simulations,” *Tire Sci. Technol.*, vol. 38, no. 2, pp. 137–154, 2010.

[41] A. J. C. Schmeitz and W. D. Versteden, “Structure and Parameterization of MF-Swift, a Magic Formula-based Rigid Ring Tire Model,” *Tire Sci. Technol.*, vol. 37, no. 3, pp. 142–164, Sep. 2009.

[42] J. P. Pauwelussen, *Essentials of vehicle dynamics*. Elsevier, 2014.

[43] M. Guiggiani, *The science of vehicle dynamics: Handling, braking, and ride of road and race cars*. 2014.

[44] C. Costitutivo, “Materiali a Comportamento Viscoelastico: Comportamento Costitutivo,” *Tecnol. E Mater. Aerospaziali*, pp. 1–19.

[45] “WHITEPAPER 2 A Basic Introduction to Rheology Shear Flow.”

[46] M. L. Williams, R. F. Landel, and J. D. Ferry, “The Temperature Dependence of Relaxation Mechanisms in Amorphous Polymers and Other Glass-forming Liquids,” *J. Am. Chem. Soc.*, vol. 77, no. 14, pp. 3701–3707, Jul. 1955.

[47] M. G. Potenger, “Contact Patch (Footprint) Phenomena,” *Pneum. Tire*, no. February, pp. 231–285, 2006.

[48] F. P. Bowden and D. Tabor, “The Area of Contact between Stationary and between Moving Surfaces,” *Proc. R. Soc. A Math. Phys. Eng. Sci.*, vol. 169, no. 938, pp. 391–413, Feb. 1939.

[49] G. Theses and J. Vishwanath Kosgolla, “Numerical Simulation of Sliding Friction and Wet Traction Force on a Smooth Tire Sliding on a Random Rough Pavement,” 2012.

[50] H. W. Kummer, “Unified Theory of Rubber and Tire Friction. Eng. Res,” *Bull. B-94, Pennsylvania State Univ.*, pp. 100–101, 1966.

[51] B. N. J. Persson, “Theory of friction and boundary lubrication,” *Phys. Rev. B*, vol. 48, no. 24, pp. 18140–18158, Dec. 1993.

[52] B. N. . Persson, “On the theory of rubber friction,” *Surf. Sci.*, vol. 401, no. 3, pp. 445–454, Apr. 1998.

[53] G. Gudehus, “SLIDING FRICTION, Physical Principles and Applications, Bo N. J. Persson, Springer-Verlag, Berlin, Germany, 1998,” *Int. J. Numer. Anal. Methods Geomech.*, vol. 24, no. 1, pp. 95–95, Jan. 2000.

[54] SAE International, “J670 Vehicle Dynamics Terminology,” 2008.

[55] M. Society of Automotive Engineers., G. Ma, S. Society of Automotive Engineers., and S. Taheri, *S.A.E. transactions.*, vol. 7, no. 1. Society of Automotive Engineers, 1927.

[56] M. Wieczorek and J. Jackowski, “Car tyres with reduced energy consumption,” vol. 25, no. 1, 2018.

[57] MSC Adams 2012, “Using the PAC2002 Tire Model When to Use PAC2002 Modeling of Tire-Road Interaction Forces,” pp. 1–58, 2012.

[58] N. Kudarauskas, “Analysis of emergency braking of a vehicle,” vol. XXII, no. 3, pp. 154–159, 2010.

[59] T. Wei and H. Dorfi, “Tire Transient Lateral Force Generation: Characterization and Contribution to Vehicle Handling Performance,” *Tire Sci. Technol.*, vol. 42, pp. 263–289, 2014.

[60] I. J. M. M. Besselink, A. J. C. C. Schmeitz, and H. B. Pacejka, “An improved Magic Formula/Swift tyre model that can handle inflation pressure changes,” *Veh. Syst. Dyn.*, vol. 48, no. SUPPL. 1, pp. 337–

352, Dec. 2010.

[61] E. J. H. De Vries and D. J. Rixen, “Non-linear dynamic vehicle model and its inverse for brake control.”

[62] G. Di Massa, S. R. Pastore, R. Russo, and F. Timpone, “Precursors of instability for a vehicle traveling in curve,” *IREMOS - Int. Rev. Model. Simulations*, vol. 12, no. 1, p. 1, Feb. 2019.

[63] A. Askarinejad, D. Akca, and S. M. Springman, “Precursors of instability in a natural slope due to rainfall: a full-scale experiment,” *Landslides*, vol. 15, no. 9, pp. 1745–1759, Sep. 2018.

[64] “Correlation coefficients - MATLAB corrcoef - MathWorks Benelux.” [Online]. Available: https://nl.mathworks.com/help/matlab/ref/corrcoef.html. [Accessed: 05-May-2019].

[65] “Optimization Toolbox™ User’s Guide R2019a,” 1990.

[66] R. Kennedy, “Road Profile Users Group Conference 1.”

[67] A. K. Bhoopalam, C. Sandu, S. Taheri, T. Furukawa, M. Ahmadian, and J. Terziyski, “Pneumatic Tire Performance On Ice,” 2015.

[68] Y. Oh and H. Lee, “Research Article,” 2014.

[69] M. T. Do and H. Zahouani, “Influence of the road-surface texture on the speed dependency of tire/road friction,” 2005.

[70] X. Lu, M. M. Khonsari, and E. R. M. Gelinck, “The Stribeck Curve: Experimental Results and Theoretical Prediction,” *J. Tribol.*, vol. 128, no. 4, p. 789, Oct. 2006.

[71] A. J. Tuononen, L. Hartikainen, F. Petry, and S. Westermann, “Parameterization of in-plane rigid ring tire model from instrumented vehicle measurements.”

[72] A. Tuononen, L. Hartikainen, F. Petry, and S. Westermann Goodyear, “Modeling tire vibrations in ABS-braking,” 2012.

[73] A. van Zanten, W. D. Ruf, and A. Lutz, “Measurement and Simulation of Transient Tire Forces,” 1989.

[74] P. W. A. Zegelaar, “The dynamic response of tyres to brake torque variations and road unevenesses.” 1998.

[75] “Linear Products Automotive AntiiLock Brake System Control Using Power+™ Control Devices.”

[76] P. W. A. ZEGELAAR and H. B. PACEJKA, “Dynamic Tyre Responses to Brake Torque Variations,” *Veh. Syst. Dyn.*, vol. 27, no. sup001, pp. 65–79, Jan. 1997.

[77] “Société de Technologie Michelin 23, rue Breschet, 63000 Clermont-Ferrand Grip on road surfaces.”

[78] B. N. J. Persson, “Theory of rubber friction and contact mechanics,” *J. Chem. Phys.*, vol. 115, no. 8, pp. 3840–3861, 2001.

[79] M. Ciavarella, “A Simplified Version of Persson’s Multiscale Theory for Rubber Friction Due to Viscoelastic Losses,” *J. Tribol.*, vol. 140, no. 1, p. 011403, 2017.

[80] F. Farroni, M. Russo, R. Russo, and F. Timpone, “A physical-analytical model for a real-time local grip estimation of tyre rubber in sliding contact with road asperities,” *Proc IMechE Part D J Automob. Eng.*, vol. 228, no. 8, pp. 955–969, 2014.

[81] C. Canudas-De-Wit, P. Tsiotras, E. Velenis, M. Basset, and G. Gissinger, “Vehicle System Dynamics Dynamic Friction Models for Road/Tire Longitudinal Interaction Dynamic Friction Models for Road=Tire Longitudinal Interaction,” vol. 39, no. 3, pp. 189–226, 2003.

[82] C. Canudas De Wit and P. Tsiotras, “Dynamic tire friction models for vehicle traction control,” *Proc. 38th IEEE Conf. Decis. Control (Cat. No.99CH36304)*, vol. 4, no. December, pp. 3746–3751, 1999.

[83] J. P. Maurice, M. Berzeri, and H. B. Pacejka, “Pragmatic Tyre Model for Short Wavelength Side Slip Variations,” *Veh. Syst. Dyn.*, vol. 31, no. 2, pp. 65–94, Feb. 1999.

[84] PerkinElmer Inc., “Dynamic Mechanical Analysis (DMA) - A Beginner’s Guide,” *Introd. to DMA*, pp. 1–23, 2008.

[85] W. C. Oliver and G. M. Pharr, “An improved technique for determining hardness and elastic modulus using load and displacement sensing indentation experiments,” *J. Mater. Res.*, vol. 7, no. 06, pp. 1564–1583, Jun. 1992.

[86] A. C. Fischer-Cripps, “Contact Mechanics,” 2004, pp. 1–20.

[87] A. C. Fischer-Cripps, *Nanoindentation*. Springer, 2004.

[88] Y. I. Golovin, “Nanoindentation and mechanical properties of solids in submicrovolumes, thin near-surface layers, and films: A Review,” *Phys. Solid State*, vol. 50, no. 12, pp. 2205–2236, Dec. 2008.

[89] X. Li and B. Bhushan, “A review of nanoindentation continuous stiffness measurement technique and its applications,” *Mater. Charact.*, vol. 48, no. 1, pp. 11–36, Feb. 2002.

[90] S. R. Cohen and E. Kalfon-Cohen, “Dynamic nanoindentation by instrumented nanoindentation and force microscopy: a comparative review,” *Beilstein J. Nanotechnol.*, vol. 4, pp. 815–833, Nov. 2013.

[91] M. L. Oyen and R. F. Cook, “Load–displacement behavior during sharp indentation of viscous–elastic–plastic materials,” *J. Mater. Res.*, vol. 18, no. 01, pp. 139–150, Jan. 2003.

[92] Y.-T. Cheng and C.-M. Cheng, “Scaling, dimensional analysis, and indentation measurements,” *Mater. Sci. Eng. R Reports*, vol. 44, no. 4–5, pp. 91–149, Aug. 2004.

[93] E. G. Herbert, W. C. Oliver, and G. M. Pharr, “Nanoindentation and the dynamic characterization of viscoelastic solids,” *J. Phys. D. Appl. Phys.*, vol. 41, no. 7, p. 074021, Apr. 2008.

[94] J. J. Aklonis and W. J. MacKnight, *Introduction to polymer viscoelasticity*. Wiley-Interscience, 2005.

[95] L. Wang and X. Liu, “Characterization of viscoelastic materials by quasi-static and dynamic indentation,” *Meas. Sci. Technol.*, vol. 25, no. 6, 2014.

Appendix

A.1 Method for the characterization of the load sensitivity of the tire from vehicle measurements

In this paragraph, a method for the characterisation of the load sensitivity of the tire from vehicle measurements is proposed. It has been designed to improve for the full characterisation of the tire in wet conditions. However, since it has not been proposed in the tire model, it is described in the Appendix.

Therefore, once obtained the desired μ-slip shape through the tire characterization of the studied tires with a trailer on wet surface, the second step has been to guarantee a load sensitivity closer to the real behaviour of the tire. Assumed that a reference tire model was the starting point of this procedure, it can be understood that the load sensitivity would remain the same for the 2 different tires.

It has been studied a simple approach to get the load sensitivities from vehicle data. It is based on some steps as shown below:

- Calculation of slip ratio κ, longitudinal force F_x and vertical load F_z;
- Evaluation of F_x in the slip range where the peak is expected for the 2 tires
    - Tire A, κ = [4%,7%];
    - Tire B, κ = [6%,8%];
- Evaluation of F_x for small ranges of the vertical load, with steps by 100N;
- Average of the obtained grip values per each vertical load.4

The results are shown in the Figure A-1. It is possible to consider these results with the aim to change the load sensitivity of the reference tire. Practically, since the new shape has been obtained, it is possible to replace the peak value at the different vertical loads with the new data from vehicle measurements. Finally, the estimated load sensitivity has been fitted by a cubic function, as shown below:

$$F_x = aF_z{}^3 + bF_z{}^2 + cF_z + d \tag{A.1}$$

with a, b, c and d the parameters of the equations. That could allow to make a model of the load sensitivity of the tire and allow to change the peak condition of a certain tire model.

In Figure A-2 and A-3, it is clear the different slope of the F_x between Tire A and B with respect to the vertical load, by focusing on the higher differences of the grip peaks among the different vertical loads.

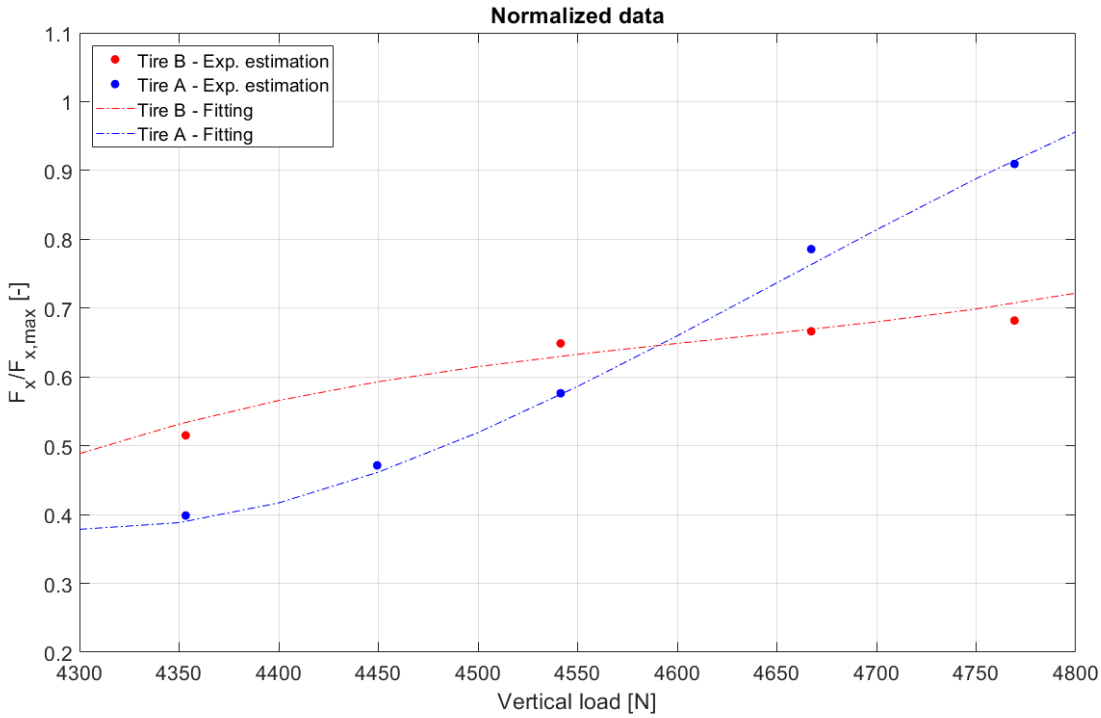

Figure A-1 - Estimation of the load sensitivity of the tires from vehicle data.

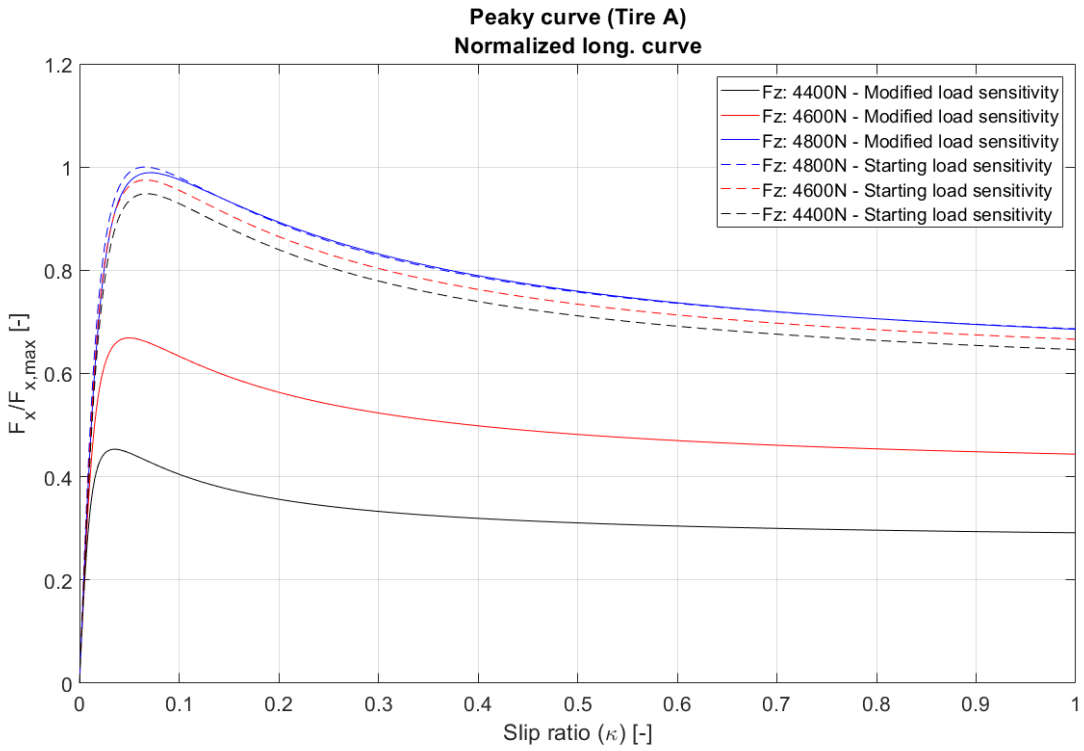

Figure A-2 - Variation of the peak values based on the estimated load sensitivities (Tire A).

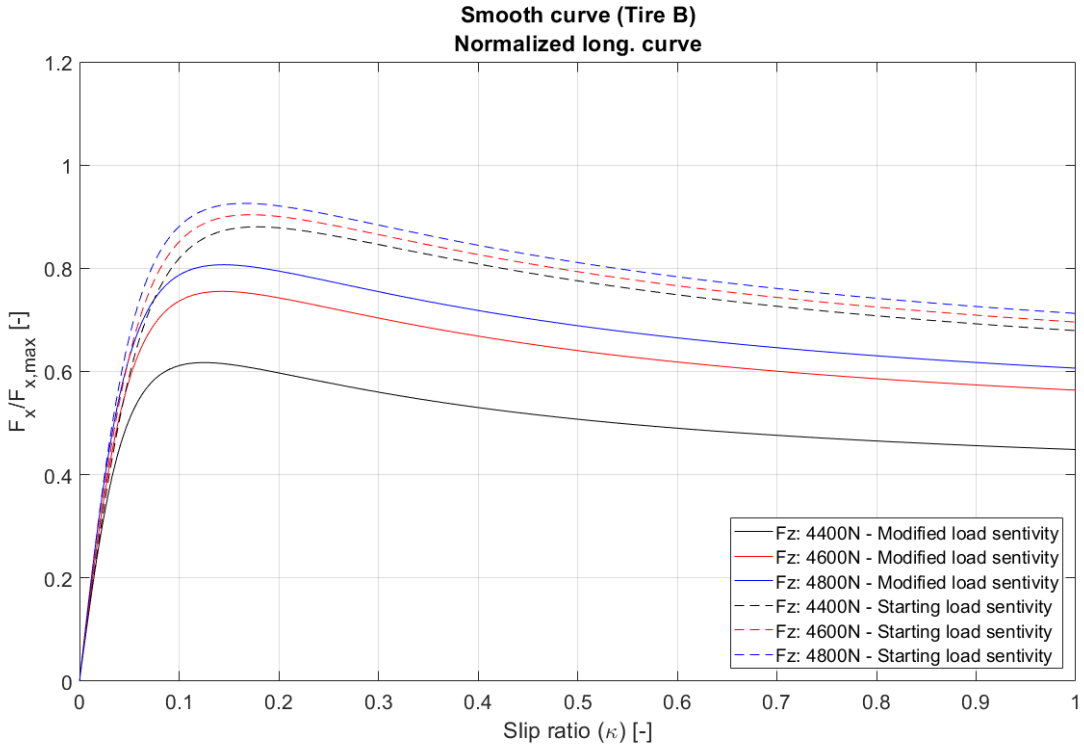

Figure A-3 - Variation of the peak values based on the estimated load sensitivities (Tire B).

It is possible to manage the only value of the grip because the outdoor test with the trailer at the same velocity are considered. In this sense, despite the load sensitivity from vehicle data are obtained at different velocities, the trailer test has been carried out at an only velocity.

A.2 Model for frequency influence on relaxation length variations

As already described, although several dynamic tire-road contact models are available in the literature [81][82][83], the MF-Tire model is the most popular one and the MF Relax proposed by Braghin et al. [40] is computationally very "light": in this thesis a new dynamic tire -road contact model is proposed that combines both the merits of the two relaxation length models previously described: low computational effort and high reliability.

The following equation tries to propose the relation between the relaxation length and the excitation frequency with which the longitudinal slip changes during the braking. This formula has not been included in the model, but it can be considered as a proposal for future development of the activity and improvement of the MF-Tire model for the ABS braking simulations, as also described in Chapter 5, Paragraph 5.2:

$$\sigma_{\kappa,f} = \left(\sigma_{\kappa,slip} - STX1\right) \cdot f \cdot e^{-STX2 \cdot f} - \operatorname{atan}(STX3 \cdot f) + STX1 \qquad \text{(A.2)}$$

where $STX1$, $STX2$ and $STX3$ are empirical parameters which can be experimentally obtained. As it is possible to see in the equation above, a similar approach to the MF Relax model has been used. In the following Figure A-4 an example is shown, between fitted (line) and calculated relaxation length from filtered data (dotted curve) at three different vertical loads.

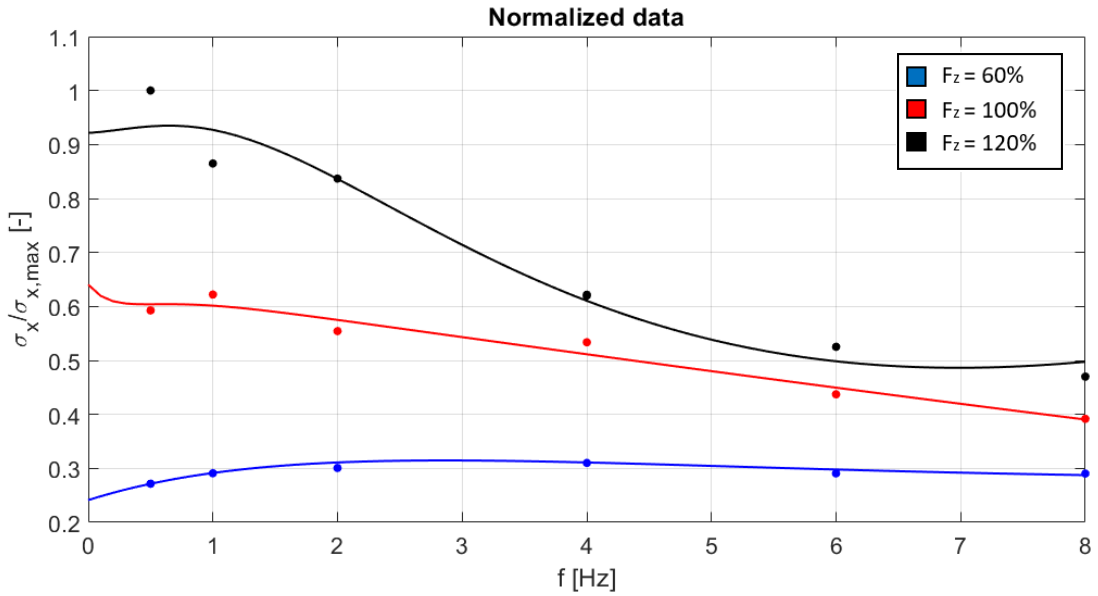

Figure A-4 – Example of the dependency of the relaxation length on excitation frequency, fitted with the proposed model, at V_x = V_3 and slip amplitude 1%.

Inserting the so determined relaxation length in the same first order differential equation in the longitudinal deformation of the tire carcass u as before,

$$\sigma_{\kappa,freq}\frac{du_x}{dt} + |V_x|u_x = -\sigma_{\kappa,freq}\kappa\, V_x \tag{A.3}$$

the longitudinal contact force can be determined, where V_x is the longitudinal speed component of the hub and κ the longitudinal slippage. In the Figure A-5, it is possible to a see logic flow-chart that can be considered for the implementation of the proposed model.

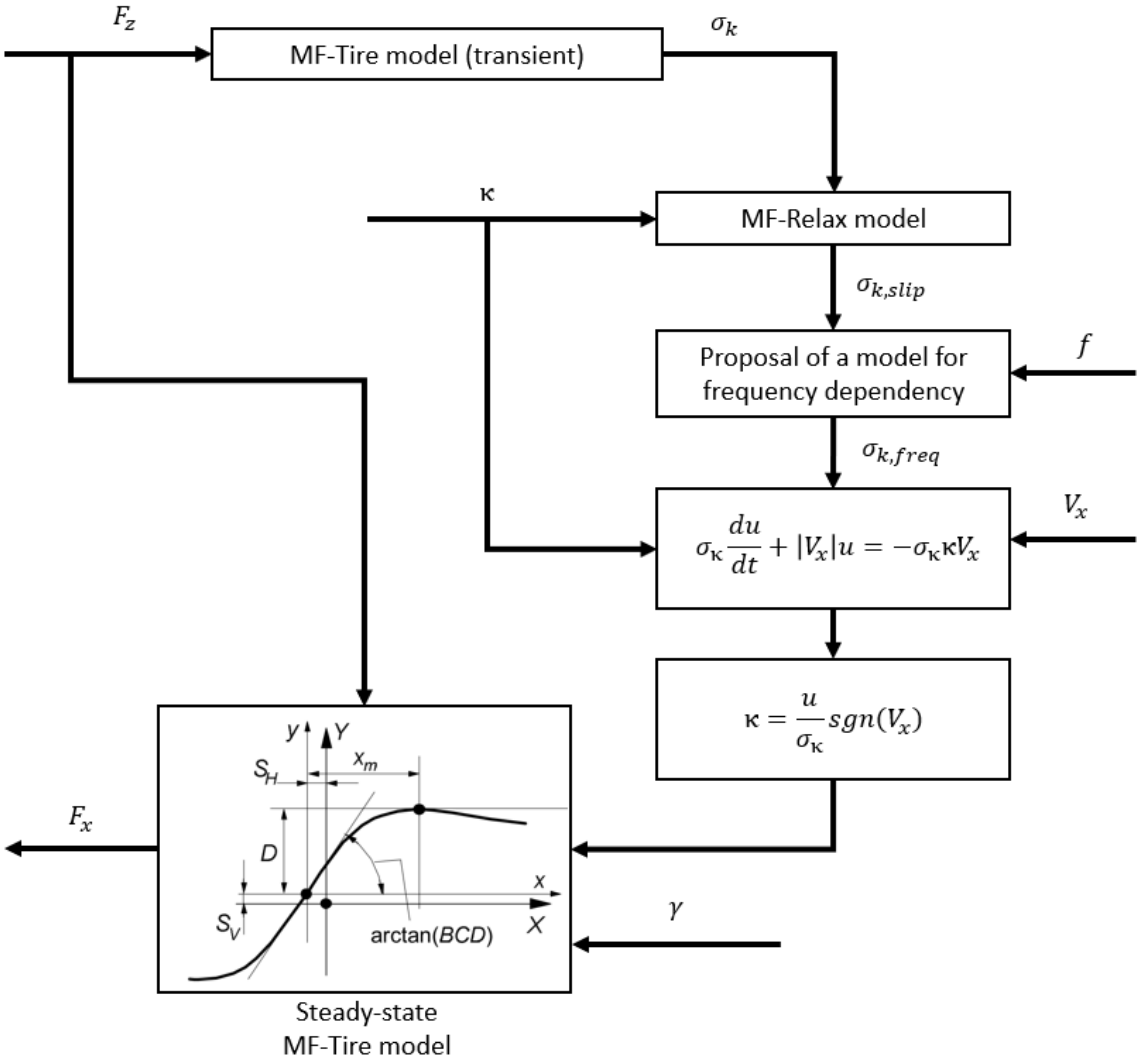

Figure A-5 - Flow chart for the implementation of the frequency-based model.

As future development of the activity, the dependency of the parameters $STX1$, $STX2$ and $STX3$ on the vertical load and slip ratio amplitudes will be investigated.

A.3 An in-house made instrument for non-disruptive viscoelastic characterisation: V-ELA

To better monitor how the tire can change its behaviour during a manoeuvre such as the emergency braking and how it can affect the ABS performance, it has been considered that it is crucial to know the rubber properties of the tire tread. It is important to focus on this topic for a better correlation between braking results from outdoor testing and compound characteristics. In this paragraph, an innovative instrument called V-ELA (Visco-ELAstic) for the evaluation of tire rubber moduli is described. The development of the instrument has started during this PhD work at the Department of Industrial Engineering at the University of Naples "Federico II", with the aim to make a procedure to get viscoelastic moduli (E' and E'') of rubber and find a correlation with results from DMA test. Despite it has been designed for motorsport purposes, the V-ELA can play an important role for the goal of this Thesis (Paragraph 7.2.3): because of its purpose to be suitable for measurements directly from tire, it can help to monitor the status of the rubber during the tests and estimate any changes in E', E'' and $tan(\delta)$. Both static and dynamic test methods will be shown, with the description of the optimization process expected for viscoelastic

parameter determination. The most important innovation that this instrument wants to introduce is the possibility to allow reliable characterizations of the rubber compounds directly from the tested tire thanks to non-disruptive tests.

A.3.1 Description of the DMA test approach

The DMA (Dynamic Mechanical Analysis) test is the common one used for rubber characterizations: a small deformation is applied to a sample in a cyclic manner. This allows to study the materials response to stress, temperature, frequency and other values [84]. The DMA test allows to measure stiffness and damping by applying a sinusoidal force: these are reported as moduli and tan(δ). It is also possible to split the modulus as an in-phase component (the storage modulus) and an out of phase component (the loss modulus), as already explain in Paragraph 4.2 and shown in Figure 4-4.

The DMA test can give a very reliable picture of the compound behaviour (at different temperatures and frequencies) by analysing a rubber block. The sample can be subjected to a controlled stress or a controlled strain. For a known stress, the sample will then deform a certain amount. How much it deforms is related to its stiffness. A force motor is used to generate the sinusoidal excitation and this is transmitted to the sample via a drive shaft.

A.3.2 Introduction to the indentation approach

The indentation test is one of the most widely investigated techniques for measuring the mechanical properties of the rubber. Traditionally, the instrumented indentation test is based upon successively recording the loading force and the penetration depth throughout the entire process of the testing period. The recent development of this technique has enabled depths of penetration to be measured at nano-meter resolution or less [85][86][87][88].

The instrument for the indentation approach is especially suitable for testing materials with a small volume, which is difficult to perform in a tensile test [89]. It is not surprising that the extension of the indentation technique to soft or compliant materials such as polymers, hydro-gels and biomaterials is becoming a hot research topic in recent years.

However, for the characterization of the viscoelastic properties an alternative method has been developed, because the indentation data analysis assumes that deformation during unloading is purely elastic in nature. In addition, during the loading and unloading process, the response of such material depends not only on the applied force, but also on the loading duration. If the material displays viscoelastic properties, errors in the determined modulus will be observed [90]. Consequently, the greatest problem with this kind of application is that the traditional technique used for elastic–plastic material does not accurately describe the response of these viscoelastic materials.

When it comes to viscoelastic material, indentation experiments are usually performed using two different approaches:

- the static test procedure, for the creep (load control) and the relaxation (displacement control) phenomena [91][92];
- the dynamic test procedure.

This static test method establishes a viscous–elastic–plastic model [91] which is on the basis of a set of mechanical elements (viscous, elastic, plastic) in series for the indentation of time-dependent materials; another method is performing dynamic indentation in the frequency domain to characterize the materials' properties over a range of frequencies instead of an extended time [93]. More specifically, the dynamic indentation expects the application of an oscillatory load to a pin: the dynamic properties can be determined by monitoring the phase lag between displacement response and load measurement.

A.3.3 Description of V-ELA

In the following Figure A-6, it is possible to see a scheme to describe the instrument. The instrument consists of a fixed part, connected to the ground/sample (the external cylinder), and a movable part.

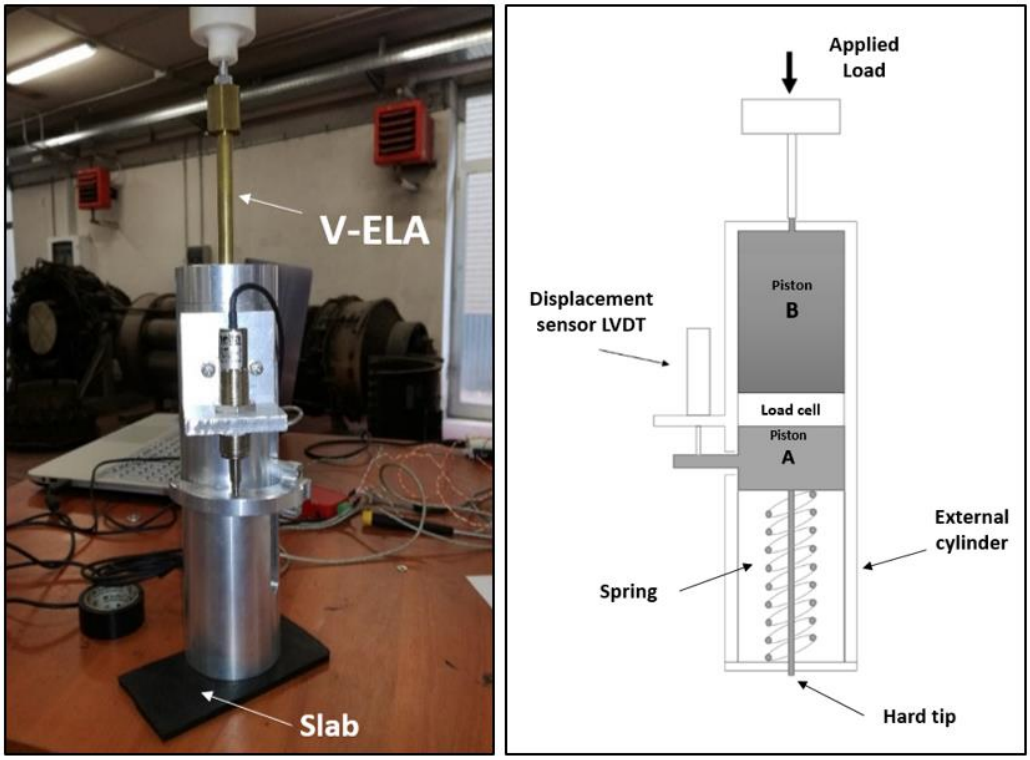

Figure A-6 - V-ELA: the scheme of the instrument.

The hard tip component transmits the force to the sample, by means of the action of pressure on the surface of the latter. It is considered infinitely rigid. The tip can penetrate the sample, moving from the cylinder through a hole, as shown in the Figure A-7.

Figure A-7 – Hard tip.

A Spring allows the ascent of the Piston A (both shown in the Figure A-7), which plays a fundamental role because it allows the transmission of the force coming from the reaction of the sample to the load cell. At the same time, it allows to measure the deformation of the sample. The Piston B is bound to the upper piston, where the force is applied and transmitted to the load cell, from which it will then come through the Piston A to the sample.

The Load cell allows to measure the applied vertical force when it is in contact with the slab: normally, it is a transducer used to measure a force applied on an object. It is a tool that detects the mechanical deformation of an element and it is capable to convert the force into an electrical signal that is proportional to deformation by the element itself. This component is usually made of a metal body, often made of hardened steel, to which they apply one or several strain gauges (a sensor that reads both the mechanical compression of traction deformations of the material) through the variation of electric resistance strain that causes on its electric circuit).

The load cell and a displacement sensor (LVDT transducer) allow to do the force and displacement measurements. The LVDT Transducer is an electromagnetic device used to measure the small displacements of the rod. It can be seen in the Figure A-8 below. The measurements are carried out once the sensors are connected to a special analogue-digital card for data acquisition, by applying a load on the upper part of the instrument.

Figure A-8 - The scheme of the LVDT transducer for displacement measurements.

The V-ELA allows to do several test methods at several vertical loads. In the case of a creep test, the applied vertical load is constant while in the case of a dynamic test it is used to apply a sinusoidal load. Finally, the displacement sensor will detect displacements.

A.3.4 Test procedures

Static test

Experiments and data processing will be described in this paragraph: both static and dynamic tests have been carried out with the goal of characterizing stiffness and damping initially, and then calculate the values of E', E'' and $tan\ (\delta)$.

Some assessments have been carried out to check the calibration of the instrument, by force and displacement. To adjust the zero of the load cell, the instrument has been positioned horizontally to prevent the weight of the structure from weighing on the cell itself; as far as the displacement sensor is concerned, it has been calibrated by placing the instrument in a vertical position and managing the upper piston work so that the ends of the hard tip coincides with the lower surface of the external cylinder.

The goal is to evaluate the behaviour of the compound subjected to a constant load over time through the analysis of stress and deformation induced by this applied load. The stiffness (K) is defined as the ability of a body to oppose the elastic deformation caused by an applied force (Hooke's law). This can be expressed by:

$$K = \frac{F}{\delta} \tag{A.4}$$

referring to a body that deforms a quantity δ because of a force applied F. To evaluate the sensitivity of the device, the tests were carried out on samples (better known as slab), from three different types of rubber compounds called hard, medium and soft. The instrument allows to indent the rubber sample through an applied force or displacement: in this way it would be possible to investigate both the phenomena of relaxation and creep.

A constant load is applied by calibrated weights: in this way, the instrument will warp the compound thanks to the sliding of a piston that moves the tip. The sample rate of the load cell and the LVDT transducer is 100Hz.

The sample shows a creep behaviour that is a characteristic of viscoelastic materials: if stressed with a constant load, it has an instantaneous initial deformation and then continues to deform over time to a certain threshold value in which the internal reaction of the compound essentially equate the external stress.

Through this static analysis, the stiffness of the rubber will be calculated: measuring the asymptotic value of the displacement or the value corresponding to the maximum deformation of the sample measured at the end of the test.

The system can be studied by considering a first order differential equation with response to the unitary step (Figure A-9). The pattern of deformation over time, starting from the point of end of the instantaneous deformation, can be represented by an exponential equation.

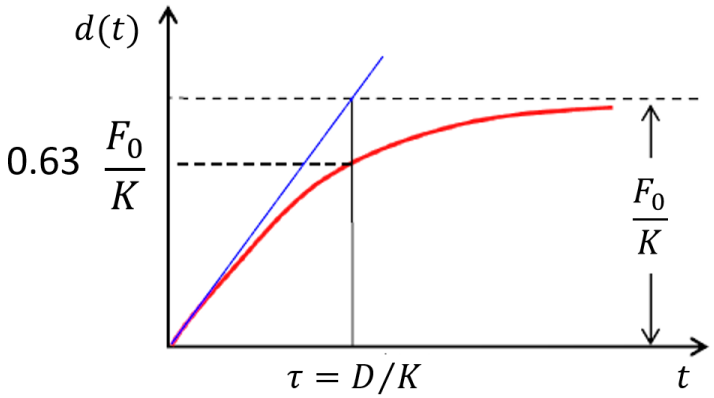

Figure A-9 - Kelvin-Voigt model response for the static procedure.

In order to calculate the stiffness and damping values of the rubber sample by following the approach showed in the Figure A-9. The approach used is based on the following points:

1. Calculation of the fitted curve using last points of the raw data, to calculate $d_{max} = \frac{F_0}{K}$.
2. Calculation of the time lag τ, by considering the 63% of d_{max}.as maximum displacement. In this way, assuming $\tau = \frac{D}{K}$, it is possible to calculate the damping effect D of the viscoelastic material (that will not be considered in this analysis).

The average of the stiffness values obtained from different repetitions is then calculated in such a way as to obtain a single reference value referring to the variation of the load and the kind of compound tested. The calculated values show a certain variability, as show in Figure A-10.

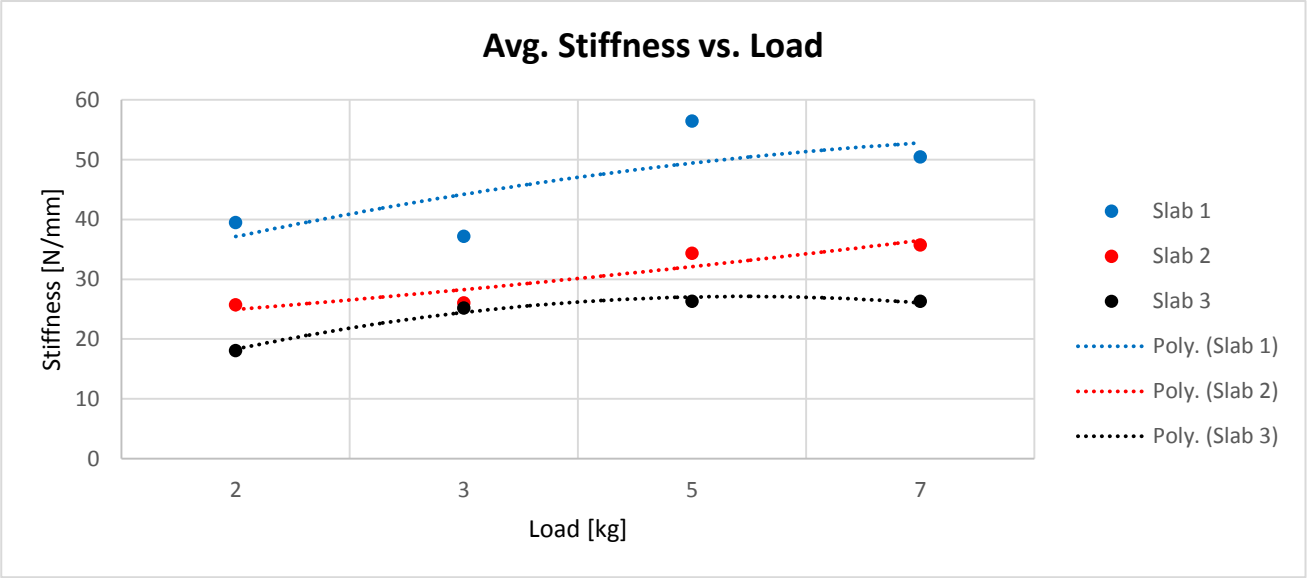

Figure A-10 – Average Stiffness values at different applied vertical loads.

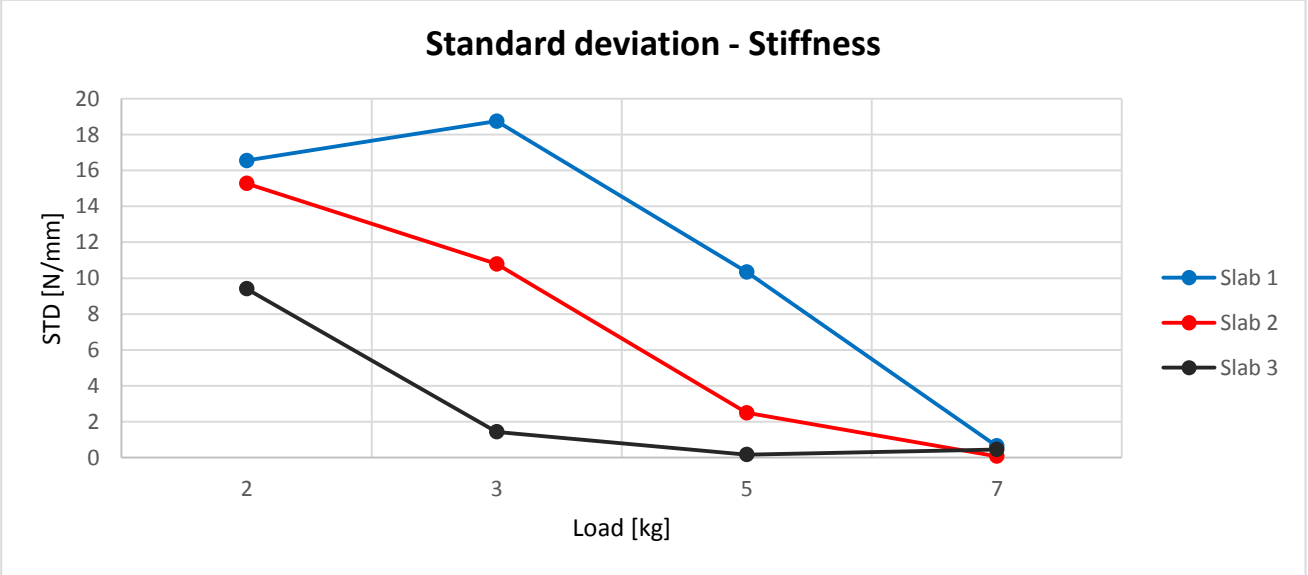

Figure A-11 - Standard deviation of the rubber stiffness.

In Figure A-11, it is possible to see that the stiffness is increasing with the vertical load. It is also possible to observe that it saturates at the higher loads. As shown in Figure A-11, the standard deviation at the different loads is showing that the higher the load, the lower the variability of the calculated stiffness. Moreover, the STD is lower for the soft compound and it increase when the medium and the hard ones are evaluated, respectively. In the Table A-1, the data about the average stiffness and the related standard deviations per each vertical load are shown.

Table A-1 - Stiffness of the rubber samples with a static procedure at different loads from experimental data.

Load [kg]	Average stiffness			STD		
	Slab 1	Slab 2	Slab 3	Slab 1	Slab 2	Slab 3
2	39.5	25.7	18.1	16.6	15.3	9.4
3	37.2	26.0	25.2	18.7	10.8	1.4
5	56.4	34.3	26.3	10.3	2.5	0.2
7	50.4	35.7	26.3	0.6	0.1	0.5

Therefore, it has been considered that the average stiffness value from the highest load must be more reliable with respect to the lower ones. Moreover, because of the repeatability of the measurement (that must be improved), it has been observed that the highest stiffness estimations coming from the several repetitions at the lower load reach similar values that is possible to find at the higher loads.

Dynamic test

As shown in Figure A-6, the rubber slab is placed below the instrument which is positioned vertically and through the upper piston a cyclic load is applied manually by the user. A certain preload is applied before starting with the sinusoidal input. The first test was carried out at different temperatures T = [-20°C, 90°C] for a time duration of 10 s and a sampling frequency of 50 Hz.

The Load cell and LVDT sensors will provide the values of force and displacement recorded in relation to the elapsed time.

The signal has been filtered and reduced by its average value, since a preload was applied (Figure A-12 and Figure A-13). It has been done in order to prepare the signal for the data processing algorithm, where the harmonic component is required as input.

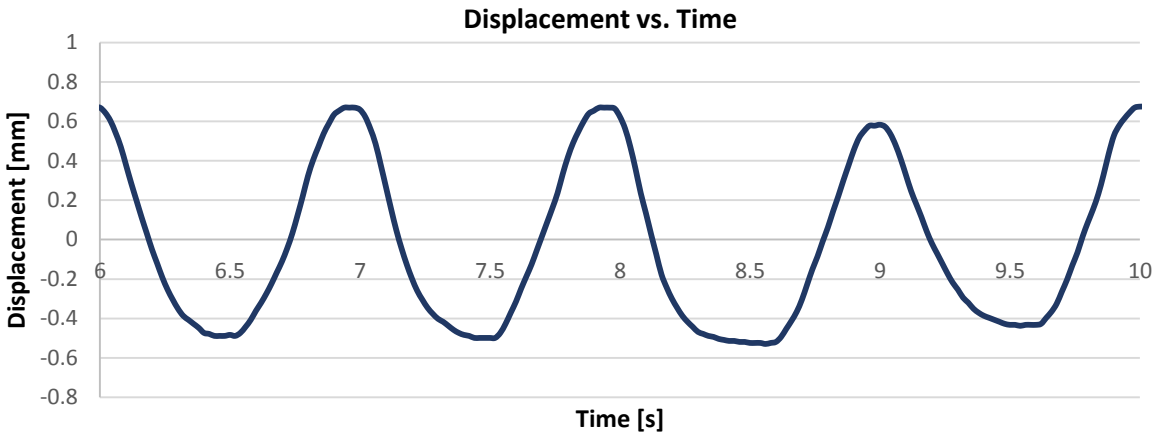

Figure A-12 - Cyclic displacement input with the time.

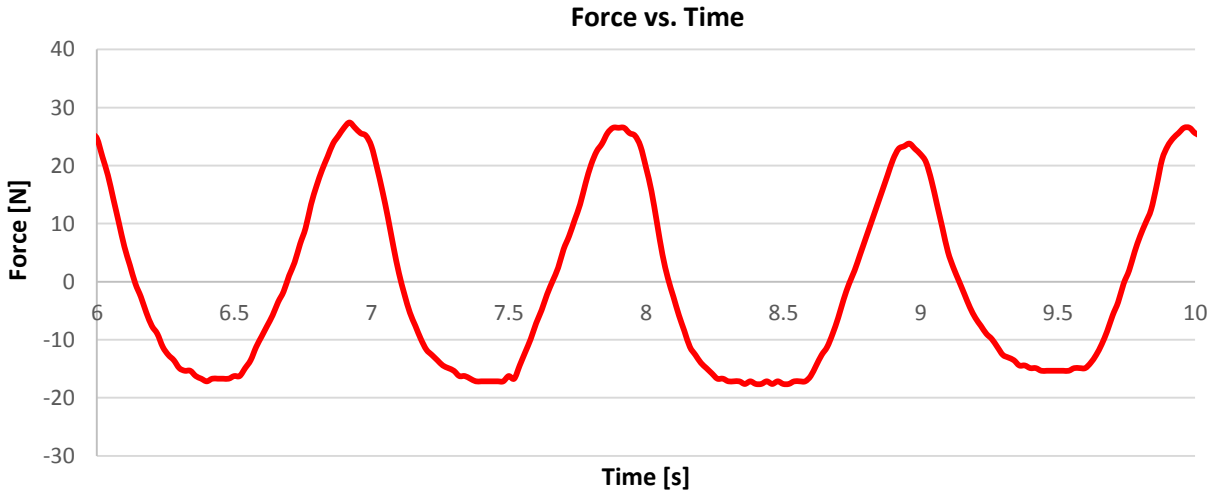

Figure A-13 - Cyclic force output with the time.

The same operation is repeated for all the different compounds under evaluation. The described test procedure has been performed at room temperature. As far as high and low temperature tests are concerned, the procedure has been essentially the same, unless a few steps are required to bring the test to the desired temperature. As for the cold tests, the samples were placed in the fridge in order to reach a temperature around -20 °C.

Once the desired temperature has been reached, the sample is taken and placed on a flat surface. The above-described dynamic test has been done and repeated several times, following the heating of the rubber and trying to cover the wider possible temperature range [-20°C, 16°C]. For each test, the initial and final temperature was recorded with an infrared thermometer, in order to use an average of the two temperatures as the test reference one.

As concerns warmer tests, the compounds have been warmed up inside an oven up to a temperature around 90 °C. The slab is then taken and placed on the previously heated surface by the temperature heat gun, to avoid excessive heat exchange. Even in this case the goal will be to cover the wider temperature range of [18°C, 80°C]. It has been experienced a too rapid cooling down of the rubber slab due to the thermal dispersion in the laboratory. Therefore, at the end of each test the surface has been heated further, with the help of the temperature heat gun, in order to make the cooling phase more gradual and reach the desired temperatures.

This step will be repeated until the heat exchange is small enough to accommodate the normal cooling of the compound. As for the cold tests for each test the initial and final temperature of the test was recorded and their values used as test reference temperature.

A.3.5 Calculation of the loss, storage moduli and loss factor from Dynamic test

The viscoelastic models described in Paragraph 4.3 will be take into account for the current analysis. The Maxwell model is much more appropriate for viscous fluid and the Voigt model is more suitable for viscoelastic solids. Therefore, the Voigt model is used to represent the sample in this work[94][95], as shown in Figure A-14.

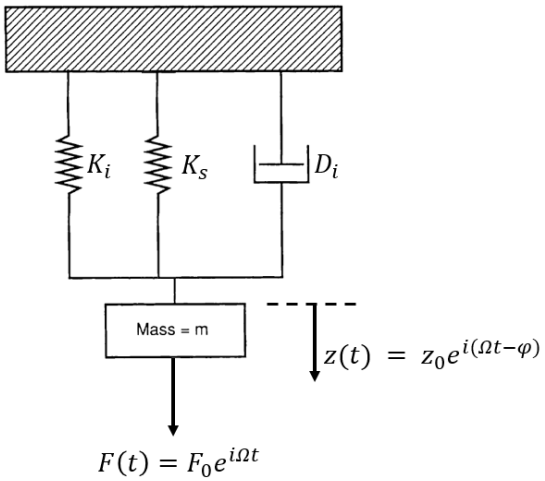

Figure A-14 - Simple harmonic oscillator model (free hanging).

The system is excited by an oscillating force:

$$F(t) = F_0 e^{i\Omega t} \tag{A.5}$$

with Ω the fundamental harmonic. It expects a response of the form:

$$z(t) = z_0 e^{i(\Omega t-\varphi)} \tag{A.6}$$

that is, the oscillation of the mass at the same fundamental harmonic frequency with a phase lag of φ. The equations (A.7):

$$\begin{aligned} K_i - m_i\Omega^2 &= \frac{F_0}{z_0}\, cos\varphi|_{free-hanging} \\ D_i &= \frac{F_0}{z_0}\, sin\varphi|_{free-hanging} \end{aligned} \tag{A.7}$$

are describing the scheme of the instrument when the tip of the instrument is not in contact. The model components are those of the indenter itself: $K = K_i$, $m = m_i$ and $D = D_i$. When the indenter is in full contact with the sample, the indentation components and sample are modelled together: K_c and D_c represent the stiffness and damping of the contact, respectively (Figure A-15).

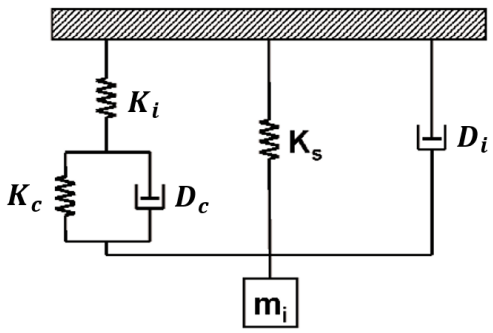

Figure A-15 - Scheme of the V-ELA in contact with the rubber sample [95].

The dynamic stiffness of the system in Figure A-15 is given by:

$$(K_i + K_c) - m_i\Omega^2 = \frac{F_0}{z_0} cos\varphi|_{contact} \tag{A.8}$$

assuming that two springs in parallel can be set as one by adding their stiffness. Likely, the dynamic damping is given by:

$$(D_i + D_c)\Omega = \frac{F_0}{z_0} sin\varphi|_{contact} \tag{A.9}$$

and the equations (A.8) and (A.9) show that both contact stiffness and damping are independent of the mass of the indenter.

The reference dynamic model is described by the equations (A.10), where some hypotheses have been considered in order to simplify the model:

$$\begin{aligned} K_c - m_i\Omega^2 &= \frac{F_0}{z_0} cos\varphi|_{contact} \\ D_c\Omega &= \frac{F_0}{z_0} sin\varphi|_{contact} \end{aligned} \tag{A.10}$$

and shown in Figure A-16. Based on the configuration of the V-ELA, K_i and D_i can be neglected. The stiffness K_i of the spring does not give a direct contribution on the calculation of the equivalent stiffness because it is considered as infinitely rigid. The damping compliance of the spring D_i is neglected as the coil spring is considered with no damping effect.

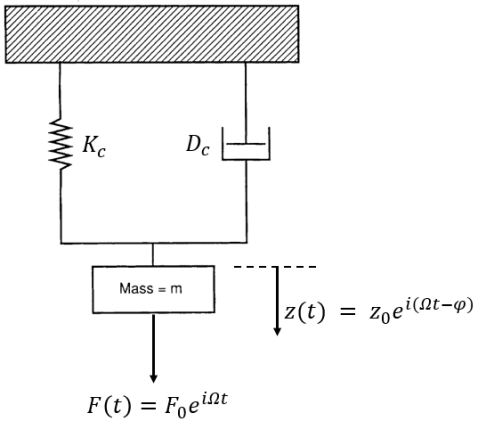

Figure A-16 - Kelvin-Voigt model based on some simplifications [95].

Once the contact stiffness and damping are obtained, values for the storage modulus E', loss modulus E'' and loss factor $tan(\delta)$ are calculated as [95]:

$$\begin{aligned} E' &= \frac{\sqrt{\pi}}{2}\frac{K_c}{\sqrt{A}} \qquad E'' = \frac{\sqrt{\pi}}{2}\frac{\Omega D_c}{\sqrt{A}} \\ \tan(\delta) &= \frac{E''}{E'} = \frac{\Omega D_c}{K_c} \end{aligned} \tag{A.11}$$

where A is the contact area between the tip and the sample and Ω the fundamental harmonic frequency of the sinusoidal signal. The calculation of the contact area depends on the geometry of the tip (in this case, $A = \pi {r_{tip}}^2$ for a flat tip with a circular cross-section.

A.3.6 The identification method: optimization and validation

In both static and dynamic cases, the main aim of the identification method is to convert the vertical force and the rod displacement signals into viscoelastic modules: E', E'' and tan(δ). The above described Kelvin-Voigt model will be considered as reference and its stiffness and damping parameters will be identified. As described in the previous Paragraph A.3.5, the equations (A.11) has been used to convert K_c and D_c to E' and E'' respectively.

An optimization method has been introduced and the mean square deviation between the predicted and the measured characteristics is minimized. To determine the quality of the optimization results, the root mean square error RMSE% in percent is calculated, as shown below:

$$RMSE = \sqrt{\frac{\sum_{i=1}^{n}(y_i - \hat{y}_i)^2}{n}} \tag{A.12}$$

whereas n corresponds to the number of values, $\hat{y}$ to the measured and y to the calculated value.

This approach has been considered for the calculation of the loss modulus E", storage modulus E' and loss factor tan(δ), based on the Kelvin-Voigt mathematical model described in the Chapter 2. The algorithm is based on some sub sections that are listed below:

1. importing section of the raw data;
2. filtering with a low-pass filter;
3. extracting the fundamental frequency;
4. identification of stiffness and damping compliances of the rubber through the Matlab function "lsqcurvefit", normally used to solve nonlinear data-fitting problems in least-squares sense.

The calculation of the stiffness and damping values have been taken directly from the raw data. We can divide the process in 2 phases, with the Phase 1 as shown in Figure A-17.

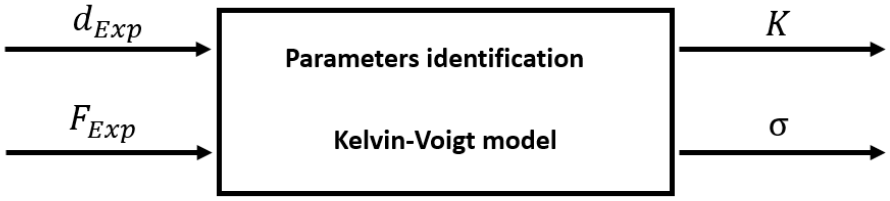

Figure A-17 - Phase1: estimation of stiffness and damping of the Kelvin-Voigt model.

The two parameters $d_{Exp}$and F_{Exp} are the measured displacement and force, respectively. The Phase 2 is dedicated to the validation of the identified model, as shown in Figure A-18.

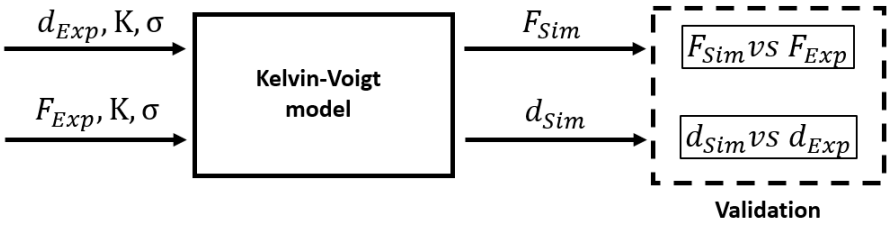

Figure A-18 - Phase 2: validation of the identified model parameters.

For the validation of the proposed method, the obtained vertical force results (of the optimization process), are used as input signals for the viscoelastic model: therefore, it has been considered the comparison between the displacement values obtained from optimization process and those ones obtain from measurements (Figure A-19).

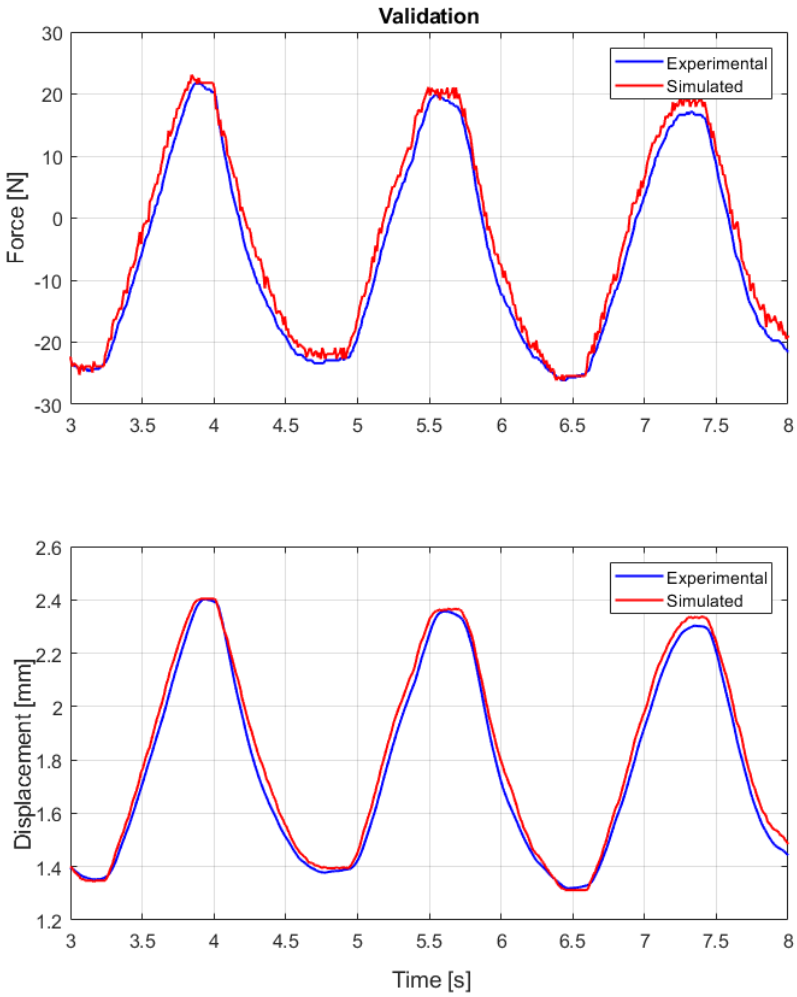

Figure A-19 - Validation of the Kelvin-Voigt model with the identified parameters.

No boundary conditions have been considered for the setup of the "lsqcurvefit" Matlab function. In the following figures results about the E', E'' and tan(δ) are shown.

The DMA analysis, provided by the rubber company, have been considered at different frequencies and strain values, as shown in Table A-2 below.

Table A-2 – Frequency and Strain of the DMA for A, B and C rubber samples.

Frequency [Hz]	**Strain [%]**
0.1	0.1
1.0	0.1

In the following Figure A-20, A-21 and A-22 the estimated storage modulus, los modulus and loss tangent are compared with the DMA data of the same rubber slabs.

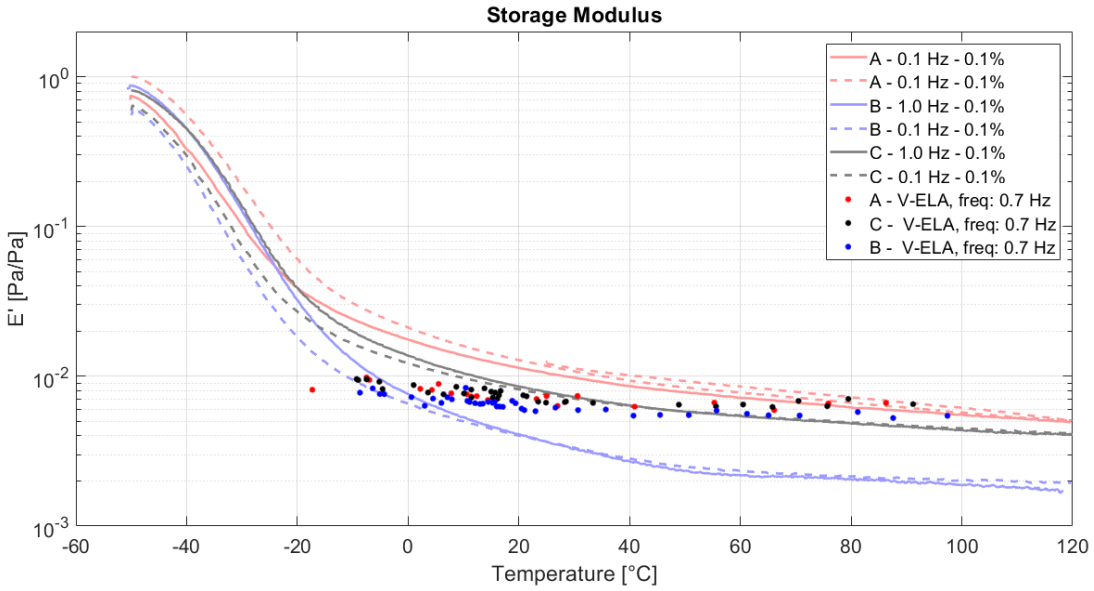

Figure A-20 – Storage modulus comparison between DMA at different frequencies and strains and V-ELA results with the 2 studied methods. Normalized data.

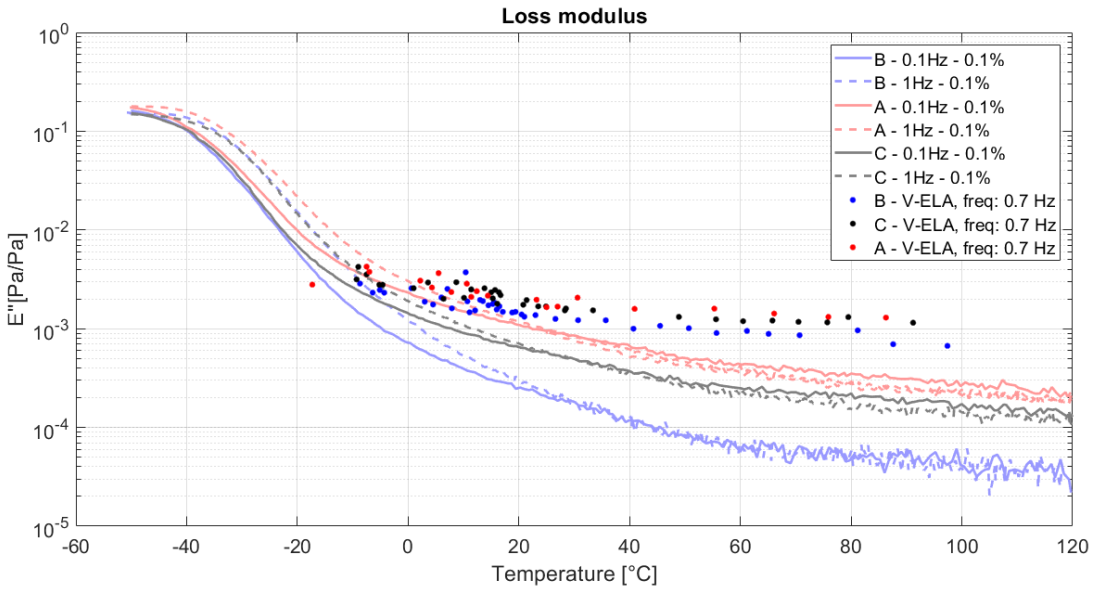

Figure A-21 – Loss modulus comparison between DMA at different frequencies and strains and V-ELA results with the 2 studied methods. Normalized data.

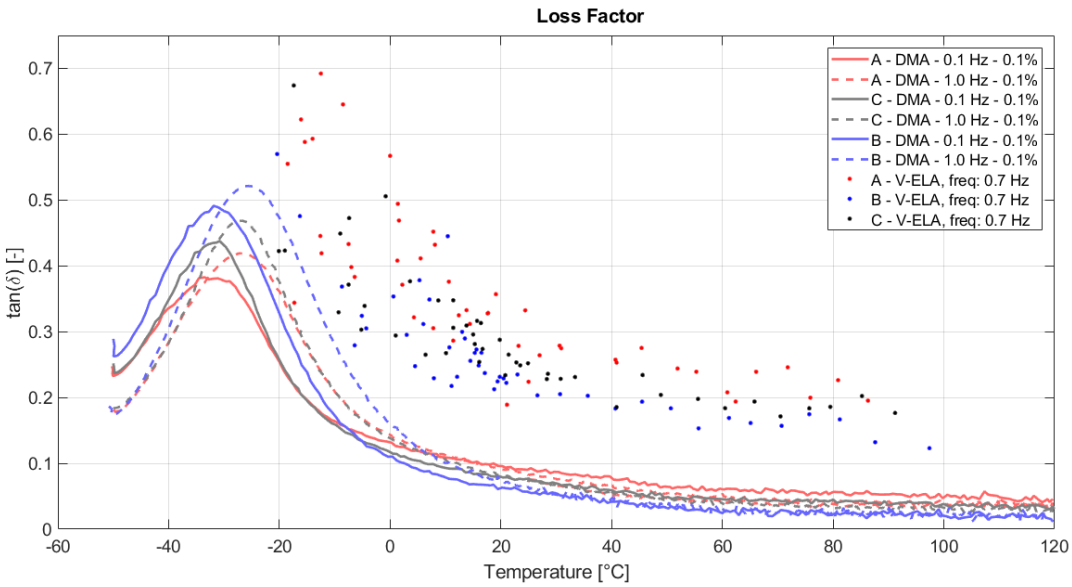

Figure A-22 - Loss tangent comparison between DMA at different frequencies and strains and V-ELA results with the 2 studied methods.

The graph in Figure A-22 above are showing the results of the optimization, based on Kelvin-Voigt model. The points (related to Identification method, explained in this paragraph), can show a similar trend with respect to the DMA analysis of the same slabs. Regarding the test performed with V-ELA, the only frequency that has been possible to reach was around and 0.7 Hz.

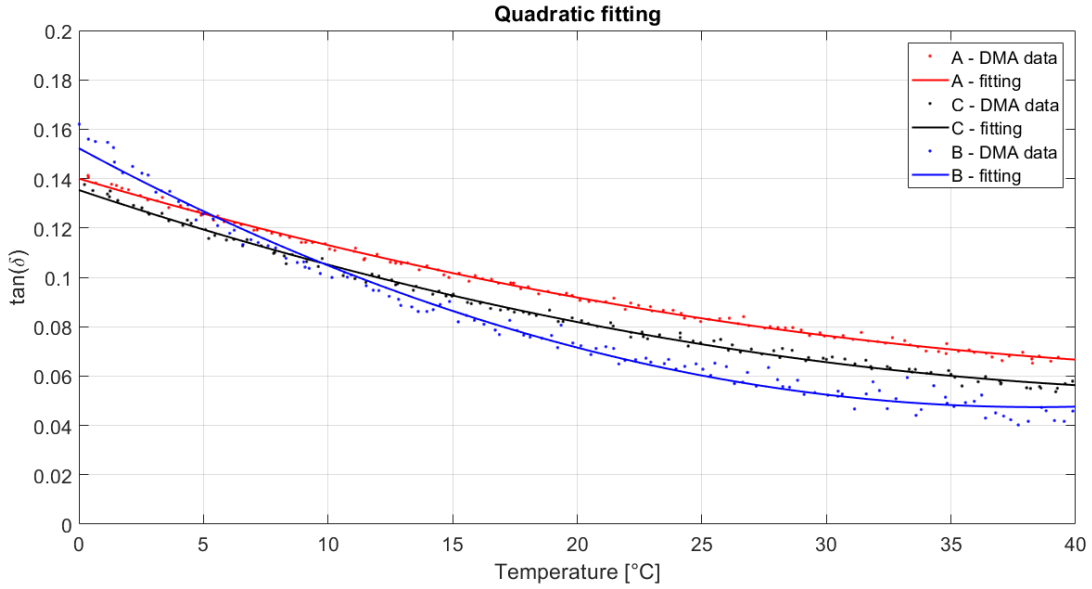

Figure A-23 – Quadratic fitting of the DMA data in the Temperature range [0; 40°C], at f = 1 Hz and strain = 0.1%.

In the Figure A-23, quadratic fitting of the DMA data has been done in the temperature range [0; 40°C]. The quadratic equation is shown below:

$$\tan(\delta) = aT^2 + bT + c \qquad \text{(A.13)}$$

where a, b and c are the estimated coefficients. This range has been chosen because it can be defined as the more reliable one due to the difficult control of temperature at very low and high values. Because of it, the estimated stiffness and damping parameters could show higher errors with respect to the range that has been considered for the current assessment.

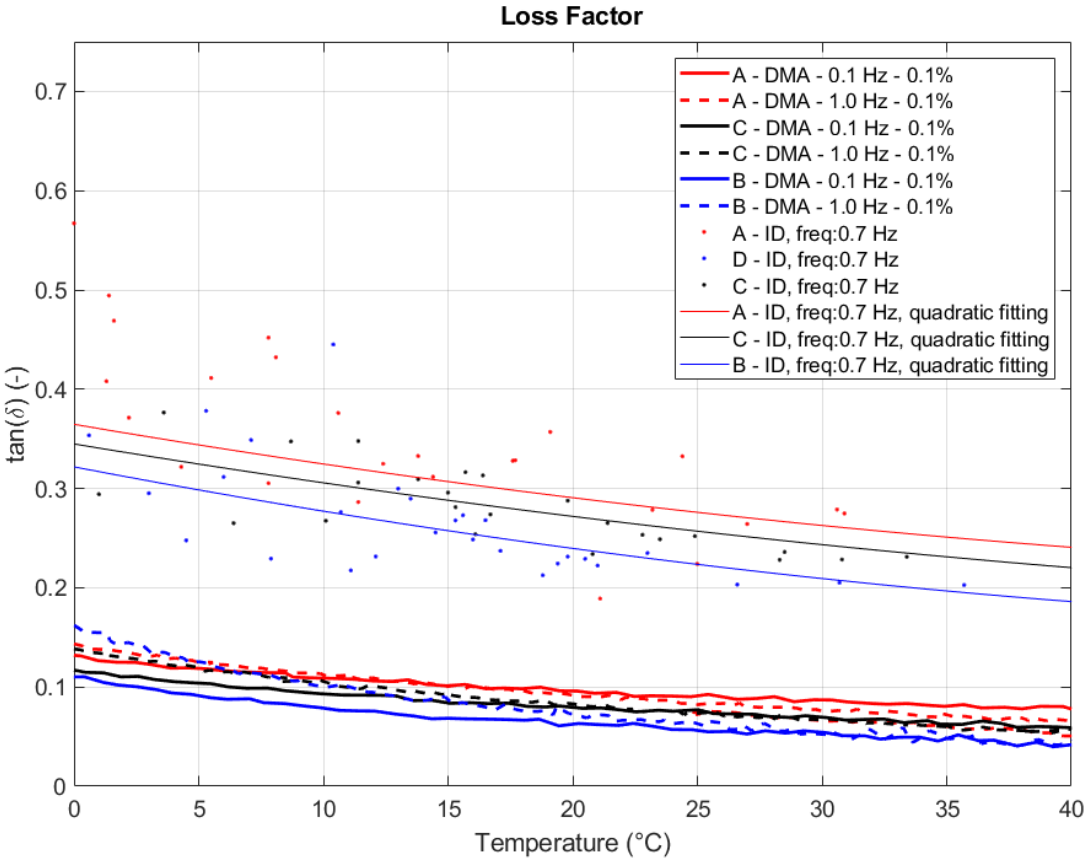

Figure A-24 – Fitting of the experimental data and comparison with the DMA results.

In Figure A-24 it can be observed that there is a good correlation between DMA and V-ELA in terms of trends of loss factor. Probably this is due to the fact that in the interval [0; 40°C], the temperature condition was more efficiently kept during the test, it is then expected that the results can be more reliable. The absolute values are not directly comparable, it could depend on several reason:

- the applied frequency is not always the same;
- the strain values are not comparable because of the nature of the indentation approach is different from the one used for DMA test (traction of the rubber sample);
- the limitation of the instrument to allow micro or nanoindentations.

Regarding the last point, the strain percentage could be considered around 20%, if it is assumed that the average indentation depth is 1,20 mm and the thickness of the slab is 5 mm. The indentation depth has been calculated by considering the RMS of the harmonic displacement signal.

The future development of this instrument will expect the improvement of the following points: temperature conditioning, correlating the 2 different kind of strains (which cannot be considered directly comparable with DMA, because of the 2 different test procedures) and automating the harmonic displacement signal.